REPORT DOCUMENTATION PAGE

1a. REPORT SECURITY CLASSIFICATION Unclassified		1b. RESTRICTIVE MARKINGS		
2a. SECURITY CLASSIFICATION AUTHORITY		3. DISTRIBUTION/AVAILABILITY OF REPORT Approved for public release; distribution unlimited.		
2b. DECLASSIFICATION/DOWNGRADING SCHEDULE				
4. PERFORMING ORGANIZATION REPORT NUMBER(S)		5. MONITORING ORGANIZATION REPORT NUMBER(S)		
6a. NAME OF PERFORMING ORGANIZATION Research Laboratory of Electronics Massachusetts Institute of Technology	6b. OFFICE SYMBOL (If applicable)	7a. NAME OF MONITORING ORGANIZATION U. S. Army Research Office		
6c. ADDRESS (City, State, and ZIP Code) 77 Massachusetts Avenue Cambridge, MA 02139		7b. ADDRESS (City, State, and ZIP Code) P. O. Box 12211 Research Triangle Park, NC 27709-2211		
8a. NAME OF FUNDING/SPONSORING ORGANIZATION U. S. Army Research Office	8b. OFFICE SYMBOL (If applicable)	9. PROCUREMENT INSTRUMENT IDENTIFICATION NUMBER DAAL03-86-K-0002		

8c. ADDRESS (City, State, and ZIP Code) P. O. Box 12211 Research Triangle Park, NC 27709-2211	10. SOURCE OF FUNDING NUMBERS			
	PROGRAM ELEMENT NO.	PROJECT NO. P-23223-EL	TASK NO.	WORK UNIT ACCESSION NO.

11. TITLE (Include Security Classification)

RLE Progress Report No. 130

12. PERSONAL AUTHOR(S)

Jonathan Allen and Daniel Kleppner

13a. TYPE OF REPORT Annual Report	13b. TIME COVERED FROM 1/1/87 TO 12/31/87	14. DATE OF REPORT (Year, Month, Day) July 1988	15. PAGE COUNT 317

16. SUPPLEMENTARY NOTATION The view, opinions and/or findings contained in this report are those of the author(s) and should not be construed as an official Department of the Army position, policy, or decision, unless so designated by other documentation.

17. COSATI CODES			18. SUBJECT TERMS (Continue on reverse if necessary and identify by block number)
FIELD	GROUP	SUB-GROUP	

19. ABSTRACT (Continue on reverse if necessary and identify by block number)

Work by J. Allen and his collaborators is summarized here.

20. DISTRIBUTION/AVAILABILITY OF ABSTRACT ☒ UNCLASSIFIED/UNLIMITED ☐ SAME AS RPT. ☐ DTIC USERS	21. ABSTRACT SECURITY CLASSIFICATION Unclassified	
22a. NAME OF RESPONSIBLE INDIVIDUAL Kyra M. Hall	22b. TELEPHONE (Include Area Code) (617) 253-2469	22c. OFFICE SYMBOL

DD FORM 1473, 84 MAR   83 APR edition may be used until exhausted. All other editions are obsolete.
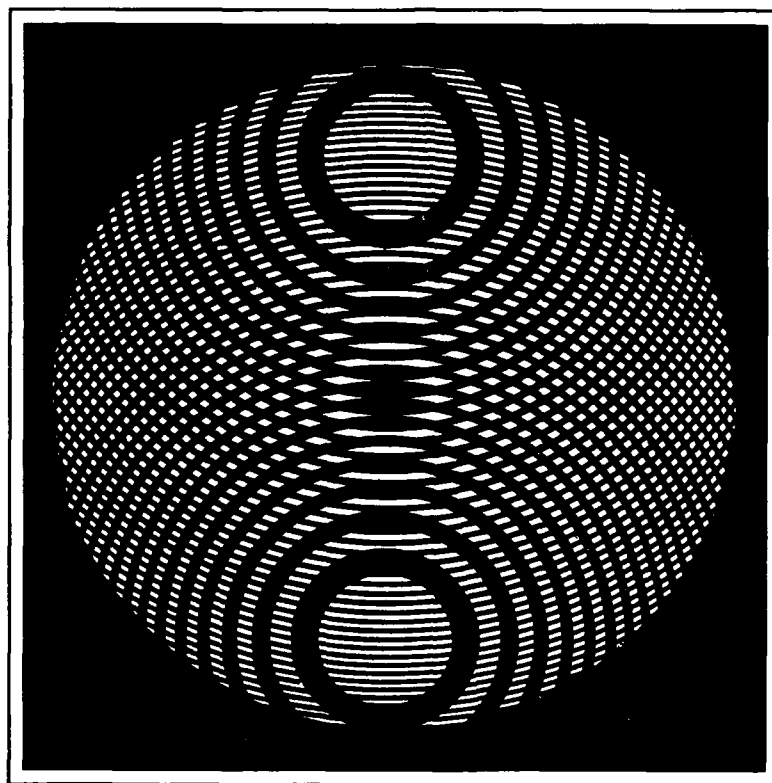
RLE Progress Report

No. 130

January 1 - December 31, 1987

Submitted by:

Prof. Jonathan Allen
Prof. Daniel Kleppner

Research Laboratory of Electronics
Massachusetts Institute of Technology
Cambridge, MA 02139 USA

RLE Progress Report No. 130

Cover and title page: Moiré patterns produced by the overlay of three zone plate *transparencies illustrate the nonlinear interaction leading to artifacts in the recon-*structed images.

The use of zone plates to focus light in place of lenses was probably invented by Lord Raleigh in 1871. A modern application of zone plates is for focusing x-rays; lenses can not be used at these short wavelengths.

Research at MIT on zone plates is reported in the 1976 doctoral dissertation of Natale M. Ceglio, Jr., *Zone Plate Coded Imaging of Laser Produced Plasmas*. Dr. Ceglio is presently at the Lawrence Livermore National Laboratory in Livermore, California.

This report was produced with IBM's Generalized Markup Language and Document Composition Facility. Mylar printing plates were printed on an IBM 4250-II electro-erosion printer. RLE personnel photographed by John F. Cook.

Table of Contents

MIT Building 36: Home of the Research Laboratory of Electronics since 1973.

RLE Director Professor Jonathan Allen

Introduction

The Research Laboratory of Electronics (RLE) was established in 1946 as the Institute's first interdepartmental laboratory. Originally organized under the joint sponsorship of the Departments of Physics and Electrical Engineering, RLE has broadened its interests to cover a wide range of research.

The RLE environment provides both the freedom of action essential in an academic institution and the availability of large-scale laboratory facilities and services required by researchers. RLE's interdisciplinary setting offers many opportunities for creative and collaborative research. By fostering this powerful combination of research and education, RLE effectively penetrates beyond the horizon of new ideas and information.

Progress Report No. 130 describes research programs at RLE for the period January 1 through December 31, 1987. This report contains both a statement of research objectives and a summary of research efforts for each of the research groups within RLE. Faculty, research staff and students who participated in these projects are identified at the beginning of each chapter, along with sources of funding.

We would like to highlight the following features of this report. Chapter 30 is a bibliography of RLE publications and papers presented by RLE staff during 1987. Chapter 31 is a roster of current RLE staff. In addition, indexes of project personnel and sponsored research projects are located at the end of this report.

Progress Report No. 130 was produced by the RLE Communications Office. Further inquiries may be addressed to:

<div style="text-align:center">

Communications Office
Research Laboratory of Electronics
Building 36-412
Massachusetts Institute of Technology
Cambridge, Massachusetts 02139
(617) 253-2566

</div>
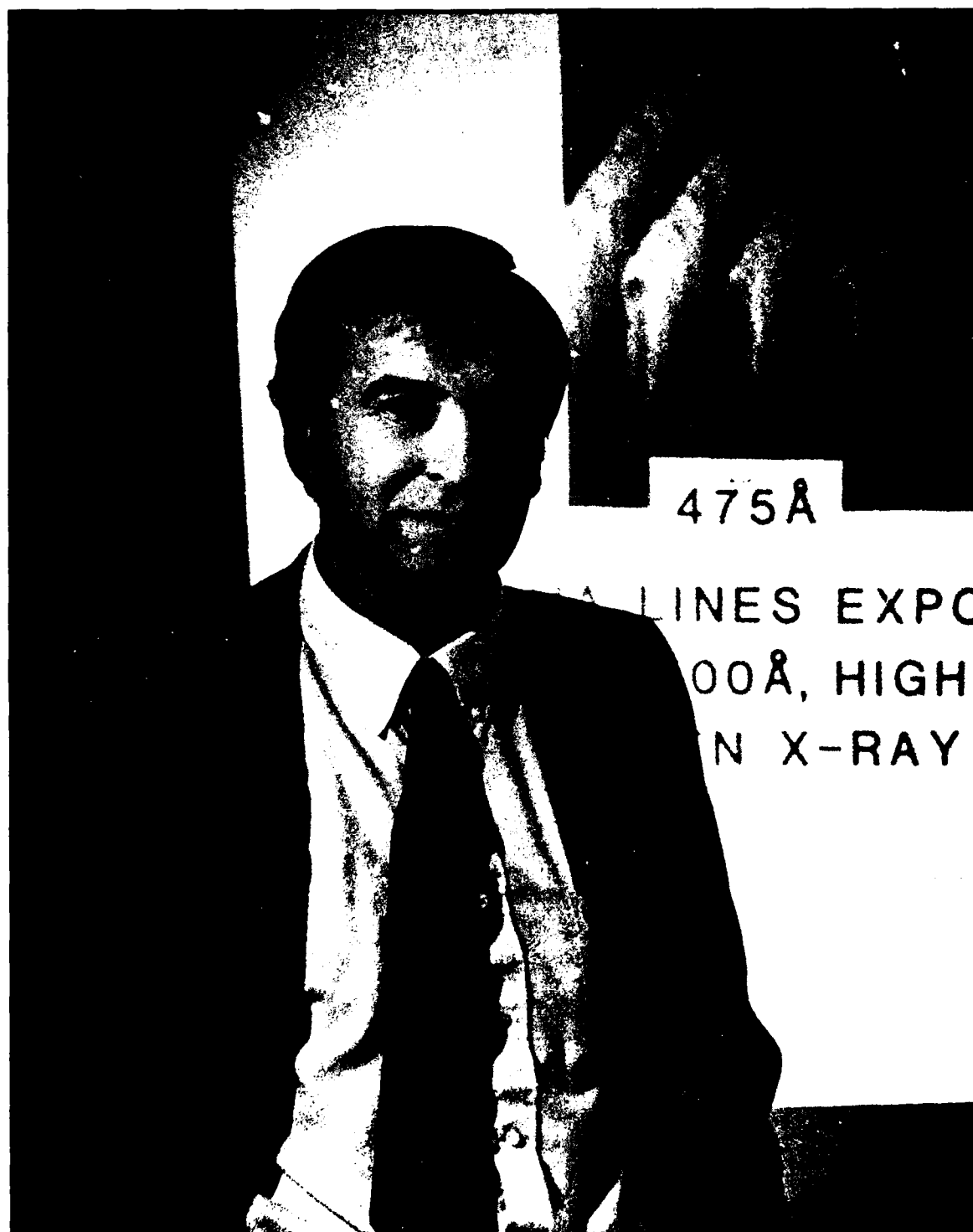
Professor Henry I. Smith

1.0 Submicron Structures Technology and Research

Academic and Research Staff

Prof. H.I. Smith, Dr. M.L. Schattenburg, J.M. Carter

Visiting Scientists

H. Kawata,[1] I. Plotnik,[2] I. Tanaka[3]

Graduate Students

S. Ajuria, E.H. Anderson, H.A. Atwater, P. Bagwell, W. Chu, L. Clevenger, J. Floro, S.M. Garrison, J. Im, K. Ismail, E. Jiran, H.J. Kim, Y-C. Ku, U. Meirav, P. Meyer, A. Moel, J.E. Palmer, S.L. Park, H.M. Quek, J. Scott-Thomas, G. Shahidi, M. Toth, A.T. Yen

1.1 Submicron Structures Laboratory

The Submicron Structures Laboratory at MIT develops techniques for fabricating surface structures with linewidths in the range from nanometers to micrometers, and uses these structures in a variety of research projects. These projects of the laboratory, which are described briefly below, fall into four major categories: development of submicron and nanometer fabrication technology; deep-submicron electronics and quantum-effect electronics; crystalline films on amorphous substrates; and periodic structures for x-ray optics and spectroscopy.

1.2 Microfabrication at Linewidths of 100nm and Below

Joint Services Electronics Program (Contract DAAL03-86-K-0002)
National Science Foundation (Grant ECS 87-09806)

Erik H. Anderson, James M. Carter, William Chu, Hui M. Quek, Irving Plotnik, Mark L. Schattenburg, Anthony T. Yen, Henry I. Smith

A variety of techniques for fabricating structures with characteristic dimensions of 0.1 μm (100 nm) and below are investigated. These include: x-ray nanolithography, holographic lithography, achromatic holographic lithography, electron-beam lithography, reactive-ion etching, electroplating and liftoff. Development of such techniques is essential if we are to explore the rich field of research applications in the deep-submicron and nanometer domains. X-ray nanolithography is of special interest

---

[1] Hampshire Intruments, Inc.

[2] Nippon Sheet Glass

[3] Osaka Prefecture University

because it promises to provide high throughput and broad process latitude at linewidths of 0.1 μm and below, something that cannot be achieved with scanning- electron-beam lithography. We are developing a new generation of x-ray masks made from inorganic membranes (Si, Si_3N_4 , and SiC) and are investigating means for precisely controlling mask-wafer gap, and achieving nanometer alignment. Phase shifting and transform x-ray masks (i.e., in-line x-ray holography) may permit us to achieve sub-50 nm linewidths at finite gaps. In this year we showed that if the absorber introduces a pi-phase shift in addition to about 10db attenuation the intensity profile at the edge of a feature is steeper than with conventional masks. This is because low levels of radiation that diffract into the shadow region behind an absorber are partially cancelled by the phase shifted radiation transmitted by the absorber. This enables either an increase in the allowable mask-sample gap at a given linewidth or improves the process latitude at a given gap.

A new tri-level technique for making, by electron-beam lithography, x-ray masks with linewidths of 50 nm was developed in collaboration with IBM. This technique allows us to fabricate x-ray masks with patterns of arbitrary geometry and replicate them in our own laboratory, as illustrated in figure 1.1.
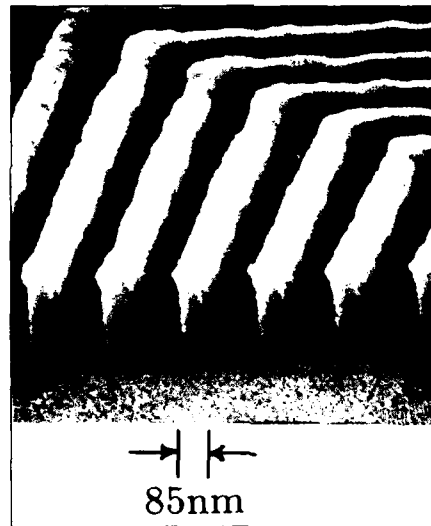
85nm

Figure 1.1 X-ray nanolithographic replication of 85 nm-linewidth patterns created on the x-ray mask by scanning e-beam lithography.

Techniques for making x-ray masks from crystallographic templates are being improved. We hope to achieve x-ray replication in PMMA with nanometer scale line-edge smoothness.

An achromatic holographic lithography configuration was developed which allows us to produce periodic structures with linewidths $\sim$ 50 nm over large areas, using deep-UV sources that have poor temporal and spatial coherence, such as the ArF laser. We have also developed a means of feedback stabilizing the fringe pattern against vibrations and other disturbances. Although holographic techniques can be used to

prepare experimental samples, there are important advantages to using them only for preparing x-ray masks. These masks are then replicated using x-ray nanolithography. With C_K and Cu_L x-ray lithography high-aspect-ratio (almost 8:1) structures with linewidths less than 50 nm have been produced in PMMA.

1.3 Improved Mask Technology for X-Ray Lithography

Semiconductor Research Corporation (Contract 87-SP-080)

Yao-C. Ku, Irving Plotnik, Henry I. Smith

In order to utilize x-ray lithography in the fabrication of submicron integrated electronics, distortion in the x-ray mask must be eliminated. Distortion can arise from stress in the absorber, which is usually gold or tungsten. Tungsten is preferred because it is a closer match in thermal expansion to Si, and other materials used as mask membranes. However, W is usually under high stress when deposited by evaporation or sputtering. We have demonstrated that tensile stress in W can be compensated by ion implantation. Strain-induced deflection of Si_3N_4 or Si membranes is measured in a Linnik interferometer. Membrane deflection due to stresses $\sim 7 \times 10^9$ dynes/cm^2 are reduced to zero by implantation of 1×10^{16} Si atoms/cm^2 at 25 keV. Stress compensation occurs because the implantation into the top 10nm of the W film causes a compressive stress which in turn produces a torque to compensate the torque produced by the native tensile stress. In the future we will develop a capacitive method of measuring membrane deflection so that stress correction can be done in situ, during film deposition, or in real time during ion implantation.

1.4 Theoretical Analysis of the Lithography Process

Semiconductor Research Corporation (Contract 87-SP-080)

Henry I. Smith

In an earlier theoretical analysis of lithography we studied the effects of statistical fluctuations on linewidth control, and compared the pixel transfer rates of the various lithographic techniques. This analysis has been expanded to include the effects of nonuniform illumination and other non-ideal factors. We have also derived a method for quantifying process-latitude in lithography, a critically important figure-of-merit in manufacturing. The normalized-process-latitude-parameter was evaluated, as a function of minimum linewidth, for several UV and deep UV projection system, and for an x-ray system based on a laser-produced plasma source. As expected, the x-ray system showed a significantly larger process latitude in the important linewidth range between 0.1 and 1 μm.

1.5 Studies of Electronic Conduction in One-Dimensional Semiconductor Devices

Joint Services Electronics Program (Contract DAAL03-86-K-0002)
National Science Foundation (Grant ECS 85-03443)

S.B. Field, Jerome C. Licini, Udi Meirav, Samuel L. Park, John Scott-Thomas, Dimitri A. Antoniadis, Marc A. Kastner, Henry I. Smith

At low temperatures, Si inversion layers of two-dimensional-electron-gas, with widths less than 100 nm in Si, and less than 1 μm in GaAs, become quasi-one-dimensional. This happens when inelastic scattering is sufficiently reduced that the electronic wave functions have phase coherence over distances larger than the device width.

Three techniques are being employed to fabricate one-dimensional devices. In the first, field-effect transistors are fabricated in Si with widths as narrow as 50 nm. The narrow gate of these MOSFET's is created by glancing-angle evaporation of tungsten onto a 50-nm high step etched in a 100-nm thick oxide on a Si (100) surface. In a second technique, the inversion layer is created under a narrow slot in a wide metal gate by applying a potential to an upper metal gate separated from the first by a layer of SiO_2. The lower gate with the narrow slot is fabricated using x-ray lithography and lift-off. To create one-dimensional devices in GaAs we are exploring the possibility of using p-implants to confine the two-dimensional electron gas created by modulation doping or by a gate.

Recently, using devices fabricated by the first and second techniques, a new collective state of the electron gas in high magnetic fields was discovered. Initial experiments were done on quasi-one dimensional Si inversion layers, about 100 nm wide and 7 μm long. At 100 mK and low magnetic fields the usual small negative magnetoresistance, and the universal conductance fluctuations associated with localization in one dimension, were observed. In a larger magnetic field of about 4T, however, there is a magnetic-field-induced transition to a new state, with conductance almost ten times larger than in zero field. This giant negative magnetoresistance is astonishing. The conductance per square of the Q1D device, once the new state is formed, is ten times larger than its 2D counterpart. Figure 1.2 shows that in high magnetic fields the conductance rises sharply at certain gate voltages and has plateaus in between. This is reminiscent of the quantum-Hall effect, and it is likely that the high-field state in the Q1D inversion layer is related to the quantum-Hall state in the 2D electron gas. However, the pattern of the plateaus and the temperature dependence of the structure in the conductance-versus-gate voltage provides strong evidence that new many-body effects are important.

There is no model that predicts these phenomena in detail. However, it has been suggested that 1D confinement of the 2D gas might lead to a charge or spin density wave instability when the width is comparable to, but somewhat larger than, the magnetic length (i.e., the radius of the Landau orbit). Such instabilities lead to a gap which remains at the Fermi energy over a wider range of filling factors than for the quantum-Hall state. The plateaus would then reflect plateaus in p_{xy} because p_{xx} would be zero. Experiments are underway to explore how the properties of the high-field state depend on the channel width and mobility. The split, dual-gate configuration produces an inversion layer $\sim$ 30 nm wide. The high-field state has been observed in this structure as well, but at much higher magnetic fields, as expected.
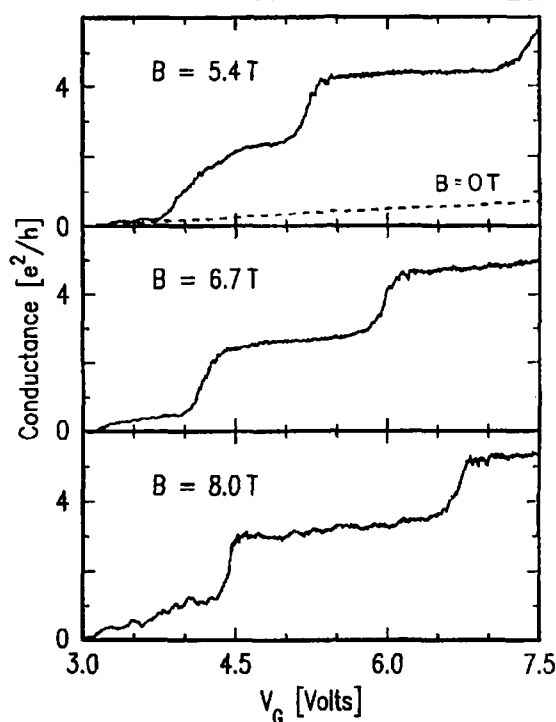
Figure 1.2 Conductance as a function of carrier density (V_G) at three magnetic fields and T=100 mK. Note that, although the values are not integral multiples of e^2/h , the largest steps have $2e^2/h$. The risers shift linearly in magnetic field. The dashed curve in the top panel is the conductance at B=0.

1.6 Surface Superlattice Formation in Silicon Inversion Layers using 200 μm Period Grating-Gate Field-Effect Transistors

Joint Services Electronics Program (Contract DAAL03-86-K-0002)
U.S. Air Force - Office of Scientific Research (Grant AFOSR 85-0376)

Phillip F. Bagwell, Anthony T. Yen, Dimitri A. Antoniadis, Marc A. Kastner, Terry P. Orlando, Henry I. Smith

We have been investigating electronic conduction and distinctly quantum-mechanical effects in a surface superlattice (SSL) device. The device is a Si MOSFET with a dual stacked gate configuration. The lower gate is a tungsten grating of 200 nm period (100 nm nominal linewidth), and the upper gate is a uniform metal pad separated from the grating by 200 nm of deposited SiO_2 . We call these devices grating-gate-field-effect transistors (GGFET's). The grating gate is fabricated using x-ray nanolithography and grating contact pads are made with deep-UV lithography. Drain-to-source current in the SSL device runs perpendicular to the grating wires. A distinguishing feature of our GGFET's is that the strength of the periodic modulation in the channel, and the inversion-layer electron density, can be independently controlled by external voltage supplies. At low temperatures we observe a modulation of the inver-

sion layer conductance with gate voltage that is about one hundred times larger than the universal fluctuations predicted by the theory of Lee and Stone. This is consistent with electron back diffraction from the imposed periodic potential.

The first generation of devices had low fabrication yields due to poor gate contacts, adhesion problems, metallization problems and shorts to the substrate. Devices also had low mobility due to radiation damage. These problems have been resolved and second generation devices have been fabricated and tested. The first set suffered from unfavorable line-to- space ratio in the grating gate, making it impossible for us to invert regions in between grating lines. A third set of devices is being fabricated with proper line-to-space ratio.

We have also developed a semiclassical algorithm to calculate the effects of free electron motion perpendicular to the superlattice, elastic impurity scattering, inelastic scattering between electrons and by phonons, and finite temperature on the conductance of these devices. The observability criterion arising from this model is that energy averaging $\sim \kappa t$ from finite temperature and $\sim h/\tau$ from a random impurity configuration must be smaller than the energy gaps at each mini-Brillouin zone boundary. Elastic scattering, by itself, does not lead to energy averaging but, coupled with inelastic scattering, sets the scale of the energy averaging. If no inelastic scattering is present in the device, elastic scattering leads to fluctuations in conductance of size e^2/h . In this regime, the observability criterion is that we must impose an average conductance modulation larger than e^2/h. We are currently implementing this semi- classical algorithm to calculate the conductance of GaAs superlattice devices, described in the next section.

1.7 Study of Surface Superlattice Formation in GaAs/GaAlAs Modulation Doped Field-Effect Transistors

William Chu, Khalid Ismail, Dimitri A. Antoniadis, Marc A. Kastner, Terry P. Orlando, Henry I. Smith

We have used the modulation-doped field-effect transistor (MODFET) as a test vehicle for studying electron back diffraction in a GaAs/GaAlAs material system. In a regular MODFET the current transport is modulated by a continuous gate positioned between source and drain. In our device, the grating-gate MODFET, shown in figure 1.3, we have combined x-ray nanolithography and liftoff to achieve a 0.2 μm-period grating-gate (100nm linewidth). By biasing this gate we can introduce a periodic modulation of the charge concentration in the 2D-gas residing at the GaA1As/GaAs interface. As a result an electron traveling from source to drain sees a periodic array of barriers. The height of these barriers and the electron concentration can be altered by changing the bias condition on the gate. Theory predicts that such a structure would result in energy gaps opening up in the energy band. This should be manifest as a drop in conductance whenever the Fermi energy is swept across any of those gaps. In our first batch of working devices current we observed plateaus while sweeping the grating-gate voltage. This effect was repeatable from one device to another. In com-

parison, regular MODFET's, which were fabricated on the same sample, had a smooth current increase. This gives evidence that the observed plateaus are a manifestation of electron back diffraction caused by the periodic modulation. Differentiating our results, the effect is more pronounced, as shown in figure 1.4, and had distinct features which were quadratically spaced, as expected for a parabolic energy band.
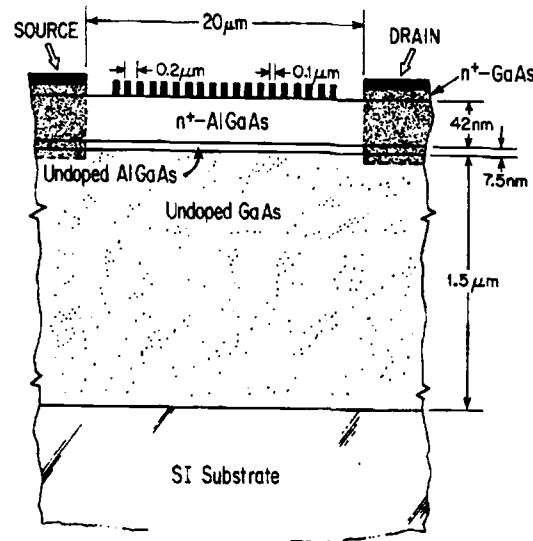
Figure 1.3 Schematic cross section of a grating-gate MODFET device. The channel width and length are both 20 μm. An undoped GaAs/GaAlAs superlattice (not shown) was used to trap impurities diffusing out of the substrate.

Because this sample had a mobility of 250,000 cm²/V sec at 4 K the calculated mean free path of electrons is ~ 1.2 μm. We believe that due to the high material purity, universal conductance fluctuations have been suppressed, since in this regime both the elastic and the inelastic scattering times are comparable. Preliminary magnetoresistance measurements confirm this idea.

We are planning to fabricate devices with grid-gates (figure 1.5) to confine the electron motion in two dimensions. We also intend to exploit our lithographic capabilities to push our grating-gate periodicity down by a factor of two to 100nm period (50nm linewidth). Under those conditions the superlattice effects should become more prounounced at 4 K, and might also become observable at much higher temperatures.
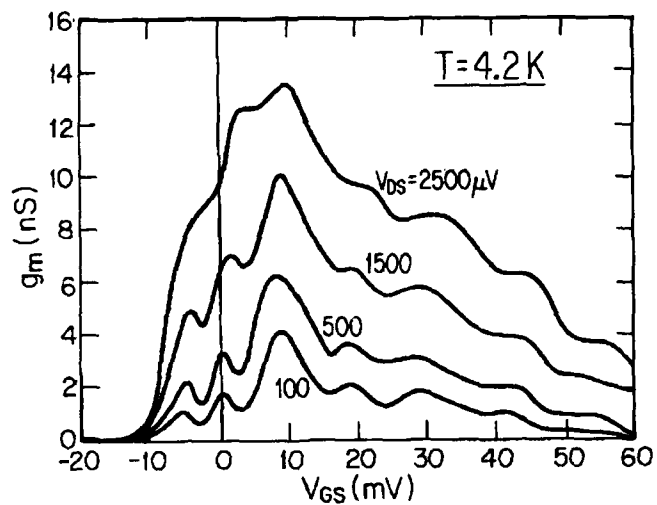
Figure 1.4   Plots of transconductance, g_m , versus gate-to-source voltage, V_{GS} , for several values of the source-drain voltage, V_{DS}.
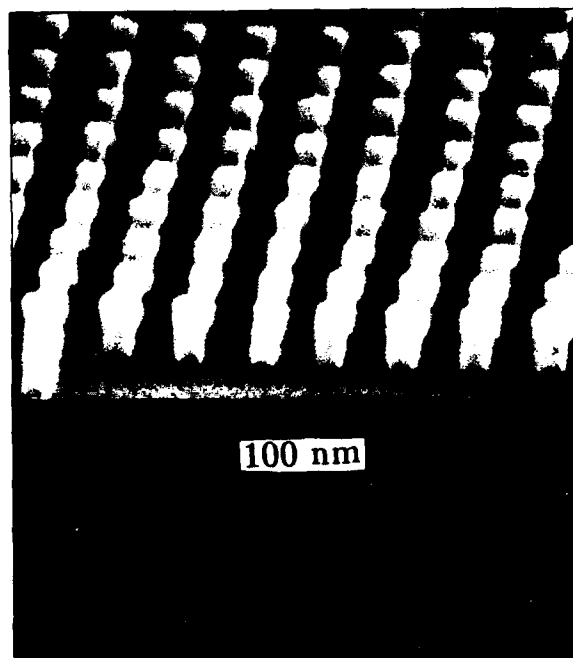
Figure 1.5 X-ray lithographic replication of a grid pattern in PMMA.

1.8 Investigation of One-Dimensional Conductivity in Multiple, Parallel Inversion Lines

Phillip F. Bagwell, Anthony T. Yen, Dimitri A. Antoniadis, Marc A. Kastner, Terry P. Orlando, Henry I. Smith

In order to study one-dimensional conductivity without the statistical fluctuations normally associated with small systems, field-effect devices have been fabricated which use a submicron-period grating-gate structure to produce 250 narrow inversion lines in parallel. The device is fabricated on the same substrate and by the same procedures as the Si GGFET's discussed in section 1.6. In fact, the major difference is that the grating lines are now parallel to the electron flow. Others have reported a variety of devices which produce a single narrow "micro-channel," but the expected quasi-one-dimensional density of states has generally been obscured by large random fluctuations inherent in small systems. Here, the parallel measurement of many such one-dimensional conductors results in an improved signal-to-noise ratio in the density-of-states sampling. This is due to the incoherence of random fluctuations in different micro-channels in the same device. Proper independent biasing of the two gate electrodes results in the formation of a parallel array of 50 to 100-nm-wide lines of inversion charge connecting the source and drain. Transconductance measurements demonstrate a weak, regular modulation that is consistent with the expected quasi-one-dimensional density-of-state. These experiments are being repeated with a new generation of devices.

We understand the conductance modulation in a quasi-one-dimensional wire as arising from scattering between subbands. As the Fermi level passes into a new subband, we expect a large decrease in conductance. Inelastic scattering at finite temperature will tend to destroy this effect. The same semi-classical modeling techniques used for the surface-superlattice devices have been used to model conductance in single-wire, and multiple wire arrays. We have developed an analytic formula showing that conductance in the wire array closely approximates a quasi-1D wire for a Fermi energy small compared to the scale of the confining potential.

1.9 Study of Electron Transport in MOSFET's in Si with Deep-Submicron Channel Lengths

Ghavam Shahidi, Dimitri A. Antoniadis, Henry I. Smith

Electron conduction in sub-100-nm channel length, Metal-Oxide- Semiconductor Field-Effect Transistors (MOSFET's) in Si is investigated. The devices were fabricated with a combination of x-ray nanolithography and optical projection lithography. The x-ray mask, which defined the minimum lithographic features, was fabricated with conventional photolithography, anisotropic etching of a Si template, and oblique shadowing of the absorber. The gate oxide thickness for these devices was typically

7.5 nm, but in some cases as thin as 2.5nm . Electron velocity overshoot, to values exceeding bulk saturation values of 10^7 cm sec^{-1} at room temperature and 1.5×10^7 cm sec^{-1} at liquid nitrogen temperature, was observed. A non-uniform channel doping was employed to achieve high electron mobility in the inversion layer, while at the same time preventing punchthrough. The doping in the inversion layer is about 10^{16} cm^{-3}. Control of punchthrough is achieved by a boron implant in the channel of 4×10^{12} cm^{-2} at 50 keV. After oxidation at 900°C for 10 min in O_2, to grow the gate oxide, the boron profile remains abrupt with a peak concentration of about 2.2×10^{17} cm^{-2} at 0.19 μm depth. The low-field mobility was estimated from long channel MOSFET's on the same substrate to be about 450 cm²/Vsec.

In addition to velocity overshoot we have also investigated hot electron effects, specifically channel-hot-electron-generated substrate currents. For channel lengths in the range 0.15 μm $< L < 0.5$ μm the normalized substrate current at constant (V_{DS} - V_{DSAT}) increases with decreasing channel length, presumably because of an increase in the maximum field near the drain. However, as the channel length is decreased below 0.15 μm, a decrease of the normalized substrate current is observed. We believe that this effect accompanies the onset of electron velocity overshoot over a large portion of the channel, and is due to either a decrease of carrier temperature or a relative decrease of the carrier population in the channel, or both.

We have also used indium as an alternative channel implant. Because of higher atomic number one can achieve lower surface doping, and bring the implant peak very close to the surface, thus resulting in higher threshold voltages and a reduction in short-channel effects. Short-channel MOSFET's with indium as the channel implant and gate oxide thickness of 2.5 nm gave transconductances of 720 mS/mm, and reduced short-channel and hot-electron effects. Further work in characterization of devices with indium implants is continuing.

1.10 Crystalline Films on Amorphous Substrates

Sergio Ajuria, Harry A. Atwater, Jerrold A. Floro, Hui Meng Quek, Henry I. Smith, Carl V. Thompson

We are investigating methods for producing crystalline films on amorphous substrates. This is motivated by the belief that the integration of future electronic and electrooptical systems will be facilitated by an ability to combine, on the same substrate, a broad range of materials (Si, III-V's, piezoelectrics, light guides, etc.). Zone melting recrystallization (ZMR) of Si on amorphous SiO_2 has been highly successful, but device-quality films are obtained only at the expense of high processing temperatures since the Si must be melted. Other materials, such as Ge and InSb, have also been successfully zone melted. ZMR has been an important testing ground for materials combination, and for a number of novel concepts based on the use of lithography to control in-plane orientation and the location of defects (so-called defect entrainment).

The most promising approach in the long-term to crystalline films on amorphous substrates is, in our view, based on surface-energy-driven secondary grain growth

(SEDSGG). In this approach, no melting or phase change occurs. Instead, we take advantage of the very large surface energies inherent in ultrathin (20 nm) films to drive the growth of large secondary grains having specific crystallographic planes parallel to the surface. This phenomenon has been demonstrated, as has the use of very fine gratings (~100 nm linewidths) to control the in-plane orientation (i.e., graphoepitaxy in combination with SEDSGG). Currently, research is focused on basic studies of grain growth and coarsening phenomena in ultra-thin films of model materials such as Ge, Si, Ag and Au. We also investigate means of promoting grain growth at temperatures many hundreds of degrees below the melting point. These include ion-bombardment-enhanced grain growth (IBEGG), laser illumination, and use of selective dopants. Theoretical models for surface-energy-driven secondary grain growth were developed and have, for the most part, been confirmed by experiments on Si, Ge and Au films. If our basic studies prove fruitful we may be able to develop a low temperature method, applicable to all crystalline film materials, for producing device-quality films on amorphous substrates. By means of lithography, defects in the films, such as dislocations and stacking faults, would be localized at predetermined positions, out of the way of devices.

1.11 Ion-Bombardment-Enhanced Grain Growth in Thin Films

Harry A. Atwater, Jerrold A. Floro, Henry I. Smith, Carl V. Thompson

Grain growth in polycrystalline films can lead to formation of low-defect-density or single-crystal film. We have been investigating the effect of ion bombardment on the motion of grain boundaries in normal and secondary grain growth, so called ion-beam-enhanced grain growth (IBEGG). The scientific objective is to better understand how grain boundaries move. The technological objective is to develop a low temperature process for obtaining crystalline films on amorphous substrates. IBEGG has been studied experimentally in thin (i.e., < 1000 Å) Ge, Au and Si films. Ion beams in the 40 - 100 keV range have been employed, resulting in an ion damage profile whose peak is approximately in the center of the thin film. Concurrent with ion bombardment, samples were annealed at 500 and 1050°C for Ge and Si, and at room temperature for Au. The temperature is chosen so that ion damage is annealed dynamically. IBEGG has been characterized by varying the ion dose, ion energy, ion flux, ion species, temperature, and thin film deposition conditions. The effect of these parameters on grain size and microstructure has been analyzed both qualitatively and quantitatively using transmission electron microscopy (TEM). A transition state model has been developed to describe the motion of grain boundaries during ion bombard-ment. The model accounts for the dependence of IBEGG on experimental para-meters. An atomistic picture of the jump rate at grain boundaries during IBEGG has been proposed. Monte-Carlo simulation of ion range and defect production was performed using the TRIM code and a modified Kinchin Pease formula. The calculated defect yield per incident ion was correlated with enhanced grain growth, and used to estimate the number of atomic jumps at the grain boundary per defect generated at the boundary for a given driving force, a quantity which is approximately constant for a given film material. The IBEGG and thermal growth rates have been related to their respective point defect populations.

That is, grain growth rate appears to depend only on the concentration of vacancies and interstitials, irrespective of whether they are created thermally or by ion bombardment.

Recently, we have extended the study of IBEGG to the low energy range (≤ 1 keV). Experiments are done in an ultrahigh vacuum system so that material lost through sputtering can be replaced by deposition from a separate source.

1.12   Epitaxy via Surface-Energy-Driven Grain Growth

Jerrold A. Floro, Joyce E. Palmer, Carl V. Thompson, Henry I. Smith

Grain growth in polycrystalline films on single-crystal substrates can lead to formation of low-defect-density or single-crystal films. This process is expected to minimize the production of extended defects in large misfit systems, a problem difficult to avoid in conventional heteroepitaxy. We are investigating surface-energy-driven secondary grain growth in semiconductor and metal films on single crystal substrates. We are also further developing the theory of epitaxy by surface-energy-driven secondary grain growth, including effects due to grain boundary motion and due to coarsening via surface diffusion.

1.13   Submicrometer-Period Gold Transmission Gratings for X-Ray Spectroscopy

Erik H. Anderson, Mark L. Schattenburg, Henry I. Smith

Gold transmission gratings with periods of 0.1 to 0.2 μm, and thickness ranging from 0.5 to 1 μm are fabricated using x-ray lithography and electroplating. The x-ray masks are made either with holographic lithography or scanning-electron-beam lithography. Transmission gratings are either supported on polyimide membranes or are made self-supporting by the addition of crossing struts. They are used for spectroscopy of the x-ray emission from plasmas produced by high-power lasers. Gratings fabricated in our lab by these techniques are used in key diagnostic instruments associated with the soft x-ray laser research at Lawrence Livermore National Laboratory.

1.14   High-Dispersion, High-Efficiency Transmission Gratings for Astrophysical X-Ray Spectroscopy

Erik H. Anderson, Mark L. Schattenburg, Claude R. Canizares, Henry I. Smith

Gold gratings with spatial periods of 0.1 - 1.0 μm make excellent dispersers for high resolution x-ray spectroscopy of astrophysical sources in the 100 eV to 10 KeV band.

These gratings are planned for use in the Advanced X-ray Astrophysics Facility (AXAF) which will be launched in the mid 1990's. In the region above 3 KeV, the requirements of high dispersion and high efficiency dictate the use of the finest period gratings with aspect ratios approaching 10:1. To achieve this we first expose a grating pattern in 1.5 μm -thick PMMA over a gold plating base using x-ray nanolithography. To date, we have worked with gratings having periods of 0.3 or 0.2 μm (linewidth 0.15 - 0.1 μm). Gold is then electroplated into the spaces of the PMMA to a thickness of 1 μm. Flight prototype gratings have been fabricated and are undergoing space worthyness tests. In the initial stage of this program we used the carbon K x-ray (λ=4.5nm) which required that the mask and substrate be in contact to avoid diffraction. This, in turn, caused distortion of the grating. To avoid this problem we are developing a new technology of microgap x-ray nanolithography using the copper L x-ray (λ=1.33nm).

1.15 Soft X-Ray Interferometer Gratings

Collaboration with KMS Fusion, Inc.

Erik H. Anderson, Henry I. Smith

In the soft x-ray region of the electromagnetic spectrum (1-10 nm) reliable optical constant data is scarce or non-existent. In order to fill this gap, an achromatic interferometer instrument is under construction at KMS Fusion Inc. The critical optical components of this instrument are a set of matched, 200-nm-period transmission gratings which will be fabricated at MIT. Because these gratings will be used in an interferometer, the phase-front quality must be extremely good and at the same time, the lines must be free-standing, i.e., have no support structure that would attenuate the x-rays. The fabrication process uses a thin membrane of silicon oxynitride which is then etched to make free-standing lines. Gold lines were found to have too much distortion for this application.

Theses

Atwater, H.A., *Ion Beam Enhanced Grain Growth in Thin Films*, Ph.D. diss., Dept. of Electr. Eng. and Comp. Sci., MIT, 1987.

Modiano, A.M., *Real Time Control, Acquisition, and Image Processing for the Scanning Tunneling Microscope*, S.M. thesis, Dept. of Electr. Eng. and Comp. Sci., MIT, 1987.

Journal Articles

Anderson, E.H., A.M. Levine, and M.L. Schattenburg, "Transmission X-Ray Diffraction Grating Alignment using a Photoelastic Modulator," submitted to *Appl. Opt.*

Anderson, E.H., K. Komatsu, and H.I. Smith, "Achromatic Holographic Lithography in the Deep UV," to be published *J. Vac. Sci. Technol.*

Atwater, H.A., C.V. Thompson, and H.I. Smith, "Interface-Limited Grain Boundary Motion During Ion Bombardment," to be published *Phys. Rev. Lett.*

Canizares, C.R., H.V.D. Bradt, G.W. Clark, A.C. Fabian, P.C. Joss, A.M. Levine, W.H.G. Lewin, T.H. Market, W. Mayer, J.E. McClintock, S.A. Rappaport, G.R. Ricker, M.L. Schattenburg, H.I. Smith, and B.E. Woodgate, "The MIT Spectroscopy Investigation on AXAF and the Study of Supernova Remnants," *Astro. Lett.* 26:87 (1987).

Chou, S.Y., D.A. Antoniadis, H.I. Smith, and M.A. Kastner, "Conductance Fluctuations in Ultra-Short-Channel Si MOSFET's," *Solid State Commun.* 61:571 (1987).

Chou, S.Y., and D.A. Antoniadis, "Relationship between Measured and Intrinsic Transconductances of FET's," *IEEE Trans. Electron Devices* ED-34:448 (1987).

Chou, S.Y., D.A. Antoniadis, and H.I. Smith, "Application of the Shubnikov-de Haas Oscillations in Characterization of Si MOSFET's and GaAs MODFET's," *IEEE Trans. Electron Devices* ED-34:883 (1987).

Garrison, S.M., R.C. Cammarata, C.V. Thompson, and H.I. Smith, "Surface-Energy-Driven Grain Growth During Rapid Thermal Annealing (<10s) of Thin Silicon Films," *J. Appl. Phys.* 61:1652 (1987).

Im, J.S., H. Tomita, and C.V. Thompson, "Cellular and Dendritic Morphologies on Stationary and Moving Liquid-Solid Interfaces in Zone-Melting Recrystallization," *Appl. Phys. Lett.* 51:685 (1987).

Ismail, K., W. Chu, D. Antoniadis, and H.I. Smith, "Surface-Superlattice Effects in a Grating-Gate GaAs/GaA1As Modulation-Doped Field-Effect Transistor," to be published *Appl. Phys. Lett.* March 1988.

Kastner, M.A., S.B. Field, J.C. Licini, and S.L. Park, "Anomalous Magnetoresistance of the Electron Gas in a Restricted Geometry," submitted to *Phys. Rev. Lett.*

Kastner, M.A., R.F. Kwasnick, J.C. Licini, and D.J. Bishop, "Conductance Fluctuations Near the Localized-to-Extended Transition in Narrow Si MOSFET's," *Phys. Rev. B* 36:8015 (1987).

Ku, Y-C., E.H. Anderson, M.L. Schattenburg, and H.I. Smith, "Use of a Pi-Phase Shifting X-Ray Mask to Increase the Intensity Slope at Feature Edges," to be published *J. Vac. Sci. Technol.*

Palmer, J., C.V. Thompson, and H.I. Smith, "Grain Growth and Grain Size Distribution in Thin Germanium Films on SiO_2," *J. Appl. Phys.* 62:2492 (1987).

Shahidi, G.G., D.A. Antoniadis, and H.I. Smith, "Observation of Electron Velocity Overshoot at Room and Liquid Nitrogen Temperatures in Silicon Inversion Layers," *IEEE Electron Devices Lett.* EDL-9:94 (1988).

Shahidi, G.G., D.A. Antoniadis, and H.I. Smith, "Reduction of Channel- Hot-Electron-Generated Substrate Current in Sub-150 nm Channel Length Si MOSFET's," submitted to *IEEE Electron Device Lett.*

Shahidi, G.G., D.A. Antoniadis, and H.I. Smith, "Electron Velocity Overshoot in Sub-100 nm Channel Length MOSFET's at 77K and 300K," to be published *J. Vac. Sci. Technol.*

Smith, H.I., "A Model for Comparing Process Latitude in UV, Deep-UV and X-Ray Lithography," to be published *J. Vac. Sci. Technol.*

Conference Proceedings

Anderson, E.H., D. Kern, H.I. Smith, "Fabrication by Tri-Level Electron Beam Lithography of X-Ray Masks with 50 nm Line Widths and Replication by X-Ray Nanolithography," Microcircuit Engineering '87, International Conference on Microlithography, Paris, France, September 22-25, 1987.

Antoniadis, D.A., "Quantum Mechanical and Non-Steady-State Transport Phenomena in Nanostructured Silicon Inversion Layers," Extended Abstracts, 19th Conference on Solid State Devices and Materials, Tokyo, Japan, August 25-27.

Cammarata, R.C., C.V. Thompson, and S.M. Garrison, "Secondary Grain Growth During Rapid Thermal Annealing of Doped Polysilicon Films," presented at the spring Materials Research Society meeting, 1987.

Plotnik, I., M.E. Porter, M. Toth, S. Akhtar, and H.I. Smith, "Ion- Implant Compensation of Tensile Stress in Tungsten Absorber for Low Distortion X-Ray Masks," International Conference on Microlithography and Related Microelectronics Technologies, September 23-25, 1986, Interlaken, Switzerland; published in *Proceedings Microcircuit Engineering '86*, eds. H.W. Lehmann and C. Bleiker, 51. New York: North-Holland Press, 1987.

Schattenburg, M.L., I. Tanaka and H.I. Smith, "Microgap X-Ray Nanolithography," Microcircuit Engineering '87, International Conference on Microlithography, Paris, France, September 22-25.

Thompson, C.V., and H.I. Smith, "Secondary Grain Growth in Thin Films, Phase Transitions in Condensed Systems - Experiment and Theory," In *Materials Research Society Symposium Proceedings*, eds. G.S. Cargill III, F. Spaepen, and K.N. Tu, 499, Pittsburgh, Pennsylvania: Materials Research Society, 1987.

Professor Carl V. Thompson

2.0 Kinetic Phenomena in Thin Film Electronic Materials

Academic and Research Staff

Prof. C.V. Thompson, Prof. C.G. Fonstad, Prof. H.I. Smith, Dr. R.C. Cammarata, Dr. J. Melngailis

Visiting Scientist

H. Tomita,[1]

Collaborators

H.J. Frost,[2] D.A. Smith,[3] K.N. Tu[3]

Graduate Students

S. Ajuria, H.A. Atwater, J. Cho, T. Chong, L. Clevenger, A.D. Dubner, J. Floro, J.S. Im, E. Jiran, H. Kahn, H-J. Kim, H. Longworth, J.E. Palmer, H.M. Quek, J.S. Ro

Undergraduate Students

H. Meng, H. Zolla

Support Staff

C. Slattery

2.1 Grain Growth in Thin Films

Sergio Ajuria, Hui M. Quek, Carl V. Thompson, Henry I. Smith

Polycrystalline metallic and semiconductor films are used in a wide variety of electronic and magnetic devices and circuits. Grain sizes, grain orientations, and grain size distributions strongly affect the properties of these films. We are studying microstructrual evolution through normal and secondary grain growth in thin films. Secondary grain growth often leads to very large grains (up to 500 times the film thickness) with restricted crystallographic orientations. We are studying the effects of

---

[1] Sony Corporation

[2] Thayer School of Engineering, Dartmouth College

[3] International Business Machines, Inc., Thomas J. Watson Research Center

film thickness and deposition conditions, as well as other parameters, on thermal grain growth. We are also investigating grain growth under laser irradiaton and during alloy formation.

2.1.1 Dopant Enhanced Grain Growth in Silicon Thin Films

Hyoung -J. Kim , Carl V. Thompson

Polycrystalline silicon films are used as gates in metal oxide semiconductor field effect transistors, as base and emitter contacts and diffusion sources in bipolar transistors, in sensors, and as active device films in thin film transistors. Performance in all of these applications is affected by the microstructure of the films. Microstructural evolution, specifically grain growth, is strongly affected by electronically active dopants. The rates of both normal and secondary grain growth are increased when electron donors (P and As) are added to silicon. This rate enhancement can be reduced or eliminated through codoping with boron. We have developed a model which accounts for the dependence of grain boundary atomic mobilities on the free electron concentration. The concepts developed here are also being applied to other solid state kinetic processes in silicon.

2.1.2 Ion Bombardment Enhanced Grain Growth in Thin Films

Harry A. Atwater, Jerrold A. Floro, Carl V. Thompson, Henry I. Smith

We have demonstrated that ion bombardment of thin films leads to grain growth at temperatures well below those required for thermally induced grain growth. In germanium, silicon, and gold films it has been shown that the grain size increases with ion dose, independent of ion flux and with only a very weak temperature dependence. It appears that grain growth is promoted through ion-bombardment-induced generation of point defects at grain boundaries. A transition state model for grain boundary motion during ion bombardment has been developed. This model is being tested and extended for application to other ion-assisted solid state kinetic processes. We are also investigating the effects of ion bombardment on microstructural evolution during film deposition.

2.1.3 Graphoepitaxy by Grain Growth in Thin Films

Hui M. Quek, Sergio Ajuria, Henry I. Smith, Carl V. Thompson

Surface-energy-driven secondary grain growth in thin films on amorphous substrates normally leads to films with grains having restricted or uniform texture but random in-plane orientations. By using sub-micron lithographic techniques to pattern amorphous substrates, we have shown that artificial surface topography can be used to control the in-plane orientation of secondary grains. Use of artificial surface topography to control crystalline orientation in thin films is known as graphoepitaxy. We are optimizing this process through development of improved patterning techniques. We are also investigating techniques for patterning the top surface of polycrystalline films in order to investigate whether graphoepitaxy can occur due to top-surface patterning.

2.1.4 Modeling of Microstructural Evolution in Thin Films

Carl V. Thompson and Harold J. Frost

We are developing analytic models for normal and secondary grain growth in continuous thin films as well as particle coarsening in discontinuous films. The effects of surface or interface energy anistropy play especially important roles in these processes. We have also developed computer models for film formation by crystal nucleation and growth to impingement under a variety of conditions. The topology and geometry of grain structures have been shown to strongly depend on the conditions of film formation. We have developed a computer model for two-dimensional normal grain growth and have extended this model for treatment of secondary grain growth.

2.2 Post-Nucleation Heteroepitaxy in Lattice Mismatched Systems

Joyce E. Palmer, Tow Chong, Carl V. Thompson, Clifton G. Fonstad, Henry I. Smith

Heteroepitaxial growth of films with poor lattice matching on single crystal substrates often leads to films with high bulk as well as interface defect densities. When atom by atom or layer growth occurs, bulk defects are generally generated during strain accommodation well after film nucleation. Alternatively, strain accommodation can occur through formation of low energy interfaces during competitive growth of grains or nuclei which initially have a variety of orientations. We are investigating these post-nucleation epitaxial processes in continuous and discontinuous films. Model systems include GaAs-on-silicon and epitaxial metals on silicon.

2.3   Thin Film Zone Melting Recrystallization of Silicon

International Business Machines, Inc.
Sony Company

James S. Im, Hisashi Tomita, Carl V. Thompson, David A. Smith

Techniques for producing device-quality single-crystal films of semiconductors on insulator (SOI) are of interest for multilayer or multimaterial integrated circuits, display devices and low-cost, high-efficiency solar cells. Such films can be obtained through directional solidification of confined thin films (zone melting recrystallization, ZMR). While there are analogies to bulk crystal growth, in ZMR there are also phenomena and mechanisms unique to thin-film solidification of radiatively heated silicon. Direct observation of dynamic and static liquid-solid interfaces complements theoretical modeling of solidification. We are studying these phenomena in order to develop means of controlling and optimizing thin film growth by ZMR.

2.4   Capillary Instabilities in Thin Solid Films

National Science Foundation (Grant ECS 85-06565)

Eva Jiran, Carl V. Thompson

Very thin metallic and semiconductor films (< 200 Å) are being used in an increasing variety of applications. Most solid films are used on substrates with which they would, in equilibrium, form non-zero contact angles. Therefore, even solid films tend to become discontinuous or bead in order to reduce their total film/substrate interface energy. This phenomena occurs in both continuous and patterned films. The rate of solid state beading is a strong function of the dimensions of a film or line as well as the microstructure of the film or line. For example, the beading rate rapidly increases with decreasing film thickness. We are experimentally characterizing the kinetics of beading of thin films of gold on SiO_2. Film patterning allows independent study of both hole formation and hole growth. These eventually lead to complete beading.

2.5   Kinetics of Thin Film Silicide Formation

International Business Machines, Inc.

Robert C. Cammarata, Lawrence Clevenger, Carl V. Thompson, King N. Tu

There is considerable current interest in the use of refractory metals or refractory metal silicides as interconnects, as gate materials in MOS devices and for low contact resistance diffusion barriers at metal-silicon contacts in integrated circuits. These applications raise fundamental questions about the rate and products of thin film metal-silicon reactions. One method of silicide formation is through reaction of metallic thin films with silicon substrates or polycrystalline silicon films. There are four critical parameters in analysis and modelling of these reactions; interdiffusivities, free energy changes, surface energies and interface reaction constants. Of these, the first two parameters are fairly well understood and can be predicted. The purpose of this project

is to develop a better understanding and predictive capability for the last two parameters. Surface energies are being determined through silicide precipitation experiments and interface reaction rate constants are being determined through thermal and X-ray analysis of interface limited reactions of thin films.

2.6 Reliability and Microstructures of Interconnects

Jaeshin Cho, Hal Kahn, Hai Longworth, and Carl V. Thompson

We are developing new techniques which allow statistical characterization of failure of contacts and interconnects for silicon-based integrated circuit technology. We are using these techniques to correlate failure rates and mechanisms with microstructures of interconnect lines and contact barriers. We are also investigating techniques for controlling microstructures in order to improve contact and interconnect reliability, especially under conditions which can lead to electromigration. For example, very large grained (100 μm), 0.75 μm-thick, electromigration-resistant films have been made using layered deposition and post-deposition annealing of Al- 2% Cu - 0.3% Cr films.

2.7 Focused Ion Beam Induced Deposition

Jaesang Ro, Andrew D. Dubner, John Melngailis and Carl V. Thompson

It is now possible to produce ion beams with diameters as small as 500Å. This permits use of focussed ion beams for high spatial resolution implantation, sputtering and deposition. In principal, the latter can be used in integrated circuit mask repair or high resolution direct writing of interconnects. We are investigating the mechanisms of ion-beam-induced chemical vapor deposition from metal-bearing gases.

Thesis

Atwater, H.A., *Ion Beam Enhanced Grain Growth in Thin Films*, Ph.D. diss., Dept. of Electr. Eng. and Comp. Sci., MIT, 1987.

Publications

Atwater, H.A., H.I. Smith, and C.V. Thompson, "Ion Beam Enhanced Grain Growth in Thin Films," In *Materials Research Society Symposium Proceedings 74*, 499, 1987.

Cammarata, R.C., C.V. Thompson, and K.N. Tu, "NiSi$_2$ Precipitation in Nickel Implanted Silicon Films," *Appl. Phys. Letts.* 51:1106 (1987).

Frost, H.J., and C.V. Thompson, "The Effect of Nucleation Conditions on the Topology and Geometry of Two-Dimensional Grain Structures," *Acta Metallurgica* 35:529 (1987).

Frost, H.J., J. Whang, and C.V. Thompson, "Modeling of Grain Growth in Thin Films, Annealing Processes-Recovery, Recrystallization and Grain Growth," In *7th Riso International Symposium on Metallurgy and Materials Science,* eds. N. Hanson, T. Lerrere, and B. Ralph, 315, 1986.

Garrison, S.M., R.C. Cammarata, C.V. Thompson, and H.I. Smith, "Surface-Energy-Driven Secondary Grain Growth During Rapid Thermal Annealing (<10s) of Thin Silicon Films," *J. Appl. Phys.* 61:1652 (1987).

Im, J.S., H. Tomita, and C.V. Thompson, "Cellular and Dendritic Morphologies on Stationary and Moving Liquid-Solid Interfaces in Zone Melting Recrystallization," *Appl. Phys. Letts.* 51:685 (1987).

Im, J.S., C.V. Thompson, and H. Tomita, "Solidification Interface Morphologies in Zone-Melting Recrystallization," In *Materials Research Society Symposium Proceedings 74,* 555, 1987.

Palmer, J.E., C.V. Thompson, and H.I. Smith, "Grain Growth and Grain Size Distributions in Thin Germanium Films," *J. Appl. Phys.* 62:2492 (1987).

Srolovitz, D.J., and C.V. Thompson, "Beading Instabilities in Thin Film Lines with Bamboo Microstructures," *Thin Solid Films* 139:133 (1986).

Thompson, C.V., and J. Cho, "A New Electromigration Testing Technique for Rapid Evaluation of Interconnect Technology," *IEEE Electron Devices Lett.* EDL-7:667 (1986).

Thompson, C.V., H.J. Frost, and F. Spaepen, "The Relative Rates of Secondary and Normal Grain Growth," *Acta Metallurgica* 35:887 (1987).

Thompson, C.V., and C.D. Maiorino, "Very Large Grained Aluminum Alloy Films for Interconnects," In *Proceedings of the 1986 International Conference on Solid State Devices and Materials,* Tokyo, Japan, 491, 1986.

Thompson, C.V., and H.I. Smith, "Secondary Grain Growth in Thin Films," In *Materials Research Society Symposium Proceedings 57,* 499, 1987.

3.0 Focused Ion Beam Fabrication

Academic and Research Staff

Dr. J. Melngailis, Prof. D.A. Antoniadis, Prof. C.V. Thompson

Collaborating Scientists

L.J. Mahoney,[1] T.O. Herndon[1]

Research Specialist

Mark I. Shepard

Postdoctoral Associate

P.G. Blauner

Graduate Students

A.D. Dubner, K. Ismail, J.B. Jacobs, H. Lezec, C.R. Musil, J.S. Ro

3.1 Focused Ion Beam Program

Research in focused ion beam applications is being carried out in two areas: maskless implantation patterning and ion induced deposition. In each area, the work is centered around a special machine. For implantation, we have a system capable of mass separation and submicron beam writing on the wafer, which was bought as part of the Microsystems Technology Program. It was delivered to MIT in March 1987, and was put into operation in June 1987. A number of implantations have been carried out as described below. The system can produce a beam of 0.1 μm diameter at 150 kV with several ion species which include the dopants of Si and GaAs.

We have also purchased a 50 kV column without mass separation, which will be used mainly with Ga$^+$ ions. It can produce a beam of 0.05 μm diameter, and is intended for ion induced deposition and ion milling. An ultrahigh vacuum chamber is being constructed to house this column. In the meantime, experiments have been carried out using a standard implanter.

3.1.1 Development of Focused Ion Beam Patterning

---

[1] Lincoln Laboratory

Henri Lezec, Mark I. Shepard, John Melngailis

To develop and test the patterning capability of the focused ion beam system, we have carried out exposure of PMMA, i.e., ion beam lithography. Features of 0.1 μm width were exposed using Be^{++} ions at 260 keV (accelerated by 130 kV) in 0.3μm thick PMMA. Gold features of 0.1μm thickness and 0.1μm width were then produced by electron-beam evaporation and lift-off. Field stitching was demonstrated by accurately calibrating the beam deflection against the laser interferometer controlled table motion. The pattern discontinuities observed in crossing the field boundaries were less than 0.1 μm. In addition, software for transferring patterns from the computer aided design facility, where they are drawn in standard workstations, directly to the focused ion beam computer was developed. These capabilities will make possible wider use of the machine in the future.

3.1.2 Fabrication of Devices by Direct Focused Ion Beam Implantation

Henri Lezec, Mark I. Shepard, Leonard J. Mahoney, Christian R. Musil, Khalid Ismail, Dimitri A. Antoniadis, John Melngailis

Focused ion beam implantation provides a new degree of freedom in device fabrication: the implantation dose can be varied as a function of position on the surface. Our goal is to exploit this capability in new devices or in improvements to existing devices. A novel device which we have conceived is a tunable Gunn diode. It is fabricated by implanting a gradient of doping between the two contacts. The distance that a Gunn domain can travel depends on D.C. bias, and the frequency can be tuned by tuning the bias. In one device the oscillation frequency was tuned from 6 to 23 GHz by tuning the bias from 37 to 27 volts. The operation of the device has also been simulated on the computer. We have, in addition, implanted GaAs MESFET's with a gradient of doping from source to drain. Compared to uniformly doped devices, these MESFET's showed a 15% increase in transconductance. The gate length was 1 μm. We plan to grade submicrometer gate lengths MESFET's, where the improvements are expected to be larger. Similarly, we plan to implant Si MOSFET's with doping gradients from source to drain.

3.1.3 Planar Vias Through Si_3N_4 Fabricated by Focused Ion Beam Implantation

John Melngailis, Terry O. Herndon, Mark I. Shepard, Henri Lezec

Previous work has demonstrated that silicon implanted into Si_3N_4 at doses above 10^{17} cm^{-2} can render the insulator conducting. This has been proposed as a means of

making planar via. We have used a focused ion beam to make such level to level interconnects in Si_3N_4, thus avoiding the need for resist or mask. Implants were carried out at a single energy, 160 keV, using Si++ ions, or at two energies, 80 keV and 160 keV, using Si+ and Si++ ions, respectively. Films of 0.25-μm-thick Si_3N_4 over Al metal were implanted. Then the upper layer was deposited, patterned, and the structure was sintered at 425°C for 30 minutes. The dose threshold for conduction was between 2 x 10^{17} and 5 x 10^{17} cm^{-2} and depended on whether the 160 keV or the two-energy implants were carried out. Interconnects formed in areas 1.6 x 1.6 μm had resistance as low as 0.15 Ω, while the minimum dimension implants, made with an unscanned beam in 6 to 12 s, had resistances of 1.5 to 5 Ω. For vias exposed with doses below threshold, permanent conduction could be induced by breakdown at voltages well below those needed to break down an unimplanted film. Even with the present state of technology, focused ion beam implantation appears to be a useful technique for making level-to-level interconnects through Si_3N_4 in limited, critical areas of devices.

3.1.4 Growth of Gold Films by Ion Induced Deposition

Charles Stark Draper Laboratory, Inc. (Contract DL-H-261827)
Hitachi Central Research Laboratory
Nippon Telegraph & Telephone
U.S. Army Research Office (Contract DAAL03-87-K-0126)

Jaesang Ro, Andrew D. Dubner, Patricia G. Blauner, Carl V. Thompson, John Melngailis

A beam of ions incident on a surface can cause absorbed gas molecules to break up, resulting in material deposition. With a focused ion beam, we have demonstrated deposition of lines of 0.25 μm width, as well as lines of 0.5 μm width and 0.4 μm thickness. The gas used is dimethyl gold hexafluoro acetylacetonate ($C_7H_7F_6O_2Au$).

The resistivity of the films was 100 to 500 times higher than that of bulk gold. To study the deposition process, we have deposited films using a broad beam from an ion implanter. Various substrate temperatures were used, and the films were examined by transmission electron microscopy. Films grown at room temperature were discontinuous even up to the thickness of 0.25 μm, while films grown at higher substrate temperatures were continuous even ι lower thicknesses. Deposition carried out on substrates at 100°C and 160°C using 70 keV Ar+ ions resulted in resistivities approaching the bulk value and a deposition yield of 60 to 75 atoms/ion. If such high quality films can also be deposited by the focused ion beam, this technique may be useful for integrated circuit restructuring and repair, and for repair of x-ray lithography masks.

Publications

Dubner, A.D., G.M. Shedd, H. Lezec, and J. Melngailis, "Ion Beam Induced Deposition of Gold by Focused and Broad Beam Sources," extended abstract, *J. Vac. Sci. Technol.* B5:1434 (1987).

Melngailis, J., D.J. Ehrlich, S.W. Pang, and J.N. Randall, "Cermet as an Inorganic Resist for Ion Lithography," *J. Vac. Sci. Technol.* B5:379 (1987).

Melngailis, J., "Focused Ion Beam Technology and Applications," (a review paper), *J. Vac. Sci. Technol.* B5:469 (1987).

Melngailis, J., A.D. Dubner, J.S. Ro, G.M. Shedd, H. Lezec, and C.V. Thompson, "Focused ion beam induced deposition," *Proceedings of the NATO Symposium on Emerging Technologies for In-Situ Processing* Cargèse, May 1987 (to be published).

Melngailis, J., T.O. Herndon, M.I. Shepard, and H. Lezec, "Planar Vias through Si_3N_4 Fabricated by Focused Ion Beam Implantation," presented at Seminar on Focused Ion Beam Technology and Applications, Osaka, Japan, November 16-20, 1987, and to be published in *J. Vac. Sci. Technol.*

Ro, J.S., A.D. Dubner, C.V. Thompson, and J. Melngailis, "Microstructure of Gold Films Grown by Ion Induced Deposition," presented at Materials Research Society Meeting November 30 - December 5, 1987, Boston, Massachusetts, to be published in proceedings.

Ro, J.S., A.D. Dubner, C.V. Thompson, and J. Melngailis, "Ion Induced Deposition of Gold Films," presented at Seminar on Focused Ion Beam Technology and Applications, Osaka, Japan, November 16-20, 1987, and to be published in *J. Vac. Sci. and Technol.*

Shedd, G.M., H. Lezec, A.D. Dubner, and J. Melngailis, "Focused Ion Beam Induced Deposition of Gold," *Appl. Phys. Lett.* 49:1584 (1986).

4.0 Chemical Reaction Dynamics at Surfaces

Academic and Research Staff

Prof. S.T. Ceyer

Graduate Students

J.D. Beckerle, D.J. Gladstone, A.D. Johnson, M.B. Lee, M. McGonigal, M. Schulberg, R.J. Simonson, Q.Y. Yang

4.1 Methane Dissociative Chemisorption: Origin of the Pressure Gap in Catalysis

Sylvia T. Ceyer, Qingyun Yang, Myung B. Lee

Many surface chemical reactions appear to proceed at high pressures but not at low pressures ($< 10^{-5}$ torr), despite favorable thermodynamics. This lack of reactivity at the low pressures where ultrahigh vacuum-surface science techniques are operable is known loosely as the pressure gap and casts doubt on the relevance of UHV surface science to high pressure processes such as heterogeneous catalysis and chemical vapor deposition.

Our group proposed that an origin of the pressure gap in the catalytic reactivity was the presence of a barrier to the dissociative chemisorption of at least one of the reactants. Since it is the translational energy of the incident molecule that is important, in surmounting this barrier and <u>not</u> the surface temperature, the rate of the reaction is limited by the flux of incident molecules with energies above the energy of the barrier. High pressures simply increase the absolute number (not the fraction) of high energy molecules, thereby increasing the reaction rate sufficiently for the products to be detected.

To verify this hypothesis, we used molecular beam techniques coupled with high resolution electron energy loss spectroscopy to probe the effect of translational energy on the dissociative chemisorption of CH_4 on Ni(111). We chose this system because the steam reforming of CH_4 over a Ni catalyst is an example of a reaction which appears to proceed only at high pressures. We showed that there is indeed a barrier to the dissociation of CH_4 and that the normal component of the translational energy and vibrational energy are effective in overcoming it. Rates for CH_4 decomposition under high pressure conditions have been shown to agree very well with rates calculated from our low pressure dissociation probability measurements as a function of energy. The agreement between the <u>low and high pressure experiments carried out in different laboratories firmly establishes the presence of a barrier along the reaction coordinate as an origin of the pressure gap in heterogeneous catalysis.</u>

Besides providing a link between UHV surface science and high pressure catalysis, our studies of the dynamics of CH_4 dissociation and our ability to identify chemically the product of the dissociative chemisorption event have also provided a detailed microscopic picture of the mechanism of the C-H bond breaking process. A deformation model explains the role of translational and vibrational energy in promoting dissociative chemisorption and suggests that tunneling is the final step in the C-H bond cleavage. In short, the barrier arises largely from the energy required to deform or splatter the methane molecule sufficiently to allow a strong attractive interaction between the carbon and the Ni surface atoms.

4.2 New Mechanisms for Dissociative Chemisorption and Desorption

Sylvia T. Ceyer, John D. Beckerle, Andrew D. Johnson, Qingyun Yang

If the deformation model dicsussed above is correct, then the impact of an Ar atom beam on a physisorbed layer of CH_4 should deform the molecule into the configuration for the transition state that leads to dissociation. Execution of this experiment shows indeed that dissociation of CH_4 to adsorbed CH_3 and H fragments does occur under the impact of an Ar atom. This observation represents <u>the discovery of a new mechanism for dissociative chemisorption:</u> collision induced dissociation of adsorbates (or chemistry with a hammer). In competition with collision induced dissociation another process, collision-induced desorption occurs. The desorption of adsorbates by the impact of an inert, neutral species has been predicted previously but this is the first experimental observation of this process.

The impact of the observation of these collision induced processes for understanding the chemistry in a high pressure environment is potentially large because, in a high pressure environment, an adsorbate-covered catalyst is continually bombarded by a large flux of high energy molecules. Therefore, having shown that collision induced processes occur, we believe that no mechanism for surface reactions under high pressure conditions can now be considered complete without an assessment of the importance of collision processes as a major reaction step. Collision induced chemistry and desorption are additional reasons why surface chemistry at high pressures is often very different from the chemistry in UHV environments.

This work was featured in *Chemical and Engineering News*, June 8, 1987, p. 20.

4.3 Chemical Reaction Dynamics on Semiconductor Surfaces

Joint Services Electronics Program (Contract DAAL-03-86-K-0002)

Sylvia T. Ceyer, David J. Gladstone, Marianne McGonigal, Michelle Schulberg

The etching of semiconductor materials in halocarbon plasma environments is a complex chemical process. The purpose of the plasma is the production of radical species that are highly reactive with the semiconductor surface. Since many different species, including neutral dissociation products of the halocarbon to atomic halogens and halocarbon radicals and ions and fragment ions produced by electron bombardment, are produced in the plasma, the chemistry is difficult to probe in this environment. Our program is aimed at systematically probing with molecular beam reactive scattering techniques the role of the neutral radical species in the etching process.

In this experimental arrangement, a beam of reactant atoms is aimed at a semiconductor surface and the volatile product molecules are detected after desorption from the surface by a quadrupole mass spectrometer. Since the molecular beam allows the production of a single reactive neutral species, the chemistry of the reactive species can be studied in a controlled fashion. The product molecule is unperturbed by collisions before detection allowing the reaction probabilities and the nascent product distribution to be determined unambiguously. We are studying the reaction probability of F atoms, a common neutral radical species present in plasma environments, with silicon to determine the identities of the reaction products and the dynamics of the chemical reaction. We are also probing the chemistry of HF with silicon with the long range goal of studying the effect of the electronic excitation of silicon on the HF reactivity.

4.4 Spectroscopic Study of the Adsorption of C_2H_4 and C_2H_2 on Oxidized Gd(0001)

Joint Services Electronics Program (Contract DAAL03-86-K-0002)

Sylvia T. Ceyer, Robert J. Simonson

The adsorption of ethylene and acetylene on a rare earth oxide surface has been studied primarily by ultraviolet photoemission and Auger electron spectroscopy. The Gd oxide surface is produced by exposure of the clean Gd(0001) surface at 300 K to O_2. The adsorption probability for ethylene is at least a factor of 3 and probably a factor of 100 lower than that for acetylene on the oxidized surface at 165 K. The surface species formed upon low-temperature acetylene adsorption is identified as molecular C_2H_2. The molecularly adsorbed C_2H_2 decomposes below a substrate temperature of 350 K, leaving carbon on the surface. These results are compared with those of a previous study of C_2H_2 and C_2H_4 adsorption on the metallic Gd(0001) surface. The possible catalytic significance of the selectivity of the oxidized Gd surface toward acetylene adsorption is immense.

4.5 Synthesis and Chemistry of New Kinds of Adsorbates

Sylvia T. Ceyer, Qingyun Yang

Having established this link between high pressure catalysis and UHV surface science, we now know how to bypass the high pressure requirement simply by raising the energy of the incident molecule or collisionally inducing dissociation. We have used the former trick to synthesize and identify spectroscopically, by high resolution electron energy loss spectroscopy, an adsorbed CH_3 radical for the first time in low pressure, ultrahigh vacuum conditions. Because of our unique ability to produce CH_3 species, we have been able to probe its stability and chemistry. From these studies, a complete picture of the relative stabilities of C_xH_n species on Ni has emerged.

4.6 Definition of the CO Precursor Molecule to Molecular Chemisorption

Sylvia T. Ceyer, John D. Beckerle, Qingyun Y. Yang, Andrew D. Johnson

Two years ago we showed that a precursor molecule to molecule chemisorption exists. We presented two models for the precursor molecule. To distinguish between these models, we have designed, constructed and assembled a liquid He cryostat that enables us to cool a Ni(111) crystal to 8 K. We observed that we could not stabilize the CO precursor molecule at 8 K. This implies that the precursor molecule to molecular chemisorption is a dynamical hindered rotor rather than a stable single configuration of the CO molecule. These results enable us to complete our picture of the precursor molecule to chemisorption.

Publications

Beckerle, J.D., Q.Y. Yang, A.D. Johnson, and S.T. Ceyer, "Collision-Induced Dissociative Chemisorption of Adsorbates: Chemistry with a Hammer," *J. Chem. Phys.* 86:7236 (1987).

Beckerle, J.D., A.D. Johnson, Q.Y. Yang, and S.T. Ceyer, "Collision-induced Dissociation and Desorption: CH_4 and CO on Ni(111) - Summary Abstract," *J. Vac. Sci. Technol.* A6:000 (1988).

Beckerle, J.D., Q.Y. Yang, A.D. Johnson, and S.T. Ceyer, "The Adsorption of CO and O_2 on Ni(111) at 8 K," *Surface Sci.* 195:77 (1988).

Ceyer, S.T., D.J. Gladstone, M. McGonigal, and M.T. Schulberg, "Molecular Beams: Probes of the Dynamics of Reactions on Surfaces," In *Physical Methods of Chem-*

istry, eds. B.W. Rossiter, J.F. Hamilton, and R.C. Baetzold. New York: Wiley, 1988 (in press).

Ceyer, S.T., M.B. Lee, Q.Y. Yang, J.D. Beckerle, and A.D. Johnson, "The Mechanism for the Dissociation of Methane on a Nickel Catalyst," In *Proceedings of a Symposium on the Production of Fuels and Chemicals from Natural Gas,* eds. D. Bibby, C. Chang, R. Howe, S. Yurchak. Amstersdam: Elsevier Science, 1987 (in press).

Ceyer, S.T., J.D. Beckerle, M.B. Lee, S.L. Tang, Q.Y. Yang, and M.A. Hines, "Effect of Translational and Vibrational Energy on Adsorption: The Dynamics of Molecular and Dissociative Chemisorption," *J. Vac. Sci. Tech. A* 5:501 (1987).

Lee, M.B., J.D. Beckerle, S.L. Tang, and S.T. Ceyer, "Lack of Translational Energy Activation of the Dissociative Chemisorption of CO on Ni(111)," *J. Chem. Phys.* 87:723 (1987).

Lee, M.B., Q.Y. Yang, and S.T. Ceyer, "Dynamics of the Activated Dissociative Chemisorption of CH$_4$ and Implication for the Pressure Gap in Catalysis: A Molecular Beam-High Resolution Electron Energy Loss Study," *J. Chem. Phys.* 87:2724 (1987).

Simonson, R.J., J.R. Wang, and S.T. Ceyer, "Spectroscopic Studies of the Adsorption of C$_2$H$_2$ and C$_2$H$_4$ on a Rare Earth Single Crystal. I. Metallic Gd(0001)," *J. Chem. Phys.* 91:5681 (1987).

Simonson, R.J., J.R. Wang, and S.T. Ceyer, "Spectroscopic Studies of the Adsorption of C$_2$H$_2$ and C$_2$H$_4$ on a Rare Earth Single Crystal. II Oxidized Gd(0001)," *J. Chem. Phys.* 92:000 (1988).

Yang, Q.Y., and S.T. Ceyer, "The Chemistry and Stability of Adsorbed Methyl Radicals - Summary Abstract," *J. Vac. Sci. Technol.* A6:000 (1988).
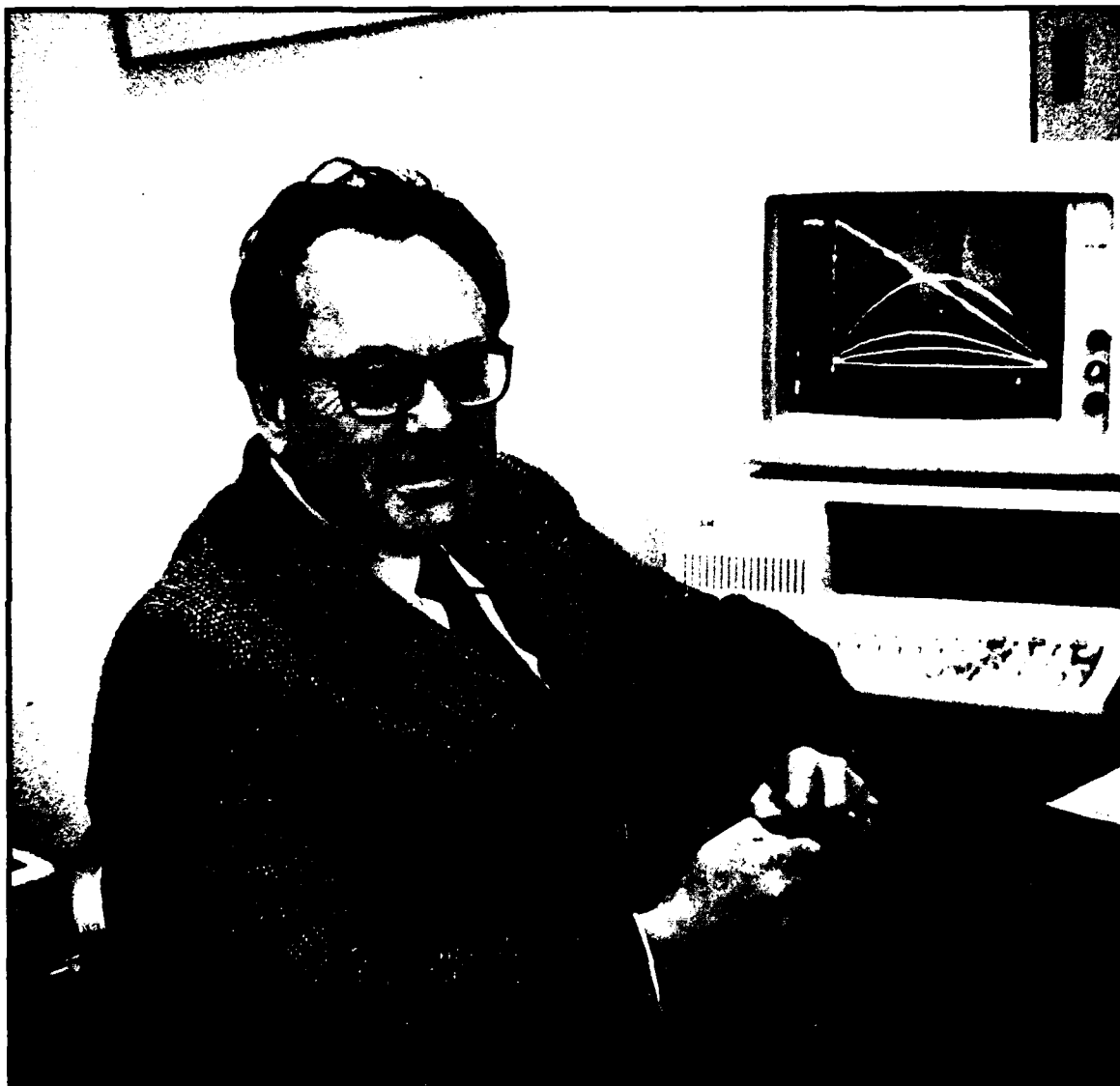
Professor Hermann A. Haus

5.0   Optics and Quantum Electronics

Academic and Research Staff

Prof. H.A. Haus, Prof. E.P. Ippen, Prof. C.G. Fonstad, Jr., Prof. J.G. Fujimoto, Prof. P.L. Hagelstein, R.E. Hillman, E. Towe

Visiting Scientists

R. Birngruber,[1] W.Z. Lin,[2] C. Mailhoit,[3] P. Mataloni,[4] S. Oho,[5] M. Shirasaki,[6] D. Smith[7]

Postdoctoral Associate

B. Zysset

Graduate Students

K.K. Anderson, J.P. Braud, S.D. Brorson, K. Delin, K. Elcess, C. Eugster, W. Huang, J.M. Huxley, S. Kaushik, M.J. LaGasse, Y. Lai, L.Y. Liu, A. Morganthaler, L. Molter-Orr, J. Moores, M. Muendel, M. Phillips, R.W. Schoelein, R. Singer, J. Vlcek, D.L. Wong,

Undergraduate Students

L. Balents, T. Farkas, J. Hung, K. Lam

5.1   The Nonlinear Waveguide Interferometer

James G. Fujimoto, Hermann A. Haus, Michael J. LaGasse, Shigeru Oho, John Moores, Masataka Shirasaki, Dilys L. Wong

All-optical switching can be accomplished with femtosecond pulses. Devices that utilize optical control signals may be classified as resistive or reactive. Resistive modulators utilize the change of absorption, reactive the change of index as a function

---

[1]   H. Wacker Laboratory, University of Munich

[2]   Zhongohan University, Guagnshou, People's Republic of China

[3]   Xerox, Webster Research Center

[4]   University of Rome, Italy

[5]   Hitachi Corporation

[6]   Fujitsu Laboratories

[7]   Los Alamos National Laboratory

of an optical control signal. The reactive modulators have the advantage that their insertion loss can be made small in principle, whereas the absorption of resistive modulators cannot be fully eliminated in the "on state." The phase modulation produced by index changes can be transformed interferometrically into amplitude modulation.

Our previous work with nonlinear optical waveguide interferometer switches using the bulk nonlinearity of GaAs[1] has revealed that, not only the required peak intensities tend to damage the waveguides, but that the thermal changes of the waveguide prevent high throughput rates.[2] For this reason, we investigated optical fiber interferometers as all-optical switches. The single fiber interferometer proposed by M. Shirasaki[3] uses two polarizations for the two "arms" of the interferometer. The pulse to be switched is separated into two mutually orthogonally polarized and time delayed pulses. If one of the two pulses is phase shifted by a cotraveling pulse, polarization rotation ensues and switching action can be accomplished. The advantage of this scheme is that long-term (nanosecond) changes of the fiber index do not affect the interferometer operation. It is also immune to heating effects. Preliminary experiments were reported at CLEO.[4] In more recent experiments,[5] switching of subpicosecond pulses was demonstrated in a 3 m length fiber interferometer. Also, in a 400m interferometer using 100 ps pulses from a modelocked Nd:YAG laser, switching was accomplished with 2 W peak power. The interferometer had excellent stability.

5.2 Picosecond Optical Signal Sampling

Hermann A. Haus, Lynne Molter-Orr, Weiping Huang

The work on waveguide couplers and interferometers as basic components for optical switches concentrated on the theory of coupled waveguides and their dispersion characteristics, on the fabrication of such waveguides in GaAs, and on the experimental verification of the theoretical predictions.

In work reported in the last progress report,[6] Dagli described an equivalent circuit method for the analysis of rib waveguides, based on a mode matching technique. The method uses both guided and radiation modes and is very computation intensive. Also, it was limited to a scalar analysis and did not yield modal birefringence. We have developed a variational method for the evaluation of the dispersion characteristic. The program is "user friendly" and is implemented on a PC. Its accuracy as compared with Dagli's results and other published work is excellent. Birefringence effects are included as corrections to the results of the scalar analysis. The program was made available to the Celanese Research Division in Summit, New Jersey.

The fabrication of two- and three-guide couplers in GaAs carried out by L. Molter-Orr with rib waveguides, in cooperation with Dr. J. Donnelly of the MIT Lincoln Laboratory, tested the idea of the waveguide lens described previously.[7] The mode confinement in rib waveguides is weaker than in channel waveguides and thus enhances effects associated with the non-orthogonality of modes pointed out by Hardy and Streifer.[8] In our own work[9] we had shown that the crosstalk produced by the effect in a two-guide coupler switch could be essentially eliminated by proper detuning and

length adjustment of the coupler. This prediction was confirmed with the rib-waveguide couplers tested by L. Molter-Orr.[10]

In the coming year, the switching techniques developed in connection with the single fiber (two polarizations) fiber interferometer described in the preceding section will be applied to optical waveguides, both as a means of measuring the nonlinear optical parameters and as a means of all-optical switching.

5.3 Solitons

Hermann A. Haus, Erich P. Ippen, Janice M. Huxley, Y. Lai, Ling-Yi Liu, John Moores

The soliton laser first realized by Mollenauer is the only means to date for the production of femtosecond pulses in the wavelength regime above 1.5 microns.[11] Direct saturable absorber modelocking of the *F*-center laser, or the metal ion laser, the only sources of high power within this frequency regime, is not possible because of the long relaxation times of these laser media. In another section of this report, the operation of such a laser is described. As part of the general theory of solitons, the operation of the two-cavity soliton laser is the subject of investigation. The aim is to determine the limit on pulse energy and pulse width imposed by the system parameters. A paper detailing the theory of the two-cavity soliton laser is currently in preparation.

Solitons are also candidates for high rate all-optical switching. The fact that a soliton can propagate undistorted along a dispersive fiber, the nonlinearity of the fiber balancing the spreading of the pulse by group velocity dispersion, suggests that the all-optical nonlinear interferometer switch described above could use solitons for the switching operation. We have started a theoretical investigation, both analytic and numerical, of the interaction of two orthogonally polarized "solitons." This entails the solution of two coupled nonlinear Schroedinger equations. It turns out that this problem is not "integrable" in general. For the values of the parameters describing an isotropic fiber, "solitons" do not fully recover after a collision; the pulses are solitary waves and not solitons. The perturbation from "soliton" behavior is small, if the collision is weak (the pulses pass each other rapidly), and the mutually induced phase shift is much smaller than π. Unfortunately, this is not adequate for switching operation of the interferometer. In future work we intend to pinpoint operating conditions for which switching may be feasible.

In work sponsored by Draper Laboratory, we initiated experimental and theoretical studies of soliton formation in an anomalously dispersive fiber using a Raman pump pulse at 1.3 microns from a modelocked Nd:YAG laser. The ultimate goal is to explore the use of solitons in a laser gyro using counterpropagating solitons. Since quantum noise is the ultimate source of noise in such a gyro, it is necessary to investigate the soliton quantization problem. This study has just begun.

References

[1] N.A. Whitaker, *All-Optical Signal Processing in Semiconductor Waveguides,* Ph.D. diss., Dept. Electr. Eng. and Comp. Sci., MIT, 1986.

[2] M.C. Gabriel, H.A. Haus, and E.P. Ippen, "Thermal Index Changes by Optical Absorption in Group II!-V Semiconductor Waveguides," *J. Lightwave Tech.* LT-4:1482 (1986).

[3] H.A. Haus, S. Oho, R. Seif, M. Shirasaki, N.A. Whitaker, and D.L. Wong, "The Nonlinear Waveguide Interferometer," RLE Progress Report No. 129, p. 29, MIT, 1987.

[4] H.A. Haus, M. Shirasaki, and D.L. Wong, "A Nonlinear Fiber Interferometer and Logic Gate," presented at CLEO '87, Baltimore, Maryland, April 27, 1987.

[5] M.J. LaGasse, D.L. Wong, J.G. Fujimoto, and H.A. Haus, "Femtosecond pump-probe interferometry," submitted for presentation at IQEC '88, Tokyo, Japan, April 1988.

[6] N. Dagli, C.G. Fonstad, and H.A. Haus, "Analysis and Characterization of III-V Guided Wave Optics Rib Waveguide Couplers," RLE Progress Report No. 129, p. 33, MIT, 1987.

[7] H.A. Haus, L. Molter-Orr, and F.J. Leonberger, "Multiple Waveguide Lens," *Appl. Phys. Lett.* 45:19 (1984).

[8] A. Hardy and W. Streifer, "Coupled Mode Theory of Parallel Waveguides," *J. Lightwave Tech.* LT-3:1135 (1985).

[9] J.P. Donnelly, H.A. Haus, and L.A. Molter, "Cross Power and Cross Talk in Waveguide Couplers," *J. Lightwave Tech.,* accepted for publication.

[10] L.A. Molter, *Integrated Optical Multiple Waveguide Coupler Switches and Lenses,* Ph.D. diss., Dept. of Electr. Eng. and Comp. Sci., MIT, 1987.

[11] L.F. Mollenauer and R.H. Stolen, "The Soliton Laser," *Opt. Lett.* 9:13 (1984).

5.4 Strained Layer Superlattices on <111> Oriented Substrates for Optical Devices

Kimberley Elcess, Stuart D. Brorson, Richard Singer, Clifton G. Fonstad, Jr., and Hermann A. Haus, in collaboration with Chrishen Mailhoit and Daryl Smith

When sufficiently thin layers of semiconductors possessing different lattice constants are grown on top of each other, the lattice mismatch can be accommodated by straining the individual layers. That such "strained layer super-lattices" can be grown without defects was first pointed out by Osbourn.[1] Strained layer superlattices are a topic of

considerable current interest since they promise increased flexibility in fabricating superlattices tailored to particular purposes.

Recent theoretical work predicts that the strain in In_xGa_{1-x} As/GaAs superlattices fabricated on <111> GaAs induces a polarization in each layer via the piezoelectric effect.[2] The built-in polarization fields are oriented along the growth axis and alternate in sign between the $In_xGa_{1-x}As$ well and the GaAs barrier. This affects the electronic properties of the bound quantum well states, and hence the optical properties of the structure.[3] In particular, superlattices possessing such built-in fields display a linear electrooptic effect, instead of the weaker quadratic effect present in conventional (non-polarized) quantum wells. This renders these structures ideal for optical device applications.

Molecular beam epitaxial growth on <111> substrates has proven to be different in significant ways from <100> growth, specifically in terms of the oxide desorption and growth initiation procedures which must be followed, the growth temperatures, and the sensitivity of the growth process to the arsenic flux.[4] The critical temperatures, fluxes, and flux ratios have now been determined and high quality layers can now be grown reproducibly.

We used the growth procedures we have developed to grow what are, to our knowledge, the first <111> oriented strained layer superlattices with built-in polarization fields. We have constructed a system for measuring near-infrared linear absorption in the quantum well samples, and are focusing on identifying features in the absorption data. Future work will center around measuring the dependence of the absorption edge on an externally applied DC electric field. From this one will be able to verify the existence of a built-in polarization field and deduce its actual magnitude. Further research will include fabricating slab waveguides which exploit the linear electro-optic effect to make optical phase modulators.

Finally, we are collaborting with Dr. D. Smith and colleagues at Los Alamos and with Prof. B.A. Weinstein and colleagues at the State University of New York at Buffalo on various characterization studies of these superlattices including Rutherford backscattering and ion channeling, low temperature optical absorption and photoluminescence, and transport.

References

[1] G.C. Osbourn, *J. Appl. Phys.* 53:1586 (1982).

[2] D.L. Smith, *Solid State Commun.* 57:919 (1986).

[3] D.L. Smith and C. Mailhoit, *Phys. Rev. Lett.* 58:1264 (1987).

[4] K. Elcess, J-L. Lievin, and C. G. Fonstad, to be published, *J. Vac. Sci. Tech. B*, March-April (1988).

5.5 Diffraction Coupled Diode Laser Arrays

Elias Towe, Robert E Hillman, Clifton G. Fonstad, Jr.

We have continued development of our novel phase-locked laser diode array, the mixed mode phase locked (M²PL) laser array. This array achieves phase-locking and operation in the fundamental, single-lobed super-mode by diffraction in a region introduced into the middle of the array. On either side of the mode-mixing region the modes are guided in ridge waveguides which terminate at the laser facets, but within the mode-mixing region the radiation is not confined laterally. Thus a small fraction of the radiation in each element of the array is coupled in this region to the adjacent elements. If the length of the mode-mixing region is properly designed, coupling will occur in phase, and the radiation in the adjacent guides will be locked in phase and single-lobed emission will result.

The M²PL laser concept was very successfully demonstrated for the first time last year.[1] The structure has been shown to routinely produce stable, single-lobed far-field patterns, and in this respect appears to be unique amongst the multitude of array structures which have been proposed. Moreover, it is one of the simplest to produce.

Work in the past year has focused largely on theoretical analysis of the M²PL structure. More detailed modeling of the optimum mode-mixing region length has been performed. Calculation of the strength of the coupling across the mode-mixing region for various device geometries, and estimates of the loss introduced by the use of the mode-mixing region, have also been completed. These predictions have been confirmed experimentally by measurements made viewing the M²PL lasers as passive waveguide structures.[2]

Very recently, we have begun a collaboration with an industrial laboratory interested in applying the M²PL concept to high power arrays. A mask set having a variety of mode mixing region lengths corresponding to phase shifts between adjacent guides ranging from under 2π to over 3π has been designed. Thus, in addition to independently confirming the importance of the M²PL concept, we expect these studies to provide verification for the theoretical analyses already completed, and data for use in more refined and extensive modeling, and optimization.

References

[1] E. Towe and C.G. Fonstad, "Mixed-Mode Phase-Locked Quantum Well Laser Arrays," *Technical Digest of the IEEE International Electron Devices Meeting*, 1987.

[2] R. Hillman, *Characterization of the Coupling Coefficient Induced by the Mode Mixing Region of the Mixed-Mode Phase-Locked Array Laser*, S.B. thesis, Dept. of Electr. Eng. and Comp. Sci., MIT, 1987.

5.6 Multiple Quantum Well Semiconductor Waveguide Optical Devices

Kristen Anderson, Richard Singer, Mary Phillips, James Vlcek, Clifton G. Fonstad, Jr., Hermann A. Haus

Multiple quantum well semiconductor optical modulators and switches in integrated waveguide structures have important application in all-optical processing systems. Research in this area is focused on theoretical optimal device design and novel material processing techniques.

In semiconductor materials, thermal effects due to nonradiative carrier recombination have a significant effect on optical device performance,[1] and are a limiting factor in many device designs. The effects are particularly crucial when a multiple quantum well material is excited with photons of energy corresponding to the exciton absorption peak where the optical nonlinearity is large. One way to benefit from the large optical non-linearity, and reduce thermal effects, is to use short device active lengths, restricting the size of the quantum well region within the waveguide.

Device performance and thermal effects in both loss modulation devices, and non-linear Mach-Zender interferometers were examined theoretically. The results indicated the feasibility of devices with small active regions. Loss modulation devices with active regions 5 μm long are expected to exhibit contrast ratios of as much as 6 dB using conventional diode laser light sources. Interferometric configurations with insertion losses of < 2.5 dB are predicted in which carrier induced heating effects are negligible.

A new material processing technique, disordering of GaAs-GaAlAs multiple quantum well materials via thermal annealing, is currently under investigation as a possible method to achieve small active lengths. Quantum wells under a silicon oxide capping layer are unstable and will disorder when annealed at temperatures above 825°C. This causes a shift to higher energy of the material band edge. With a silicon nitride capping layer, however, quantum wells subject to the same annealing conditions remain stable. In a multiple quantum well sample grown by molecular beam epitaxy, using the different dielectric capping layers, we have successfully demonstrated patterned disordered regions. These results were verified by transmission measurements and scanning electron microscopy. Buried waveguide structures are also currently being fabricated using this technique.

The ultimate goal is to use this disordering technique to compositionally mix, or homogenize, the GaAs-GaAlAs MQW's everywhere we wish to eliminate them. Subsequently shallow rib waveguides will be defined to produce the desired integrated optical circuitry.

Optical absorption measurements were performed on the disordered material. The measured band edge corresponds to that of an $Al_xGa_{1-x}As$ alloy with a fractional aluminum content, x, which would be expected if the original multiple quantum well layer were completely disordered. Future studies of linear and nonlinear absorption and

refractive index as well as carrier relaxation phenomena will provide further comparison of the disordered material to an epitaxially grown alloy. These studies well lead to specific device designs and eventual fabrication of nonlinear modulators and switches in integrated optical waveguide ge metries.

In addition to working with the well established GaAs-GaAlAs system, we are also studying the InGaAs-InAlAs system lattice-matched to InP. This system is compatible with operation in the 1.3-1.5 μm wavelength region commonly used in single-mode optical fiber telecommunications systems. Furthermore, the energy band discontinuities in this system are larger than they are in the GaAs-GaAlAs system, and larger non-linear optical effects are anticipated. The work in the InGaAs-InAlAs system is less advanced than that on the GaAs-GaAlAs system, and efforts are being directed first at simply producing and characterizing multiple quantum well structures, prior to addressing the issue of incorporating them into guided wave optical devices.

Reference

[1] M.C. Gabriel, H.A. Haus, and E.P. Ippen, "Thermal Index Changes by Optical Absorption in Group III-IV Semiconductor Waveguides," *J. Lightwave Tech.* LT-4:1482 (1987).

5.7 Femtosecond Laser Systems and Pulse Generation

James G. Fujimoto, Erich P. Ippen, Robert W. Schoenlein, Michael J. Lagasse

One of the key issues in the study of ultrafast phenomena is the availability of laser sources with femtosecond pulse durations at suitable wavelengths. Our research on femtosecond laser generation techniques has centered on the development of high repetition rate femtosecond amplification techniques as well as the development of tunable femtosecond laser sources. These sources provide the basis for a wide range of experimental investigations of ultrafast phenomena.

We have recently completed the construction of a high repetition rate femtosecond laser amplifier which can generate high intensity pulses with 50 fs duration at 620 nm. The laser source is a colliding pulse modelocked ring dye laser which uses internal prisms for the compensation of dispersion.[1] This laser is amplified with a copper vapor laser pumped dye jet amplifier operating at an 8 kHz repetition rate.[2] Using a six pass configuration, a gain of 10^4 is obtained to generate pulse energies of a few microjoules. The high repetition rate of the laser source is a key factor in improving time resolved measurements since it permits the use of signal averaging and lock-in detection techniques to enhance sensitivity. In addition, the high peak intensities allow the direct observation of nonlinear optical processes.

The high peak intensities produced by this laser are also important since they permit the application of nonlinear optical techniques for generating other wavelengths or performing optical pulse compression. By focusing intense pulses into a medium with an intensity dependent index of refraction, nonlinear self phase modulation can be used

to generate additional frequencies. A broadband femtosecond continuum can be produced which contains wavelengths ranging from 400 nm to 900 nm. This source is especially useful as a broadband probe of transient absorption or reflectivity line shape. We have applied our high repetition rate amplifier to perform pump and continuum probe measurements of a variety of femtosecond processes including non-equilibrium electron heating in metals, carrier relaxation in GaAs and AlGaAs, and transient excited state dynamics in polydiacetylene.

One of our principal objectives in continuing our development of high repetition rate sources is to extend the temporal resolution and bandwidth of femtosecond continuum pump and probe measurements. Previously, temporal resolutions for broadband continuum probe measurments were limited to ~ 100 fs. Because of the extremely large bandwidths and short pulse durations involved, one of the key problems in femtosecond measurement is controlling dispersion produced by the frequency generation processes and propagation through the optical components which are present in the experimental apparatus. Group velocity dispersion causes different frequency pulses to propagate with a varying time of flight through an optical system and thereby produce pulse broadening. The use of diffraction grating pairs or prism pairs has been demonstrated for the compensation of linear group velocity dispersion. However, for our pulse durations and experimental bandwidths, higher order dispersion was also found to play a critical role in limiting experimental resolution. We have been investigating dispersion compensation techniques in an effort to perform broadband measurements over several tens of nanometers with resolutions on the 10-20 fs time scale.

Complementing our high repetition rate femtosecond amplifier we have recently completed the construction of a tunable femtosecond laser. The approach that we are using is similar to that developed by Kafka and Baer,[3] and combines pulse compression techniques with synchronous modelocking. The laser system is based on a conventional modelocked Nd:YAG laser which produces 90 ps pulse durations at 1.06 μm Pulses from this laser are compressed using an optical fiber and diffraction grating pair to 5 ps. After frequency doubling, this laser is used to pump a synchronously modelocked, cavity dumped dye laser which generates 500 fs pulse durations. Finally, a second optical fiber and prism pair pulse compressor is used to obtain pulse durations as short as 55 fs.

Since this laser system uses pulse compression techniques and synchronous modelocking, the wavelength of the output pulse can be easily tuned. Using different laser dyes, we have generated femtosecond pulses in the wavelength range from 580 nm to 950 nm with typical pulse durations of 75 fs. The tunability and short pulse duration of this laser make it especially promising for femtosecond studies of GaAs and AlGaAs materials and devices. The laser can be tuned both above and below the bandgap of these semiconductors, thereby permitting the investigation of excited carrier relaxation processes as well as dynamic processes in guided wave devices.

References

[1] J.A. Valdmanis, R.L. Fork, and J.P. Gordon, "Generation of Optical Pulses as Short as 27 Femtoseconds Directly from a Laser Balancing Self-Phase Modulation, Group-Velocity Dispersion, Saturable Absorption, and Saturable Gain," *Opt. Lett.* 10:131 (1985).

[2] W.H. Knox, M.C. Downer, R.L. Fork, and C.V. Shank, "Amplified Femtosecond Optical Pulses and Continuum Generation at 5-kHz Repetition Rate," *Opt. Lett.* 9:552 (1984).

[3] J.D. Kafka and T. Baer, "A Synchronously Pumped Dye Laser Using Ultrashort Pump Pulses," *Proc. Soc. Photo-Opt. Instrum. Eng.* 533:38 (1985).

5.8 Femtosecond Carrier Dynamics in GaAs

Erich P. Ippen, James G. Fujimoto, Wei-Zhu Lin, Beat Zysset, Robert W. Schoenlein, Michael J. Lagasse

The investigation of transient carrier dynamics in GaAs and AlGaAs semiconductors is relevant to electronic and optoelectronic devices which depend on high speed transient carrier phenomena. Our research program focuses on the study of carrier dynamics using optical techniques which can provide measurements on the time scale of the fundamental scattering processes. Using pump and probe absorption saturation spectroscopy, we have investigated carrier scattering, energy relaxation, and intervalley scattering on a femtosecond time scale.

Pump probe absorption saturation measurements have been performed to measure the initial scattering time of carriers as they relax from their initial optically excited states. Using pulse durations of 35 fs generated by a CPM laser at a fixed wavelength of 620 nm, we have previously measured[1] initial scattering times as rapid as 13-30 fs. Because the laser source for these measurements was not tunable, studies were performed by varying material composition[2] of AlGaAs.

In order to investigate the energy relaxation of excited carriers, femtosecond pump and continuum probe measurements were performed using our recently developed high repetition rate amplifier system. By generating optically excited carriers at the pump pulse wavelength and probing absorption saturation over a range of wavelengths using a broadband continuum, the energy relaxation dynamics of the excited carriers could be observed. Our investigations provide evidence for transient nonthermal carrier distributions which occur on a femtosecond time scale.[3,4] Probing absorption saturation using transitions from the split-off band permits an investigation of the electron distribution as distinct from the hole distribution. This suggests possible methods for studying carrier-carrier scattering and separating electron-hole scattering contributions. Systematic measurements performed using different material compositions of AlGaAs permit an exploration of the effects of generating carriers with different excess energy. Intervalley scattering was found to contribute significantly to the initial energy relaxation of carriers which are excited above the X and L valleys.

Our recently developed tunable femtosecond laser system provides a unique opportunity to perform complementary investigations of transient carrier dynamics. One process of special importance to electronic device operation is intervalley scattering. Scattering of energetic carriers from the Γ valley to the L and X satellite valleys is one

of the dominant mechanisms which limit carrier transport and give rise to negative differential resistivity effects.[5]

Using our tunable femtosecond laser, we have begun an investigation of intervalley scattering and energy relaxation in GaAs and AlGaAs. A tunable femtosecond source is a particularly important tool for investigating carrier dynamics since the excess energy of the excited carriers can be continuously varied by adjusting the laser wavelength. Preliminary measurements[6] show dramatic changes in carrier scattering times when the excess energy of the carriers are increased to permit $\Gamma - L$ and $\Gamma - X$ intervalley scattering. While intervalley scattering has recently been investigated using a number of different techniques, including transient conductivity and luminescence measurements, femtosecond pump probe probe measurements represent one of the few approaches which has sufficient temporal resolution to directly measure the initial carrier scattering times.

References

[1] W.Z. Lin, J.G. Fujimoto, E.P. Ippen, and R.A. Logan, "Femtosecond Carrier Dynamics in GaAs," *Appl. Phys. Lett.* 50:124 (1987).

[2] W.Z. Lin, J.G. Fujimoto, and E.P. Ippen, "Femtosecond Dynamics of Highly Excited Carriers in AlGaAs," *Appl. Phys. Lett.* 51:161 (1987).

[3] R.W. Schoenlein, W.Z. Lin, E.P. Ippen, and J.G. Fujimoto, "Femtosecond Hot Carrier Energy Relaxation in GaAs," *Appl. Phys. Lett.* 51:1442 (1987).

[4] R.W. Schoenlein, W.Z. Lin, S.D. Brorson, E.P. Ippen, and J.G. Fujimoto, "Femtosecond Hot Carrier Energy Redistribution in GaAs and AlGaAs," *Solid State Electron.* 31:443 (1988).

[5] M.A. Littlejohn, J.R. Hauser, T.H. Glisson, D.K. Ferry, and J.W. Harrison, "Alloy Scattering and High Field Transport in Ternary and Quaternary III-V Semiconductors," *Solid State Electron.* 21:107 (1978).

[6] W.Z. Lin, M.J. LaGasse, R.W. Schoenlein, B. Zysset, and J.G. Fujimoto, "Femtosecond Studies of Excited Carrier Energy Relaxation and Intervalley Scattering in GaAs and AlGaAs," invited paper presented at the SPIE Symposium on Advances in Semiconductors and Superconductors, Newport Beach, California, March 1988.

5.9   Femtosecond Spectroscopy of Electronic and Optoelectronic Materials

James G. Fujimoto, Erich P. Ippen, Wei-Zhu Lin, Paolo Mataloni, Robert W. Schoenlein, Janice M. Huxley, Stuart D. Brorson

Femtosecond optical studies of electronic and optoelectronic materials are of importance since they provide an approach for directly investigating the transient dynamics associated with these materials. These studies are relevant to both increasing the understanding of fundamental physical processes as well as to applications of these materials in high speed electronic and optical signal processing.

In addition to studies in semiconductors, another topic of special interest is transient electronic processes in metals. Metals and semiconductors are the principal constituents of devices. In contrast to semiconductors, relatively few investigations have been performed in metals. Because of the high densities inherent in metals, nonequilibrium processes occur on an extremely rapid time scale and changes in optical properties are usually quite small. Thus, transient spectroscopy in metals has been made possible only through the recent development of new femtosecond laser technology which provides high temporal resolution and sensitivity.

Using femtosecond laser excitation, it is possible to generate and measure nonequilibrium electron heating phenomena. If the incident laser pulse duration is less than the electron-phonon energy transfer time, a transient nonequilibrium between the electrons and lattice may be produced. Since the heat capacity of the electron gas is much less than that of the lattice, electron temperatures in excess of the lattice temperature can be generated. We have investigated nonequilibrium electron energy relaxation and temperature dynamics in metals. Using noble metals, changes in electron temperature may be investigated optically by monitoring optical transitions from the *d* bands to the Fermi level. By performing pump and continuum probe transient reflectivity lineshape measurements on a femtosecond time scale, nonequilibrium electron heating was demonstrated.[1] Electron energy relaxation to the lattice was observed on a 1-2 ps time scale.

Since measurements can be performed on a time scale less than the electron lattice energy transfer time, it is possible to directly measure nonequilibrium properties of the electron gas. We have performed a study of transient energy transport in thin metal films using pump probe time-of-flight measurements.[2] A femtosecond pulse is used to heat the electron distribution on one side of a thin film while changes in electron temperature on the opposite side of the film are monitored with a probe pulse. Subpicosecond energy transport times are observed in 500 Å - 3000 Å thick gold films. This corresponds to an effective transport velocity of $\sim 10^8$ cm/sec, almost two orders of magnitude faster than equilibrium lattice heat diffusion. This experiment is the first observation of nonequilibrium energy transport in metals.

As an extension of these studies, we are currently working in collaboration with researchers at the General Motors Research Laboratories to investigate the transient dynamics of image potential states in metals.[3] When an electron is photoexcited from a bulk metal, it can relax into a state where it is bound to the surface in an image potential. These states are not surface states associated with the bulk. The electron wavefunction is maximized outside rather than inside the metal. We are currently developing techniques for transient photoemission spectroscopy in an effort to measure the transient dynamics of the image potential state. Femotsecond spectroscopy can be performed by populating the optical states using a short laser pulse, then subsequently photoemitting from these states using a second pulse. The photoemission energy spectrum may be obtained with a conventional energy analyzer to determine the transient photoemission spectrum from the metal. These experiments are relevant for the

measurement of fundamental physical processes and also represent a step toward combining femtosecond optical techniques with surface science diagnostics.

The investigation of nonequilibrium electronic effects in metals can provide new information on the fundamental physical processes in condensed matter. An increased understanding of these processes is important for problems such as the generation of plasmas and x-ray and UV laser sources which involve the interaction of high intensity laser pulses with metals. In addition, nonequilibrium electronic processes and transport are relevant for future high speed semiconductor devices where nonequilibrium processes can occur at semiconductor-metal interfaces.

In addition to semiconductors and metals, we are also investigating transient processes in polydiacetylenes. Polydiacetylenes are a class of organic polymers which are of technological importance because they exhibit large third order optical nonlinearities.[4] Thus they are an attractive candidate for all optical signal processing applications. The enhanced nonlinear optical response of these materials is the result of their unique chemical structure which is characterized by long carbon chains with bond superalternation and delocalized electronic states. Polydiacetylenes are also a model system for investigating one dimensional electron behavior.

We have investigated the transient excited state dynamics of polydiacetylene Langmuir-Blodgett films and crystals of PTS using pump probe absorption saturation spectroscopy.[5] Measurements performed at 620 nm just above the absorption edge indicate a recovery response consisting of a picosecond time scale process combined with an initial ultrafast relaxation occurring on a 100 fs time scale. Further studies of excited state dynamics were performed using continuum probe spectroscopy. The initial absorption saturation recovery was correlated with the onset of an induced absorption at a lower energy which is produced by relaxation of the excited state. Transient absorption saturation hole burning was observed near the excitation energy.

In addition to studies of absorption saturation, we have also investigated effects in thin PTS crystals. This system presents a natural Fabry-Perot cavity so that measurements of transmission versus wavelength provides information on both absorption and index. Pump and continuum probe measurements which investigate the spectrum at discrete time intervals after the occurrence of a pump pulse provide can permit the measurements of both the nonlinear absorption saturation corresponding to energy relaxation of the electronic excitations as well as the nonlinear index changes associated with excited state relaxation. At present there are a number of competing theories which explain the electronic nature of the excited state and the origin of the enhanced nonlinear effects observed in the polydiacetyelene system. Further studies of excited state transient dynamics could provide important information which could distinguish between different theoretical pictures and also describe the rate limiting processes in potential signal processing applicatons.

References

[1] R.W. Schoenlein, W.Z. Lin, J.G. Fujimoto, and G.L. Eesley, "Femtosecond Studies of Nonequilibrium Electronic Processes in Metals," *Phys. Rev. Lett.* 58:1680 (1987).

[2] S.D. Brorson, J.G. Fujimoto, and E.P. Ippen, "Femtosecond Electronic Heat Transport Dynamics in Thin Gold Films," *Phys. Rev. Lett.* 59:1962 (1987).

[3] D. Straub and F.J. Himpsel, "Identification of Image-Potential Surface States on Metals," *Phys. Rev. Lett.* 52:1922 (1984).

[4] G.M. Carter, M.K. Thakur, Y.J. Chen, and J.V. Hyrniewicz, "Time and Wavelength Resolved Nonlinear Optical Spectroscopy of a Polydiacetylent in the Solid State Using Picosecond Dye Laser Pulses," *Appl. Phys. Lett.* 47:457 (1985).

[5] J.M. Huxley, J.G. Fujimoto, E.P. Ippen, G.M. Carter, and P.Mataloni, "Femtosecond Absorption Saturation Dynamics in Polydiacetylene," *Technical Digest of the Conference on Lasers and Electro-Optics,* CLEO '87, Baltimore, Maryland, April 1987, paper ThF2, p. 226.

5.10   Ultrashort Pulse Laser Medicine

James G. Fujimoto, Wei-Zhu Lin, Reginald Birngruber, Beat Zysset, Robert W. Schoenlein

Working in collaboration with researchers at the Massachusetts Eye and Ear Infirmary and the Wellman Laboratories of the Massachusetts General Hospital, we are investigating the application of short and ultrashort pulses lasers and time resolved spectroscopic techniques to problems in laser medicine. In contrast to more established applications of cw lasers to surgery which relay primarily on thermal effects to acheive the desired therapeutic response, the use of high intensity ultrashort pulsed lasers is promising since it permits the possibility of nonlinear laser tissue interactions. In addition, the application of measurement techniques traditionally used in time resolved spectroscopy to studies of transient processes in laser tissue interaction and medical diagnostics can yield new and significant information which will allow the optimization of desired laser tissue interaction processes.

One area of special interest is the application of high intensity short pulsed lasers for ophthalmic surgery. In particular, the Q-switched and mode-locked Nd:YAG lasers have recently emerged as important tools for ophthalmic surgery.[1,2] High intensity laser pulses in the nanosecond or picosecond regime can be used to produce optical breakdown which is used for surgical incision of transparent structures in the anterior eye. We have developed and applied techniques of time resolved spectroscopy to investigate the transient processes of plasma absorption, acoustic wave generation, and cavitation which are associated with laser induced breakdown.[3] Our ultimate objective is to characterize physical processes, determine correlations with physical effects in ophthalmic surgery, and finally to optimize the laser surgical process.

Our initial investigations were performed using a nanosecond laser, since this is the most widely used system clinically. During the past year we have extended our investigations using pulse durations of 30 ps generated by a modelocked Nd:YAG laser.[4] The rationale for performing measurements with shorter pulses is twofold. By developing and applying time resolved techniques such as pump probe studies, we can perform measurements of physical processes with a temporal resolution limited only by the

pulse duration. In addition, since peak intensities scale up as laser pulse duration is increased, the desired nonlinear laser-tissue interactions can be generated at lower energy densities. We have performed pump and probe optical measurements to characterize the spatial and temporal evolution of the plasma, acoustic wave, and cavitation in optical breakdown. Comparison of nanosecond and picosecond lasers show that the transverse dimensions of the physical processes can be reduced by using shorter pulse laser sources, thereby producing an increased localization of surgical effects.

In order to establish a correlation of the physical phenomena in laser induced breakdown to a clinically observable effect in a biological system, the cornea endothelium was used as a model system. Studies were performed with enucleated bovine corneas. The corneal endothelium is a monolayer of cells on the posterior surface of the cornea which can provide a sensitive indicator of laser surgical effects.[5] Laser induced breakdown was generated both directly on the endothelium and at varying distances from the endothelium immersed in saline solution. Ultrastructural changes, including removal of cells and production of an incision were characterized using light and scanning electron microscopy. The localization of surgical lesions was observed to vary roughly as (energy)$^{1/3}$ for both nanosecond and picosecond laser pulses. This implies that shorter pulse durations with reduced energy can be used surgically to significantly enhance controlability over currently utilixed nanosecond laser sources.

The limiting case of short pulse laser surgery was investigated using high intensity femotsecond laser pulses with pulse durations of 70 fs and peak exposure intensities of greater than 10^{12}w/cm^2. Because of the high peak intensities but low pulse energies, strongly nonlinear effects could be observed. Laser ablation of the cornea could be performed using pulses at 620 nm wavelength where the cornea is nominally transparent.[6] Ultrastructural studies including light and transmission electron microscopy were performed to characterize the degree of collateral damage. These findings show a surprisingly small degree of thermal denaturation and a localization of the damage on a 10 μm scale. This high degree of incision control approaches results which can be obtained with some types of ultraviolet ablation.[7] Our study represents one of the first investigations using a high intensity visible laser for corneal ablation. Preliminary findings indicate that in contrast to UV ablation, nonlinear absorption plays a key role in energy deposition processes. The use of femtosecond lasers may thus provide a technique for the microsurgcial treatment of internal intraocular structures where UV ablation is not feasible.

References

[1] D. Aron-Rosa, J. Aron, J. Griesemank, and R. Thyzel, "Use of the Neodymium-YAG Laser to Open the Posterior Capsule after Lens Implant Surgery," *J. Intraocular Implant Soc.* 6:352 (1980).

[2] R.F. Steinert and C.A. Puliafito, "The Nd:YAG Laser in Ophthalmology," in *Principles and Clinical Applications of Photodisruption.* Philadelphia: W.B. Saunders Co., 1985 (and references therein).

[3] J.G. Fujimoto, W.Z. Lin, E.P. Ippen, C.A. Puliafito, and R.F. Steinert, "Time-Resolved Studies of Nd:YAG Laser Induced Breakdown: Plasma Formation, Acoustic Wave Generation, and Cavitation," *Invest. Ophthalmol. Vis. Sci.* 26:1171 (1985).

[4] B. Zysset, G. Dalickas, T. Deutsch, and J.G. Fujimoto, "Time Resolved Studies of Picosecond Photodisruption," presented at the Conference on Lasers and Electro-Optics (CLEO '88), Anaheim, California, April 1988, paper ThS3.

[5] H.D. Schubert and S. Trokel, "Endothelial Repair following Nd:YAG Laser Injury," *Invest. Ophthalmol. Vis. Sci.* 25:971 (1984).

[6] R.W. Schoenlein, D. Stern, C.A. Puliafito, J.G. Fujimoto, and R. Birngruger, "Ablation of the Cornea using Visible Femtosecond Pulses," presented at the Conference on Lasers and Electro-Optics (CLEO '88), Anaheim, California, April 1988, paper ThL3.

[7] C.A. Puliafito, R.F. Steinert, T.F. Deutsch, F. Hillenkamp, E.J. Dehm, and C.M. Adler, "Excimer Laser Ablation of the Cornea and Lens," *Ophthal.* 92:741 (1985).

5.11   Short Wavelength Lasers

Peter L. Hagelstein, John P. Braud, Kevin A. Delin, Cris C. Eugster, Sumanth Kaushik, Anne Morganthaler, Martin H. Muendel, Leon Balents, Thomas Farkas, Tsen-Yu Hung, Kevin Lam

A major objective of our research is to develop a small scale (table top) extreme ul-traviolet laser (EUV) which operates in the 200-300 Å spectral regime. The purpose of this research effort is to explore the new short wavelength laser technology and its associated scientific applications. Serious exploitation of x-ray laser applications will require an economical, reliable and high-repetition-rate x-ray laser system. As a result, our initial efforts (and efforts of our colleagues at a number of laboratories) are primarily aimed at developing such a short wavelength laser source.

The scientific applications of x-ray lasers probably include:

1. Phase sensitive soft x-ray surface reflection probing.

2. Soft x-ray/optical nonlinear studies, and mixing to provide bright and tunable soft x-ray sources.

3. Short pulsed holographic imaging of microscopic surfaces, including biological surfaces.

4. Source of accurate wavelength standards in the soft x-ray regime.

5. Source for the creation of microscopic plasmas.

Undoubtedly many additional applications will become apparent in time. Our hope is that our efforts will help this technology to mature to the point of being of significant use to the scientific and industrial communities.

Our research group is also interested in a number of atomic physics and quantum electronics projects which we will report on in the next RLE Progress report.

5.11.1 Monopole Collisional Excitation Scheme

Electron collisional excitation as a mechanism to produce population inversions at EUV and soft x-ray wavelengths has played a key role in the successful demonstration of short wavelength amplification in recent years. Amplification has been observed in a number of highly stripped neon-like ions,[1-3] and more recently in nickel-like ions.[4] Searches for amplification in Nd-like ions are currently underway at a number of laboratories. We plan to pursue the electron collisional excitation scheme experimentally at lower Z in coming years at MIT.

The monopole excitation scheme is based on the occurrence of very large electron collisional excitation cross sections for the excitation of a highly stripped ion from a closed shell $^1S_0$ ground state to a singly excited state of the same parity and total angular momentum. For example, in neon-like ions, transitions of the type $1s^22s^2p^6\ ^1S_0 - 1s^22s^2p^53p^1S_0$ can lead to strong population inversions on 3p-3s laser lines.[5] In nickel-like ions, the dominant electron collisional excitation drives the $1s^22s^2p^63s^2p^6d^{10}\ ^1S_0 - 1s^22s^2p^63s^2p^6d^94d^1S_0$ transition which leads to gain on 4d - 4p transitions.[6]

The upper laser state in these schemes cannot radiatively back down to the ground state due to the parity selection rule, and as a result, inter-shell population inversions readily develop. The lower laser state is a short-lived $J = 1$ state, which radiatively decays rapidly back to the ground state.

The observation of significant amplification in nickel-like yterbium has been reported down to 50.2 Å,[4] which for the time being appears to be the shortest wavelength at which such amplification has been demonstrated in a laboratory. One of our goals is to study the 4d-4p laser lines in low Z nickel-like ions up to molybdenum (the strongest of which in molybdenum is computed to lie near 195 Å).

We have been involved during the past years in the simulation and analysis of collisional excitation schemes in Ne-like, Ni-like, and Nd — like[7] systems. The design of our low Z lasers is being carried out with the physics simulation codes LASNEX, XRASER and YODA, which have previously been used to design[8-12] nearly all of the laboratory x-ray laser experiments to date that have been done at Livermore.

5.11.2 Concept of a Benchtop Short Wavelength Laser Facility

One of the advantages of using the monopole collisional excitation scheme in the proposed wavelength regime is that the required intensity of the pump laser scales very rapidly with increasing wavelength of the output beam, $(\sim \lambda^{-6})$. Thus, by exploiting the isoelectronic transitions in lower Z ions ($Z = 38-45$), it is possible to not only reach the desired wavelength regime but also to achieve the necessary pump intensity on an academic laboratory scale. Currently no cheap optical pumping source is readily available; one of the objectives of this research is to develop such a system.

Once a population inversion has been generated, it is desirable to use a cavity to provide feedback and collimation of the short wavelength light. By allowing the signal to travel through an inverted plasma several times, the required pump energy is further reduced by approximately an order of magnitude. Because the EUV radiation is highly

energetic, traditional cavity designs used in the infra-red and optical regimes will not sufficiently contain the radiation. Therefore, a second objective of this research is the development of a practical resonant cavity for the EUV regime.

Finally, to be considered a useful scientific device, a practical EUV laser must have at least a moderate repetition rate. Currently, there exists no short wavelength laser in the world that can generate pulses of EUV light at a repetition rate that is even close to rates normally associated with optical systems. Therefore, the entire system will be constructed to operate at rates on the order of 1 pulse every few seconds. Specifically, the third major goal of this work, is to develop a method of replenishing the target material that is used to make the EUV plasma at a rate consistent with this design criterion.

Some of these objectives are discussed in more detail in the following sections.

5.11.3 The Optical Pumping System

The pump laser system which will be used to create the laser plasma will consist of a conventional modelocked oscillator and preamplifier system which is commercially available, followed by a thin slab Nd-glass power amplifier.[13,14] (See figure 5.1). Our goal is to obtain approximately 50 Joules out of two power amplifiers in series.
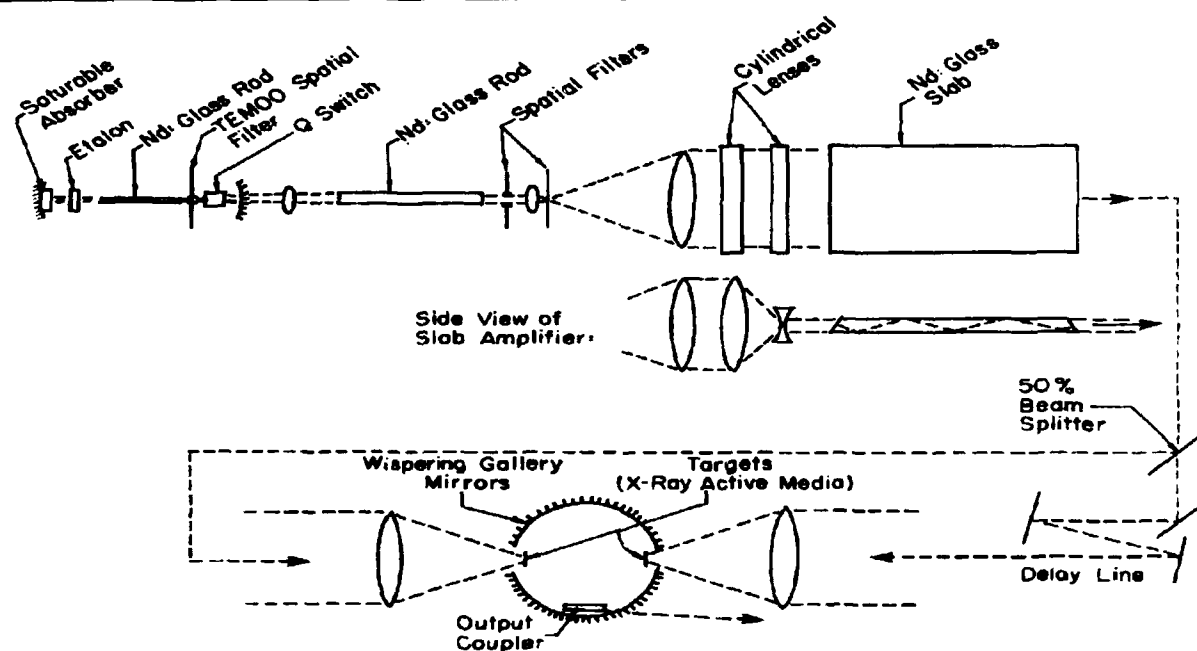
Figure 5.1 Schematic of pump system for a small scale short wavelength laser system.

Glass rod amplifiers are commonly used in high-power laser facilities, and we could in principle construct our power amplifiers using rods instead of slabs. Since glass is a poor thermal conductor, high-power glass laser amplifiers tend to cool rather slowly. The characteristic thermal relaxation time of a phosphate glass rod is approximately

$$\tau = 45R(cm)^2 sec. \tag{1}$$

In order to stay below the damage threshold for the glass, we would require a rod of radius 2.5 cm, and would be faced with a corresponding cooling time of close to 250 seconds between shots.

The primary advantage of a thin slab amplifier over a rod amplifier is in the relative cooling rates of the two geometries. The double requirements of moderately high optical laser energy high repetition rate places severe constraints on the design of the pump laser, and these considerations have lead us to consider the more unconventional approach of thin slab power amplifiers. For example, a slab amplifier of thickness 0.4 cm which is cooled from one side would have a thermal relaxation time of 17 seconds. Cooling from both sides reduces this number to 4 seconds.

5.11.4   Whisper-Gallery Mode Mirrors in the Soft X-Ray Regime

A single pass amplification scheme for the EUV portion of the system for applications is impractica' (although most soft x-ray laser work done to date has been on single-or double-pass systems), as it would require roughly an order of magnitude increase in the required pump energy. Normal incidence reflection is most often obtained using lossy multilayer mirrors in the EUV and soft x-ray regimes, with observed reflection coefficients approaching 50% per bounce. The extension of this technique to the construction of stable short wavelength laser cavities has not yet been explored.

An alternate approach using successive glancing angle reflection has lead to higher observed reflection coefficients for 180 degrees turning (the equivalent of a normal incident reflection for a multilayer mirror) from 100-140 eV.[15] This approach should scale favorable to the somewhat longer wavelengths of interest to us.

We have therefore examined the construction of such a cavity by exploiting whisper gallery modes (multiple glancing angle reflection modes), as shown in figure 5.2. Originally analyzed by Rayleigh in connection with acoustic waves, these modes can guide waves that are in grazing incidence to the mirrors. Stable cavities are easily constructed by arranging for the shape of the mirror to cause refocusing of the expanding beam which emerges from the plasma amplifier.
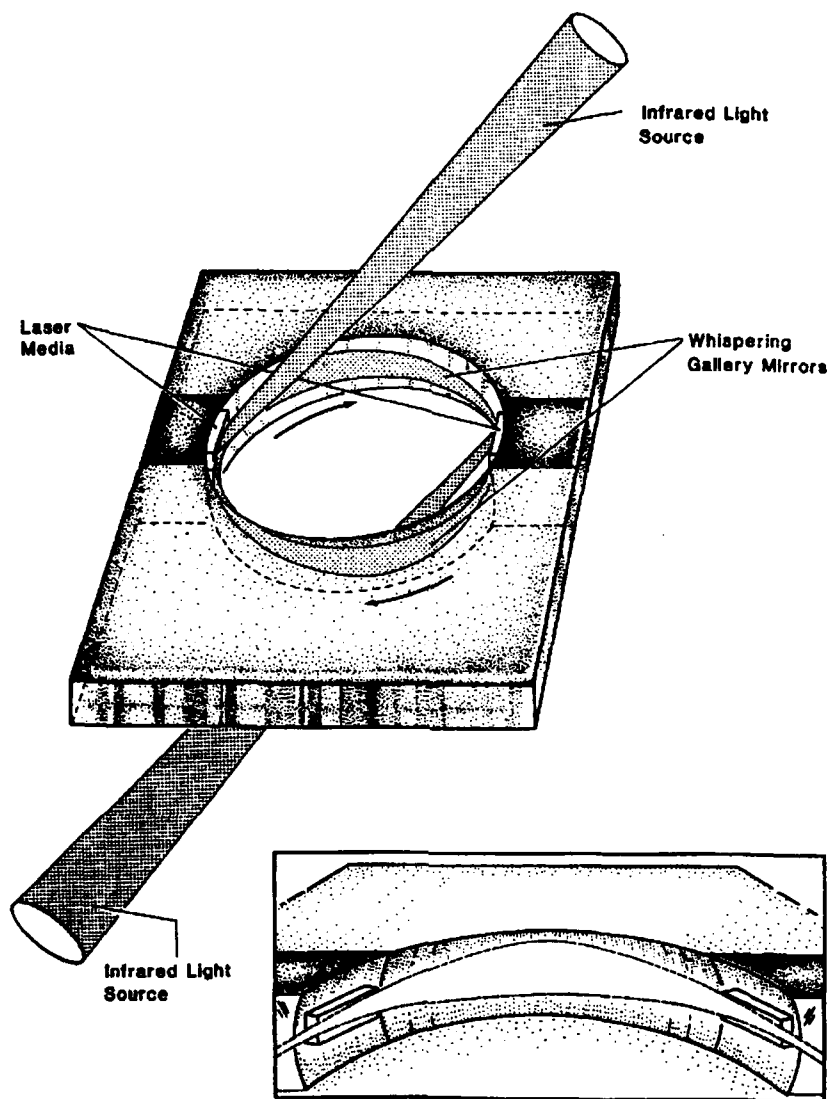
Figure 5.2 Illustration of concept of whispering gallery mirror for a short wavelength laser cavity.

As envisioned, the EUV resonant cavity will be spherical. Arranging two inverted plasmas antipodally will therefore guarantee that radiation in the cavity will always pass through the amplifying media, since any great circle on a sphere that passes through one antipode will necessarily pass through the other. Laser amplification is therefore possible twice for every round trip in the cavity.

Moreover, it can be shown that the radius of the cavity does not affect the efficiency of the whisper modes to first order. Thus the cavity can be constructed to a size convenient to the EUV pumping scheme. By subdividing the optical pulse to a train of 15 pulses, the inverted population of the plasma can be refreshed for each pass of the beam through the plasma amplifier. If the subpulses come 1 ns apart, a spherical cavity 10 cm in diameter will allow a complete round trip between plasma reheating.

5.11.5 A Fast High Resolution Soft X-Ray Detector

In conjunction with the development of the x-ray laser, research efforts have been made in our group developing schemes for time-resolved and time-gated x-ray detectors which are both efficient and have excellent spatial resolution.[16] Applications for these soft x-ray detectors include time-gated spectrometers and cameras for the soft x-ray laser beam, diagnostics for the plasma amplifiers, and imaging instruments for microscopic and holographic applications.

The proposed schemes are based on the use of optical nonlinearities of multiple quantum well (MQW) structures to obtain potentially fast (10 psec) and efficient x-ray detection with submicron spatial resolution. Specifically, two related schemes have been devised that are based on: 1) the scattering; and 2) the reflection of a pulsed optical probe beam by carriers produced by the absorption of a single energetic soft x-ray photon.

The mechanism of the detection relies on the strong carrier density dependence of the (complex) index of refraction of the exciton absorption lines in MQW GaAs/AlGaAs layers. In optical experiments, the carriers are usually generated by the absorption of an optical laser above the bandgap. In our schemes, we propose to create carriers directly by soft x-ray absorption.

Figure 5.3 shows the setup for the reflection scheme where the probe beam is incident from the back and the soft x-rays are incident on the front of the MQW structure. The pixels give the necessary spatial and temporal resolution. The pixels are essentially Fabry-Perot cavities whose refractive index can be altered by the carriers generated by the x-ray. The optical signal is reflected from individual pixels where soft x-ray absorption has occurred and is then imaged onto a CCD.
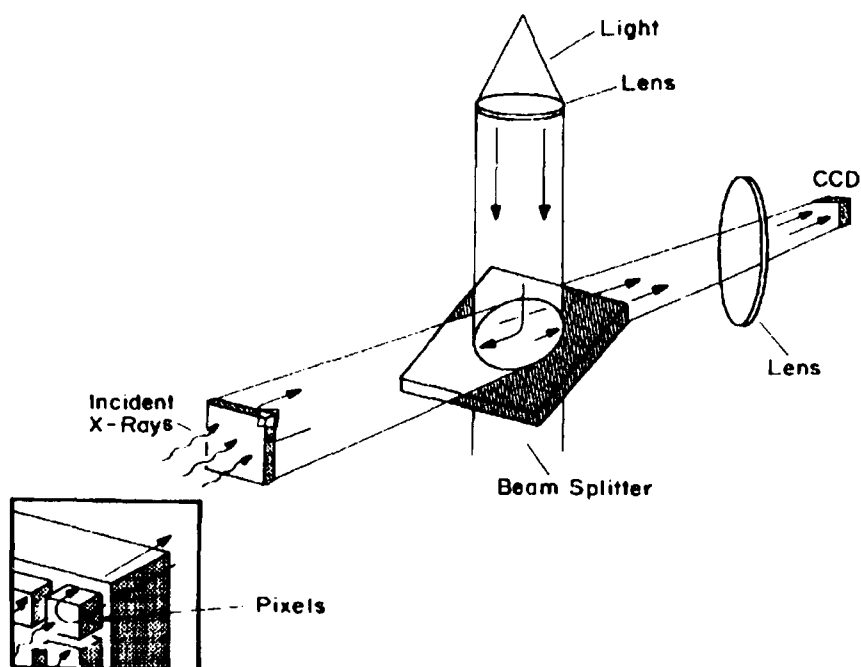
Figure 5.3 Microetalon approach to sort x ray detection.

References

[1] D.L. Matthews, P.L. Hagelstein, M.D. Rosen, M.J. Eckart, N.M. Ceglio, A.U. Hazi, H. Medecki, B. MacGowan, J. Trebes, B.L. Whitten, E.M. Campbell, C.W. Hatcher, A.M. Hawryluk, R.L. Kauffman, L.D. Pleasance, G. Rambach, J.H. Scofield, G. Stone, and T.A. Weaver, "Demonstration of a Soft X-Ray Amplifier," *Phys. Rev. Lett.* 54:110 (1985).

[2] T.N. Lee, E.A. McLean, and R.C. Elton, *Phys. Rev. Lett.* 59:1185 (1987).

[3] B.J. MacGowan, M.D. Rosen, M.J. Eckart, P.L. Hagelstein, D.L. Matthews, D.G. Nilson, T.W. Phillips, J.H. Scofield, G. Shimkaveg, J.E. Trebes, R.S. Walling, B.L. Whitten, J.G. Woodworth, *Observation of Soft X-Ray Amplification in Neonlike Molybedenum, J. Appl. Phys.* 61:5243 (1987).

[4] B.J. MacGowan, S. Maxon, P. Hagelstein, C.J. Keane, R.A. London, D. Matthews, M. Rosen, J. Scofield, and D.A. Whelan, "X-Ray Laser Experiments in Ni-like ions," *Phys.Rev. Lett.* 59:2157 (1987).

[5] A.V. Vinogradov, I.I. Sobelman, and E.A. Yukov, "Population Inversion of Transitions in Neon-Like Ions," *Sov. J. Quantum Electron.* 7:32 (1977).

[6] P. Hagelstein, "Relativistic Distorted-Wave Results for Nickel-Like Gadolinium," *Phys. Rev. A* 34:874 (1986).

[7] P.L. Hagelstein and S. Dalhed, "On Strong Monopole Collisional Excitation in Highly Stripped Ions," *Phys. Rev. A* 37:1357 (1988).

[8] P.L. Hagelstein, "Review of Radiation-Pumped Soft X-Ray Lasers," *Plas. Phys.* 25:1345 (1984).

[9] M.D. Rosen, P.L. Hagelstein, D.L. Matthews, E.M. Campbell, A.U. Hazi, B.L. Whitten, B. MacGowan, R.E. Turner, R.W. Lee, G. Charatis, G.E. Busch, C.L. Shepard, and P.D. Rockett, "Exploding-Foil Technique for Achieving a Soft X-Ray Laser," *Phys. Rev. Lett.* 54:106 (1985).

[10] S. Maxon, P. Hagelstein, K. Reed and J. Scofield, "A Gas Puff Soft X-Ray Laser Design," *Appl. Phys. Lett.* 57:971 (1985).

[11] S. Maxon, P. Hagelstein, J. Scofield and Y. Lee, "Estimated Gains for a Ni-Like Exploding Foil Target," *J. Appl. Phys.* 59:293 (1986).

[12] S. Maxon, P.L. Hagelstein, B. MacGowan, M.D. Rosen, R. London, S. Dalhed, J. Scofield, and M.H. Chen, "Calculation and Design of a Ni-like Eu Soft X-Ray Laser," *Phys. Rev. A* 37:2227 (1988).

[13] G.F. Albrecht, J. Eggleston, and J.J. Ewing, "Design and Characterization of a High Average Power Slab YAG Laser," *IEEE J. Quantum Electron.* QE-22:2099 (1986).

[14] J. Eggleston, G.F. Albrecht, R.A. Petr, and J.F. Zumdieck, "A High Average Power Dual Slab Nd:Glass Zigzag Laser System," *IEEE J. Quantum Electron.* QE-22:2092 (1986).

[15] A. Vinogradov, "XUV Cavity and Pumping Optics," In *Proceedings of the International Colloquium on X-Ray Lasers,* eds. P. Jaegle and A. Sureau, 1986.

[16] C.C. Eugster and P.L. Hagelstein, "Soft X-Ray Detection Using the Quantum Well Exciton Nonlinearity," submitted to *IEEE J. Quantum Electron.* (1988).

Professor Jeffrey H. Shapiro

6.0   Optical Propagation and Communication

Academic and Research Staff

Prof. J.H. Shapiro, Dr. R.H. Rediker, Dr. N.C. Wong

Graduate Students

B.T. Binder, D.E. Bossi, C.J. Corcoran, R.H. Enders, S.M. Hannon, S.-T. Ho, R.K. John, K.-W Leong, S.K. Liew, L. Pang, D. Park, G. Saplakoglu, S.R. Shepard, S.D. Lau Shiple, P.T. Yu, N.E. Zirkind

The central theme of our programs has been to advance the understanding of optical and quasi-optical communication, radar, and sensing systems. Broadly speaking, this has entailed: 1) developing system-analytic models for important optical propagation, detection, and communication scenarios; 2) using these models to derive the fundamental limits on system performance; and 3) identifying, and establishing through experimentation the feasibility of techniques and devices which can be used to approach these performance limits.

6.1   Atmospheric Optical Communications in Local Area Networks

Jeffrey H. Shapiro, Bradley T. Binder, Peter T. Yu

The distribution of computing resources to a community of users often calls for the use of a local area network (LAN). LANs are characterized by limited geographic scopes and data rates in excess of 1 Mbps. Atmospheric optical communication links can support data rates in the Mbps to Gbps range over kilometer path lengths in clear weather, but are subject to outages caused by fog, snow, etc. These characteristics suggest that atmospheric optical communication links may find LAN applications as bridges between buildings containing cable subnetworks, or as temporary quick-connects for new outlying hosts for which cable runs are initailly unavailable. The viability of such applications will depend on the degree to which network users can be insulated from the vagaries of atmospheric optical communication through a judicious combination of link and network design. In this program, we have have established an experimental 10 Mbps token-ring local area computer network that uses atmospheric optical communications over a 170 m outdoor path on the MIT campus. Objective and subjective performance results have been obtained with this system.

In its initial incarnation, our LAN links two IBM-PC microcomputers that are located along a line-of-sight path in Buildings 36 and NE43 (see figure 6.1). Each of these computers is equipped with a PROTEON proNET interface card. The proNET is a commerical 10 Mbps wire-based token-passing ring network that, along with a variety of other commerical and experimental networks, is presently in use on the MIT campus. We have constructed a pair of atmospheric optical communication transceivers that

complete the proNET connections between the IBM-PCs in an electrically transparent fashion.

Each transceiver consists of a 10 Mbps Manchester-coded GaAlAs semiconductor laser diode transmitter and a Si avalanche photodiode direct-detection receiver.[1-3] The transmitters employ feedback power-stabilization circuitry, and the receivers are equipped with automatic gain control circuitry.[3] Status information concerning the transmitted and receiver power levels is accumulated at regular intervals by data-acquisition systems attached to each transceiver.[3,4] These data are time-logged and stored by the computers that comprise the network.

The experimental network has been studied in several ways. Objective measurements of packet-level performance have been obtained by having one microcomputer continuously recirculate a packet around the ring, accumulating error statistics.[3] Clear-weather measurements of this type have been made with optical attentuation inserted into the links and used to corroborate a theoretical model for the noise-induced degradation of link performance. Bad-weather measurements of this type have shown significantly different behavior, which we attribute to the burst-error nature of bad weather operation. This hypothesis, which is still under investigation, is supported by data collected with burst-error sensing software.[5]

In addition to the fundamental packet-level performance measurements, we have used the standard Trivial File Transfer Protocol (TFTP) of the Transmission Control Protocol/Internet Protocol (TCP/IP) to probe the utility of our network by employing the IBM-PC in Building NE43 as a remote disk for the IBM-PC in Building 36; this remote disk is accessed through the atmospheric-optical network.[3] Here, we found that the burst-error behavior encountered in bad weather made network file-transfer operations far more fragile, at the same average received-power level, than in random-error (optically-attenuated) clear weather. This observation was supported by subjective comments culled from log files produced by network users via our network-interface software.[6]
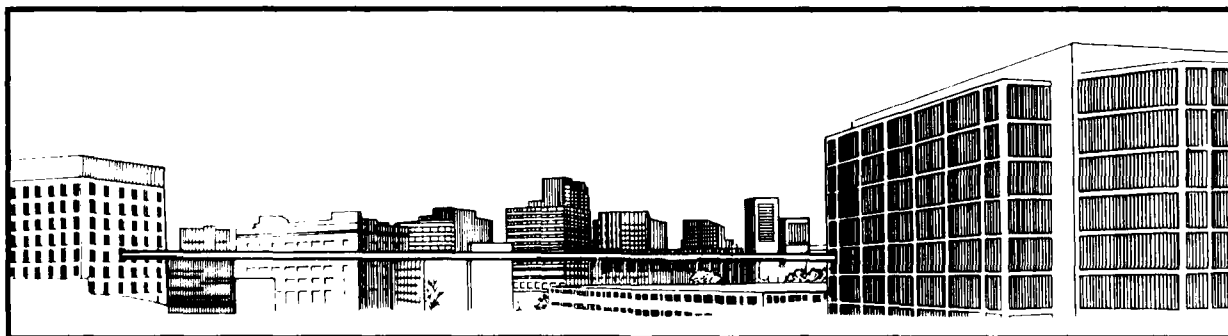
Figure 6.1   In conjunction with two microcomputers and the appropriate software, two laser transmitters and companion receivers form an experimental token-ring local area network (LAN).

References

[1] A.K. Wong, *A Variable-Rate Atmospheric Optical Link for Local Area Networks*, S.M. thesis, Dept. of Electr. Eng. and Comp. Sci., MIT, 1984.

[2] D.R. Lane, *A Modified Atmospheric Optical Link for Local Area Networks*, S.B. thesis, Dept. of Electr. Eng. and Comp. Sci., MIT, 1985.

[3] B.T. Binder, *Remote Computation with an Atmospheric Optical Ring Network*, S.M. thesis, Dept. of Electr. Eng. and Comp. Sci., MIT, 1987.

[4] A. De Rozairo, *A Data Acquisition System for Atmospheric Optical Links*, S.B. thesis, Dept. of Electr. Eng. and Comp. Sci., MIT, 1986.

[5] B.S. Wong, *Statistics of Error-Free Seconds in an Atmospheric Optical Communication Ring Network*, S.B. thesis, Dept. of Physics, MIT, 1987.

[6] B.T. Hou, *Atmospheric Optical Ring Network User Interface*, UROP Report, Dept. of Electr. Eng. and Comp. Sci., MIT, 1987.

6.2   Squeezed States of Light

Jeffrey H. Shapiro, Ngai C. Wong, Seng-Tiong Ho, Kin-Wai Leong, Gurhan Saplakoglu, Roy K. John, Scott R. Shepard

The squeezed states of light (also called the two-photon coherent states) are minimum uncertainty states for the quadrature components of the electromagnetic field which possess an asymmetric noise distribution between the two quadratures. The standard minimum uncertainty state that appears in quantum optics is the Glauber coherent state; it has an equal noise division between the two quadratures and is the quantum analog of the classical electromagnetic wave. Squeezed states are nonclassical, and are of interest because their asymmetric noise division can lead to lower noise in photodetection measurements than that achievable with coherent states of the same energy. These noise reductions have been shown, theoretically, to afford significant benefits in interferometric precision measurements and novel guided-wave optical communication devices. We have pursued a vigorous program of experimental and theoretical research on squeezed-state and related nonclassical light.

Experiments

We were one of the first groups to report experimental observation of quadrature-noise squeezing.[1] Our measurement, which was a forward four-wave mixing experiment in atomic sodium vapor, exhibited 0.2 dB of squeezing. This was the first squeezing measurement in a Doppler-broadened atomic medium, and was limited by a variety of technical difficulties.[2] Since then we have continued our atomic sodium vapor work with a greatly improved optical configuration. Moreover, the new sodium exper-

iment is preliminary to an experiment in ytterbium vapor. The ytterbium experiment will benefit from a simpler atomic level system than sodium, and will use a pump-recirculation cavity to enhance the squeezing.

The greatest observed quadrature-noise squeezing to date has come from a LiNbO$_3$ optical parametric amplifier,[3] i.e., a below-threshold optical parametric oscillator (OPO). We have begun work on a somewhat similar arrangement in which we intend to concentrate on the above-threshold OPO regime. As compared to the atomic vapor work, the OPO experiment benefits, because it uses a transparent medium, from lower loss and absence of spontaneous emission.

Theory

Our theoretical work on nonclassical light has addressed issues relevant to our experimental work as well as topics concerned with the application of such light beams. In support of the atomic vapor experiments, we have developed a quantum theory for nondegenerate multiwave mixing,[4,5] which includes important advances in the quantum treatment of light-beam propagation in material media in addition to providing operating-point calculations for our experiments. In conjunction with possible experiments in self-phase modulation (SPM) media, such as optical fibers, we have developed a multi-temporal mode single-spatial mode treatment of the classical and quantum noise tranformations of lossless dispersionless SPM.[6] Here we were the first to indicate the necessity of including a medium-dependent time constant in assessing the limit of validity of coupled-mode theory, and in evaluating the quantum-mechanical periodicity of the full nonlinear regime.

We have also made major advances in our understanding of the quantum nature of feedback photodetection. Our initial interest in this area stemmed from its possible use, in conjunction with a quantum nondemolition measurement, for generating nonclassical light.[7] We were able to fully elaborate the relationships between the semiclassical and quantum treatments of these closed-loop systems and to emphasize the importance of explicitly treating the optical delay within the apparatus in order to properly understand the in-loop field commutators.[8] Lately, we have been examining the dual relationships between the state-generation and state-measurement descriptions of closed-loop photodetection.[9]

Finally, we have begun a new fundamental investigation of the sensitivity of quantum phase measurements. This work, which is still in very preliminary form, predicts that substantially lower phase-measurement errors can be obtained, at the same average photon number, than those predicted for optimized squeezed-state interferometers.

References

[1] M.W. Maeda, P. Kumar, and J.H. Shapiro, "Observation of Squeezed Noise Produced by Forward Four-Wave Mixing in Sodium Vapor," *Opt. Lett.* 12:161 (1987).

[2] M.W. Maeda, P. Kumar, and J.H. Shapiro, "Squeezing Experiments in Sodium Vapor," *J. Opt. Soc. Am. B* 4:1501 (1987).

[3] L-A. Wu, M. Xiao, and H.J. Kimble, "Squeezed States of Light from an Optical Parametric Oscillator," *J. Opt. Soc. Am. B* 4:1465 (1987).

[4] S-T. Ho, P. Kumar, and J.H. Shapiro, "Quantum Theory of Nondegenerate Multiwave Mixing," *Phys. Rev. A* 35:3982 (1987).

[5] S-T. Ho, P. Kumar, and J.H. Shapiro, "Quantum Theory of Nondegenerate Multiwave Mixing: General Formulation," *Phys. Rev. A* 37 (1988).

[6] R.K. John, J.H. Shapiro, and P. Kumar, "Classical and Quantum Noise Transformations Produced by Self-Phase Modulation," *J. Opt. Soc. Am. B* 4:P226 (1987).

[7] H.A. Haus, and Y. Yamamoto, "Theory of Feedback-Generated Squeezed States," *Phys. Rev. A* 34:270 (1986).

[8] J.H. Shapiro, G. Saplakoglu, S.-T. Ho, P. Kumar, B.E.A. Saleh, and M.C. Teich, "Theory of Light Detection in the Presence of Feedback," *J. Opt. Soc. Am. B* 4:1604 (1987).

[9] G. Saplakoglu, *Photodetection Feedback Systems,* Ph.D. diss. proposal, Dept. of Electr. Eng. and Comp. Sci., MIT, 1987.

6.3 U.S.-Japan Seminar on Quantum Mechanical Aspects of Quantum Electronics

Jeffrey H. Shapiro

The continuing rapid developments taking place in quantum electronics cut across a wide swath of research activities including atomic and solid-state physics, nonlinear optics and spectroscopy, and quantum light beams and quantum measurement. Strong research programs in these areas presently exist in the United States and Japan. The fourth in a series of U.S.-Japan Seminars on Quantum Electronics was held from July 21 to July 24, 1987 in Monterey, California. Professor J.H. Shapiro, of MIT, served as the U.S. Coordinator for this event, and Professor H. Takuma, of the University of Electro-Communications, Tokyo, served as the Japanese Coordinator. Major funding for this Seminar was obtained from the U.S. National Science Foundation, and the Japan Society for the Promotion of Science. The Seminar program focused on topics of very current interest including: neutral atom trapping; ultrahigh stability sources and ultrahigh resolution spectroscopy; squeezed states of light; and nonlinear optics of semiconductors. A Proceedings was produced under funding from the U.S. Office of Naval Research.[1]

Reference

[1] J.H. Shapiro and H. Takuma, *United States - Japan Seminar on Quantum Mechanical Aspects of Quantum Electronics,* Final Report, U.S. Office of Naval Research Contract N00014-87-G-0198, MIT, Oct. 1987.

6.4 Laser Radar System Theory

Jeffrey H. Shapiro, Dongwook Park, Robert H. Enders, Stephen M. Hannon, Naomi E. Zirkind

Coherent laser radars represent a true translation to the optical frequency band of conventional microwave radar concepts. Owing to the enormous wavelength disparity between microwaves and light, laser systems offer vastly superior space, angle, range, and velocity resolutions as compared to their microwave counterparts. However, the resolution benefits associated with the shortness of laser wavelengths are accompanied by the penalties of this wavelength region: the ill-effects of atmospheric optical wave propagation in turbulent or turbid conditions, and the speckle patterns resulting from target roughness on wavelength scales. The ensuing trade-off between resolution advantages and propagation/speckle disadvantages makes it likely that laser radars will fill new application niches, rather than supplant existing microwave systems. We have been working to quantify the preceding issues through development and experimental validation of a laser radar system theory. Our work includes a collaboration arrangement with the Opto-Radar Systems Group of the MIT Lincoln Laboratory, whereby the experimental portions of the research are carried out with measurements from their CO_2 laser radar test beds.

Multipixel Detection Theory

We have been developing the appropriate target-detection theory for multipixel multidimensional laser radar imagers. We have established the structure of quasi-optimum intensity-only, range-only, and joint range-intensity processors for deciding whether or not a speckle target is present within an image frame.[1] This problem has been solved for the realistic case in which the target, if it is present, has unknown azimuth, elevation, range, and reflectivity, and in which there is a spatially-extended speckle background of unknown reflectivity. The structure of these processors coincides with those employed in ad hoc designs, i.e., the intensity-only system searches for intensity contrast, and the range-only processor seeks out vertical objects. The great advance in our work over ad hoc treatments is its associated performance results,[1] which allow analytical trade-off assessments to be made between radar-system parameters and target-detection performance. Our initial performance results, which were limited to intensity-only and range-only processors, have since been generalized to relax certain structural assumptions.[2] They have also been verified through computer simulation of the fundamental pixel-statistics developed and experimentally confirmed in earlier work.[3] This simulation program is now being used to obtain performance results for the joint range-intensity processor; a laser radar experiment is being planned to test the performance predictions obtained from the simulation.

Multipixel Laser Radar Target Tracking

The preceding target detection work is a multipixel multidimensional single-frame theory. Once a laser radar has detected a target, it will usually need to track that target. Here we have a multipixel multidimensional multiframe task. In recent work,[4] we have

established a basic theory for such tracking problems. The correct pixel-level statistics are used to develop the first and second moments of an observation equation for use in a Kalman-filter track-while-image linear least-squares algorithm. For a variety of observation structures, e.g., intensity-only, range-only, joint range-intensity, etc., it turns out the the Kalman filter problem that results is non-standard in that the nth-frame observation statistics involve a signal-dependent noise term. Nevertheless, we have been able to develop a filtering procedure and performance equations for the resulting observation equations.

High-Resolution Optical Imagers

A microwave synthetic aperture radar (SAR) exploits coherent target-return processing to achieve an along-track spatial resolution better than its antenna's diffraction limit. It also uses its range resolution capability to enhance its cross-track spatial resolution. In a similar vein, a microwave range-Doppler (RD) radar uses its range and Doppler resolutions to obtain high spatial-resolution imagery of rotating objects. We have been studying the translation of SAR and RD techniques into the optical-wavelength region.[5] Like our previous studies of angle-angle imagers, this work on high-resolution imagers has focused on the following key performance measures: spatial resolution, carrier-to-noise ratio (CNR), and signal-to-noise ratio (SNR). We have developed results for performance under ideal operating conditions, and then examined the effects of laser frequency instability, turbulence, and target/radar motion errors on system performance.

Adaptive Optics for Laser Radars

The speckle-target performance of coherent laser radars improves with increasing aperture size in free space. In the presence of atmospheric turbulence, however, the performance of a conventional coherent laser radar does not improve above turbulence-limited values as aperture size is increased beyond an atmospheric coherence length. We have been studying the use of adaptive optics to compensate for the turbulence-induced degradations of spatial resolution and CNR in an angle-angle imager.[6] The goal of this work is to understand the improvement in performance that can be obtained, in principle, with adaptive optics, and to specify the structure of the systems needed to approach this improved performance. To date, the performance gains that accrue when turbulence can be perfectly measured and corrected have been established. A scheme for measuring the turbulence parameters from target returns has been postulated, and shown to suffer from an unfortunate coupling between fluctuations that are due to turbulence and those that are due to target speckle. Work is continuing on both the separation of the turbulence and speckle contributions, and on what can be done with combined turbulence/speckle information if the preceding separation cannot be effected.

References

[1] M.B. Mark and J.H. Shapiro, "Multipixel, Multidimensional Laser Radar System Performance," *Proc. SPIE* 783:109 (1987).

[2] S.M. Hannon, *Performance Analysis of Quasi-Optimal, Multipixel Laser Radar System Processors,* S.M. thesis, Dept. of Electr. Eng. and Comp. Sci., MIT, 1987.

[3] J.H. Shapiro, R.W. Reinhold, and D. Park, "Performance Analyses for Peak-Detecting Laser Radars," *Proc. SPIE* 663:38 (1986).

[4] R.H. Enders, *Laser Radar Tracking Theory,* Ph.D diss. proposal, Dept. of Electr. Eng. and Comp. Sci., MIT, 1987.

[5] D. Park, *High-Resolution Laser Radar Performance Analysis,* Ph.D. diss., Dept. of Electr. Eng. and Comp. Sci., MIT, 1988.

[6] N.E. Zirkind, *Adaptive Optics for Large Aperture Coherent Laser Radars,* Ph.D. diss. proposal, Dept. of Electr. Eng. and Comp. Sci., MIT, 1987.

6.5 Fiber-Coupled External-Cavity Semiconductor High Power Laser

Robert H. Rediker, Christopher J. Corcoran, So Kuen Liew, Lily Pang, Asli Ural

We have reported in previous progress reports the high-spectral-purity pulse and cw coherent output that has been obtained from a linear array of five discrete external-cavity diode lasers by placing in the cavity a spatial filter at the Fourier plane of the lens system between the AR-coated diodes and the feedback mirror. We now report results on the intensity and phase distribution of the near field of the ensemble. Results were obtained for spatial filters with various ratios of slit opening to the slit center-to-center spacing. For all filters of practical interest, two eigenmodes are shown to exist: in one, the outputs from adjacent diodes are in phase: in the other they are 180° out of phase. These eigenmodes are switched by moving the filters laterally by half the 10.42 μm spacing between the centers of their slits. The theoretical explanation of the experimental results clearly validates the model that has been used to explain the operation of the coherent ensemble. With this validation, extrapolation of the performance obtained with the ensemble of five lasers to that of an ensemble with a large multiplicity of lasers is possible.

Limited tuning of the output wavelength has also been accomplished by effectively varying the center-to-center slit spacing.

Publication

Rediker, R.H., S.K. Liew, and C. Corcoran, "Near Field Distribution and Output Wavelength Tuning of a Coherent Array of Discrete Diode Lasers," *J. Opt. Soc. Am. A* 4 (13):74 (1987).

6.6 Analog Processing of Optical Wavefronts Using Integrated Guided-Wave Optics

Robert H. Rediker, Donald E. Bossi, Suzanne D. Lau Shiple

This program, which was initiated in March 1987, seeks to explore the fundamental issues associated with optical wavefront correction using integrated guided-wave optical devices in GaAlAs. Device fabrication and optimization are performed at MIT Lincoln Laboratory and evaluation will be performed at the Research Laboratory of Electronics. During 1987, two key areas of research have been addressed. Namely, we have begun to examine the design, fabrication, and optimization of 1) dielectric waveguides in GaAlAs for single-mode operation at $\lambda = 0.85$ μm, and 2) adiabatic antennas to efficiently couple light between these waveguides and free space.

Heterojunction ridge waveguides have been fabricated in GaAlAs. For these first devices epitaxial layers of $Ga_{1-x}Al_xAs$ were grown upon a GaAs substrate using a metal-organic chemical vapor deposition (MOCVD) technique. A waveguide ridge was then chemically etched in the epitaxial film. The performance of these waveguide devices is currently being evaluated at GaAlAs laser wavelengths. The goals of this experiment are to optimize the fabrication of GaAlAs waveguides for single-mode operation at $\lambda = 0.85$ μm and to examine the optical attenuation (loss) of these waveguide structures at the same wavelength.

For the antennas the concept of a tapered waveguide (a waveguide which tapers to a point) is being pursued. This dielectric antenna is the optical analog to the polyrod antenna which is used at microwave frequencies. The advantages of adiabatic waveguide antennas are as follows: 1) they serve as a means to increase the coupling efficiency between free-space radiation and the guided optical modes; and 2) for an array of single-mode waveguides they will increase the efficiency with which the radiating (or receiving) surface is filled. Our first experimental tapered antennas were fabricated in Ti:LiNbO$_3$ because this is currently a more established waveguide technology. The devices which were incorporated on the first sample include a variety of taper lengths and taper angles. Experimental evaluation of these devices is currently underway. Using a fabrication technique that has been independently developed at Lincoln Laboratory, a program is underway which we believe will produce two-dimensional tapered waveguide antennas in GaAlAs.

Professor Peter A. Wolff

7.0 Infrared Nonlinear Optics

Academic and Research Staff

Prof. P.A. Wolff, Prof. L.R. Ram-Mohan, Dr. P. Becla, Dr. S.Y.C. Yuen

Graduate Students

C. McIntyre, J. Stark, D. Walrod, S. Wong

7.1 Nonlinear Optics in HgCdTe

DARPA/Universities Research Initiative (Contract N00014-46-K-0760)

Sunny Y.C. Yuen, Peter A. Wolff

We have recently demonstrated[1] a third order optical susceptibility of 1.5×10^{-3} esu in a $Hg_{0.84}Cd_{0.16}Te$ epilayer with small band gap at 80 K. The relaxation time for the nonlinear effect was measured to be 5 psec., and identified as the thermalization of the electrons. The observed $\chi^{(3)}$ is ten times larger than that we reported[2] in HgTe, which then was the largest known $\chi^{(3)}$ with picosecond response times. The non-linear susceptibilities were measured with four-wave mixing experiments using a pair of Q-switched CO_2 lasers.

The nonlinear mechanism in small-gap HgCdTe is different from the band filling effect observed in larger gap HgCdTe alloys. Band filling provides larger nonlinear susceptibilities, but the response is slow and the nonlinearity saturates at quite low pump intensities. By contrast, the fast nonlinear mechanism we observe in small-gap HgCdTe decreases only mildly with pump intensity.

The optical nonlinearity of small-gap HgCdTe is attributed to interband population modulation, caused by carrier temperature fluctuations. Laser heating modulates the carrier temperature relative to the lattice; the resulting nonlinearity is large because the electron mass is small. Calculations suggest that a $\chi^{(3)} \simeq 2 \times 10^{-2}$ esu can be achieved in a material in which the $\Gamma_8 - \Gamma_6$ band gap approaches zero.

7.2 Optical Nonlinearity in Superlattices

SDI/IST managed by the Naval Research Laboratory (Contract N00014-87-K-2031)

L. Ramdas Ram-Mohan, Sunny Y.C. Yuen, Peter A. Wolff

Some years ago, Yuen[3] suggested that spatially varying effective masses could cause large, free-carrier-induced optical nonlinearities in superlattices. To further explore this proposal, that has never been tested experimentally, we are developing accurate general techniques for computing superlattice band structures in materials such as HgTe/CdTe. The analysis involves a 16x16 transfer matrix technique that rigorously describes that spatial evolution of eight coupled conduction and valence bands in diamond type

semiconductors. The program involves a novel routine for calculating the exponential of a 16x16 matrix (8 wave functions and their derivatives). Preliminary calculations give excellent agreement with previous superlattice band structures.

These techniques will next be used to compute superlattice dielectric constants and optical nonlinearities. In optimizing the latter, we will be guided by previous studies of the free-carrier-induced optical nonlinearities of semiconductors which suggest that the largest nonlinearities occur when the character of the carrier wave functions changes rapidly with temperature.[4]

This theoretical work is being performed in collaboration with NRL, which is doing experimental studies of carrier dynamics and band structure in HgTe/CdTe superlattices.

7.3 Negative Magnetoresistance and Current-Voltage Characteristics of HgTe/CdTe superlattices.

7.4 Negative Magnetoresistance and Current-Voltage Characteristics of HgMnTe

Stephen Wong, Piotr Becla, Peter A. Wolff

At low temperature, p-type HgMnTe has an enormous negative magnetoresistance;[5] in some cases magnetic fields of 6 T decrease the resistivity by factors as large as $10^5 - 10^6$. This dramatic effect has been ascribed to "magnetic boil-off" or a field-induced metal-insulator transition. To explore the mechanisms of the large conductivity change, we have performed pulsed, high field measurements of current-voltage characteristics in p-HgMnTe. Avalanche breakdown is observed in large electric fields; short pulse experiments assure that the effect is electronic rather that thermal. The form of the i-v curves precludes the boil-off mechanism, as also implied by low temperature conductivity measurements.[6]

Theoretical calculations suggest that magnetic field-induced acceptor overlap, resulting from the unusual valence splittings of p-HgMnTe, could cause the metal-insulator transition. This hypothesis will be tested with higher field (to 19 T) magnetoresistance measurements. Unusual non-linear optic effects are also anticipated in p-HgMnTe.

References

[1] S.Y. Yuen, P.A. Wolff, K.A. Harris, J.W. Cook, Jr., and J.F. Schetzina, *J. Vac. Sci. Tech.* In press.

[2] P.A. Wolff, S.Y. Yuen, K.A. Harris, J.W. Cook, Jr., and J.F. Schetzina, *Appl. Phys. Lett.* 50:1858 (1987).

[3] S.Y. Yuen, *Appl. Phys. Lett.* 42:331 (1983).

[4] P.A. Wolff, S.Y. Yuen, and G.A. Thomas, *Solid State Commun.* 60:645 (1986).

[5] A. Mycielski and J. Mycielski, *J. Phys. Soc. Japan* 49, Suppl. A:807 (1980).

[6] T. Wojtowicz, T. Dietl, A. Sawicki, W. Plesiewicz, and J. Jaroszynski, *Phys. Rev. Lett.* 56:2419 (1986).

Professor Marc A. Kastner and Research Assistant Jerome C. Licini

8.0 Phase Transitions in Chemisorbed Systems

Academic and Research Staff

Prof. A.N. Berker

Graduate Students

K. Hui, J.F. Marko

8.1 Selenium Chemisorbed onto Nickel (100): Deviations from the Ashkin-Teller Model

A. Nihat Berker

In view of the interpretation of electron scattering experiments, the microscopics of selenium atoms chemisorbed onto the nickel (100) surface is considered. An exact mapping onto Ashkin-Teller variables is reviewed. It is seen that the adatom-adatom interactions deviate from the Ashkin-Teller Hamiltonian. These interactions involve helicity and also otherwise violate the Ashkin-Teller symmetry. A phase diagram excluding the Ashkin-Teller topology is presented for selenium on nickel (100) from an extensive renormalization-group calculation in agreement with published finite-size scaling calculation. This phase diagram exhibits, in addition to 2x2 and $\sqrt{2}$ x $\sqrt{2}$ phases, a 2x1 phase with a disordering boundary with non-universal critical behavior.[1]

8.2 HCP versus FCC Freezing of Hard Spheres: A Variational Density Functional Study

John F. Marko

A density-functional calculation is used to study the crystallization transition in the three-dimensional hard-sphere fluid, determining lattice parameter, density, and real-space peak width of the ordered phase variationally for hexagonal-close-packed, face-centered-cubic, and body-centered-cubic lattices. Using the short-range Percus-Yevick approximate structure factor, it is found that the HCP and FCC lattices have very nearly the same transition properties, with HCP the slightly more stable phase at the melting point. The BCC phase is highly metastable, having a free energy higher than the isotropic liquid phase. When the more realistic and longer-ranged Waisman-Henderson-Barker structure factor is used, the degeneracy of the HCP and FCC phases is broken, HCP being the favorable structure, while the BCC phase continues to be highly metastable. Also, the effect of anharmonicity in the density functional is investigated and is seen to shift the real-space lattice peaks only slightly away from being pure Gaussians.[2]

8.3 Reentrant Behavior of an Anti-Metamagnet in Magnetic Field

Kenneth Hui

We introduce an "anti-metamagnet" model, which is an Ising cubic lattice with nearest-neighbor antiferromagnetic couplings in the x and y directions, and nearest-neighbor ferromagnetic couplings in the z direction. It is called an anti-metamagnet because it can be derived from a metamagnet by reversing the signs of all the interactions in a metamagnet. The anti-metamagnet in a uniform magnetic field is studied by an extended mean-field method. In this method, the lattice is divided into "bundles" of spins along the z direction. Each bundle is composed of four columns (lines) of spins along the z direction and each of them is imbedded in the mean field of its neighboring bundles. The interactions within the bundle and the mean field due to the neighbors are solved exactly using the transfer-matrix method along the z direction. Within this extended mean-field calculation, the system exhibits a reentrant second-order phase boundary which separates the disordered phase from the antiferromagnetic phase. In the reentrant region, the system approaches a picture of effectively one-dimensional disordered Ising models surrounded by fully magnetized lines of spins.[3]

8.4 The Hard Ellipsoid Fluid: First-Order Phase Transitions to Plastic Crystal, Liquid Crystal, and Crystal Phases using Optimized Direct Pair Correlations

John F. Marko

The statistical mechanics of a fluid of prolate ellipsoids of revolution is addressed using density-functional methods. The direct pair correlation function of the isotropic liquid required by this method is adjusted from the Pynn-Wulf form using a variational approach, and then is used in a density-functional theory for the transitions to ordered phases. For the first time, calculations have been done with a density functional that can properly describe the narrow real-space peaks at crystallization transitions, and that can accommodate simultaneous translational and orientational ordering. As a result, transitions to the (orientationally ordered) solid, as well as to the (orientationally disordered) plastic crystal and nematic fluid phases can be described, and the resulting phase diagram is in quantitative agreement with Monte Carlo results.[4]

8.5 Exact Statistical Mechanics of a One-Dimensional Fluid of Hard Cores with Orientational and Translational Degrees of Freedom

John F. Marko

A fluid of anisotropic hard cores with orientational as well as one-dimensional translational degrees of freedom is studied using the Ornstein-Zernicke integral equation for the direct and usual pair correlation functions. For the class of systems studied, this integral equation can be solved to yield the exact correlation functions, and thus an exact description of thermodynamic properties. Application of these results to improving approximations for direct correlation functions of three-dimensional fluids with orientational degrees of freedom is discussed.[5]

References

[1] A.N. Berker, R.G. Caflisch, and A. Aharony, preprint (1988).

[2] J.F. Marko, *Phys. Rev. Lett.*, submitted (1988).

[3] K. Hui, *Phys. Rev. B*, to be published (1988).

[4] J.F. Marko, preprint (1988).

[5] J.F. Marko, preprint (1988).

Left to right: Dr. Paul Horn, Professor Robert J. Birgeneau, Alan Mak

9.0 X-Ray Diffuse Scattering

Academic and Research Staff

Prof. R.J. Birgeneau, Dr. J.W. Chung, Dr. C.J. Peters

Graduate Students

K. Evans-Lutterodt, J. Hill, H. Hong, B. Keimer, A. Mak, D.Y. Noh, E. Specht, T. Thurston

Joint Services Electronics Program (Contract DAALO3-86-K-0002)

Robert J. Birgeneau

In this research program, modern x-ray scattering techniques are used to study structures and phase transitions in thin films and on surfaces. We have two principal experimental facilities. At MIT we have four high-resolution computer-controlled x-ray spectrometers using high intensity rotating anode x-ray generators. The angular resolution can be made as fine as 1.8 seconds of arc; this enables one to probe the development of order from distances of the order of the x-ray wavelength, $\sim 1\text{Å}$, up to 30,000Å. The sample temperature may be varied between 2K and 500K with a relative accuracy of $2\text{X}10^{-3}$K. We also have, in collaboration with IBM, a two spectrometer system at the National Synchrotron Light Source at Brookhaven National Laboratory. A third beam line desig̣ ꞏd to operate at short wave lengths is currently being implemented. These make pussible high resolution scattering experiments with a flux more than three orders of magnitude larger than that from a rotating anode x-ray generator; this, in turn, has opened up a new generation of experiments.

As part of this JSEP program we have built an x-ray compatible high vacuum single crystal apparatus. This enables us to use synchrotron radiation to study the structure and transitions occurring at a single surface; the first generation of such experiments has now been performed. Our current experiments in this program are concentrated in two areas: 1) the phases and phase transitions of metal and semiconductor surfaces and surface overlayers; and 2) the structure and phase transitions of rare gas multilayers on simple substrates.

9.1 Metal Surface Studies

For our first detailed studies of metal surface reconstruction we have chosen tungsten, both pure and coated with hydrogen or oxygen. The tungsten system has been exhaustively studied with all of the standard surface techniques including LEED, STM, atom beam scattering, and Rutherford back scattering. In spite of this effort, there are still major controversies concerning the nature of the structures and surface transitions. Our most successful experiments were for W (100) with sub-monolayer coverages of H.

The system of atomic hydrogen chemisorbed onto the surface of tungsten has long been considered a model system for the study of chemisorption. Extensive experimental

studies have shown that the W(100) surface goes through an elaborate sequence of phases and phase transitions as a function of increasing hydrogen coverage; however, the microscopic nature of these successive states remains problematic. We carried out a synchrotron x-ray glancing-angle diffraction study of W(100) at room temperature for a range of hydrogen coverages. The experiments illustrate clearly the utility of x-rays in obtaining quantitative information about the structures and the nature of the disorder in such chemisorbed surface systems.

Our data suggest a simple picture in which at very low coverages there is a tradeoff with increasing coverage, analogous to that in a two-phase coexistence region, between hydrogen-poor and hydrogen-rich regions until a uniform but still disordered $(\sqrt{2} \times \sqrt{2})R45°$ −H phase is attained. This disagrees with the currently accepted model which assumes that the hydrogen atoms are always uniformly distributed on the tungsten surface. With further increase in coverage the surface layer exhibits a commensurate-incommensurate transition (CIT) which, rather than being a solid-solid transition as previously assumed, is actually a lattice-gas melting transition into a domain-wall fluid phase. Such surface domain-wall fluid phases should occur commonly in chemisorbed systems.

We find that the line-shape in the $(\sqrt{2} \times \sqrt{2})R45°$ −H phase is well-described as a Lorentzian raised to the 3/2 power. This line-shape is indicative of random field effects in two dimensions. Specifically, in surface lattice-gas systems, impurities and defects which fix the sublattice locally act as random fields which round the freezing transition and prevent the achievement of true long range order. Such random field effects have not been seen in previous surface diffraction experiments; only x-rays provide the resolution and simple kinematical interaction to allow such quantitative line-shape analysis.

9.2 Rare Gases on Graphite

In the last year, we completed two major experiments on monolayer rare gas films. First we carried out an encyclopaedic high resolution x-ray diffraction study of the structures and phase transitions of monolayer krypton, adsorbed on both powder and single crystal graphite substrates. A comprehensive series of powder diffraction profiles was used to construct the two-dimensional phase diagram. The melting of the commensurate solid was shown to be strongly first order throughout the region where tricritical behavior was previously thought to occur; fluid-solid coexistence extends up to the termination of the commensurate phase at 130 K. A disordered, weakly incommensurate phase with lattice constant smaller than that of the $\sqrt{3} \times \sqrt{3}$ phase was shown to be reentrant fluid, a system which may be described as a disordered network of domain walls and which evolves continuously into a more conventional 2D fluid. This evolution is marked by the disappearance of satellite peaks which are caused by the modulation of the overlayer by the substrate. The freezing of the reentrant fluid into the commensurate phase was shown to be consistent with a chiral Potts transition, its freezing into the incommensurate solid consistent with a dislocation binding transition. Single crystal experiments revealed the orientation of the weakly incommensurate phase. The reentrant fluid was found to have no visible orientational fluctuations, manifesting isotropic diffraction peaks. This is attributed to the strong epitaxy of domain walls. The incommensurate solid was shown to undergo an aligned-rotated transition which is well described by zero-temperature calculations.

Second, we carried out an extensive synchrotron x-ray study of monolayer xenon on single crystal graphite. A monolayer of xenon freezes at ~135K into an incommensurate solid. The incommensurate solid undergoes the sequence of phases with decreasing temperatures aligned → rotated → reentrant aligned, before transforming at ~70K into a commensurate $\sqrt{3} \times \sqrt{3}$ R45° solid. The current theory of orientational epitaxy correctly predicts only the point at which the rotated → reentrant aligned transition occurs. None of the current theories can explain the entire sequence. The reentrant aligned phase at intermediate temperatures is an incommensurate solid with a network of superlight domain walls. The observed phase transition into the commensurate phase is first order consistent with domain wall theories. The incommensurability decreases as

$$\left[\frac{T - T_0}{T_0} \right]^{1/3}$$

until the first order C-IC transition point is encountered. This 1/3 power law is apparently a universal behavior shared with Kr on graphite.

We have estimated the potential corrugation of the surface adsorbtion from the intensity ratios between the main and satellite peaks in the domain wall incommensurate phsae. The corrugation of the potential estimated is close to that predicted by Steele. Along with this estimation from the onset of the rotated phase, we are able to set the limits for the dimensionless wall width, $36 < \ell_0 < 42$. Also we estimated the wall crossing energy which turned out to be +60K. However, the striped phase, predicted by Halpin-Healy using a similar value was not observed.

9.3 Surface Roughening of Ag

Direct evidence of the thermal roughening of Ag (110) surface has been observed in a high resolution x-ray scattering experiment at the National Synchrotron Light Source of the Brookhaven National Laboratory. Information about the surface roughness, as manifested in the height-height correlation function, is obtained from the scattering intensity profile of the bulk forbidden $(1\bar{1}0)$ surface peak. The results indicate that surface roughening occurs at $T_r = 450 \pm 25$°C. Below T_r, the Ag (110) surface is smooth, as characterized by delta function Bragg scattering, whereas above T_r, the scattering intensity obeys a power law lineshape, indicating a rough surface with logarithmically divergent height fluctuations. Since the transition is reversible with temperature, it is indeed an equilibrium phase transition. Furthermore, the fact that the integrated intensity of the bulk Ag (111) peak undergoes little change during the transition, apart from the Debye-Waller factor, demonstrates that the observed changes in bulk forbidden $(1\bar{1}0)$ peak are due exclusively to changes in the surface morphology. In contrast to atom scattering and LEED experiments which have significant multiple scattering and inelastic scattering, x-ray experiments allow relatively simple data analysis. Coupled with the high resolution of our experiment, we have demonstrated a very powerful technique for studying surface roughening.

Publications

Mochrie, S.G.J., A.R. Kortan, P.M. Horn, and R.J. Birgeneau, "Novel Melting Transition in a Two-Dimensional Stripe-Domain System," *Phys. Rev. Lett.* 58:690 (1987).

Chung, J.W., K. Evans-Lutterodt, E.D. Specht, R.J. Birgeneau, P.J. Estrup, and A.R. Kortan, "Grazing-Incidence X-Ray Study of the Structures and Phase Transitions of Hydrogen on Tungsten (100)," *Phys. Rev. Lett.* 59:2192 (1987).

Specht, E.D., A. Mak, C. Peters, M. Sutton, R.J. Birgeneau, K.L. D'Amico, D.E. Moncton, S.E. Nagler, and P.M. Horn, "Phase Diagram and Phase Transitions of Krypton on Graphite in the Extended Monolayer Regime," *Z. Phys.* B 69:347 (1987).

Held, G.A., J.L. Jordan-Sweet, P.M. Horn, A. Mak, and R.J. Birgeneau. "X-Ray Scattering Study of the Thermal Roughening of Ag(110)," *Phys. Rev. Lett.* 59:2075 (1987).

10.0 Semiconductor Surface Studies

Academic and Research Staff

Prof. J.D. Joannopoulos, Dr. G. Gomez-Santos, Dr. E. Kaxiras, Dr. O. Alerhand

Graduate Students

T. Arias, M. Needles, A. Rappe, E. Tarnow, J. Wang

John D. Joannopoulos

Understanding the properties of surfaces of solids and the interactions of atoms and molecules with surfaces has been of extreme importance both from technological and academic points of view. The recent advent of ultrahigh vacuum technology has made microscopic studies of well-characterized surface systems possible. The way atoms move to reduce the energy of the surface, the number of layers of atoms involved in this reduction, the electronic and vibrational states that result from this movement, and the final symmetry of the surface layer are all of utmost importance in arriving at a fundamental and microscopic understanding of the nature of clean surfaces, chemisorption processes, and the initial stages of interface formation. Actually, one of the most difficult and fundamental problems in surface studies, both from the experimental and theoretical points of view is simply the determination of the precise positions of the atoms on a surface. Currently, there are many surface geometries, even for elemental surfaces, that remain extremely controversial.

The theoretical problems associated with these systems are quite complex. We are, however, currently in the forefront of being able to solve for the properties of real surface systems (rather than simple mathematical models). In particular, we are continuing our goal of calculating the total ground-state energy of a surface system from "first principles" so that we may be able to provide accurate theoretical predictions of surface geometries. Our efforts in this program have concentrated in the areas of surface growth reaction pathways, surface reconstruction geometries, structural phase transitions, and hyrdogenation.

10.1 Surface Reconstruction Geometries

Using "first principles" total energy calculations, it is possible to determine on a microscopic scale how atoms behave when they are on the surface of a solid. This is a fundamental problem that has plagued both theorists and experimentalists for decades. The difficulty lies with the very strong interactions that may exist between the surface atoms and the host atoms constituting the rest of the solid. These interactions can strongly disturb the original idealized atomic arrangement at the surface changing the nature of the bonding and even the original stoichiometry.

In recent years there has been considerable activity focused on determining the exact equilibrium geometry of the [111] surfaces of the III-V compounds. In particular, the

($\overline{111}$) As-terminated surface of GaAs stands out as a system that is very poorly understood. Even the relative abundance of Ga and As atoms in the surface region is not established with sufficient accuracy. The multitude of diffraction patterns observed on this surface (e.g., (2x2), (3x3), ($\sqrt{19} \times \sqrt{19}$)) and their sensitivity to preparation conditions make the problem very intriguing. The layer of exposed As atoms that constitutes the unreconstructed ($\overline{111}$) bulk plane is apparently unstable leading to a rich variety of surface reactions and atomic arrangements. No model has yet to emerge as a satisfactory candidate for any of these reconstructions.

In this work we have focused on the most stable observed pattern, namely the (2x2) reconstruction. The variety of structural models, for the reconstructions of this surface, that we have considered are shown in figure 10.1. The total energies for these structures, calculated as a function of the relative chemical potential of Ga and As atoms are summarized in figure 10.2.
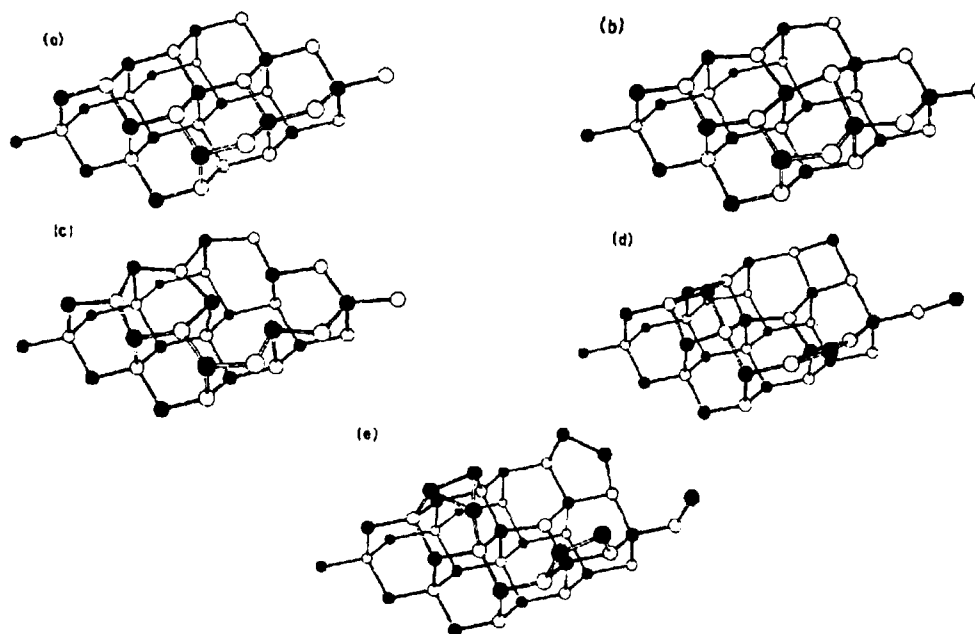
Figure 10.1. Structural models for the (111) surface (2x2) reconstructions. The first four atomic layers are shown in perspective. The atoms in each layer outline the (2x2) unit cell, in the ideal configuration. The same atoms and their nearest neighbors are shown in the other reconstructions. Solid circles represent As atoms and empty circles represent Ga atoms. (a) Ideal surface. (b) Buckled geometry; a variation of this is the substitutional geometry. (c) Vacancy geometry; variations of this are Ga-vacancy plus Ga-substitutional geometry and the Ga-vacancy plus As p -bonded geometry. (d) Adatom geometry. (e) Triangle geometry.

From these results we can predict that phase transitions will occur, as the relative chemical potential scans its range, whenever two lowest energy lines cross and different reconstructions become the lowest energy configuration. Note that two such crossings occur in figure 10.2. The results presented here are for perfectly equilibrated surfaces and care must be taken to include kinetic effects which can be crucial in certain cases. Thus the very low sticking coefficient of As indicates it is unlikely that As-adatom models (either the single As adatom of the As-triangle) will be observable on the As-
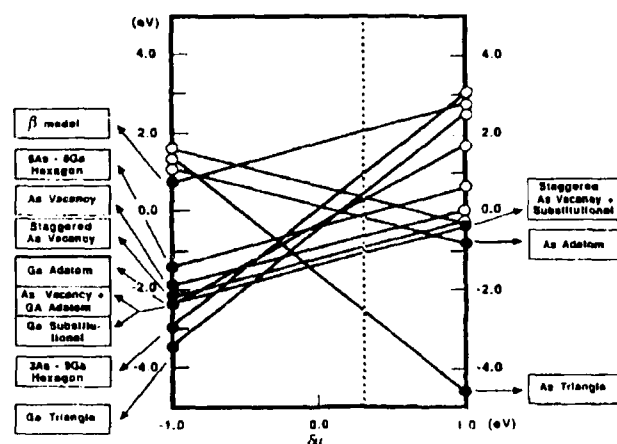
Figure 10.2. Energy versus relative chemical potential $\delta\mu$ of the different reconstruciton models of the (111) surface. The range of $\delta\mu$ scans the values conr stent with the Ga bulk and As_2 gas reservoirs. The closed dots are the calculated energies per (2x2) unit cell with respect to the ideal surface. The dashed line indicates the upper limit of $\delta\mu$ constistent with an As_4 gas reservoir.

terminated surface. It may, in fact, be rather difficult to simulate the surface As-rich environment at all. It is more reasonable to suggest that an experimentally observed As-rich reconstruction should be one of the two lowest energy geometries in the $-0.3 < \delta\mu < -0.1$ eV range. That is, either the staggered As vacancy or the Ga-adatom configurations. We are inclined to favor the staggered As vacancy. On the other hand, the Ga-rich reconstruction is most certainly the Ga-triangle, both from energetic and structural considerations. It is the lowest-energy geometry among all the negative stochiometry models and presents the most favorable coordination once all the surface As and part of the surface Ga has been removed.

10.2 Structural Phase Transitions

All the calculations described in the previous section were at zero temperature. It is now becoming possible, however, to begin studying the statistical mechanics and temperature related phase transitions of surfaces of solids. This is a completely new and unexplored area. As an example, the myriad of surface reconstructions that may exist on clean semiconductor surfaces at different temperatures is an exrremely interesting and fundamental problem that needs to be investigated. Modern studies of phase transitions utilize a powerful theoretical tool which is the renormalization group scheme. The scheme is based on scaling ideas, and has as input simple spin Hamiltonians which model the degrees of freedom of the system. Until now there has been no way of calculating what these Hamiltonian parameters shoula be for real surfaces of solids. The total energy calculations described above, however, should provide precisely the kind of information needed. The exciting possiblity then arises of coupling the results of microscopic studies of surface systems (at zero temperature) with simple spin Hamiltonians and the renormalization group approach to study phase transitions at finite temperatures from "first principles."

In the past, using a simple semi-empirical total energy approach we succeeded in developing such a scheme and have applied it to the Si(100) surface, resolving impor-

tant questions regarding the structure of the Si(100) surface. We are investigating the possible phase transitions that may occur on the Ge(100) surface. This system, however, cannot be described accurately by a semi-empirical approach so that we are forced to use the more powerful and much more complex *ab-initio* total energy method discussed in section 10.1.

To perform these studies we have been developing a new scheme for relaxing a system with many degrees of freedom to its lowest energy configuration. The scheme is based on a molecular dynamics approach to calculating quantum mechanical total energies and resembles a simulated quench.

Using this approach we have calculated the total energy of various dimer models with either (2x1) or C(4x2) symmetry. The lowest energy dimer configuration for each rconstruction is shown in figure 10.3. We find, in particular, that the C(2x4) reconstruction is lower in energy that the (2x1) by 0.05 eV/dimer. The reason for this lies in the relaxation of the atoms in the second layer with respect to the dimers. Moreover, we find for the C(2x4) case that the energy surface is surprisingly flat for lateral displacements of the dimers along the surface. This should result in a distinct soft surface-phonon mode for the system.

At present we are performing total energy calculations on P(2x2) and C(2x2) reconstructions in order to have a large enough data-base to calculate a structural phase transistion termperature for Ge(100).
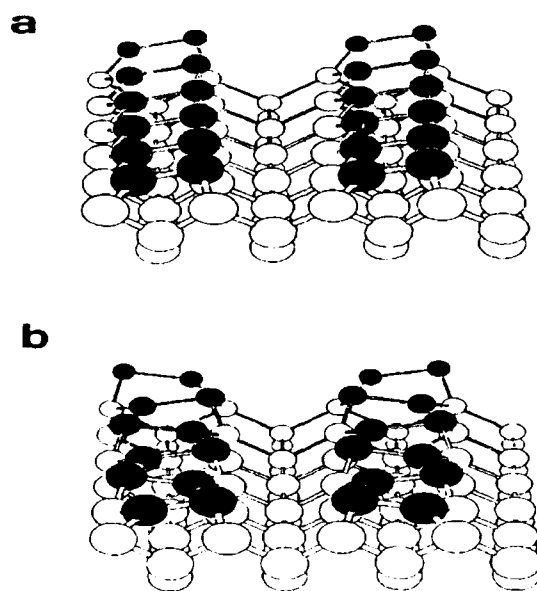
Figure 10.3. Perspective view of dimer models of the Ge(100) surface. The solid atoms are the surface layer. (a) Buckled (2x1) symmetry configuration. (b) Lowest- energy c (4x2)-symmetry dimer configuration obtained from our calculations.

10.3   Hydrogenation

The interaction of atomic hydrogen with cleaned semiconductor surfaces has been extensively studied for over a decade. Hydrogen atoms appear to saturate surface dangling bonds resulting in a nearly ideal, <u>bulk-terminated</u> plane of exposed surface atoms. It is interesting that in cases where the surface does not have the geometry and periodicity of the <u>bulk-terminated</u> plane, the interaction of hydrogen with surface atoms is strong enough to unreconstruct the complicated reconstruction patterns. This process takes place for example on the (2x1) Si(111) surface, which exhibits a low-energy π-bonded-chain reconstruction. Upon hydrogenation this chain of Si atoms with (2x1) periodicity reverts to the (1x1) pattern of the bulk-terminated plane. Similar phenomema have been observed on the Ge(111) surface. Theoretically, this process is not very well understood and a realistic, first-principles study with adequated accuracy to define precise low energy positions of atoms, corresponding total energies, and vibrational excitations above the ground state has been completely lacking.

Recently we have undertaken precisely such a study. Using *ab-initio* quantum mechanical total energy calculations, we find that the atomic positions of the hydrogenated Si and Ge(111) surfaces differ significantly from those of an ideal bulk terminated plane. In particular, the Si-H and Ge-H bonds are found to be considerably larger than the sum of covalent radii. The substrate relaxations are small and their physical origin can be explained in terms of electronic charge transfer which eliminates the surface dipole moment, by shifting charge from the hydrogen bond to the backbonds. This is very clearly illustrated for both Si(111):H and Ge(111):H by examining the total valence electron charge densities as shown in figure 10.4. As indicated in the third panel for each system, charge transfer drives the relaxations in order to cancel the dipole moment induced by the difference in electronegativity between H and Si(Ge).
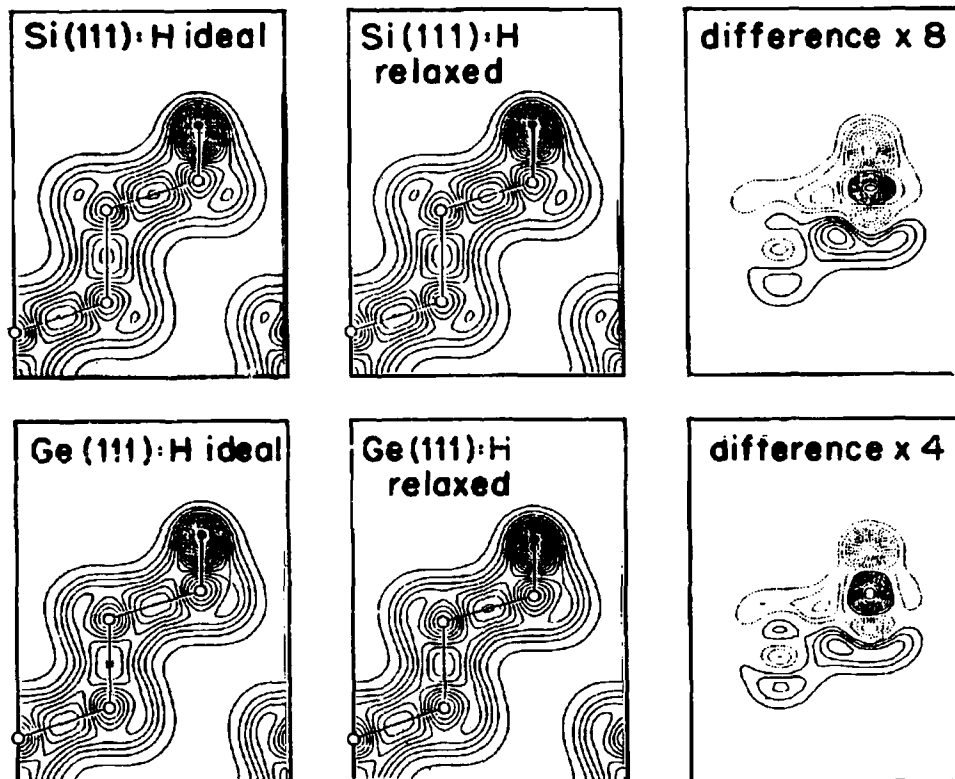
Figure 10.4. Valence charge density of Si(111):H and Ge(111):H plane. Open dots correspond to Si or Ge atoms and solid dots to H atoms. The difference between the ideal and fully relaxed configurations is given in the third panel for each case. Positive contours are shown in continuous lines, negative ones in dotted lines.

11.0 Ultralow-Temperature Measurements of Submicron Devices Nanometer-Scale Semiconductor Devices

Academic and Research Staff

Prof. M.A. Kastner, S.B Field

Graduate Students

U. Meirav, S.L. Park, J. Scott-Thomas

Marc A. Kastner, Stuart B. Field, John Scott-Thomas, Udi Meirav Sam L. Park

Project Goals:

1) To study the behavior of electrons in semiconductor devices so small that the behavior is quantum-mechanical.

2) To understand how the conductivity and other properties of electronic wavefunctions such as many body effects, are altered by confinement in nanometer-scale devices.

In studies of Si MOSFET's about 100 nm wide we discovered a magnetic-field induced transition to a different state of the electron gas, with conductance G about 10 times higher than that in zero field. Above the threshold field G rises in a series of steps as a function of gate voltage. Each of the risers moves to higher gate voltage approximately linearly in magnetic field, suggesting that they occur at fixed filling factor, the ratio of carrier density to flux quantum density. Each plateau disappears at a different temperature revealing a family of phase transitions, one for each plateau. There is no model that predicts in detail the phenomena we have observed. However, it has been suggested that confinement of the two-dimensional electron gas in one additional dimension might lead to a charge or spin density wave instability when the width is comparable to but somewhat larger than the magnetic length, the radius of the Landau orbit. Such instabilities would lead to dissipationless current flow and plateaus in the conductance analogous to those in the two-probe quantum Hall effect. The absence of the usual spin and valley splittings is evidence that the many-body effects are different in the quasi-one-dimensional electron gas than in the usual two-dimensional electron gas.

We are learning that the behavior of electrons in devices smaller than 100 nm is altered in fundamental ways from that in conventional devices. However, at the same time, it raises the possibility that completely new kinds of devices may emerge

Professor Patrick A. Lee

12.0 Quantum Transport in Low Dimensional Disordered Systems

Academic and Research Staff

Prof. P.A. Lee

Graduate Students

W. Xue

12.1 Resonant Tunnelling in Two Directions

Patrick A. Lee, Weige Xue

In devices where the electrons are localized, the dominant transport process is usually Mott variable range hopping and it has been known for some time that in small devices, the hopping conductance exhibits large fluctuations. However, since the hopping processes are thermally activated, such fluctuations are also temperature dependent. In the limit of zero temperature, a different process of charge transport, known as resonant tunnelling, will take over. This is a process where the Fermi energy of the electrons in the electrodes is almost equal to the energy of a localized state in the sample. Resonance transmission can occur and the transmission probability can be as large as unity.

Several years ago, Stone and Lee[1] predicted that a cross-over from the hopping regime to the tunnelling regime will occur for a sufficiently small sample at a sufficiently low temperature. It appears that the cross-over has been observed in two systems. Fowler et al.[2] cooled a Si - MOSFET down to mK temperature and observed temperature independent peaks in the conductance as a function of gate voltage which controls the chemical potential of the electron bath. At about the same time, experiments were done on small tunnel junctions with amorphous semiconductors as barriers,[3] and reproducible structures were observed in the differential conductance. Both these experiments were interpreted as observation of the resonant tunnelling process via localized states in the MOSFET or in the amorphous barrier.

Previous theoretical treatment of the resonant tunnelling process was restricted to one dimension, and one can obtain the result that the conductance is given by

$$G = \frac{e^2}{h} \frac{\Gamma_L \Gamma_R}{(E - E_0)^2 + \frac{1}{4}(\Gamma_L + \Gamma_R)^2} \tag{1}$$

where E_0 is the energy of the localized state, and Γ_L and Γ_R are the decay rate of the electron to the left and right electrodes respectively. Note that the maximum conductance occurs when $\Gamma_L = \Gamma_R$, $E = E_0$, $\wedge G = e^2/h$. This corresponds to perfect

transmission in one dimension. However, in two dimensions, which is appropriate for the MOSFET experiment, perfect transmission corresponds to $G = (e^2/h)N$ where N is the number of channels. (Approximately N equals the sample width divided by the electron wavelength.) Thus the natural question arises, does resonant tunnelling produce a maximium conductance of e^2/h or $(e^2/h)N$ in two dimensions?

We have studied this question both analytically and by computuer simulation.[4] Our conclusion is that the resonant tunnelling process can be described by a linear super-position of Eq. (1) over E_0 corresponding to different localized states. For tunnelling through a single localized state, the maximum conductance is e^2/h. However, if reso-nances overlap, the maximum conductance can exceed unity but never reaches the perfect transmission limit as in one dimension.

We have further studied the effect of a magnetic field normal to the plane on these resonances. We find that the resonant peaks shift in position and magnitude, in a way which provides information on the localization length. It will be interesting to observe the field dependent effects experimentally.

References

[1] A.D. Stone and P.A. Lee, *Phys. Rev. Lett.* 55:324 (1985).

[2] A.B. Fowler, G.L. Timp, J.J. Wainer, and R.A. Webb, *Phys. Rev. Lett.* 57:138 (1986).

[3] S.J. Bending and M.R. Beasley, *Phys. Rev. Lett.* 55:324 (1985).

[4] W. Xue and P.A. Lee, *Phys. Rev. B*, to be published.

13.0 Graphoepitaxy of Colloidal Crystals

Academic and Research Staff

Prof. J.D. Litster

Graduate Students

R. Francis, B. McClain

13.1 Graphoepitaxy of Colloidal Crystals

Joint Services Electronics Program (Contract DAAL03-86-K-0002)

Brian McClain, J. David Litster

This part of the project aims to use surface sensitive x-ray scattering to study the structure of Langmuir-Blodgett films pulled in the standard way from monolayers on the surface of water. These films have potential for device applications and are also model systems for studying the structure of two-dimensional materials.

Last year experiments were carried out on a Langmuir-Blodgett sample with 192 multilayers poymerized with a poly-diacetylene linkage. The layers were pulled from monomers of the cadmium salt of 10,12-nanacosa-diynoic acid dispersed on a substrate containing 10^{-2}M of $CdCl_2$. Polymerization was done by ultraviolet irradiation after the films were pulled. X-ray scattering data for this film that were taken at our beam line at the Brookhaven National Synchrotron Light Source are shown in the figure 13.1; the momentum transfer was normal to the film and shows many harmonics with an interesting alternating intensity of the peaks. No structure could be detected in the plane of the film.

Since then, effort has been devoted to the design and construction of a spectrometer for glancing-angle x-ray scattering from the surfaces of liquids. It has been designed to be used both with on-campus rotating anode x-ray sources and the storage ring at the National Synchrotron Light Source. It will be used to study the structure of the Langmuir film precursors from which the L-B films are drawn.

13.2 Growth of Colloidal Crystals

Joint Services Electronics Program (Contract DAAL03-86-K-0002)

Ronald Francis, J. David Litster

The goal of this portion of the project is to use colloidal crystals of polystyrene latex spheres as models to study epitaxial growth on patterned substrates. Using lithographic techniques, it is possible to control the texture and patterns precisely on the "atomic" scale of the model systems - which is about 0.1 μm. Thus light scattering may be used

to study ordering in these materials in a way analogous to the use of x-rays to study ordinary crystals, with the added advantage that dynamic information can be obtained.

A thin cell in which the ionic strength of the colloid can be reduced to the point where crystallization occurs has been constructed. Preliminary light scattering experiments of the freezing with smooth substrates have been carried out. Unlike the case of x-ray scattering, we have excellent energy resolution with light scattering and can use it to cleanly separate elastic (Bragg) scattering from inelastic (thermal diffuse) scattering. We may also use the technique to study quantitatively the dynamics of the "atomic" motion in the colloidal crystal. Figure 13.1 also shows both the inelastic Bragg scattering intensity, as open circles, and the thermal diffuse intensity was obtained by integrating the inelastic scattered light over the frequency, and has been multiplied by ten to display on the same scale as the elastic scattering.
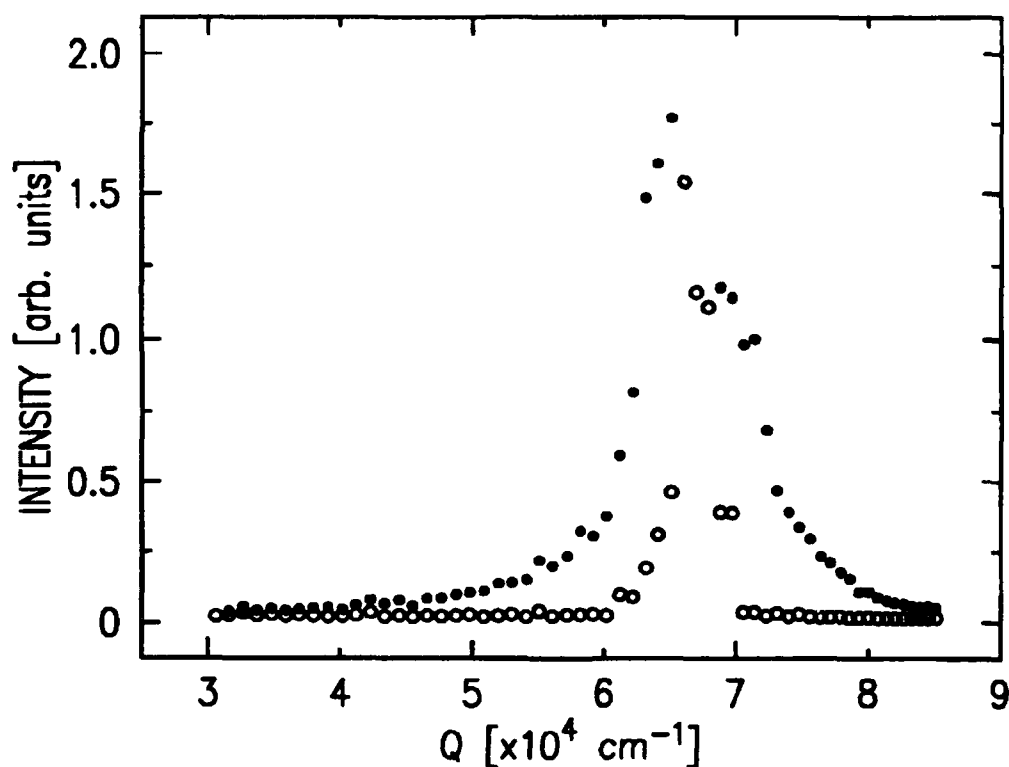
Figure 13.1 Light scattering intensity near a colloidal crystal Bragg peak.

14.0 Photon Correlation Spectroscopy and Applications

Academic and Research Staff

Prof. S-H. Chen, Dr. G. Briganti

Visiting Scientist

Prof. N.M. Zhao[1]

Graduate Students

B. Carvalho, X.H. Guo, D. Wang, X.Y. Wang, C.F. Wu

14.1 Structure, Interaction and Thermodynamics of Surfactant and Polymer Micellar Solutions

Sow-Hsin Chen, Chuan-Fu Wu, Nan Ming Zhao, Xuan-Hui Guo

Small angle neutron and x-ray scattering techniques are used to study the structure and interaction of charged surfactant and polymer micellar aggregates in solution and the distribution of counter ions around the aggregates, respectively. SANS work uses the Biology Low Angle Diffractometer at the High Flux Beam Reactor of Brookhaven National Laboratory while SAXS work uses the 20 meter small angle x-ray Difractometer located at the National Center for Small Angle Scattering Research at Oak Ridge National Laboratory.

We developed a generalized one-component macroion theory for highly asymmetric ionic liquids such as micellar solutions. Combination of the structural studies and the theoretical analyses of the inter-micellar correlations by GOCM lead to an unambiguous method for obtaining: 1) the weight average micellar aggregation number; 2) the re-normalized micellar charge; and 3) the micellar shape and size distributions as functions of the surfactant (polymer) and salt concentration in solutions. Thus the micellar growth and polydispersity can be simultaneously determined, besides various thermodynamical functions which depends on the charge of the micelles. Charged copolymer, poly (1-octadecene-co-maleic anhydride), abbreviated as C18PODMA, was shown to form cylindrical micelles when fully neutralized in aqueous solution. The cylindrical micelle has a dimension on radius R = 24.8 Å and length L = 110 Å at 1 weight percent concentrations. Owing to the high surface charge density, the counterions pile-up near the micellar surface effectively neutralizing large fraction of the

---

[1] Tsinghua University, Beijing, China

charge. We have performed SAXS measurement using C_s^+ as counterions. We were able to, for the first time, directly verify the prediction of the Poisson-Boltzman equation with regard to the counterion distribution.

14.2 Hydrophobicity of the Solvent and Phase Transition in Micellar and Mixed Micellar Solutions

Sow-Hsin Chen, Giussepe Briganti, Bruce Carvalho, Dan Wang

A series of zwitterionic micelles formed from short chain lecithins (dihexanoylphosphatidylcholine, diheptanoly PC and dioctanoyl PC, etc.) in aqueous solutions have been studied by SANS and by photon correlation spectroscopy (PCS). We have analyzed SANS data using a thermodynamic model, called the ladder model, which is expected to be a good model for rod-like micelles. This model contains three basic parameters, namely, the aggregation number of the minimum size micelle, N_0; the free energy gain of forming the minimum size micelle, Δ; and the free energy gain of inserting an additional monomer into a micelle of the minimum size or larger, δ. This model is capable of explaining the phenomenon of critical micelle concentration (CMC) and the growth and polydispersity of micelle as the surfactant concentration is increased or salt is added to the solution. SANS data was shown to yield all three parameters of the theory, i.e., N_0, $K \equiv \exp[(\Delta - N_0\delta)/k_BT]$ and $X_B \equiv \exp[\delta/k_BT]$, besides the structural parameters such as the radius of the cylindrical micelle.

It is known that pure diC_8PC solution show liquid-liquid phase separation at room temperature with an upper consolute temperature occuring at $T_c = 45°C$ in H_2O and at $T_c = 65°C$ in D_2O. We have found that an addition of certain amount of urea in the aqueous solution dramatically lowers the consolute temperatures in both H_2O and D_2O. Urea is a well-known protein denaturant which functions by weakening the hydrophobicity of water. We have shown that the phase separation phenomena in in surfacant solutions can be a very sensitive tool for studying the hyrdophobicity of water.

Another method for changing the phase separation temperatures (or sometimes called cloud points) of a surfactant solution is the addition of salt. We found, however, that a particular class of salts, for example ionic surfactants such as SDS and AOT, is particularly effective in lowering the cloud points. The effect is connected to the formation of mixed micelles in solution. The combined techniques of SANS and PCS are used to study the thermodynamics and the dynamic concentration fluctuation of the surfactant solution near its phase separation temperature. Hydrophobicity of the solvent enters through parameters such as K and X_B of the ladder model.

Publications

Brakto, D., E.Y. Sheu, and S-H. Chen, "Analysis of Intermicellar Structure Factors with the Mean Spherical and Hypernetted-Chain Approximations," *Phys. Rev. A* 35:4359 (1987).

Chen, S-H., and T.L. Lin, "Colloidal Solutions." In *Methods of Experimental Physics,* Vol. 23, Part B *Neutron Scattering,* eds. D.L. Price and K. Skold, 489-543. New York: Academic Press, 1987.

Chen, S-H., T.L. Lin, and C.F. Wu, "SANS Study of Structure, Growth and Polydispersity of Short-Chain Lecithin Micellar Systems. A Ladder Model Analysis." In *Physics of Amphiphilic Layers,* eds. O.J. Meunier, D. langevin, and N. Boccara, 242-252. New York: Springer-Verlag, 1987.

Chen, S-H., and E.Y. Sheu, "Analysis of SANS Data from Strongly Interacting Polydispere Ionic Micellar Solutions," *10th Discussion Conference on "Small Angle Scattering and Related Methods,"* Prague, Czechoslovakia, July 13-16, 1987. To appear in *Makromolekuare Chemie* (1988).

Lin, T.L., S-H. Chen, N.E. Gabriel, and M.F. Roberts, "SANS Techniques Applied to the Study of Polydisperse Rod-Like Diheptanoyl PC Micelles," *J. Phys. Chem* 91:406 (1987).

Lin, T.L., S-H. Chen, and M.F. Roberts, "Thermodynamic Analyses of the Structure and Growth of Asymmetric Linear Short-Chain Lecithin Micelles Based on SANS Data," *J. Am. Chem. Soc.* 109:2321 (1987).

Sheu, E.Y., and S-H. Chen, "Thermodynamic Analysis of Polydispersity in Ionic Micellar Systems and its Effect on SANS Data Treatment," to appear in *J. Phys. Chem* (1988).

Sheu, E.Y., S-H. Chen, and J.S. Huang, "Structure and Growth of AOT Micelles in Aqueous Solutions," *J. Phys. Chem* 91:3306 (1987).

Sheu, E.Y., S-H. Chen, and J.S. Huang, "Structure, Interaction, and Growth of Sodium Dodecyl-o-xylencanlfonate Micelles in Aqueous Solutions," *J. Phys. Chem.* 91:1535 (1987).

Wu, C.F., and S-H. Chen, "SANS Studies of Concentrated Protein Solutions: Determination of the Charge, Hydration and H/D Exchange in Cytochrome D.," *J. Chem. Phys.* 87:6199 (1987).

14.3 Basic Studies of Laser-Cell Interactions

Wan Yuan Industry, Inc., People's Republic of China

Sow-Hsin Chen. Xui-Bin Wei, Xue-Yuan Wang

The aim of this project has been to understand the various chemical processes which occur when a laser radiation of a certain wave length interacts with blood cells in the presence of a hematoporphyrin. An intrument consisting of a copper vapor laser coupled to an optical fiber/chemical injector catheter for the treatment of occluded arteries

has been constructed and tested. The combined application of three steps: the pre-irradiation injection of HPD II, a brief copper laser irradiation (at 578 nm), and an enzyme urokinase infusion after the irradiation has been shown to produce the striking effect of liquifaction and resolution of a thrombus. Due to the low imput laser power and short period of irradiation, a histological examinction of the arteries after the treatment showed no apparent damage of the arterial wall.

Publication

Wei, X.B., X.Y. Wang, and S-H. Chen, "A Copper Vapor Laser and Optical Fiber Catheter System for Liquifaction and Removal of Thrombus in Occluded Arteries," preprint, "Method and Apparatus for Laser Angiosurgery." Patent application pending.

15.0   Custom Integrated Circuits

Academic and Research Staff

Prof. J. Allen, Prof. B. Musicus, Prof. J. White, Prof. J.L. Wyatt, Jr.

Graduate Students

R.C. Armstrong, D.G. Baltus, C.S. Bamji, H. Jeong, K. Kundert, A. Lumsdaine, L.M. McCormick, S.P. McCormick, H. Miyanaga, K. Nabors, P. O'Brien, G.N.S. Prasanna, M. Reichelt, W.S. Song, D. Standley, F. Van Aelten

Undergraduate Students

J. Deroo, K. O'Connor

15.1   Custom Ingegrated Circuits

Jonathan Allen, Robert C. Armstrong, Donald G. Baltus, Cyrus S. Bamji, Lynne M. McCormick, Steven P. McCormick, Hiroshi Miyanaga, Mark Reichelt, Filip Van Aelten.

The overall goal of VLSI CAD research is to provide the means to produce custom integrated circuits correctly, quickly, and economically. In the past, correctness applied only to the desired function, but there is increasing need to design to a performance specification, expressed in terms of speed, circuit area, and power. In this research group, the main emphasis is on CAD tools for performance-directed synthesis, with particular emphasis on digital signal processing applications. This goal implies the development of algorithms for optimizing performance of the total design. These complete designs, however, are specified at several levels of abstraction, ranging from function through architecture, logic, circuit, and layout. Traditionally, optimization techniques have been applied within a single such abstraction, but total optimization implies the simultaneous specification of all levels of representation such that the desired performance goal is realized. To facilitate this process, each such representation must be constructed so that optimization algorithms can be effectively designed, often utilizing well-understood methods. Furthermore, these representations must be coordinated so that each represents a projection of a single overall design. This "consistency" requirement guarantees that the distinct levels of abstraction can all be regarded as views of one abstract underlying design object.

The major research emphases in performance directed synthesis follow from the above observations. Algorithms for design at the several levels of representation are needed, but means for characterizing performance in several aspects is also required. Furthermore, the role of formal representational techniques is central, both for specify-

ing well-formedness at each design level, and for providing the requisite framework for consistency maintenance techniques. In the following paragraphs, several research projects are described which address these concerns.

Given a circuit specification, there is a need for a flexible compiler which will produce optimized layout automatically subject to several parameter settings. These parameters specificy the location of input and output pins, as well as feedthrough busses, and the desired aspect ratio. Baltus[1,2] has constructed an algorithm for this purpose that converts both NMOS and CMOS circuits to compact layouts, while observing the pin location and aspect ratio constraints. These techniques also allow for widely varying device size, grouping devices conveniently in terms of topological connectivity, device type (e.g., N or P) and device size. Diffusion breaks are minimized, and unequal numbers of N and P devices are allowed for CMOS circuits. This program is of great interest because it is highly flexible and not constrained to a rigid layout architecture, but still manages to produce high-quality layouts. The output of the program is in symbolic form, which can then be compacted to final geometrical specifications. This algorithm can be seen as a major contribution to the overall goal of moving the designer's focus away from the detailed layout to higher levels of design, which are more directly meaningful in terms of design goals. As such it encapsulates powerful algorithmic methods for the manipulation of layout artwork, exceeding the capability of human designers for medium and large sized cells.

As the minimum dimensions of layouts decrease, noise coupling between lines becomes an increasing problem, requiring accurate modeling of electromagnetic coupling and estimation of noise signal magnitudes. McCormick,[3] building on earlier models for resistance and capacitace associated with layout, has developed a new general representation. In the past, waveform bounding, higher order approximations (up to the second order moment of the impulse response), and macromodeling have been used to capture a variety of aspects of waveforms, but this new generalized representation subsumes all of these, permitting a variable order of representation. In particular, noise waveforms require third and fourth order moments of the impulse response. The generalized representation provides a uniform representation for all CAD analyses, providing both flexibility and variable accuracy. Use of the waveform moment representation permits efficient computation of noise coupling "hot spots" in a circuit layout, thus permitting the analysis of layouts for quality of (or relative lack of) noise coupling. Clearly, advances in technology now make this additional well-formedness check mandatory, and a part of the overall assessment of an integrated circuit design.

Just as the waveform moment representation is useful for noise coupling analysis, macromodeling techniques have been introduced for circuit delay modeling. Techniques have been developed by Brocco[4] for modeling of CMOS circuits for time delay, which take into account the rise (or fall) time of the input waveform(s), the output capacitive loading, and the nature of the circuit itself. Such modeling had been introduced before, giving accuracy within 5% of SPICE results, but the modeling of transmission gates (which introduce two time constants) is novel as is the method by which all gate models are combined. Gate resistances themselves are macromodeled, instead of being represented as constant values. In fact, four different types of macromodeled resistances are introduced in order to provide the desired accuracy. The resulting models are both general and accurate, and represent the desired tradeoff between accuracy and computational efficiency.

When extremely high accuracy of simulation is needed, especially for high frequency circuits, then even macromodeling of device and circuit action is insufficient, and the drift-diffusion based partial differential equation approximation for electron transport must be used rather than lumped models usually employed in circuit simulators. Unfortunately, the computations required for such analyses are very extensive. Nevertheless, Reichelt, White and Allen[5] have recently investigated the possibility of accelerating the transient simulation of MOS devices by using waveform relaxation. Convergence has been shown for practical cases, and the discretization needed for two-dimensional MOS transient device simulation is now being investigated.

For some time, we have been searching for appropriate formalisms for the verification of VLSI layouts and circuit schematics. By introducing formal grammars, correctness is tied to a rigorous set of composition rules which govern how blocks of layout and circuit schematic may be combined. These layouts and circuit schematics are represented as graphs, so that the composition rules are defined as graph transformations. Bamji[6] has shown how individual composition rules can span both layout and circuit schematic graphs, making verification of the layout to circuit schematic correspondence possible. These grammatical composition rules permit incremental verification, and the introduction of modifications during the analysis process with minimal overhead.

Van Aelten[7] has demonstrated the use of the grammatical formalism for a variety of circuit styles. Now he is starting to extend these techniques to the logic domain through functions for mapping objects at the circuit level to objects on the logic level. These mappings are similar to valuation functions used in denotational semantics. These functions efficiently describe the abstraction of all legitimate circuit schematic structures to the logic level, utilizing the recursiveness of the grammar. This approach also captures the notion of tolerant well-formedness requirements by moving some constraints now employed at the circuit schematic level to the logic level and its behavioral representation.

While formal grammatical techniques are useful for characterizing (and recognizing) well-formed structures at the various levels of representation, there remains the problem of consistency maintainence between these levels in a design database. Armstrong[8] is developing a formal model which can serve as the basis for incremental database consistency maintainence, utilizing basic set theoretic mappings. The consistency problem can be formally stated using these mappings, and graph grammars can describe the fundamental structures to be manipulated in maintaining consistency. These techniques are expected to provide the basis for correct translations in design synthesis, so that all design views remain consistent at all points of the design evolution, including the exploration of the space of all correct designs in order to find desired performance configurations.

From the above project descriptions, it is clear that many representational techniques are being studied as part of the overall task of building CAD programs for high performance circuit design. While these studies address the area of circuit performance, architectural performance (or parallelism) must also be used when the intended task algorithms permit. Miyanaga is studying the design of a new basic element for multiprocessor systems aimed at digital signal processing tasks. Mapping algorithms for the distribution of the overall algorithm on the several processors are also being developed in a coordinated way, so that optimal performance can be readily obtained for a wide variety of digital signal processing tasks using specialized mapping transformations.

Starting from the given functional task, the studies described above aim at providing the needed design representations, the means to specify their correctness and inter-domain consistency, and the context for design exploration needed to find high performance solutions to computationally demanding tasks. Present goals do not include the construction of an overall design system, but are instead focused on fundamental formal representational issues central to efficient and correct CAD systems aimed at high-performance design.

References

[1] D.G. Baltus, *Generating Efficient Layouts from Optimized MOS Circuit Schematics*. RLE Technical Report No. 535. MIT, 1988.

[2] D.G. Baltus and J. Allen, "SOLO: A Generator of Efficient Layouts From Optimized MOS Circuit Schematics" *Proceedings of the 25th Design Automation Conference*, June 1988.

[3] S.P. McCormick, *Cross-Talk Noise Modeling for VLSI Interconnections*, Ph.D. diss. proposal, Dept. Electr. Eng. and Comp. Sci., MIT, 1987.

[4] L.M. Brocco, *Macromodeling CMOS Circuits for Timing Simulation*. RLE Technical Report No. 529. MIT, 1987.

[5] M. Reichelt, J. White, J. Allen, and F. Odeh, "Waveform Relaxation Applied to Transient Device Simulation," *Proceedings of the International Symposium on Circuits and Systems*, 1988.

[6] C.S. Bamji, *Graph-Based Representation and Coupled Verification of VLSI Schematics and Layouts*, Ph.D. diss. proposal, Dept. of Electr. Eng. and Comp. Sci., MIT, 1987.

[7] F. Van Aelten, *Constraining Mechanisms for Circuit and Logic Level VLSI Representations*, S.M. thesis proposal, Dept. of Electr. Eng. and Comp. Sci., MIT, 1988.

[8] R.C. Armstrong, *A Formal Approach to Incremental Consistency Maintainence in Multirepresentation VLSI Databases*, Ph.D. diss. proposal, Dept. Electr. Eng. and Comp. Sci., MIT, 1987.

15.2 Extracting Masks from Optical Images of VLSI Chips

Bruce R. Musicus, Hong Jeong

One of the chief difficulties in studying image modeling and image understanding is that it is difficult to find useful models to aid in interpreting unconstrained images. To better understand the role of image modeling, we have focused on the particular problem of reverse-engineering a VLSI chip given a micro-photograph of the chip. The in-

teresting feature of this problem is that it requires combining conventional image processing with a rule-based image model. An enormous amount of modeling information is available concerning the design of VLSI chips: they are fabricated in layers of known composition and optical appearance; the images are formed from strips of material delineated by clear, though ragged, boundaries; the strips must form electrical circuits with known characteristics. Given all this *a priori* information, including knowledge of minimum line and feature widths as well as rules about the composition of layers making up the chip, our goal has been to build an efficient analysis system for reconstructing the masks that were used to manufacture the chip.

Our initial work in this area focused on low-level image processing issues, such as compensating for improper focusing, imbalanced lighting, and texture, while trying to accurately segment the image into line strips. It was found that local analysis methods, analyzing small windows to decide if they contained an edge or not, worked reasonably well and were relatively insensitive to lighting and texture fluctuations.

Our latest work has been to address the back end of the analysis system.[1-4] Given a clean line drawing representing a section of the VLSI chip, how do we piece together the various strips into the masks that formed the chip? We have developed various algorithms which deduce all possible legal interpretations of a given line drawing using only information about the edges. Our programs are written in a mixture of LISP, C, and PEARL, and run under UNIX 4.3. Using a database of rules of VLSI design, the programs start with edges and vertices, piece together paths marking the edges of a strip in some mask, assign the paths to layers, and label the layers. The most difficult part is to correctly infer where mask strips cross over each other, and to properly interpret accidental edges, where several strip edges coincide in the image.

Our most efficient algorithm utilizes a depth-first search strategy which constructs the final mask layers through a series of stages, trying out all possible interpretations of each line in the original image. Pruning this search tree quickly is vital, because of the exponentially increasing number of interpretations. Geometric reasoning based on the multi-layer strip model limits the growth in the number of interpretations until we reach the stages where we must assign potential strip contours to layers, choose which part of each layer is filled, and name the layers. At this point, our package invokes elementary circuit reasoning to rule out clearly infeasible circuit constructs. At present, our package only uses rules about contact cuts and wiring.

There are two major extensions to this work which we are now contemplating. The first is to increase the level of circuit reasoning ability in the software package to prune out more infeasible circuits. In particular, we would like to incorporate more careful reasoning about the shapes of the strips, the location of contact cuts within the shapes, and strip crossings which form transistors. A second major extension would be to use feedback from the symbolic reasoning system to improve the edge and segment extraction in the front-end. At present, our software assumes that the initial line drawing is perfect, and relies heavily on this assumption to rule out invalid interpretations. Ideally, we would like to modify the system to be more robust to mistakes in the line drawing, and to be able to isolate approximately where an error may have occurred in the initial segmentation. Such feedback could be used to change the processing used in the front end, to produce a better line drawing of the chip. In addition, we would like to use more information from the original image, such as brightness, color, and texture, to further improve the interpretation process.

References

[1] H. Jeong and B.R. Musicus, "Mask Extraction from Optical Images of VLSI Circuits," *IEEE ICASSP '87*, Dallas, Texas, April 5-9, 1987.

[2] H. Jeong, "Mask Extraction from Line Drawings of Optical VLSI Images," Ph.D. diss., MIT, 1987.

[3] H. Jeong and B.R. Musicus, "Extracting Masks from Optical Images of VLSI Circuits," In *Advances in Machine Vision, Algorithms, and Architectures,* ed. Jorge L.C. Sanz. New York: Springer-Verlag, 1988.

[4] H. Jeong and B.R. Musicus. "Extracting Masks for VLSI Circuits Using the Geometrical Configurations Around Contact Cuts," to be submitted 1988.

15.3 Cellular Array for Image Processing

Bruce R. Musicus, G.N. Srinivassa Prasanna, Hong Jeong, Edward Schembor, John Deroo, Kevin O'Conner

Low-level image processing operations, such as contrast stretching, compensation for lighting variation, noise suppression, or edge enhancement, often rely on highly repetitive processing of the pixels in the image. In conventional image processing architectures, this characteristic is exploited by pipelining the image data through a computational pipeline which repetitively executes the same instruction on all the data flowing through it. An alternative approach, which we are exploring, is to build a large number of small processors, and use these processors in parallel to execute the same instructions on different parts of the image. The Connection Machine is the best-known commercial implementation of this architectural idea. Our goal is to explore much simpler and cheaper implementations, which can be carefully matched to the algorithmic domain in order to achieve high performance at low cost.

To better understand hardware, software, and algorithmic issues involved in this approach, we have built a small 16 by 16 array of 256 single-bit processors, packaged on 2 VME boards with data memory, a horizontally microcoded sequencer, and a host interface.[1,2,3] Combined with a frame grabber and a 68000 controller card, we have a very high performance machine capable of extremely high speed computation for a particular class of signal processing problems. The array is built from four AAP chips from OKI Semiconductor, and operates at a 6.5 MHz rate, performing 256 bit operations on every clock tick. Both bit-serial and bit-parallel arithmetic are supported. Data memory is specially designed to supply overlapping frames of bit-serial or bit-parallel data to the processor array. The machine is programmed with a microP-assembler with high-level control constructs and expression evaluation. Various algorithms for low-

level image processing and matrix arithmetic are under development, and we are finishing final system debugging.

The purpose of building this system was to better understand the consequences of using a high degree of parallelism in signal processing tasks which would appear to be highly parallelizable. As would be expected, writing software for this array is non-trivial. The user must be highly familiar with the byzantine structure of the processor architecture, and with what operations can and cannot be performed in parallel. New algorithms must be developed for standard image processing tasks which can utilize all 256 processors in parallel. Algorithms must be carefully partitioned so that they deal with 16 by 16 chunks of the image. Much programming effort and run time must be devoted simply to moving the image data in and out of the array. High -level languages are difficult to design for the machine, because the hardware capabilities are highly non-orthogonal and are tightly bound to particular settings of various flag bits. In part, it was our familiarity with the difficulties of programming this machine that has motivated us to consider compilation systems capable of automating at least some part of this programming.

References

[1] J. DeRoo, *Image Processing Software Package,* S.B. thesis, Dept. Electr. Eng. and Comp. Sci., MIT, 1987.

[2] K.G. O'Conner, *Low Level System Interface for the OKI 16416 Cellular Array Project,* S.B. thesis, Dept. Electr. Eng. and Comp. Sci., MIT, 1987.

[3] E.A. Schembor, *Software Kernel for Array Processor Based Parallel Image Processing System,* S.B. thesis, Dept. Electr. Eng. and Comp. Sci., MIT, 1987.

15.4   Algorithmic Fault Tolerance in Digital Signal Processing

Charles Stark Draper Laboratory
U.S. Air Force - Office of Scientific Research (Contract AFOSR 86-0164)

Bruce R. Musicus, William S. Song

Conventional methods for achieving fault tolerant computer architectures rely on triplicating computational resources and using voter circuitry to reject incorrectly computed results. From an information theory viewpoint, however, a much better error control philosophy would be to use coding techniques to achieve a high level of error recovery with minimal overhead. Essentially, a coder distributes information across a noisy channel bandwidth in such a way that individual noise spikes may destroy a portion of many bits, but not an entire bit. A decoder at the receiver can combine information from the full channel bandwidth to reconstruct the original message, with a very high degree of reliability.

Coding techniques are used heavily in high performance memory systems and in communication networks. These techniques are excellent at protecting modules where data entering at one end is expected to arrive intact and unchanged at the other end.

However, coding techniques are not usually used to protect actual computation. Instead, high levels of fault tolerance within CPU's are traditionally achieved by duplicating or triplicating processor resources, and voting on the results. Another problem with coding is that the coding and decoding procedure adds to the latency of the channel, slowing down any machine using the protected component.

In this project, we are developing a new approach to fault tolerance, in which we can protect certain types of linear computation against processor failure, by using a small number of redundant processors to protect each other and to protect the real processors. One design uses a bank of analog-to-digital converters operating in round-robin fa 'ion to achieve an overall sampling rate somewhat above the Nyquist rate for the signal. A dither system and digital low-pass filter combine to reduce quantization errors in the front end. This same low-pass, however, can be used to detect and correct temporary or permanent errors in any of the converters, without substantially increasing the total amount of computation. The system is able to trade off additional hardware for greater accuracy and higher levels of fault protection. As converters fail, all that happens is that the effective quantization error increases.

Another application is to the FFT processor system used in range and velocity doppler sonar processing. Here we use a stack of processors to process multiple scans of sonar data from a phased-array antenna. Each processor does the same linear FFT processing, but on different sets of range cells. Adding extra processors working on linear combinations of the inputs to the other processors allows simple fault detection *and correction. Regardless of the number of processors in the system, detecting K simultaneous failures requires only K extra processors; detecting and correcting K simultaneous failures requires only 2K extra processors. When conventional truncation or rounding arithmetic is used, however, then the error checking can only be approximate. In this case, adding more processors improves the accuracy of the fault checking and correction. Generalized likelihood ratio tests are used to select the most likely failure hypothesis, and to perform the most likely fault correction. Realistic systems result which use comparatively small computational overhead (<50%) to achieve 100% single fault detection and correction. We are presently working with Draper Labs on the design of a sonar system incorporating these concepts.

Publication

Song, W., and B.R. Musicus, "A Fault-Tolerant Architecture for a Parallel Digital Signal Processing Machine," In *Proceedings 1987 International Conference on Computer and Circuit Design*, Rye, New York, 1987.

15.5   Simulation of VLSI Circuits

John L. Wyatt, Jr., Keith S. Nabors, Peter O'Brien, David Standley, Andrew Lumsdaine

We have been finishing up our previous project on delay estimation for digital integrated circuits and beginning a new one on parallel simulation methods for regular analog arrays.

One goal of this last phase of our CAD project has been to extend the waveform bounding results that Penfield et al. developed for MOS circuits so that they work for high-speed ECL as well. Our recent work consists of two major parts: 1) macromodelling of ECL logic gates acting both as drivers and as loads; and 2) delay estimation for individual nets using the gate macromodel parameters and RC tree models for metal interconnect. The success of the macromodelling approach relies on repetitive use of a library of modelled cells. A fixed computational cost (several mainframe CPU hours per cell) is paid to obtain parameter values for the simplified macromodels. The resultant timing estimates are typically within 5% - 10% of SPICE and are obtained with roughly 1000x less CPU time per run. This work has taken a very practical turn and has been extensively tested on an industrial ECL process and cell library. It is now in use in two industrial settings and will appear in Peter O'Brien's S.M. thesis this spring.

Another goal at the final phase of this project is to explore the possibility of building a very fast, arbitrarily accurate delay simulator for digital MOS circuits that is highly optimized and specialized to exploit the special mathematical structure of linear RC networks in which all capacitors are connected to ground, a common class of models for signal propagation delay in digital MOS. This work is nearly complete and will appear in Keith Nabors' M.S. thesis this spring.

We are beginning a new project on the parallel simulation of large, regular analog arrays. The goal is to produce a simulation tool that can be used for the design of smart sensors for machine vision, such as those currently being developed at Carver Mead's laboratory at the California Institute of Technology. These chips typically consist of large arrays, e.g., from 32x32 to 128x128, of moderately simple analog cells that perform a collective analog computation by communication with nearest neighbors. No currently available simulation tool is of any use on circuits of this size.

Systems of this type have two features that should influence the design of a tailor-made simulator. One is the natural hierarchy: devices in circuits in cells in arrays. The other is the designer's concern with circuit sensitivity in such systems: how do individual component variations affect overall system performance? We are studying ways to adapt the classical adjoint network approach to a hierarchical framework to solve this latter problem with acceptable computational efficiency.

Publications

Wyatt, J.L., Jr., "Signal Propagation Delay in RC Models for Interconnect," *Circuit Analysis, Simulation and Design. Part II: VLSI Circuit Analysis and Simulation,* ed. A. Ruehli, 254-291, North-Holland, 1987. (Also published as VLSI Memo 87-381, 1987, under the title *The Practical Engineer's No-Nonsense Guide to On-Chip Signal Delay Calculations.*)

Wyatt, J.L., Jr., *Nonlinear Dynamic Maximum Power Theorem:* VLSI Memo 87-371. MIT, 1987.

Wyatt, J.L., Jr. and D.L. Standley, "A Method for the Design of Stable Lateral Inhibition Networks that is Robust in the Presence of Circuit Parasitics," Proceedings of the IEEE Conference on Neural Information Processing Systems, Denver, Colorado, November, 1987.

15.6   Mixed Circuit and Device Simulation

International Business Machines, Inc.

Mark Reichelt, Jacob White, Jonathan Allen

Both digital and analog MOS circuit designers rely heavily on circuit simulation programs like SPICE to insure the correctness and to test the performance of their designs. For most applications, the lumped MOS models used in these programs accurately reflect the behavior of terminal currents and charges, but in some cases, these models are not adequate. In particular, charge redistribution between source and drain during device switching cannot easily be modeled by a lumped device, but the details of this charge redistribution can have an important effect on circuit behavior. In circuits like dynamic memory cells, sense amplifiers, analog-to-digital converters, and high frequency operational amplifiers, charge redistribution effects may not only degrade performance, but can inhibit proper function.

For these critical applications, sufficiently accurate transient simulations can be performed if, instead of using a lumped model for each transistor, some of the transistor terminal currents and charges are computed by numerically solving the drift-diffusion based partial-differential equation approximation for electron transport in the device. However, simulating a circuit with even a few of the transistors treated by solving the drift-diffusion equations is very computationally expensive, because the accurate solution of the transport equations of an MOS device requires a two-dimensional mesh with more than a thousand points.

One approach to accelerating this kind of mixed device and circuit simulation is to apply waveform relaxation to accelerating the transient simulation, not just at the circuit level, but inside the devices being simulated with a drift-diffusion description. In the present investigation, the WR algorithm is being applied to the sparsely-connected system of algebraic and ordinary differential equations in time generated by standard spatial discretization of the drift-diffusion equations that describe MOS devices. It has been proved (with J. Wyatt) that the WR algorithm contracts in a uniform norm on a model of the device simulation problem, and the result was verified on a one-dimensional experiment.[2] The implementation of the method for 2-D device simulation is in progress.

15.7   Detailed Simulation of Phase-Locked Loops

AT&T Bell Laboratories

K. Kundert, Jacob White

Switching filters and phase-locked loops are computationally expensive circuits to simulate using conventional circuit simulators like SPICE or ASTAP. This is because these kinds of circuits are all clocked at a frequency whose period is orders of magnitude smaller than the time interval of interest to the designer. To construct such a long time solution, a program like SPICE or ASTAP must calculate the behavior of the circuit for many high frequency clock cycles. The focus of this research is to develop and implement more efficient techniques for the circuit simulation of switching filter and phase-locked loop designs. The basic approach to simulating these circuits is to exploit only the property that the behavior of such a circuit in a given high frequency clock cycle is similar, but not identical, to the behavior in the preceding and following cycles. Therefore, by accurately computing the solution over a few selected cycles, an accurate long time solution can be constructed.

Simulating switched analog systems is an old problem but this novel approach has led to a recent success. The most structured of these switching problems, and therefore the easiest, is the switched-capacitor filter. A very efficent algorithm for the steady state analysis of switched-capacitor filters has been developed.[1] The idea is based on simulating selected cycles of the high-frequency clock accurately with a standard discretization method, and pasting together the selected cycles by computing the low frequency behavior with a truncated Fourier series. If carefully constructed, the nonlinear system that must be solved for the Fourier coefficients is almost linear and can be solved rapidly with Newton's method.

15.8 Numerical Algorithms for Hydrodynamics-Based Device Simulation

Keith S. Nabors, Jacob White

The model used in conventional device simulation programs is based on the drift-diffusion model of electron transport, and this model does not accurately predict the field distribution near the drain in small geometry devices. This is of particular importance for predicting oxide breakdown due to penetration by "hot" electrons. An approach for improving the accuracy of the drift-diffusion model of electron transport is to take an additional moment of the Boltzman equation, which yields a system of equations for electron transport that is similar to the drift-diffusion model, but includes the electron energies. The model is referred to as the hydrodynamic model and has been implemented in several simulators.

The hydrodynamic model is not as numerically tame as the standard drift-diffusion model, and other hydrodynamic simulators either circumvent this problem by ignoring difficult terms, or occasionally produce oscillatory results. A. research goal in this area is to try to develop a simulation program, based on the complete hydrodynamic model, whose numerical methods are efficient and are as robust as those used for the drift-diffusion model. Present work in this direction has been to implement a 2-D hydrodynamics-based simulator using standard numerical techiques in order to characterize the instabilities. Results so far demonstrate that the instabilities occur in the direction orthogonal to that of the dominant current flow.

15.9 Parallel Numerical Simulation Algorithms

Andrew Lumsdaine, Jacob White.

The key problem in parallelizing many of the numerical algorithms used in circuit and device simulators is finding efficient techniques for solving large sparse linear systems in parallel. Most parallel matrix solution algorithms fall into one of two general categories, the direct (Gaussian-elimination based) and the iterative, and each presents quite different problems. The computation in the direct approach is not very structured, and is therefore difficult to parallelize. Iterative methods are easily parallelized, but are not numerically robust.

The direct solution of circuit simulation matrices is particularly difficult to parallelize, in part because methods like parallel nested dissection are ineffective due to the difficulty of finding good separators. For this reason, the interaction between sparse matrix data structures and computer memory structure is being investigated (with Professor W. Dalley) to see how to store sparse matrices for effective parallel computation. One interesting recent result is that it is possible to store matrices in a completely scattered form, which allows for access of the sparse entries by fast indexing, in only three times the storage. This data structure is static, constructed once the matrix structure is known, and is therefore very attractive for parallel implementation.

In order to improve the reliability of relaxation methods for circuit simulation, approaches are being investigated based on extracting bands from a given sparse matrix, solving the bands directly, and relaxing on the rest of the matrix. This approach is efficient because band matrices can be solved in order *log(n)* time on order *n* processors, and this approach is more reliable than standard relaxation, because "less" relaxation is being used. This banded relaxation has been tested on circuit simulation matrices and does converge faster and more often than standard relaxation on all examples tried so far. The present work is on selecting the ordering of the matrix to best exploit the direct solution of the band, and to automatically select the band size. In addition, an implemention of the method on the Connection Machine is in progress.

Studying the behavior of parallel iterative algorithms for sparse matrix solution has lead to an interesting theoretical result indicating an optimality of Gauss-Jacobi over Gauss-Seidel relaxation, given enough processors. Of particular interest is that the result connects the spectral radius of the iteration matrices to their graphical properties.[3] The results are being extended to the waveform relaxation case, where in practice, this limiting result seems to show on as few as eight processors.

As mentioned above, relaxation algorithms for solving matrices are easily parallelized. It is also possible to apply relaxation directly to the differential equation, referred to as waveform relaxation (WR), and easily develop a parallel algorithm in which different differential equations are solved on different processors. A recently developed variant of the WR algorithm, referred to as waveform-relaxation Newton (WRN), allows for additional parallelism in that most of the computation for each of the discretization timepoints for a single differential equation can be computed in parallel. In recent

theoretical work, it has been proved that WRN converges globally even when applied to circuits with nonlinear capacitors.[4]

References

[1] K. Kundert, J. White and A. Sangiovanni-Vincentelli, "A Mixed Frequency-Time Approach for Finding the Steady State Solution of Clocked Analog Circuits," Custom International Circuits Conference, Rochester, New York, 1988.

[2] M. Reichelt, J. White, J. Allen and F. Odeh, "Waveform Relaxation Applied to Transient Device Simulation," International Symposium on Circuits and Systems, Espoo, Finland, 1988.

[3] D. Smart and J. White, "Reducing the Parallel Solution Time of Sparse Circuit Matrices using Reordered Gaussian Elimination and Relaxation," International Symposium on Circuits and Systems, Espoo, Finland, 1988.

[4] R. Saleh, J. White, A. S. Vincentelli, and A. R. Newton, "Accelerating Relaxation Algorithms for Circuit Simulation Using Waveform-Newton and Step-Size Refinement," submitted to the *IEEE Trans. Comp. Aided Design*.
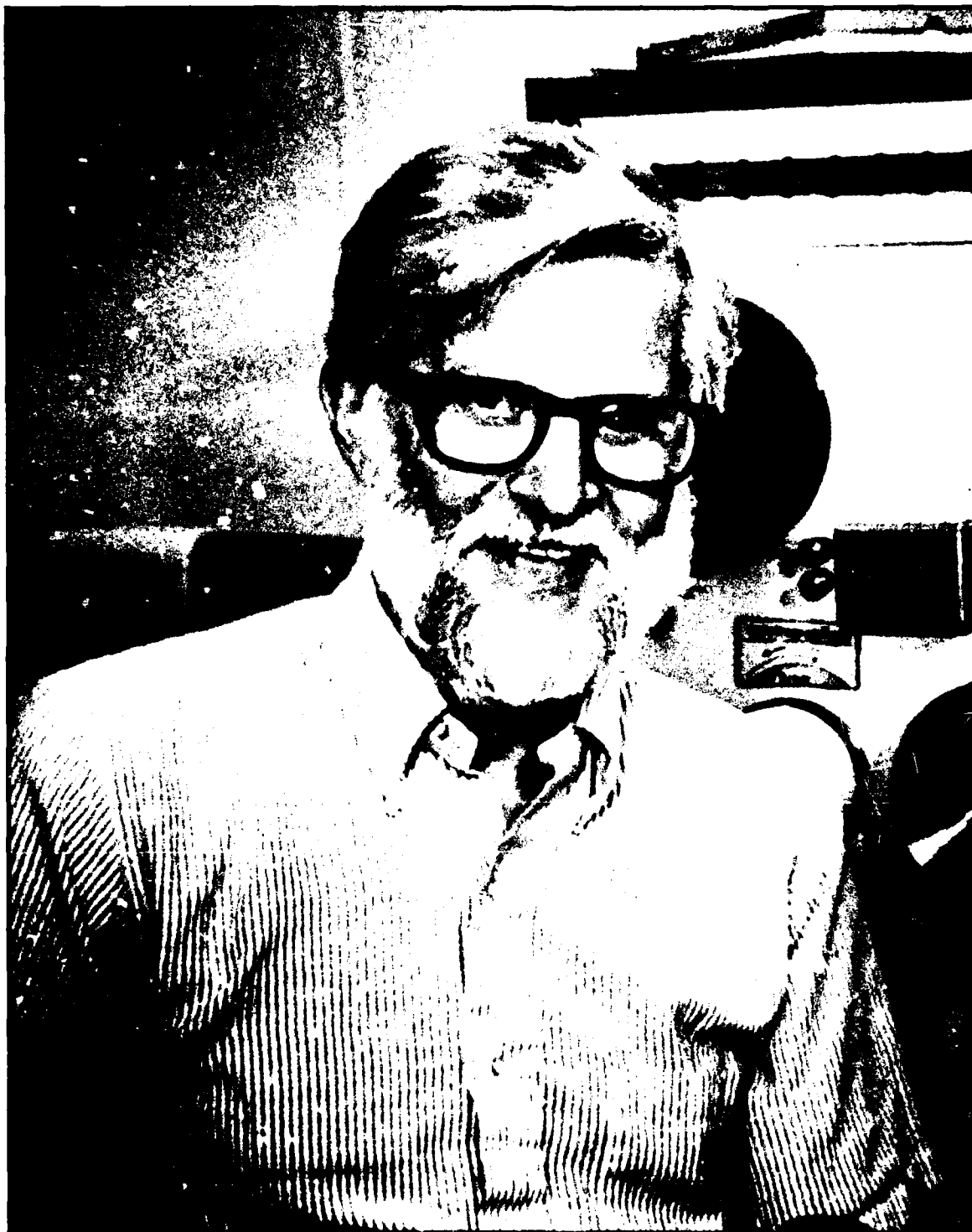
Professor Kenneth N. Stevens

16.0   Speech Communication

Academic and Research Staff

Prof. K.N. Stevens, Prof. J. Allen, Prof. M. Halle, Prof. S.J. Keyser, Dr. C. Bickley, Dr. S. Boyce, Dr. C. Chapin Ringo, Dr. C. Espy-Wilson, Dr. D.H. Klatt, Dr. S. Manuel, Dr. J.S. Perkell, Dr. S. Seneff, Dr. S. Shattuck-Hufnagel, Dr. V.W. Zue, M. Cohen, D.H. Kaufman, N. Lauritzen, M. Phillips

Collaborating Scientists

Dr. A. ni Chasaide,[1] Dr. R. Goldhor,[2] Dr. M. Gosy,[3] Dr. R.E. Hillman,[4] Dr. T. Hirahara,[5] Dr. K. Hirose,[6] E.B. Holmberg,[7] Dr. H. Kawasaki,[8] Dr. H. Lane,[9] Dr. L.S. Larkey,[10] Dr. J. Locke,[11] Dr. J.I. Makhoul,[12] Dr. N. Suzuki,[13] J. Webster,[14] Dr. L. Wheeler,[15] Dr. K. Yoshida[16]

Graduate Students

A. Alwan, M. Anderson, K.K. Key, N. Daly, S. Dubois, J.R. Glass, A.W. Howitt, C. Huang, R. Kassel, L. Lamel, H. Leung, J.N. Marcus, L. Pastel, J. Pitrelli, M. Randolph, T. Wilson

---

[1]   Visiting Scientist, Trinity College, Dublin

[2]   Kurtzweil Applied Intelligence

[3]   Visiting Scientist, Hungarian Academy of Sciences, Budapest

[4]   Boston University

[5]   Visiting Scientist, ATR, Osaka

[6]   Visiting Scientist, University of Tokyo, Tokyo

[7]   Boston University

[8]   Voice Processing Corporation

[9]   Northeastern University

[10]   Kurtzweil Applied Intelligence

[11]   Massachusetts General Hospital

[12]   Bolt, Beranek and Newman, Inc.

[13]   Visiting Scientist, Showa University, Tokyo

[14]   Massachusetts Eye and Ear Infirmary

[15]   Visiting Scientist

[16]   Visiting Scientist, NEC, Kawasaki

Undergraduate Students

M. Blush, G. Hopkins, C. Jankowski, J. Landry, A. Lim, H. Mitra, C. Pao, A. Shaw, S. Tierney, D. Whitney, A. Wong

Support Staff

A. Forestell, K. Kline, K. North, A. Wint

Part-Time Assistants/Special Projects

K. Abramson, N. Bateman, L. Glicksman, K. Isaacs, M. McCandless, L. Volaitis, D. Wong

16.1 Acoustic Correlates of Breathiness: First Harmonic Amplitude, Turbulence Noise, and Tracheal Coupling

A selected sample of reiterant speech has been collected from ten female speakers and six male controls in order to quantify acoustic correlates of perceived breathiness of the female voice, and to contrast these measures with comparable data from males. Two sentences with differing stress patterns were spoken by replacing each syllable by [hV] and by [ʔV], where V = [a, i, æ, o, ɝ]. Detailed analysis of the [a] data reveals: 1) wide variation in the strength of the first harmonic (relative to first formant amplitude), with an average increase of about 6 dB for females relative to males; 2) a greater tendency for the third formant to be excited by noise rather than voicing harmonics in the female population; and 3) indications of tracheal poles and zeros in the spectra of vowels adjacent to voiceless consonants in utterances produced by both genders. These three measures of breathiness tend to be greatest in unstressed syllables and toward the end of an utterance.

The acoustic data have been used to design a synthesis experiment in order to determine which dimensions of breathiness are perceptually most salient. Preliminary results of a listening test involving a female voice producing the vowel [a] under 16 different conditions indicate that noise in the third formant region is the most effective cue for most listeners, although a few listeners are more responsive to an increase in first harmonic amplitude and/or spectral tilt. Some changes (first formant bandwidth increase or increase to the first harmonic amplitude) induced the perception of nasality if done alone, but were interpreted as a highly breathy non-nasal vowel if accompanied by aspiration noise and spectral tilt.

16.2 Speech Recognition

The overall objectives of our research in machine recognition of speech are:

1. to carry out research aimed at collecting, quantifying, and organizing acoustic-phonetic knowledge, and

2. to develop techniques for incorporating such knowledge, as well as other relevant linguistic knowledge, into speech recognition systems.

During the past year, progress has been made on several projects related to these broad objectives.

16.2.1 Acoustic Segmentation and Classification

As part of our goal to better understand the relationship between the speech signal and the underlying phonemic representation, we have developed a procedure that segments the speech signal into an acoustic structure, and have determined an acoustically motivated set of broad classes. The segmentation algorithm makes use of the output of an auditory model. Every 5 ms, the algorithm measures the similarity of a given frame of data to its near neighbors. A frame is associated with either its past or future, depending on whether the backward or forward similarity is greater. We have initially biased the algorithm towards over-segmentation, since mechanisms exist for us to combine segments at a later stage.

Since there is no single level of segmentation that can adequately describe all the acoustic events of interest, we adopted a multi-level representation. In this representation, each initial "seed region" is associated with either its left or right region, again using a distance metric. When two regions are associated with each other, they are merged into one. The procedure is repeated until the entire utterance is described by a single acoustic event. By keeping track of the distance at which two regions merge into one, the multi-level description can be displayed in a tree-like fashion as a dendrogram. The acoustic description varies from fine at the bottom of the dendrogram, to coarse at the top. Thus, for example, the release of a stop consonant may be considered to be a single acoustic event or a combination of two events (release plus aspiration), depending on the level of detail desired.

In order to evaluate the effectiveness of this representation, we first developed an algorithm to automatically find the path through the dendrogram which best matched a time-aligned phonetic transcription. We then tabulated the insertion and deletion errors of these paths. An analysis of the acoustic structure, using 500 utterances from 100 different talkers, shows that it captures over 96% of the acoustic-phonetic events of interest with a 5% insertion rate.

Our objective with the acoustic classification algorithm is to group similar sounds into the same category, and to separate sounds that are widely different. While we did not know how many classes would be appropriate, we suspected that the number of classes would be small in order for the results to be robust against contextual and extra-linguistic variations.

To classify the acoustic segments, we first determined a set of prototype spectral templates based on training data. This was accomplished by using a stepwise-optimal agglomerative hierarchical clustering procedure, resulting in many possible codebooks of varying size and content. We then evaluated the effectiveness of various codebooks in several ways, using 500 sentences from 100 speakers. A comparison of the phonetic content of the resulting clusters over several databases indicates that the top three or four levels are quite stable, suggesting that the total number of clusters should not exceed twenty. We also measured the decrease in mean square distortion error as a function of the cluster size and found that the rate of decrease is less than 1% after the cluster size exceeds ten. In addition, we judged the relative merit of a set of clusters by examining the distribution of phonetic information within each set. This was done by performing hierarchical clustering of all phones using their distribution across the set of clusters as a feature vector. This procedure is very helpful in facilitating visualization of the data structure captured by a set of clusters. A qualitative analysis of these structures showed that after ten to twelve clusters the hierarchical organization did not change significantly.

16.2.2 Recognition of Semivowels in American English

A set of procedures has been developed for the detection and classification of the semivowels /w, y, r, l/ in American English. The detection process marks those acoustic events which may signal the occurrence of a semivowel. Once marked, the acoustic events are used by the classification process in two ways, based on their times of occurrence and their relative strengths. First, a small region from which to extract the values of particular acoustic properties is determined. Second, the number of possible classifications of the detected sound is reduced. Almost all of the acoustic properties are based on relative measures, and hence they tend to be independent of speaker, speaking rate and speaking level.

Fairly consistent overall recognition results in the range of 78.5% to 95% were obtained across different contexts. (Higher performance was obtained when /w/ and /l/ were allowed to be confusable.) These results are for corpora which include polysyllabic words and sentences produced by many speakers, both males and females, of several dialects. Thus the recognition data show that much of the across-speaker variability is overcome by using a feature-based approach to recognition where relative measures are used to extract the acoustic properties.

Several issues were brought forth by this research. First, an acoustic study revealed several instances of feature assimilation. Some of the domains over which feature spreading occurred are limited to syllables whereas others spread across syllable boundaries. Second, an analysis of the sounds misclassified as semivowels showed that, due to contextual influences, the misclassified vowels and consonants had patterns of features similar to those of the assigned semivowels. This result suggests that there may be an advantage in representing lexical items in terms of matrices of binary features as opposed to, or in addition to, phonetic labels. Finally, the system's ability to recognize semivowels which were in the underlying transcription of the utterances, but were not included in the hand transcription, suggests that caution should be exercised in using hand-transcribed data to evaluate recognition systems, without appropriate interpretation of the results.

Our experience with the recognition of the semivowels has helped us to evolve a framework for a feature-based approach to speech recognition. This approach is based on three assumptions: that phonetic segments are represented as bundles of binary features; that the abstract features have acoustic correlates which, due to contextual influences, have varying degrees of strength; and that the acoustic manifestation of a change in the value of a feature or a group of features is marked by specific events in the sound. These acoustic events correspond to maxima or minima in particular acoustic parameters.

16.2.3 Recognition of Continuously-Spoken Letters by Listeners and Spectrogram Readers

Because of acoustic similarities between the pronunciation of some letters of the alphabet, automatic recognition of continuously-spoken letters is a difficult task. The goal of this study is to determine and compare how well listeners and spectrogram readers can recognize continuously-spoken letter strings from multiple speakers. Our interest in spectrogram reading results is motivated by the belief that this procedure may help us identify acoustic attributes and decision strategies that are useful for system implementation. Listening and spectrogram reading tests involving eight listeners and six spectrogram readers, respectively, were conducted using a corpus of one thousand word-like strings designed to minimize the use of lexical knowledge. Results show that listeners' performance was better than readers' (98.4% vs 91.0%). In both experiments, string lengths were determined very accurately (98.1% and 96.2%), presumably due to the large number of glottal stops inserted at letter boundaries to facilitate segmentation. Most of the errors were due to substitution of one letter for another (68% and 92%), and they generally fall into two categories. Asymmetric errors can often be attributed to subjects' disregard for contextual influence, whereas symmetric errors are largely due to acoustic similarities between certain letter pairs. Our subsequent acoustic study of four of the most confusable letter pairs has resulted in the identification of a number of distinguishing acoustic attributes. Using these attributes, we achieved overall recognition performance better than that of the readers.

16.2.4 Vowel Recognition Using Artificial Neural Nets

This study is concerned with the application of artificial neural nets to phonetic recognition. Our work is motivated by the observation that our improved knowledge of acoustic-phonetic feature extraction is often overshadowed by our relative ignorance on how to combine them into a robust decision. We suspect that artificial neural nets may provide a natural self-organizing mechanism for different acoustic cues to simultaneously interact, cooperate and compete. Our goal is to investigate how the mathematically well-defined framework of artificial neural nets can be exploited in phonetic recognition when they are augmented with acoustic-phonetic knowledge. Specifically, we explored issues such as the selection of an appropriate network, the choice of the error metric, the use of contextual information, and the determination of the training procedure. Our investigation is couched in a set of experiments that attempts to recognize the 16 vowels in American English independent of speaker.

Our experimental results were based on some 10,000 vowel tokens that appear in all phonetic contexts. They were extracted from 1,000 sentences spoken by 200

speakers, 140 male and 60 female. We found that by replacing the mean-squared error metric with a weighted one to train a multi-layer perceptron, we consistently obtained better recognition accuracy and rank order statistics. Using the two-layer perceptron in a *context-independent* manner, we were able to achieve a top-choice vowel recognition accuracy of 54%, which compares favorably with results reported in the literature. Our *context-dependent* experiments reveal that heterogeneous sources of information can be integrated to improve recognition performance. Our top-choice accuracy of 67% is comparable to the average agreement on vowel labels provided by listeners when they are given the immediate phonetic context. Finally, we found that the rate of improvement of recognition accuracy may be used as a terminating criterion for training, and that reasonable performance can be achieved using as few as 800 training tokens.

We are presently investigating ways to improve recognition performance by incorporating additional acoustic attributes, including those that preserve temporal aspects of the signal. In addition, we want to understand how different sources of information are being used in the network. Finally, we plan to move on to the recognition of other classes of phonemes.

16.3   Speech Planning

We are pursuing the development of a speech production planning model in three areas, and are beginning to explore interactions among them. The first is word structure, the second is lexical stress, and the third is phrasal prosody.

1.   Word Structure.   Earlier experimental results showed the importance of word structure in production planning, by demonstrating that segmental speech errors are more likely to occur between word-onset consonants than between non-word-onset consonants. This is true even when the word-onset consonants occur before vowels with mixed stress levels, showing that the special susceptibility of word-onset segments is not due to the fact that in English word onsets are usually in stressed syllables. We have now extended these results from the original set of list stimuli ("parade fad foot parole") to a second set of list stimuli with a different metrical structure ("fad parade parole foot") and to phrasal stimuli, ("It's a fad to parade with parole on your foot") with nearly identical findings. Since the preferential occurrence of interaction errors among word-onset consonants is not diminished by changing the metrical structure of the stimuli or by introducing syntactic and prosodic structure, we conclude that it is a robust and reliable effect. Interestingly, the effect is even more pronounced for non-word stimuli like "pareed fid fet perile," suggesting that word structure imposes this effect not during the process of lexical access, but during the integration of the accessed segments into the planning frame.

2.   Lexical Stress.   Although word-onset consonants appear to be the strongest candidates for segmental interaction errors, prestressed consonants also participate in errors, although at a reduced rate. For example, in the pair of stimuli "parade fad foot parole" and "repeat fad foot repaid," /p/ and /f/ interact about twice as often in the first (word-onset) twister as in the second (prestressed), but both error rates are significantly higher than that for "ripple fad foot rapid," where the /p/ is neither in the word onset nor in prestressed position. This result suggests that lexical stress may also play a role in the planning frame.

3. Phrasal Prosody. Although list versus phrasal context did not affect the error pattern in the Word Structure experiment described above, an earlier pilot experiment had suggested that phrasal stimuli do have one significantly different effect: word-final consonants are protected against errors when the elicitation stimuli are phrases but not when they are lists. That is, when the four words of the list twister "peal tone pan tool" are placed in a phrasal context of "From the peal of the tone to the pan of the tool," the number of /l/-/n/ (final-position) errors is reduced significantly from that of the number of /p/-/t/ (initial position) errors. However, these pilot results were obtained in a between-subject experimental design, raising the possibility that the two sets of speakers were differentially susceptible to the effects of list versus phrasal contexts. A replication of the experiment, using within-subject design, has now shown the same effect. We are currently pursuing the question of whether this final-position protection effect in phrases is associated: 1) with the computation of syntactic structure for these phrases; or 2) with the computation of metrical structure to support their more complex prosody.

4. Interactions: Lexical vs. Phrasal Prominence. In a separate experimental domain, we are following up on the hypothesis that the pitch gestures traditionally associated with lexical stress are actually associated with the pitch accents of phrase-level intonation patterns. In measurements made on a single speaker, when the pitch accent is moved off of a target word (by any one of a number of means), the lexically-stressed syllable of that word exhibits no residual pitch gesture. If confirmed in a number of speakers, this finding would support the view that lexical stress or prominence is a rhythmic or durational phenomenon.

16.4 Studies of the Acoustics and Perception of Speech Sounds

16.4.1 Stops, Fricative, and Affricate Consonants

As one component of our study of the acoustics and perception of a variety of speech sounds, we are examining the mechanisms of sound generation during the constricted interval and at the release for stop, affricate, and fricative consonants. This research includes a theoretical component in which the events at the implosion, during the constricted interval, and at the release of these consonants are calculated through the analysis of models of the processes. The analysis includes: 1) the effects of intraoral pressure on the release of the closure for stop consonants and on the shaping of the constriction for fricative consonants; 2) the role of the yielding walls of the vocal tract in determining airflows during the constricted interval and following the release; 3) the effects of obstacles in the airflow on the generation of turbulence noise; 4) determination of the amplitude and spectral characteristics of the initial transient at the release of stop consonants; and 5) calculation of formant trajectories near the consonantal implosion and release. Comparison of acoustic data for the consonants with predictions of the model show reasonable agreement. Analysis of the model is hampered, however, by the lack of quantitative data on the impedance of the vocal-tract walls at low frequencies and on the rates of movement of articulatory structures at the instant of release of stop consonants.

One outcome of the theoretical and acoustical study of the release of stop and affricate consonants is the finding that the initial transient has an amplitude that is often comparable to or exceeds that of the following noise burst. This transient is expected, therefore, to contribute significantly to the perception of the place and manner of articulation for these consonants. A perceptual experiment examining the contrast between fricative and affricate consonants in English has been carried out, and has indeed shown that the initial transient is an important contributor to the perception of the affricate-fricative distinction.

16.4.2 Vowel Perception

We have been continuing our studies of the perception of vowels in consonant contexts in which the formants undergo rising-falling-rising trajectories (i.e., concave downwards) or falling-rising-falling trajectories (concave upwards). Subjects adjusted the formants of a steady-state vowel so that this vowel matched the quality of various vowels with time-varying trajectories. The subjects did not always show perceptual compensation for undershoot in the second-formant trajectory, as might be expected based on the results of earlier experiments. That is, the subjects did not always adjust the second formant of the matching stimulus to be beyond the extreme maximum or minimum point in the trajectory of the time-varying second formant. This lack of perceptual overshoot was evident in concave downward trajectories. Studies of these effects are continuing in an effort to separate out effects that might be auditorily based from effects that are based on linguistic experience.

16.4.3 Voicing for Fricatives

The maintenance of vocal-fold vibration during voiced fricatives is expected to be subject to considerable variability, since careful adjustment of the glottal and supraglottal constrictions is required to provide an intraoral pressure in the appropriate range. We have been examining the acoustic characteristics that distinguish voiced from voiceless fricative consonants when they occur in a variety of phonetic contexts, including sequences of two fricatives that may or may not agree in voicing. The observations verify that it is quite common for voiced fricatives to be produced with vocal-fold vibration over only a portion of the time interval in which the vocal tract is constricted. The distinction between voiced and voiceless fricatives is usually carried, however, by the presence or absence of significant vocal-fold vibration over a 20-30 millisecond time interval immediately adjacent to the preceding or following sonorant interval. Preliminary listening tests with synthetic fricatives in intervocalic position have verified that glottal vibration with these temporal characteristics leads to appropriate listener identification of the fricatives as voiced or voiceless.

16.4.4 Cross-Language Study of Nasalization

In collaboration with the Linguistics Center of the University of Lisbon, we have been conducting a comparative study of the implementation of nasalization in the three languages: English, French, and Portuguese. In particular, we have examined nasalization in utterances where the nasal interval is followed by a stop consonant (as in the words *banter* in English, *tante* in French, or *tinto* in Portuguese). In a series of perceptual experiments with synthetic utterances of the form *tante*, the following parameters were

systematically manipulated: 1) the duration of nasalization in the vowel; 2) the amount of nasalization in the vowel; and 3) the duration of the nasal murmur following the vowel.

The stimuli were presented to native speakers of Portuguese, English and French, which differ with respect to the occurence of nasal vowels in their phonological systems. The listeners were asked to judge, for each stimulus: 1) the presence or absence of nasalization; and 2) the adequacy of the stimulus as a natural utterance with respect to its nasalization.

The different language groups gave similar responses with regard to the presence or absence of nasalization. However, judgments of the naturalness of the stimuli in the different languages depend on the temporal characteristics. French listeners preferred a longer duration of nasalization in the vowel and were indifferent to the presence of murmur, English listeners preferred some murmur and accepted briefer nasalization in the vowel, and Portuguese responses were intermediate. Preliminary acoustic data from utterances in the three languages are in accord with these perceptual findings.

16.5   Physiology of Speech Production

16.5.1   Articulatory Movement Transduction

Work has continued on refinement of techniques for transduction of articulatory movements with the use of alternating magnetic fields. This effort has concentrated on exploration of a system which uses three magnetic-field transmitters as an alternative to the already-completed two-transmitter system (see RLE Technical Report No. 512). A successful three-transmitter system is potentially more desirable because: 1) it would simplify the complicated and time-consuming protocol for running experiments; 2) the data might be more reliable; 3) its transducer/receivers are much less expensive; and 4) it uses field strengths which are several times lower than the two-transmitter system. The last factor has potential implications for the use of humans as experimental subjects, because a very recent epidemiological study has found an increased incidence of cancer in children who live in proximity to magnetic fields generated by high-tension power lines.

The function of both the two- and three-transmitter systems has been simulated. The simulations predict: the characteristics of fields generated by solenoidal transmitters, the signal strengths induced in the transducer/receivers, and the resulting transduced displacements. An important requirement of the device is that it transduce displacements with sufficient accuracy in the face of a moderate amount of receiver tilt, and with receivers mounted slightly lateral to the midsagittal plane (because it is impossible assure absolutely midsagittal transducer placement). Use of the simulation suggests that a three-transmitter system could perform adequately only if the transducers are mounted within about 2 mm of the midline of the transmitter assembly. The simulation predicts that the two-transmitter system allows for more off-midline displacement error, but at the expense of having to calibrate each transducer separately and mount it on the subject with the same orientation in which it was calibrated. The simulations have also been used to investigate and specify the transmitter characteristics

117

and spacing for new versions of both designs. These new versions have been built, along with additional testing and calibration devices, and final testing is in progress.

16.5.2 A Quantitative Study of Anticipatory Coarticulation

Analysis is almost complete on lip-protrusion movement data for the vowel /u/ from four speakers of American English. Test utterances consisted of pairs of words such as "leak hoot" and "leaked coot," each pair embedded in a carrier phrase. Word pairs were chosen so that different numbers of consonants intervene between the unrounded vowel /i/ and the rounded /u/. Utterances were repeated 15-20 times in random order. Protrusion movements of the upper lip and the acoustic signal were recorded, digitized and processed. Times of end of voicing of the vowel /i/ and onset of voicing of the vowel /u/ were marked interactively in the acoustic signal stream. Times of protrusion onset (onset of positive velocity) and of maximum acceleration were identified algorithmically in the movement signal stream.

Consistent with previous qualitative observations on one subject, there was a lot of variation in the relative timing of the identified events. Lip protrusion movements were partitioned into two components: an initial slow one, with onset of positive velocity occurring around the end of the preceding unrounded /i/ (possibly corresponding to relaxation of spreading for the /i/), and a later faster one, with its onset marked by the largest acceleration peak, occurring after the end of the /i/.

Quantitative analysis shows that as the duration of the acoustic interval between the end of the /i/ and the onset of the /u/ increased (with increasing numbers of intervocalic consonants), the interval between the onset of the slow movement component and onset of the /u/ also increased, but at a lesser rate. Thus, for the shortest intervocalic intervals the protrusion onset occurred slightly earlier than the end of the /i/, and for the longest intervocalic intervals, the initial protrusion onset occurred slightly later than the end of the /i/. This finding suggests that the time of the initial protrusion onset is somewhat constrained by the end of the acoustic requirement of lip spreading for the /i/, but that constraint interacts with a competing tendency to produce the protrusion gesture at a relatively invariant, (biomechanically) optimal velocity. The analysis also suggests that when the consonant string contains a /k/, the movement onset is slightly delayed in comparison to utterances not containing /k/. It is speculated that this effect is due to the coordination of the lip and tongue body gestures for the vowel /u/, in which lip protrusion onset "waits" for completion of the tongue body gesture for the /k/. Further experimentation is required to explore these ideas.

16.5.3 Glottal Airflow and Pressure Measurements for Male and Female Speakers with Normal Voices

Measurements on the inverse filtered airflow waveform (the "glottal waveform") and of estimated average transglottal air pressure and glottal airflow were made from non-invasive recordings of productions of syllable sequences in soft, normal and loud voice and in normal, low and high pitch for 25 male and 20 female speakers. Analysis of the

results for intensity manipulation is complete and shows a large amount of inter-subject variation in most parameters. There was an almost universal DC offset in the glottal airflow waveform, indicating incomplete closure of the inter-arytenoid portion of the glottis. With change from normal to loud voice, both males and females produced loud voice with increased pressure, accompanied by increased AC flow and increased rate of change of airflow during the glottal closing phase (called "closing velocity"). Soft voice was produced with decreased pressure, decreased AC flow and closing velocity and increased DC and average flow. Within the loudness conditions, there was no significant male-female difference in pressure. Several glottal waveform parameters separated males from females in normal and loud voice. The waveforms evidenced higher AC flow and higher closing velocity for males. In soft voice, the male and female glottal waveforms were more alike, and there was no significant difference in closing velocity. The DC flow did not differ significantly between males and females in all three loudness conditions. Because of the DC flow component, previously-employed measures of glottal resistance and vocal efficiency may be less useful indicators of vocal-fold function than other measures. Most of the findings may be related to biomechanical differences and differences in voice source acoustic characteristics between males and females and across loudness conditions.

Analysis of the same measures for normal, low and high F0 is almost complete. It shows increased pressure for change both from normal to high and normal to low pitch. The unexpected finding for low pitch may be due to the nature of the task, in which low pitch is below the normal speaking range. A lack of correlations of the measured parameters with F0 change and strong correlations with change in sound pressure level (SPL) suggest that the measured aerodynamic parameters are more closely related to mechanisms which determine SPL than F0.

16.5.4 Objective Assesment of Vocal Hyperfunction: An Experimental Framework and Preliminary Results

This study is part of the initial phase of a project which focuses on the development and use of quantitative measures to provide objective descriptions of conditions called "vocal hyperfunction." Some of these conditions can be manifested in the form of vocal-fold edema, nodules, polyps, and contact ulcers. They are accompanied by acoustic abnormalities and are believed to be due to abuse and/or misuse of the vocal apparatus. More advanced cases may require surgical treatment. Experimental design for the project is based on a descriptive theoretical framework which maintains that there are different types and stages of hyperfunctionally-related voice disorders. Data consist of indirect measures made from non-invasive aerodynamic and acoustic recordings, including: 1) parameters derived from inverse filtered approximations of the glottal volume velocity waveform; 2) estimates of transglottal air pressure, average glottal airflow, glottal resistance and vocal efficiency; and 3) measures of vocal intensity and F0. Preliminary results (based on comparisons among 15 voice patients and the above-mentioned 45 normal speakers) support major aspects of the theoretical framework and indicate that the measurement approach is capable of differentiating hyperfunctional from normal voices and different hyperfunctional conditions from one another. Organic manifestations of vocal hyperfunction (nodules, polyps, contact

ulcers) are accompanied by abnormally high values of AC flow and maximum closing velocity, suggesting an increased potential for vocal fold trauma due to high collision forces. In contrast, non-organic manifestations of vocal hyperfunction (called "functional disorders") tend to be associated with abnormally high levels of unmodulated DC flow, without high values of AC flow and maximum closing velocity, suggesting reduced potential for vocal fold trauma. The measures also suggest different underlying mechanisms for nodules and polyps vs. contact ulcers. The results are interpreted with respect to predictions based on the theoretical framework. These interpretations have led to refinement of the experimental approach for use in the next phase of the work. Currently, completed measures from an additional 15 voice patients are being examined.

16.5.5 The Speech of Cochlear Implant Recipients

National Institutes of Health (Grant 1 P01-NS23734), subcontract with the Massachusetts Eye and Ear Infirmary

Work has begun on studying the speech of post-lingually-deafened cochlear implant recipients as part of an NIH Program Project entitled "Basic and Applied Research on Cochlear Prostheses" (J.B. Nadol, MD, Principal Investigator). The aims of this component project are to: 1) characterize the speech of post-lingually deafened adults before and after they receive cochlear implants to help evaluate and improve prostheses; and 2) understand the role of hearing (auditory feedback) in speech production. These aims will be met by making: 1) perceptually-based measurements of sound segment deletions and substitutions and ratings of prosodic variables and overall intelligibility; 2) acoustically based measures of segmental productions (temporal and spectral) and prosody (F0 and temporal variables); and 3) physiological measures of respiration and air flow regulation and articulatory coordination. The measures will be compared within each implanted subject across time and between aided and unaided conditions, as well as between implanted subjects and normal-hearing controls. The measures are derived from recordings of the acoustic signal, oral and nasal air flow, nasal and throat vibrations (for a nasality index), an electroglottographic signal and, chest and abdominal cross-sectional areas (for a measurement of lung volume). Thus far, experimental protocols have been established, longitudinal recordings have been made of four implant patients, individual recordings have been made of several controls, initial signal processing and data extraction procedures have been devised, and preliminary measures of respiration have been examined longitudinally for two implant recipients. Analysis will be resumed and expanded when a new data processing facility (currently being completed) comes on line.

17.0 Linguistics

Academic and Research Staff

Prof. M. Halle, Prof. N.A. Chomsky

The work of the Linguistics group is directed towards obtaining a better grasp of the mental capacities of human beings through the study of the nature, acquisition and use of language. Language is a uniquely human faculty in that only humans appear to be capable of learning and using a language and that every normal human acquires knowledge of one or more languages during his/her lifetime. This knowledge is represented somehow in the speaker's mind, which is a special organ located in the human brain. Viewed from this vantage point, the central issues of linguistics research are:

1. What is the nature of this knowledge? What do speakers of a particular language - Lattvian, Spanish or Walpiri - know, and how does knowledge of one language differ from and resemble that of some other language?

2. How do speakers acquire this knowledge?

3. How do speakers put this knowledge to use in producing and understanding utterances?

4. What are the physiological mechanisms that provide the material basis for the storage, acquisition and utilization of linguistic knowledge?

There are considerable differences in our ability to answer these questions. It would seem that at present we have advanced more with regard to question 1 and least with question 4. These differences are also reflected in the research conducted by the group. At this time, it is most heavily concentrated on issues concerned with the nature of the knowledge that characterizes fluent speakers of various languages. Yet the other three questions have not been overlooked, and significant efforts are being devoted to their solution.

The study of these topics is being carried out along a number of parallel lines. On the one hand, linguists have investigated the principles by means of which words are concantenated to form meaningful sentences. These principles have been the primary domain of inquiry of the disciplines of syntax and semantics. Phonology studies the sound structure of words while morphology examines the manner in which different languages combine different meaning-bearing units (specifically, stems, prefixes, suffixes and infixes) to form words. The latter topic has attracted increasing interest in recent years and is likely to become more prominent in the future.

The English Noun Phrase in its Sentential Aspect

Steven Paul Abney

*Submitted to the Department of Linguistics and Philosophy in
partial fulfillment
of the requirements for the degree
of Doctor of Philosophy in Linguistics*

Abstract

This dissertation is a defense of the hypothesis that the noun phrase is headed by a functional element (i.e., non-lexical category) D, identified with the determiner. In this way, the structure of the noun phrase parallels that of the sentence, which is headed by Infl(ection), under assumptions now standard within the Government-Binding (GB) framework.

The central empirical problem addressed is the question of the proper analysis of the so-called Poss-ing gerund in English. This construction possesses simultaneously many properties of sentences, and many properties of noun phrases. The problem of capturing this dual aspect of the Poss-ing construction is heightened by current restrictive views of X-bar theory, which, in particular, rule out the obvious structures for Poss-ing, $[_{NP}NP\ VP_{ing}]$, by virtue of its exocentricity.

Consideration of languages in which nouns, even the most basic concrete nouns, show agreement (AGR) with their possessors, points to an analysis of the noun phrase as headed by an element similar to Infl, which provides a position for AGR; I call this Infl-like element D. D and Infl belong to the class of non-lexical categories, which I prefer to call <u>functional</u> categories. The analysis in which D heads the noun phrase I call the DP-analysis.

Importing the DP-analysis into English yields an immediate solution for the problem of the Poss-ing gerund: Poss-ing gerunds (and by extension, noun phrases generally) have a more sentence-like structure than hitherto throught, namely, $[_{DP}\ DP's\ D\ DP_{ing}]$. (In non-gerundive noun phrases, VP is replaced by a projection of N. This projections of N, despite being a maximal X-bar projection, corresponds to N-bar in the standard analysis.)

Current trends in the treatment of minor categories - so-called non-lexical categories - lead us to a similar conclusion. Until recently, minor categories like complementizers and modals had been treated as syncategorematic. Under current assumptions, however, they participate fully in the X-bar schema. In this way, two simplifications are achieved simultaneously: we eliminate syncategorematic elements, and we acquire an endocentric analysis of the sentence, which had been exceptional in being the only exocentric major category. To make these results fully general, we are led to treat the remaining syncategorematic elements - in particular, determiners in noun phrases and degree words in adjective phrases - as heads of full phrases. The analogy with complementizers and modals indicates that determiners and degree words should head noun phrases and adjective phrases, respectively. In other words, determiners are lexical instantiations of D in the same way that modals are lexical instantiations of Infl.

However, despite the conceptual links, the question of the existence of a functional head of the noun phrase (the DP-analysis), and the question of the place of the determiner, are independent questions, and I treat them separately. Chapters 1 through 3 are concerned predominantly with the former question, Chapter 4 with the latter.

Chapter 1 provides a brief introduction. In Chapter 2, I present the DP-analysis, motivating it by examining languages with agreement between noun and possessor. I also discuss issues raised by the DP-analysis, with emphasis on the parallelism between noun phrase and sentence hypothesized under the DP-analysis. In particular, I treat the question of PRO in the noun phrase; and I show that the numerous differences between sentence and noun phrase do not invalidate the parallelism of structure proposed under the DP-analysis. In Chapter 3, I apply the analysis to the three gerundive constructions, Acc-ing, Poss-ing, and Ing-of. Finally, in Chapter 4, I turn to the question of whether the determiner is the lexical instantiation of D, the functional head of the noun phrase.

Null Operator Constructions

Marguerite Browning

Abstract

This dissertation defends the hypothesis that certain constructions involve covert A'-movement resulting in the creation of A'-chains headed by null categories commonly referred to as null operators. The constructions which have been widely analyzed as involving null operators fall into two categories. In the first category, designated OWM (Oh WH-movement) constructions, are relative clauses (tensed and infinitival), purpose clauses, degree clauses, adjectival complements, clefts and comparatives, all of which are treated as covert wh-movement structures in Chomsky (1977). More recently, the null operator hypothesis has been extended to parasitic gap constructions, which constitute the second category. The goal of this dissertation is to develop an analysis of the nature of null operator chains and the conditions which apply to them which will account for the similarities and differences between the two categories of constructions in a unified manner. Three types of constraints are discussed and proposed: constraints governing the licensing of the null operator itself, the licensing of the variable created by null operator movement, and the licensing of the null operator chain as a whole. Chapter 1 contains a history of the development of the null operator analysis, reviews the basic phenomena to be examined and sets out the framework, essentially that of Chomsky (1986a, 1986b), within which the research has been carried out.

Chapter 2 examines the relation between predication and the operators, both overt and null, which allow clausal categories to function as predicates in OWM constructions. It is proposed that predication relations which are not licensed by θ-role assignment must be licensed by the existence of an agreement chain between the sub-

ject of predication and a predicate internal category. An agreement chain exists when two categories are connected by an unbroken sequence of independently motivated instances of agreement, e.g., subject-predicate agreement, SPEC-HEAD agreement, etc. It is futher argued that null operators arepure pronominals, i.e., pro, and that the agreement chain which licenses predication is sufficient to identify A'-pro.

Since A'-pro in OWM constructions receives ϕ-features via the agreement chain, it is licensed as the head of an A'-chain. In Chapter 3, it is shown that the fundamental difference between OWM constructions and parasitic gap constructions is that A'-pro in the latter does not participate in an agreement chain and, therefore, does not receive phi-features. The result is that A'-pro in parasitic gap constructions is not licensed to head a chain; however, under the appropriate assumptions about the constraints governing A'-chains, unidentified A'-pro may act as an intermediate empty category. This position is embedded in an analysis of parasitic gap constructions which treats the parasitic chain and the real chain as a single complex chain derived by chain formation, a non-exceptional, non-construction specific process. The Subjacency Condition is interpreted as a condition on chain links which applies at SS to the output of all chain formation operations and which, therefore, governs the formation of complex chains. Conditions on the identification of variables are also shown to affect the distribution of parasitic gaps. At LF A'-pro in these constructions, like other intermediate empty categories in argument chains, deletes via Affect α, yielding representations identical to those resulting from the Chomsky (1982) analysis, in which the matrix operator directly binds two variables. The anti-c-command constraint is once again analyzed as a Binding Condition C violation. The chapter ends with some speculative remarks concerning the typology of empty categories and the nature of chains.

Other aspects of A'-chains involving both null and overt operators are explored in Chapter 4, in particular, the greater sensitivity of extracted subjects in a variety of contexts to the presence of intervening barriers. It is shown that this senstitivity is not a unified phenomenon and that it does not motivate certain revisions of the ECP which have been proposed in recent work. The marginality of subject gaps in OWM constructions, parasitic gap constructions and within certain types of islands in English is attributed to the Subjacency Condition, in a revised relativized form which imposes a stricter SS bounding constraint on non-complement chains than on complement chains. Another group of constructions which exhibit stronger violations and which share the property that extraction of an argument requires the obligatory presence of an intermediate empty category in an A'-position at LF, are brought within the scope of the ECP by means of a condition on LF argument chains involving A'-positions. A discussion of several other topics, including the appropriate formulation of the Minimality Condition, the nature of antecedent government and head government, the proper definition of barrier, ends the chapter.

Planar Phonology and Morphology

Jennifer Sandra Cole

*Submitted to the Department of Linguistics and Philosophy in partial
fulfillment of the requirements of the Degree of Doctor of Philosophy in
Linguistics*

Abstract

The development of the non-linear theory of phonological representation has lent
great depth to our current understanding of long-distance phonological processes like
harmony, and, in particular, to our understanding of transparent and opaque segments
in harmony systems. This thesis argues for an analysis of harmony systems in which the
properties of transparency and opacity are not primitive, but instead derive from prop-
erties of the phonological representation to which harmony applies. Blocking segments
can be characterized either by their specification for the harmonic feature, or in cases
of parasitic harmony, by their specification for a contextual feature on which harmony
is dependent. Central to this analysis is the idea that all phonological processes are
governed by a locality constraint which requires that two elements related in a
phonological rule be adjacent at some level in the phonological representation.

The harmony rules of four languages are examined in detail; these rules seem to vi-
olate the adjacency constraint, allowing harmony to skip over segments that are speci-
fied for the harmonic feature-segments which in other harmony systems would be
expected to block harmony. In all four cases, harmony is a reflex of a morphological
affixation process. To explain the unusual properties of these morphologically governed
harmony systems, I adopt McCarthy's (1981) proposal that morphemes occupy sepa-
rate planes in the phonolgical representation of a word. The special property of
morphologically governed harmony is that it applies to multi-planar representations. In
a morphologically governed rule of F harmony, the harmonic feature (F) spreads on a
plane that is distinct from the (F) plane of stem segments. Since adjacency is always
calculated between elements on a single plane, F Harmony will never be blocked by a
(F) specification of a stem segment.

The multi-planar representations created by morphological affixation are collapsed
uni-planar representations at some stage in the derivation. It is shown that certain
non-morphologically governed harmony systems apply after this process of Plane
Conflation. The role of Plane Conflation in phonological systems is investigated,
focussing on the proposal made by Younes (1983) and McCarthy (1986) that Plane
Conflation is the formal mechanism that effects Bracket Erasure. A close look at the
empirical evidence for Bracket Erasure reveals that Bracket Erasure, as a universal con-
vention, does not apply internal to the lexical level of morpho-phonological derivation.
Regarding Plane Conflation, the available data from syncope systems (McCarthy, 1986)
and harmony systems only weakly suggest that Conflation may in some cases need to
apply internal to the lexical level. The conclusion is that Plane Conflation and Bracket
Erasure can only be equated insofar as Plane Conflation can be restricted to apply only
where Bracket Erasure applies: at the end of the lexical level.

125

Observations about the locality constraints on morphological and phonological processes have been used to argue for the Bracket Erasure Convention. It is shown that computational limitations of morpho-phonolgical parsing motivate such locality constraints, independent of the Bracket Erasure Convention. An Adjacency Constraint is formulated which requires that phonological elements relted in a rule be adjacent (on the skeleton, or on the plane of some distinctive feature or feature class node), and that morphological elements related in a rule meet a condition on morphological c-command and peripherality.

The role of morpheme planes in explaining phonological phenomena is further illustrated by analyses of four phonological rules from Fula, Malayalam, Dakota and Hausa.

Syntactic Features: Parametric Variation in the History of English

John Stewart Lumsden

*Submitted to the Department of Linguistics and Philosophy
in partial fulfillment of the requirements for the degree of
Doctor of Philosophy*

Abstract

This study compares the syntax of Old English and early Middle English with particular attention to the annals of the Peterborough Chronicle. It provides an account of the immediate changes in syntactic representations during this period and relates these changes to the revisions which swept the English lexicon during the Middle Ages.

This thesis argues that the properties of substantive inflection (i.e., number, gender and Case) are best represented as binary features in underspecified matrices. These grammatical features are syntactic features. Grammatical feature matrices define phrases in the syntactic representation.

The thesis proposes that a single binary feature distinguishes structural Case from inherent Case. In Old English, only structural Case was underlyingly marked. Inherent Case was assigned by a general rule in each derivation. In later English, this markedness was reversed in verb and adjective phrases. Because the Case feature is listed in verbal lexical entries, this reversal altered the markedness of verb classes in the English lexicon. During the Middle Ages, hundreds of verbs which had assigned inherent Case in Old English were revised to become structural Case assigners. More immediate changes in the syntax of early Middle English are evident in adjective phrases and in other constructions were Case is not specified in lexical entries.

The analysis provides support for a principles and parameters view of variation in natural language. The grammars of Old English and early Middle English are argued to be massively similar. Relatively simple changes in the distribution of grammatical features can account for complex differences in the surface structures of these languages.

Copular, Nominal and Small Clauses: a Study of Israeli Hebrew

Tova Rebecca Rapoport

*Submitted to the Department of Linguistics and Philosophy in
partial fulfillment of the requirements for the degree of Doctor of
Philosophy in Linguistics.*

Abstract

This dissertation is a study of structures of verbless predication in Israeli Hebrew and English. Predicative and equative nominal and copular constructions are closely examined, as are embedded subject-predicative constructions (small clauses).

Chapters 2 and 3 explore the thematic relations and corresponding syntactic properties of two major classes of nominal and copular constructions: predicative and equative. It is claimed that while in predicative sentences the predicate XP assigns a θ-role to the referential subject; in equatives, both NP's are referential, and neither assigns a theta-role. The identity relation of equative sentences is shown to require the mediation of a functional head (e.g., INFL), whereas the predication relation of predicative sentences does not. It is assumed that small clauses have no functional head; they, therefore, are never read as equative. The study of small clauses in Chapter 4 allows, in turn, a refinement in the principles constraining the predication relation.

In Hebrew, the present tense equivalents of copular constructions contain no verb. Such nominal sentences are discussed in Chapter 2 of this thesis, and their syntactic and semantic properties are studied. Under the assumptions about copular constructions argued for in this thesis, the Israeli Hebrew nominal sentences are seen to offer strong evidence in favor of a syntactic and thematic division of such verbless constructions into two classes: predicative and equative.

There are two nominal sentence types. One type is analyzed as a matrix small clause, an analysis which, along with certain assumptions about small clause structures in general, correctly predicts its properties and behavior. A second nominal sentence construction is analyzed as a full (tenseless) clause, headed by the Case-assigning AGR in INFL. This analysis, together with a strict view of AGR as a bundle of features, accounts for the distribution and semantic properties of this nominal sentence type.

In Chapter 3, the properties of precidative and equative copular constructions in general, and in English, in particular, are discussed. Arguments are given to support a thematic and syntactic distinction between predicatives and equatives. It is claimed further that the relevant characterization of this distinction is to be made solely in terms of the thematic relation involved in each construction type. This makes possible a simple classification of copular constructions.

In the theory of copular constructions outlined in this chapter, noun phrases of every type (e.g., definite, or proper NP's) can be used predicatively, under specific interpre-

tations. The verb be is argued to have no semantic content, nor thematic role, in either predicative or equative constructions. Thus, it follows that noun phrases can be licensed even when they do not receive a theta-role projected from a predicator's argument structure.

Chapter 4 deals with the facts of embedded subject-predicate constuctions in Israeli Hebrew. It is demonstrated that there is a limited class of argument small clauses in Hebrew, and it is argued that the small clause possibilities are limited due to the presence in Hebrew of a restriction on Case assignment: all verbal Case assignments must be θ-related. Small clauses are found in Hebrew only in those sentences whose matrix verb is causative. The fact that causative verbs and affixes require the incorporation of the second predicate is what allows the requirement in Hebrew Case assignment to be met. Embedded subject-predicate constructions which are not an argument of the verb, on the other hand, are comparatively free in Israeli Hebrew, since they do not constitute a violation of the Case-marking restriction.

As part of the account of small clauses, an analysis of their structure in terms of projections sets is presented. This analysis, in turn, allows the revision of the restriction on the domain of θ-marking, in general, and on the predication relation, in particular.

Null and Displaced Subjects

Ur Shlonsky

Abstract

This work explores three problems related to the syntactic position of clausal subject: Do all clauses require subjects? What conditions must be met for subjects to appear postverbally? Where are postverbal subjects attached?

The discussion begins with a study of expletives, in particular, of the relationship between expletives and postverbal subjects. It is hypothesized that expletives are fillers for the syntactic subject position at S-structure amd that they are replaced, in Logical Form, by the semantic subject of the clause. Various consequences of this hypothesis are probed, in particular, for Case theory and Binding theory.

Chapter 3 develops a theory of Case which incorporates both the Case Filter and the condition that heads of chains must be Case marked. The particular statement of this module of Universal Grammar has consequences for the status of null expletives and variables. There follows a discussion of the Case status of variables, in particular, in positions which are clitic doubled.

Chapter 4 studies subject inversion. First, the licensing conditions for postverbal subjects are discussed and the relevant facts from Hebrew are presented. It is then ar-

gued that Hebrew has a rule of subject postposing which adjoins a subject to VP, on the left. It is argued that Spanish utilizes the option of left, as opposed to right, adjunction to VP, while Italian does not. Various crosslinguistic differences can be accounted for on the basis of this distinction, especially with regards to the distribution of the definiteness effect.

Chapter 5 considers the pro module of UG. It is shown that null expletives which are replaced, in LF, by arguments which are personal, need to be supported as S-structure by coindexing with over-grammatical features.

A study of the possessive/existential alternation in Hebrew is the topic of the final chapter. It is proposed that the verb be/have is ambiguous between an unaccusative predicate taking a single argument to which nominative Case is assigned and verb subcategorized for two internal arguments, one of which is marked with accusative Case, the other with inherent dative Case. The questions relating to this verb are considered with the intention of clarifying further the notion of syntactic subject.

Grammaticalizing Aspect and Affectedness

Carol Tee Tenny

Abstract

This thesis is an investigation of the interaction of aspect and syntax. More particularly, the syntactic repercussions of the aspectual property of delimitedness are examined. Delimitedness - the temporal boundedness of an event - is shown to have an effect on a wide range of syntactic phenomena, including resultative secondary predicates, verb-particle constructions, and certain Case phenomena. Affectedness is also shown to depend on delimitedness. The interaction between affectedness and syntax is proposed to take place in the Case module of the grammar.

An analysis of the property of affectedness in aspectual terms leads to a theory in which the direct argument of a verb measures out the event described by the verb over time, as if on a scale. Affected arguments are direct arguments that delimit the event on that scale. Non-affected direct arguments also measure out the event, though they do not delimit it.

This aspectual property of direct arguments is the first of a set of aspectual principles of argument structure. Three additional principles are proposed: An event may be delimited only by its internal arguments-arguments within the verb phrase at deep structure. Indirect arguments may delimit the event parasitically through the direct argument, while external arguments may not delimit the event at all. Secondly, there may be only

one delimiting to a verb phrase. And, finally, secondary objects are always delimiting elements.

Two specifically syntactic issues are addressed. First, it is proposed that aspect is a syntactic category, and several possible instantiations of aspect in phrase structure are discussed. Secondly, the aspectual principles of argument structure are applied to verb-particle constructions, resultative secondary predicates, and double object constructions; and these principles are shown to shed some light on the syntactic behavior and structure of these constructions. The usefulness of aspect as a tool for syntactic investigations is demonstrated.

The aspectual principles of argument structure place constraints on the kind of event participants that can be internal arguments. In this way, these principles provide a principled mapping between the meaning of verbs and their syntactic representations. The Aspectual Interface Hypothesis is proposed, which maintains that the two systems communicate only through a common aspectual vocabulary. Under this view only the aspectual information in thematic roles is visible to the syntax, and thematic hierarchies are not necessary in the mapping between meaning and syntax. The Aspectual Interface Hypothesis is consonant with a highly autonomous syntax.

18.0   Auditory Physiology

18.1   Signal Transmission in The Auditory System

Academic and Research Staff

Prof. L.S. Frishkopf, Prof. N.Y.S. Kiang, Prof. W.T. Peake, Prof. W.M. Siebert, Prof. T.F. Weiss, Dr. R.A. Davis, Dr. B. Delgutte, Dr. L.A. Delhorne, Dr. D.K. Eddington, Dr. D.M. Freeman, Dr. J.J. Guinan, Jr., Dr. D.R. Ketten, Dr. W.M. Rabinowitz, Dr. J.J. Rosowski, I.A. Boardman, R.M. Brown, M.L. Curby, F.J. Stefanov-Wagner, D.A. Steffens

Graduate Students

K. Donahue, S.B.C. Dynes, G. Girzon, M.P. McCue, J.R. Melcher, X-D. Pang, S.L. Phillips

18.1.1   Basic and Clinical Studies of the Auditory System

Investigations of signal transmission in the auditory system are carried out in cooperation with the Eaton-Peabody Laboratory for Auditory Physiology at the Massachusetts Eye and Ear Infirmary. The long term objective is to determine the anatomical structures and physiological mechanisms that underlie vertebrate hearing and to apply that knowledge to clinical problems. Studies of cochlear implants in humans are carried out in the Cochlear Implant Laboratory in a joint program with the Massachusetts Eye and Ear Infirmary. The ultimate goal of these devices is to provide speech communication for the deaf by using electric stimulation of intracochlear electrodes to elicit patterns of auditory nerve fiber activity that the brain can learn to interpret.

18.1.2   Signal Transmission in the External and Middle Ear

Kathleen M. Donahue, Darlene R. Ketten, William T. Peake, John J. Rosowski

We seek to relate signal-transmission properties of ears to their structural features. We have been primarily interested in interspecies variations, but in one project we have pursued our goal through anatomical and physiological measurements of intraspecies variations. In the alligator lizard, whose ear we have studied extensively, we have used individuals with a wide range of sizes. The magnitude of the acoustic admittance of the ear at low frequencies correlates well with the size (weight and snout-to-vent length) of the lizard, and with the area of the tympanic membrane. Admittance magnitudes at higher frequencies do not show this close correlation. These results, considered with earlier admittance measurements of the effects of removal of specific structures, suggest that the middle ear structures that control the low-frequency admittances grow with the animal, whereas the structures of the inner ear that are more important at higher fre-

quencies do not.[1] Another suggestion of these results is that larger individuals possess more sensitive hearing, at low frequencies, than smaller lizards.

In another project we have measured acoustic impedances of human cadaver ears to test "normality" of mechanical behavior of these ears.[2] The results show that ears that are kept frozen (when measurements are not being made) show only small alterations over periods of months. The impedance magnitudes are quite similar to those reported for ears of live humans. Thus, with cadaver ears we should be able to make measurements on human ears that are comparable to those we have made on other species.

18.1.3   Cochlear Mechanisms

Dennis M. Freeman, Lawrence S. Frishkopf, Thomas F. Weiss

Manuscripts describing the frequency dependence of synchronization of spikes discharges of cochlear nerve fibers to the phase of a tone have been completed.[3-5] The principal conclusions of these studies are: 1) the cochlea of a variety of vertebrate ears contains lowpass filter processes whose orders sum to at least 4 and which serve to degrade the timing information present in an acoustic stimulus; 2) one such process, which results from the resistance and capacitance of the hair cell membrane, limits the rate at which the membrane potential of a hair cell can change; and 3) the remaining process(es) occur in the transformation of the receptor potential of a hair cell to the spike discharge of a cochlear nerve fiber.

We have designed and built a system to measure submicron motion of inner ear structures in an *in vitro* preparation of the auditory organ of the alligator lizard. The scheme, which is similar to one described in the literature, is to project the microscope image of a structure onto a pair of photodiodes, with the image aligned so that the movement of the object sweeps across the photodiodes. Differential recording of the photodiode currents gives a measure of the displacement of the object across the photodiode surface. By mounting the photodiodes on a device that can be moved a known distance, the apparatus can be calibrated and the displacement of the object relative to the photodiodes can be determined. With this system we have measured displacements as small as 1 nm.

To better understand its structure, we have constructed a three-dimensional scale model of the inner ear of the alligator lizard. We first obtained photomicrographs (at a magnification of 50) of a contiguous series of histological sections of the ear. Tracings of key structures were made from the photographs, and used to cut sheets of balsawood which were then assembled into a three-dimensional model. Flexible polyurethane rubber was used to make a mold for each of three separate parts representing the cochlear duct, auditory nerve, and otic capsule. The molds were then used to cast transparent plastic models of each part. The parts fit together so that the relation between them can be visualized in three dimensions. The model has been used to develop surgical methods and experimental chambers for physiological studies of the alligator lizard ear. It is very useful for anyone interested in learning the anatomy of this ear.

18.1.4   Membrane Properties of Inner-Ear Neurons *In Vitro*

Robin L. Davis

The goal of this work is to characterize the electrophysiological and pharmacological properties of auditory neurons. To this end, a technique has been developed to grow single auditory neurons in tissue culture without the complicating influences of synaptic connections or hormonal regulation. This preparation enables one to ask questions such as:

1.   Are there differences in the membrane properties of the two classes of auditory neurons that can be related to the known difference in their discharge patterns?

2.   What is the distribution of ionic channel types along the length of these neurons?

3.   Are there neurotransmitter-activated channels specific to the peripheral or central projections of these neurons? If so, which transmitters activate these channels?

The goldfish (*Carassius auratus*) was the experimental animal of choice since our laboratory has extensive experience isolating and purifying neuroactive substances released by inner-ear receptor cells in this animal. Our procedure yields two groups of neurons distinguished by their location in the auditory nerve and their axon diameters. One to two weeks after being placed in culture, the cells generate action potentials and sprout processes that can extend for hundreds of microns.[6]

The properties of these neurons will be further evaluated with electrophysiological and pharmacological studies. Preliminary studies have shown that the patch clamp procedure can be successfully implemented to record single channel currents from the growing ends of the neurons as well as from membrane that has been acutely de-sheathed from its myelin covering. Experiments using the cell-attached configuration of the patch clamp technique have revealed single channel currents with conductances ranging from 16 to 120 pS in solutions that select for K^+, Cl^- or Ba^{++} currents. These conductances and their voltage dependence are being systematically categorized according to ionic specificity as well as position along the length of the neuron. Although this work is in its early stages, the results to date have been extremely encouraging, and it appears that a complete categorization of the channel types is feasible. This will aid considerably in the search for the afferent transmitter substance in the inner ear and will increase our understanding of this important link between the auditory receptors to the CNS.

18.1.5   Stimulus Coding in the Auditory Nerve

Bertrand Delgutte

Masking of tone signals might be caused either by spread of the excitation produced by the masker to the place of the signal along the cochlea, or by suppression of the response to the signal by the masker, or by a combination of the two. To separate these different forms of masking, two types of masked thresholds were measured from auditory nerve fibers in anesthetized cats, using methods mimicking the two-interval, two-alternative forced-choice paradigm of psychophysics: simultaneous masked thresholds, and nonsimultaneous thresholds.[7,8] For measuring simultaneous thresholds,

a stimulus consisting of a 1 kHz masker and a tone signal is presented in alternation with the masker alone, and the signal level is adjusted by a PEST procedure until the spike count in response to the two-tone stimulus exceeds the count in response to the masker alone for 75 percent of the presentations. This simultaneous masked threshold reflects the effects of both suppression and spread of excitation. For measuring nonsimultaneous thresholds, the signal alone is presented in alternation with the masker alone, and the signal level is adjusted until the spike counts meet the same probabilistic criterion as in simultaneous masking. The nonsimultaneous threshold must be entirely due to the spread of masker excitation because suppression does not occur when the masker and the signal are not simultaneous. Thus, the difference between simultaneous and nonsimultaneous thresholds gives a measure of the contribution of suppression to masking.

For fibers whose characteristic frequencies (CF) are close to the 1 kHz masker, the two types of masked thresholds are similar, indicating that masking is primarily due to spread of excitation. In contrast, for fibers with CF's either above or below the masker frequency, simultaneous masked thresholds are considerably higher than non-simultaneous thresholds, suggesting that two-tone rate suppression contributes significantly to masking.

To obtain a general picture of masking for a population of auditory nerve fibers, we determined for each masker and each signal frequency the auditory nerve fibers that had the lowest (or "best") masked thresholds. Profiles of best threshold against signal frequency roughly resemble psychophysical masking patterns, with a maximum near the masker frequency, and a pronounced skew towards high frequencies. Best threshold profiles are more sharply tuned in nonsimultaneous that in simultaneous masking, a phenomenon which is also found in psychophysics. Simultaneous masking patterns for a masker at 80 dB SPL extend considerably more towards high signal frequencies than they do for a 60 dB masker. In particular, for signal frequencies well above the masker, best thresholds increase by 40 to 50 dB for a 20 dB increase in masker level. This supralinear growth of masking is also found in psychophysics, and is called "upward spread of masking." It is much less apparent in nonsimultaneous masking, where the masking seems to grow more linearly. This result suggests that the upward spread of simultaneous masking is due to the rapid growth of suppression rather than to the growth of excitation.

In summary, both two-tone rate suppression and spread of masker excitation contribute to the masking of auditory nerve fiber responses, with suppression being most important for signal frequencies well above the masker frequency. Patterns of best single-fiber masked thresholds against signal frequency resemble psychophysical masking patterns in many respects. Both suppression and spread of excitation are essential to obtain this good correspondence between physiology and behavior.

During the past year a previously-written paper on the physiological basis of intensity discrimination has been published.[9]

18.1.6 Middle Ear Muscle Reflex

John J. Guinan, Jr., Xiao-Dong Pang, Michael P. McCue

We aim to determine the structural and functional basis of the middle ear reflexes. During the past year, we have completed a manuscript which describes changes in the acoustic stapedius reflex produced by brainstem lesions which destroyed selected sets of stapedius motoneurons.[10] The results of this work suggest that inputs from the two cochleas are distributed inhomogeneously across the stapedius motoneuron pool in such a way as to produce a segregation of function, with motoneurons in one brainstem region responding preferentially to contralateral sound and motoneurons in other regions responding preferentially to ipsilateral sound.

We have confirmed and extended this hypothesis by recording from single stapedius motoneurons and determining their responses to sound. During the past year we have completed a paper on the implications of our stapedius recordings with regard to motor control issues.[11] In particular, our results show that the "size principle" a commonly held hypothesis which accounts for the recruitment order of motoneurons innervating a muscle, does not hold for the stapedius muscle.

During the past year, we have completed the data gathering phase of our project in which physiologically characterized stapedius motoneurons are labeled by intracellular injections of the tracer, horseradish-peroxidase (HRP).[12] We now have labeled stapedius motoneurons in each of our five physiological categories. This work shows that stapedius motoneurons with distinctive electrophysiological properties have similar locations in the brainstem with limited overlap between categories. The results are consistent with the idea that the stapedius motoneuron pool is divided into groups which are spatially segregated in the brainstem and receive different patterns of inputs from the two ears.

During the past year, considerable progress has been made on our project to determine the effects of stapedius muscle contractions on the responses of single auditory nerve fibers. It is well known that contractions of the stapedius muscle reduce sound transmission primarily at low sound frequencies. Because of the nonlinear properties of the cochlea, intense sounds at low frequencies are particularly effective in reducing (masking) responses to sounds at higher frequencies. Our experiments have shown that stapedius contractions reduce the masking of high frequency sounds by low frequency sounds. In a typical case, a 20 dB reduction of sound transmission at 0.5 kHz can improve the threshold by 35 dB at 6 kHz. Furthermore, the data show that this effect of stapedius contractions can be fully accounted for by the masking properties of auditory nerve fibers and the attenuation of middle ear transmission produced by the stapedius. Such a reduction of masking is probably one of the most important functions of the stapedius muscle.

With other members of the Eaton-Peabody Laboratory, a paper has been written which describes the acoustic reflex properties of the middle ear muscles and the auditory efferents, and explores the implications these might have for the design of cochlear implants.[13] Also, during the past year a previously submitted paper on asymmetries in the acoustic reflexes of the cat stapedius muscle has been published.[14]

18.1.7 Cochlear Efferent System

John J. Guinan, Jr.

Our aim is to understand the physiological effects produced by medial olivocochlear (MOC) efferents which terminate on outer hair cells. During the past year our efforts have focused on the effects of electrical stimulation of medial olivocochlear efferents on single auditory nerve fibers. The work has included data analysis of previous work done with M.L. Gifford and new experiments to provide data to fill in gaps left by previous experiments. This work has led to three papers, two of which (outlined below) are completed.

In the first set of experiments,[15] we selectively stimulated medial efferents in cats, and determined the changes produced in the firing rates of auditory nerve fibers with sound level as a parameter. Efferent stimulation shifted rate vs. level functions to higher sound levels and depressed the rate in the plateau. The amplitudes of the efferent induced effects were different for auditory nerve fibers with different spontaneous rates (by as much as a factor of three for the plateau depression). The results support several hypotheses: 1) individual crossed and uncrossed MOC fibers produce similar effects; 2) efferents differentially change the information carrying properties of auditory nerve fibers in different spontaneous rate categories; and 3) that the level shifts are produced by MOC efferents acting on outer hair cells to reduce the mechanical stimulus to inner hair cells.

In the second set of experiments,[16] we measured changes in the rate of spontaneous firing (SR) of single auditory nerve fibers in response to the stimulation of medial olivocochlear efferents in cats. Efferent stimulation depressed SR. In most animals, the SR depression increased as auditory nerve fiber sensitivity increased, increased as the original SR decreased and had a maximum at characteristic frequencies (CFs) of about 10 kHz. The data are consistent with the hypotheses 1) that "spontaneous" firing of auditory nerve fibers is reduced by an efferent induced hyperpolarization of outer hair cells which is electrically coupled through the endocochlear potential to inner hair cells and 2) that the reduction is largest at CFs near 10 kHz because this CF region receives the greatest outer hair cell innervation from medial efferents.

During the past year, a paper was written which reviews recent advances in the understanding of the physiology of efferent fibers in the cochlea,[17] and a previously submitted paper was published.[18]

18.1.8 Central Neural Pathways: Evoked Responses

Jennifer R. Melcher, Nelson Y.S. Kiang

We are investigating the brainstem auditory evoked potential (BAEP) which is a time varying potential that can be recorded from electrode pairs on the surface of the head in the 10 msec immediately following the delivery of a punctate acoustic stimulus to the ear of a cat. While it is known that the BAEP is due to currents generated by cells in the auditory nerve and brainstem, exactly which of the numerous cell groups contribute to the BAEP is largely unknown. The goal of this project is to better understand which cells contribute to the BAEP. Our approach is to selectively destroy particular cell groups by

injecting kainic acid, a neurotoxin, at discrete locations along the brainstem auditory pathway. The injections result in changes in the BAEP. At the end of each experiment, the brainstem is prepared histologically and the location and number of cells destroyed is determined. The BAEP changes are then compared with the regions of cell destruction.

18.1.9 Cochlear Implants: Current Spread During Electrical Stimulation of the Human Cochlea

Donald K. Eddington, Gary Girzon

The basic function of a cochlear prosthesis is to elicit patterns of activity on the array of surviving auditory nerve fibers by stimulating electrodes that are placed in and/or around the cochlea. By modulating these patterns of neural activity, these devices attempt to present information that the implanted subject can learn to interpret. The spike activity patterns elicited by electrical stimulation depend on several factors: the structure of the cochlea (three-dimensional, electrically heterogeneous), the geometry and placement of the stimulating electrodes, the stimulus waveform, and the distribution of exitable auditory nerve fibers. Understanding how these factors interact to determine the activity patterns is fundamental to designing better devices and to interpreting the results of experiments involving intracochlear stimulation of animal and human subjects. As a first step towards this understanding, the goal of this project is to construct a software model of the cochlea that predicts the patterns of current flow due to the stimulation of arbitrarily placed, intracochlear electrodes.

Last year sections from a human temporal bone were digitized and resistivities were assigned to the major cochlear elements (e.g., bone, nerve, perilymph, endolymph). Finite element techniques were used to convert the anatomical and resistivity data to a set of equations representing a three dimensional mesh of 512 by 512 by 46 nodes. Current sources were defined at nodes representing the positions of the six intracochlear electrodes used in five human subjects implanted at the Massachusetts Eye and Ear Infirmary. The equations were solved and maps of nodal potentials located along the length of the spiraling scala tympani showed a monotonic reduction of potential from the more apically placed current sources toward the base while a potential plateau was observed as one moves from the basal current sources toward the apex. For basal current sources, "bumps" were observed in the potential plateaus between 15 and 20 mm from the base. These nonmonotonicities probably indicate significant current pathways between cochlear turns in addition to the pathway along the scala tympani.

This year we completed the measurement of potentials at unstimulated electrodes made in the initial five human subjects implanted with intracochlear electrodes. These measurements demonstrated the asymmetric potential distributions predicted by the model in all five subjects. The "bumps" predicted by the model were also present in the potential distributions measured during the stimulation of the most basal of the implanted electrodes in all five subjects.

We are now collecting psychophysical measures of current interaction to determine if the pattern of interaction between simultaneously stimulated electrodes will exhibit the same asymmetries as the potential distributions along the scala tympani. Preliminary

measurements obtained in two subjects exhibit such an asymmetric distribution of interaction. We are currently collecting these data from the other three subjects.

18.1.10 Cochlear Implants: Electrical Stimulation of the Auditory Nerve

Betrand Delgutte, Scott B.C. Dynes

This project aims at characterizing the patterns of auditory nerve activity produced by electrode configurations similar to those used in cochlear implants, and at identifying physiological limitations on schemes for encoding speech information for electrical stimulation. In these experiments, the activity of auditory nerve fibers in anesthetized cats is recorded in response to electrical currents applied at pairs of electrodes inserted into the cochlea through the round window. Initial efforts focused on measuring the phase locking (or "synchrony") of spikes to electric sinusoidal stimulation. Phase locking is an important property of the response of auditory nerve fibers because it has been suggested that it is essential for discriminating certain vowels, and because, for single channel implants, it is the only way in which information about the stimulus spectrum can be encoded.

A major experimental problem encountered was the stimulus artifact, which arises from currents generated by the stimulus and can result in an artificially elevated measure of phase locking. This problem was essentially eliminated through the development of a special electrode that records differentially between two closely spaced locations, and by the use of an adaptive filter which greatly reduces sinusoidal components at the stimulus frequency in the signal recorded by the microelectrode.

Preliminary results show that phase locking of nerve spikes to sinusoidal stimuli is more pronounced in electrical stimulation than acoustical stimulation, with the synchrony index being larger in electrical stimulation for all frequencies investigated, ranging from approximately 4 kHz to 10 kHz. Also, it seems that the synchronization index reaches its maximum at or very near electric threshold. These results suggest that electrical stimulation can, in principle, mimic some of the temporal fine structure of nerve activity which occurs in the normally functioning ear.

References

[1] J.J. Rosowski, D.R. Ketten, and W.T. Peake, "Allometric Correlations of Middle Ear Structure and Function in One Species - the Alligator Lizard," Midwinter Meeting, Association for Research in Otolaryngology, February 1988, p. 32.

[2] S.N. Merchant, P.J. Davis, J.J. Rosowski, "Normality of the Input Immitance of Middle Ears from Human Cadavers," Abstract, Midwinter Meeting, Association for Research in Otolaryngology, February 1988, p. 211.

[3] C. Rose and T.F. Weiss, "Frequency Dependence of Synchronization of Cochlear Nerve Fibers in the Alligator Lizard: Evidence for a Cochlear Origin of Timing and Non-Timing Neural Pathways," *Hear. Res.* In press.

[4] T.F. Weiss and C. Rose, "Stages of Degradation of Timing Information in the Cochlea: a Comparison of Hair Cell and Nerve Fiber Responses in the Alligator Lizard," *Hear. Res.* In press.

[5] T.F. Weiss and C. Rose, "A Comparison of Synchronization Filters in Different Auditory Receptor Organs," *Hear. Res.* In press.

[6] R.L. Davis, E.A. Mroz, and W.F. Sewell, "Isolated Auditory Neurons in Culture", Midwinter Meeting, Association for Research in Otolaryngology, February 1988, p. 240.

[7] B. Delgutte, "Physiological Correlates of Tone-on-Tone Masking in the Discharge Rates of Auditory Nerve Fibers," Midwinter Meeting, Association for Research in Otolaryngology, February 1988.

[8] B. Delgutte, "Physiological Mechanisms of Masking," In *Basic Issues in Hearing,* eds. H. Duifhuis and J.W. Horst. Groningen: University Press. In press.

[9] B. Delgutte, "Peripheral Auditory Processing of Speech Information: Implications from a Physiological Study of Intensity Discrimination," in *The Psychophysics of Speech Perception,* ed. M.E.H. Schouten, 333-353. Dordrecht, Holland: Nijhoff, 1987.

[10] M.P. McCue and J.J. Guinan, Jr., "Anatomical and Functional Segregation within the Stapedius Motoneuron Pool of the Cat," submitted to *J. Neurophysiol.*

[11] J.B. Kobler, S.R. Vacher, and J.J. Guinan, Jr., "The Recruitment Order of Stapedius Motoneurons in the Acoustic Reflex Varies with Sound Laterality," *Brain Res.* 425:372 (1987).

[12] S.R. Vacher, J.B. Kobler, and J.J. Guinan, Jr., "Brainstem Locations of Physiologically Characterized Stapedius Motoneurons in Cat: Single Unit Labeling," *Soc. Neurosci. Abstr.* 13:549 (1987).

[13] N.Y.S. Kiang, J.J. Guinan, Jr., M.C. Liberman, M.C. Brown, and D.K. Eddington, In "Feedback Control Mechanisms of the Auditory Periphery: Implications for Cochlear Implants," In *Proceedings of the International Cochlear Implant Symposium,* 1987. In press.

[14] J.J. Guinan, Jr., and M.P. McCue, "Asymmetries in the Acoustic Reflexes of the Cat Stapedius Muscle," *Hear. Res.* 26:1 (1987).

[15] J.J. Guinan, Jr. and M.L. Gifford, "Effects of Electrical Stimulation of Efferent Olivocochlear Neurons on Cat Auditory Nerve Fibers. I. Rate versus Sound Level Functions," *Hear. Res.* In press.

[16] J.J. Guinan, Jr. and M.L. Gifford, "Effects of Electrical Stimulation of Efferent Olivocochlear Neurons on Cat Auditory Nerve Fibers. II. Spontaneous Rate," *Hear. Res.* In press.

[17] J.J. Guinan, Jr., "Physiology of the Olivocochlear Efferents," in *Auditory Pathway - Structure and Function,* ed. J. Syka. New York: Plenum. In press.

[18] M.L. Gifford and J.J. Guinan, Jr., "Effects of Electrical Stimulation of Medial Olivocochlear Neurons on Ipsilateral and Contralateral Cochlear Responses," *Hear. Res.* 29:179 (1987).
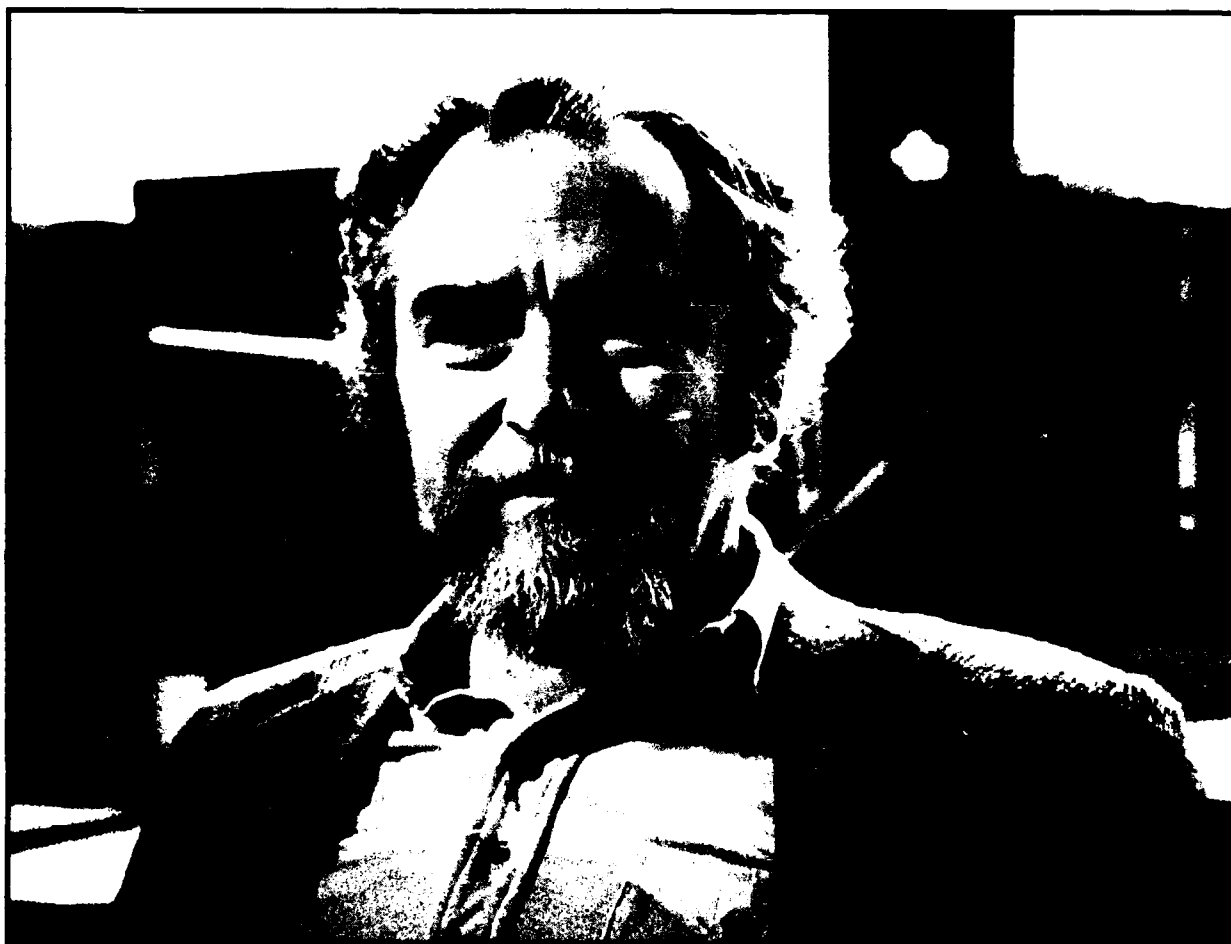
Professor Thomas F. Weiss

19.0   Sensory Communication

19.1   Auditory Psychophysics and Aids for the Deaf

Academic and Research Staff

Prof. L.D. Braida, Dr. D.K. Bustamante, Dr. H.S. Colburn, Dr. L.A. Delhorne, Dr. N.I. Durlach, Dr. J.A. Frisbie, Dr. K.W. Grant, Dr. J.D. Koehnke, Dr. H.B. Lee, Dr. N.A. Macmillan, Dr. K. Payton, Dr. W.M. Rabinowitz, Dr. C.M. Reed, Dr. B. Schneider, Dr. V.W. Zue, Dr. P.M. Zurek

Visiting Scientist

Dr. N.A. Macmillan[17]

Graduate Students

D. Barnes, P. Duchnowski, R. Hammerschlag, T.H. Im, Y. Ito, S.K. Isabelle, M.E. Machado, E.L. Markowitz, B. Mihura, G. Owen, C. Passaro, M.H. Power, P.M. Peterson, K. Rashd, B. Shinn, D. Stephan, T. Tamir, R.M. Uchanski, S-M. Wei, J.S. Yu, H. Zhang, M. Zissman

Support Staff

E.M. Luongo

Research is being conducted on a variety of topics concerned with the auditory and tactile senses, particularly with a view to the development of improved aids for the deaf. The supporting grants are listed below. Detailed progress reports are available from the investigators (listed below) and the granting agencies. Publications and talks reporting this work are listed below.

19.1.1   Perceptual Anchors

National Science Foundation (Grant BNS 84-11392)

Louis D. Braida, Neil A. Macmillan

19.1.2   Binaural Hearing

National Institutes of Health (Grant 5 R01 NS10916)

H. Steven Colburn, Nathaniel I. Durlach, Patrick M. Zurek

---

[17] Brooklyn College

19.1.3 Hearing Aid Research

National Institutes of Health (Grant 5 R01 NS12846)

Louis D. Braida, Patrick M. Zurek, Nathaniel I. Durlach, Charlotte M. Reed

19.1.4 Tactile Communication of Speech

National Institutes of Health (Grant 5 R01 NS14902)
National Science Foundation (Grant BNS 84-17817)

Nathaniel I. Durlach, William M. Rabinowitz, Charlotte M. Reed

19.1.5 Multimicrophone Hearing Aids

National Institutes of Health (Grant 1 R01 NS21322)

Patrick M. Zurek, Nathaniel I. Durlach, William M. Rabinowitz

19.1.6 Cochlear Prostheses

National Institutes of Health (Grant 1 P01 NS23734)

William M. Rabinowitz, Donald K. Eddington

19.1.7 Hand Function

National Science Foundation (Grant DMC 83-32460)

Nathaniel I. Durlach, William M. Rabinowitz

Publications

Bustamante, D.K., and Braida, L.D., "Multiband Compression Limiting for Hearing-Impaired Listeners," *J. Rehab. Res. Dev.* 24 (4):149 (1987).

Colburn, H.S., P.M. Zurek, and N.I. Durlach, "Binaural Directional Hearing - Impairments and Aids," In *Directional Hearing,* eds. W. Yost and G. Gourevitch. New York: Springer Verlag, 1987.

Durlach, N.I., C.R. Corbett, M.V. McConnell, P.M. Peterson, W.M. Rabinowitz, and P.M. Zurek, "Multimicrophone Monaural Hearing Aids," 10th Annual Conference Proceedings Rehabilitation Engineering, San Jose, California, 1987.

Durlach, N.I., C.M. Reed, C.E. Sherrick, and J.D. Miller, "Sensory Substitution: Visual and Tactual Methods," CHABA Report. In press.

Farrar, C.L., C.M. Reed, N.I. Durlach, L.A. Delhorne, P.M. Zurek, Y. Ito, and L.D. Braida, "Spectral-shape Discrimination. I. Results from Normal-hearing Listeners for Stationary Broadband Noise," *J. Acoust. Soc. Am.* 81:1085 (1987).

Furst, M., W.M. Rabinowitz, and P.M. Zurek, "Acoustic Distortion from Human Ears: Relation to Evoked Emissions and Combination Tones," submitted to *J. Acoust. Soc. Am.*

Gagne, J.-P., and P.M. Zurek, "Resonance-Frequency Discrimination," accepted for publication, *J. Acoust. Soc. Am.*

Grant, K.W., "Encoding Voice Pitch for Profoundly Hearing-impaired Listeners," *J. Acoust. Soc. Am.* 82:423 (1987).

Grant, K.W., "Frequency Modulation Detection by Normally Hearing and Profoundly Hearing-impaired Listeners," *J. Speech Hear. Res.* 30:558 (1987).

Grant, K.W., "Identification of Intonation Contours by Normally Hearing and Profoundly Hearing-impaired Listeners," *J. Acoust. Soc. Am.* 82:1172 (1987).

Held, R., and N.I. Durlach, "Telepresence, Time Delay, and Adaptation," *Proceedings of the Symposium and Workshop on Spatial Displays and Spatial Instruments,* NASA and University of California, Berkeley, Asilomar, California, 1987.

Houtsma, A.J.M., N.I. Durlach, and D.M. Horowitz, "Comparative Learning of Pitch and Intensity Identification," *J. Acoust. Soc. Am.* 81:129 (1987).

Jain, M., J.R. Gallagher, and H.S. Colburn, "Interaural Correlation Discrimination in the Presence of a Spectral Fringe," submitted to *J. Acoust. Soc. Am.*

Koehnke, J., and M.F. Cohen, "Masker Effects in Binaural Detection and Interaural Time Discrimination," *J. Acoust. Soc. Am.* 81:724 (1987).

Macmillan, N.A., "Beyond the Categorical/Continuous Distinction: A Psychophysical Approach to Processing Modes," In *Categorical Perception,* ed. S. Harnad. New York: Cambridge University Press, 1987.

Macmillan, N.A., L.D. Braida, and R.F. Goldberg, "Central and Peripheral Processes in the Perception of Speech and Nonspeech Sounds," In *The Psychophysics of Speech Perception,* ed. M.E.H. Schouten. Dordrecht, Holland: Nijhoff, 1987.

Macmillan, N.A., R.F. Goldberg, and L.D. Braida, "Vowel and Consonant Resolution: Basic Sensitivity and Context Memory," submitted to *J. Acoust. Soc. Am.*

Payton, K L., "Vowel Processing by a Model of the Auditory Periphery: A Comparison To Eight-Nerve Responses," submitted to *J. Acoust. Soc. Am.*

Peterson, P.M., N.I. Durlach, W.M. Rabinowitz, and P.M. Zurek, "Multimicrophone Adaptive Beamforming for Interference Reduction in Hearing Aids," *J. Rehab. Res. Dev.* 24 (4):103 (1987).

Peterson, P.M., and J.A. Frisbie, "An Interactive Environment for Signal Processing on a VAX Computer," In *1987 Proceedings of the International Conference on Acoustic Speech Signal Processings,* 1891-1894.

Picheny, M.A., N.I. Durlach, and L.D. Braida, "Speaking Clearly for the Hard of Hearing. III: An Attempt to Determine the Contribution of Speaking Rate to Differences in Intelligibility between Clear and Conversational Speech," submitted to *J. Speech Hear. Res.*

Rabinowitz, W.M., A.J.M. Houtsma, N.I. Durlach, and L.A. Delhorne, "Multidimensional Tactile Displays: Identification of Vibratory Intensity, Frequency, and Contactor Area," *J. Acoust. Soc. Am.* 82:1243 (1987).

Zurek, P.M., "The Precedence Effect," In *Directional Hearing,* eds. W. Yost and G. Gourevitch. New York: Springer-Verlag, 1987.

Zurek, P.M., "A Predictive Model for Binaural Advantages and Directional Effects in Speech Intelligibility," submitted to *J. Acoust. Soc. Am.*

Zurek, P.M., and L.A. Delhorne, "Consonant Reception in Noise by Listeners with Mild and Moderate Hearing Impairment," *J. Acoust. Soc. Am.* 82:1548 (1987).

Zurek, P.M., and N.I. Durlach, "Masker-Bandwidth Dependence in Homophasic and Antiphasic Tone Detection," *J. Acoust. Soc. Am.* 81:459 (1987).

Talks

Braida, L.D., "Review of Research on Signal Processing for Hearing Aids," presented as part of the Symposium on Auditory Signal Analysis and Signal Processing for the Hearing Impaired, Swedish National Board for Technical Development, Sollentuna, Sweden, October 1987.

Braida, L.D., and D.K. Bustamante, "Physical and Perceptual Effects of Amplitude Compression for Hearing Aids," presented as part of the Miniseminar on Hearing Aid Processed Speech at the American Speech-Language-Hearing Association Convention, New Orleans, November 1987.

Grant, K.W., "Evaluating the Articulation Index for Auditory-Visual Input," *J. Acoust. Soc. Am.* 82: S4(A) (1987).

Isabelle, S.K., and H.S. Colburn, "N0Spi Detection With Frozen Noise Samples at 500 Hz," *J. Acoust. Soc. Am.* 82: S109 (1987).

Koehnke, J., and H.S. Colburn, "The Dependence of Binaural Detection and Interaural Discrimination on Interaural Time and Intensity in Normal and Impaired Listeners," *J. Acoust. Soc. Am.* 81: S27 (1987).

Koehnke, J., and H.S. Colburn, "Binaural Detection and Discrimination in Normal and Hearing-Impaired Listeners," presented at the American Speech-Language-Hearing Association Convention, New Orleans, Louisiana, 1987.

Koehnke, J., and H.S. Colburn, "Effects of Roving Level on Binaural Detection and Discrimination On and Off Midline," *J. Acoust. Soc. Am.* 82: S109 (1987).

Rabinowitz, W.M., "Tactile Aids for the Deaf," Gordon Research Conference on Implantable Auditory Prostheses, New London, New Hampshire, July 1987.

Rabinowitz, W.M., "Noise Reduction Techniques for Hearing Aids," part of the Mini-seminar on Hearing Aid Processed Speech at the American Speech-Language-Hearing Association Convention, New Orleans, November 1987.

Rabinowitz, W.M., "Directional Processing for Interference Reduction in Hearing Aids," *J. Acoust Soc. Am.* 82: S38 (1987).

Reed, C.M., W.M. Rabinowitz, and N.I. Durlach, "Tactile Speech Reception Using Augmented Tadoma," *J. Acoust Soc. Am.* 82: S23 (1987).

Reed, C.M., L.A. Delhorne, and N.I. Durlach, "Tactile Reception of Fingerspelling and Sign Language," *J. Acoust Soc. Am.* 82: S24 (1987).

Uchanski, R.M., L.D. Braida, and N.I. Durlach, "Clear Speech," presented as part of the Miniseminar on Hearing-Aid Processed Speech, the American Speech-Language-Hearing Association Convention in New Orleans, November 1987.

Theses

Choi, S., *The Effect of Pauses on the Intelligibility of Sentences*, S.B. thesis, Dept. of Electr. Eng. and Comp. Sci., MIT, 1987.

Im, T.H., *Noise Reduction for Performance Improvements in the IBM Speech Recognizer*, S.M. thesis, Dept. of Electr. Eng. and Comp. Sci., MIT, 1987.

Kaomea, P., *Auditory Localization Cue Simulator*, S.B. thesis, Dept. of Electr. Eng. and Comp. Sci., MIT, 1987.

Washington, D.L., *Evaluation of an Augmented Tadoma System*, S.B. thesis, Dept. of Electr. Eng. and Comp. Sci., MIT, 1987.

Clockwise from right: Professor Louis D. Braida, Research Assistant Rosalie Uchanski, Postdoctoral Associate Dr. Diane K. Bustamante, and Research Assistant Matthew H. Power

20.0 Physiology

Academic and Research Staff

Prof. J. Lettvin, Prof. C. Searle, G. Geiger, D. Denton, A. Grant, G. Pratt, T. Sciascia, R. Webster

20.1 Introduction

We will describe four of the various studies progressing at this laboratory that have occupied the most attention over the past year. They are only remotely connected to each other in subject and method and, therefore, will be described separately. The first subject has received enough public attention and controversy that we will spend much of the report in laying out the underlying ideas associated with the work.

20.2 Visual Function in Dyslexia

Gad Geiger and Jerome Lettvin

Dyslexia is a disorder that is hard to explain. A person with good vision, skillful in sports, the graphic arts, or engineering design, nevertheless cannot read or cannot improve his defective reading ability to that general level of competence expected of a high school graduate. This trouble becomes almost inexplicable when there exist students in mathematics who can read equations but not the connecting text. In general it is supposed that dyslexia is some disorder of the "higher functions."

But we have found that the distributions of certain visual functions over the visual field differ markedly between dyslexics and ordinary readers. Specifically, if we consider the visual field as centered on the axis of gaze, there is a solid angle of about 1° − 2° radius around the axis in which ordinarily objects and details are clear and distinct. This is the region of central vision and corresponds with the area in which the photosensors are the most narrow and, therefore, the most dense. Outside this region is the peripheral field in which objects ordinarily lose clarity and distinction as they increase in angular distance from the axis of gaze.

Our discovery was that the severe dyslexic sees isolated letters or strings of letters or figures best not around the central region but in the near periphery, between 5° and 10° eccentric to the axis. This eccentriciy is on the right side if he reads a European language such as English or on the left side if he reads Hebrew. Ordinary readers and severe dyslexics do not much differ in peripheral vision if the sense of the displacement is opposite to the direction of reading. To see the difference regard the letters in the arrangement below, fixing your gaze on the x in the center.

N   X   VHNKW

The letter N is the same distance from the X on right and the X on the left. But while the letter is reasonably clear on the left, it is not clear on the right. When looking directly at the letter string you see the array clearly even if your gaze is held fixed on any letter in the string. For the severe dyslexic the array is confused on direct gaze in the same way it is confused in your vision when you are fixing on the X. On the other hand, it is clearer for him when he fixes on the X than when he regards it directly.

Reviewing the literature we found that visual function tests have almost uniformly been done on readers. College students are cheaply had subjects. But the results have been supposed not only as description of the norm but evidence of a specific built-in organization of the visual field. Prior to our study of dyslexics, we had questioned this concept. We felt that the information necessary to identify a letter in the interior of an eccentric string was not lost in early visual processing and could be retrieved.

The confusion that you see in the interior of the eccentrically viewed string is defined as "lateral masking" by Boumarn. Existence of nearby flanking letters addles the perception of a letter. We felt that lateral masking was a learned operation, a weighting function that, applied to the peripheral field, reduced an aggregate of forms to a texture. We took a texture to be that property of an aggregate that is had from discerning textural elements, e.g., the "textons" of B. Julesz, but not perceptually providing them with that connectivity that determines form. It is as if the aggregate has more a statistical rather than a formal description. To a significant degree we made the point that lateral masking is a perceptual strategy by showing that one could "demask" the laterally masked letters in the periphery.

In the case of the dyslexic, the visual strategy is to laterally mask in the center of the visual field and attend what is the case away from that center. This, which we call the "hunter" strategy, is what all of us use in driving through fast two-way traffic or playing in competitive sports, e.g., tennis or football. We know more what to do from the ambience of the ball than from watching the ball. When we read, we use the "scribe" stragegy in which we laterally mask in the visual periphery so as to attend the center of vision. We easily switch between these strategies. The severe dyslexic seems frozen in the "hunter" mode and so cannot learn conventional reading. Indeed, practicing to read with central vision reinforces the perceptual block.

Geiger's experiments tested the learning of a new strategy by showing how a 24 year-old severe dyslexic, scarcely at the third grade level in reading despite repeated attempts at remediation in the past, could be brought to tenth grade level in four months by training him to read in the peripheral field by blocking the text in the central field. This procedure, now repeated on four more cases, has *pro tem* proved effective. But what is more important is that the tests we designed for examining central versus peripheral vision have emerged not only as diagnostic, but sensitive enough to follow the improvement and degradation in reading ability of those prone to dyslexia.

This claim is borne out by finding subjects who are readers in the morning and dyslexic at night so that we can track repeatedly the clinical variation by test and correlate it with the gain and loss of ability to read. We have records now on such a case.

The report as given here is cursory and somewhat popularized. The data supporting this approach are in two papers already published. Rather more is said in two other papers now being prepared for publication in which a more extended set of results are given, but this would take too much space in this note.

20.3   Physiology of Vision in the Frog

Arthur Grant and Jerome Lettvin

The major visual center of the frog, certainly the largest, is the tectum, a paired structure on top of the midbrain. Each tectal lobe is directly connected only to the opposite eye: there is no splitting of the output of each eye as in our visual projection to cortex. Associated with each tectal lobe is a relatively small accessory nucleus, n. isthmi, that receives output only from that tectal lobe, but projects back to both tectal lobes. Ipsilaterally the axons of n. isthmi end on the dendrites of those cells that send axons to nucleus isthmi. Its topology closely resembles that of a layered "nerve net."

In the past this laboratory has shown that the crossed projection of n. isthmi is responsible for "binocular" vision in the frog. We could not account for the ipsilateral projection. Then E. Gruberg found that if n. isthmi is ablated on one side, the frog becomes visually indifferent to both prey and threat in the image seen by the opposite eye. Yet, when the frog is made to jump it avoids obstacles, and goes over barriers and does not hit walls.

We had begun recording in the tectum many years ago. Several new features have emerged this last year from Mr. Grant's investigations. First and foremost is the demonstration that the records taken from single units in the superficial neuropil do not represent the firing of the terminal bunches of primary optic nerve fibers. Instead they appear to be active responses of special dendritic appendages of certain tectal cells. An extraordinary anatomical feature of these appendages is that they form a mutually synapsing net between the tectal cells all across the tectum. This identification of the signal sources at single nodes in the net changes considerably the current view of the visual processes in amphibia.

But the second feature that has come to light seems to be that the crossed n. isthmi fibers terminate on these nodes as well. For the first time we can compare at the same recording site some of the processed output of one tectum with the optic nerve input to the other. It is premature to assert the results, but what is emerging is that, however the tectum handles its input data, it preserves almost slavishly at the output the several categories attributable to different types of retinal feature detectors. That is, the output can pe parsed easily in terms of combinations of input.

20.4   Image Processing in the Photo-receptors

Gill Pratt, Robert Webster, Jerome Lettvin

A great deal is now known about the mechanism of transduction of light by rods and cones and the first steps of amplifying the transduction into signal. But if the receptors

are taken as discrete sensors feeding the nervous part of the retina, a distinct problem emerges.

First of all, the point spread function on the retina through the optical system of the eye under optimal focus and aperture is quite large, several receptors in width - much worse than occurs with the cheapest cameras. Second, receptors of the same type, e.g., rods or cones are laterally connected among themselves ohmically in a resistive net. Each receptor is a node in such a net. And the space constant of the resistive connection is larger than the point-spread function. However, at the retinal output the ganglion cells, in their response, reflect sensitivity to details in the image as if the image had somehow been sharpened in a way familiar to modern image processing.

The existence of the resistive net between the receptors would be corruptive if each receptor signaled the effects of light on it as a current. However, if the measured signal from the outer segment drive a voltage follower in the inner segment of each rod or cone, then the nodes in the net become voltage sources. The feedback current used to clamp the voltage to that which is set by the light signal, now measures the signal level difference between any receptor and its immediate neighbors because of the resistive coupling. It this feedback current is that which drives the output signal of the receptor, the image at the output of the receptor layer has been sharpened in the same way as is used in conventional image processing.

We have modelled this system succesfully in a computer program and are now doing experiments on actual retinas to test the hypothesis.

20.5 Voltage Control of Cell Membrane

Campbell Searle and Jerome Lettvin

The mechanism of voltage control is still unknown. A large body of data from voltage clamp experiments gives the empirics of the rate processes of this control on the ionic channels of nerve. However the chemical operation has stayed obscure.

We have modeled a system in which the heads of phosphatidyl serine molecules in the membrane trimerize reversibly in the presence of Ca^{2+}, with three Ca^{2+} binding three heads in a triangle. This is an excellent electro-mechanical transducer with adsorption of Ca^{2+} sensitive to boundary density of Ca^{2+} and to the local electric field; desorption sensitive to the ionic strength of the solution and the local receptive field.

This model fits the known data, especially the rate processes, remarkably well and accounts for the voltage-sensitive component of membrane capacitance. We are preparing the study for publication.

21.0 Molecular Physics

Academic and Research Staff

Prof. J.G. King, Prof. A.P. French

Visiting Scientists

Dr. A. Essig,[1] Dr. S. Rosenthal,[1] Dr. J.A. Jarrell[2]

21.1 Molecule Microscopy

F.L. Friedman Chair
National Institutes of Health (Grant Am 25535)
Whitaker Foundation

John G. King, Alvin Essig, Joseph A. Jarrell, Stanley R. Rosenthal

During 1987 we ceased work on this project as various contracts ran out. Whereas, much progress towards our goals has been made, the project was too ambitious and speculative to be carried out in this environment. We have abandoned the development of: 1) a one nanometer resolution desorption molecule microscope in which neutral molecules desorbed from the sample surface by a pulsed, focused electron beam are collected on a movable tungsten tip for later remote field desorption and ionization and detection with time of flight mass spectroscopy; 2) an instrument to observe with one micron resolution fluxes of hydrogen through various metallurgical samples under various conditions. This project was part of a larger study on hydrogen embrittlement and corrosion; and 3) an instrument in which a sharp tungsten tip in contact with a surface in UHV is later removed and atoms which plate out on the tip are counted and identified by field desorption and ionization, and time of flight mass spectroscopy.

We are expecting to continue work on the study of the binding of water to cholesterol and lecithin using the thermal desorption method originally developed for contrast studies in molecule microscopy. The results complement x-ray and differential calorimetry data.

---

[1] Boston University Medical School

[2] Waters Corporation

21.2 Electrical Neutrality of Molecules

John G. King, Anthony P. French

We are continuing pilot experiments in preparation for applying for funds to carry out the acoustic-electric neutrality experiment described in RLE Progress Report No. 129.
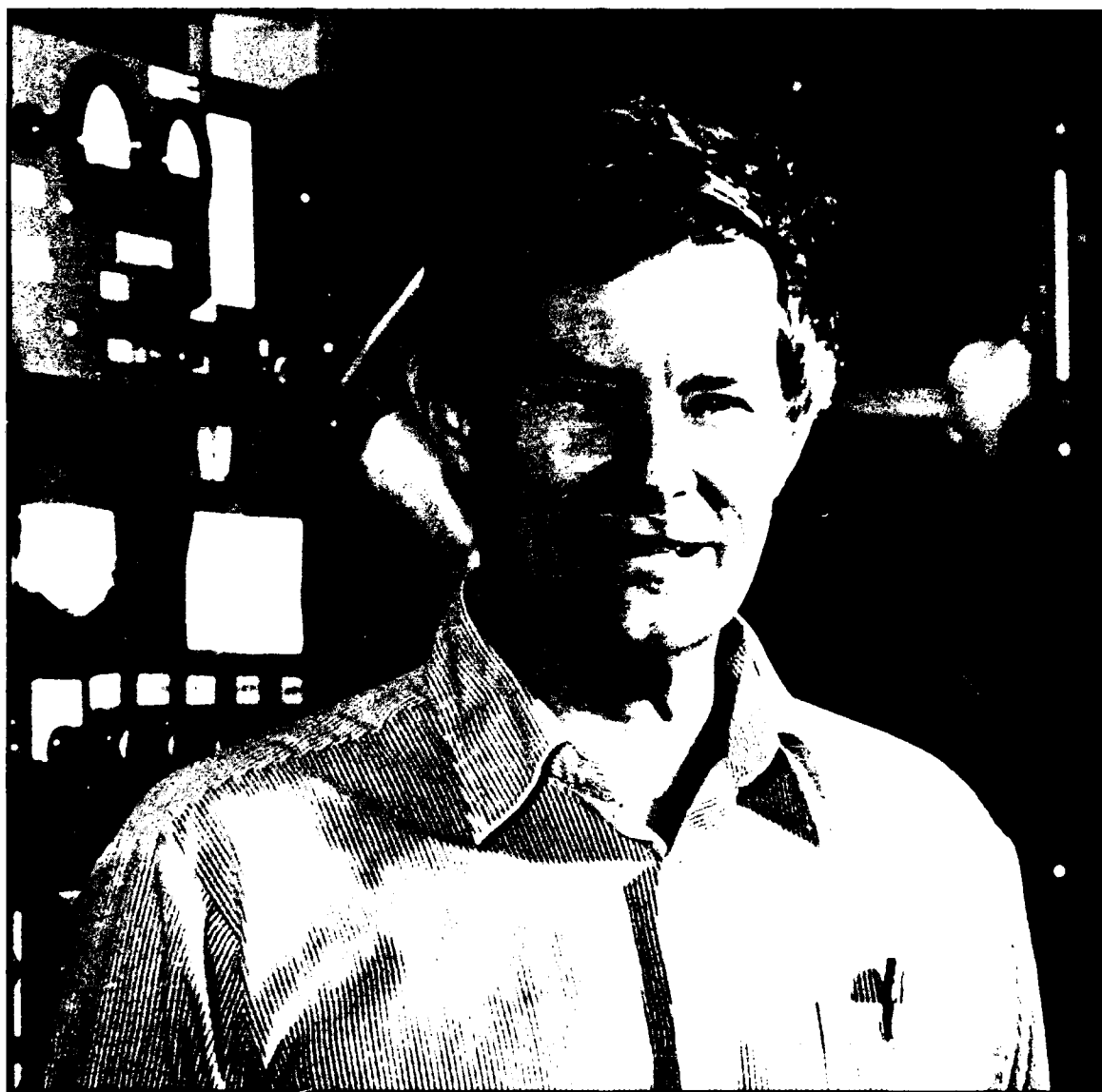
Professor John G. King

22.0 Quantum Optics and Photonics

Academic and Research Staff

Prof. S. Ezekiel, Dr. P.R. Hemmer, Dr. M.G. Prentice, Dr. H. Lamela-Rivera, B. Bernacki, D. Morris, J. Kierstead

Graduate Students

R. Barat, M.S. Shahriar, S.P. Smith, F. Zarinetchi

Undergraduate Students

J. Bevilaqua, T. Hawkeye, J. Kuchar, M.C. Neils

Sponsors

22.1 Measurement of Fresnel-Drag in Moving Media Using Aring Resonator Technique

It has been known for many years that the observed velocity of light in a moving medium differs from that in a stationary medium. This effect, namely the Fresnel-drag, was explained by the special theory of relativity. While special relativity has been very accurately tested, no tests of comparable precision can be claimed regarding the theory's predictions for light propagation in moving media.

We have performed careful measurements of the Fresnel-drag in various moving glass media and tested the dependence of the drag coefficient on refractive index and dispersion. A solid medium was used in our experiments to provide a precisely known velocity and index. To further ensure the accuracy of these measurements we have studied the drag dependence on other key parameters such as the thickness and velocity of the glass samples, as well as the angle between the light beam and glass normal.

Our technique is based on moving a glass plate of known index and dispersion back and forth inside a ring resonator as shown in figure 22.1. In this way, the Fresnel-drag generated by the motion of the glass induces a nonreciprocal phase shift which manifests itself as a difference in the resonance frequencies of the cavity for oppositely propagating field directions. The precision measurement of small resonance frequency difference in a ring cavity is similar to the measurement of nonreciprocal phase shift due to inertial rotation, i.e., Sagnac effect.

The effective drag coefficient was measured for four glass samples namely; BK-7, SF-1, SF-57 and fused silica which have different indices of refraction and dispersion. Averaging fifteen separate measurements resulted in an overall agreement with theory

153

that was well within our $\pm 2.8 \times 10^{-4}$ measurement uncertainty, thus verifying the drag dependence on both the refractive index as well as the dispersion of the moving medium. These measurements provided the most accurate verification of Fresnel-drag thus far.

The use of a solid medium together with ac detection techniques contributed to the improved experimental verification of the Fresnel-drag reported here. Aside from varying sample index and dispersion we also varied sample thickness, velocity and angle of incidence. Further improvement in the accuracy of the measurements can be made by placing the cavity within an evacuated chamber to exclude air currents, and by using a smoother bearing for guiding the motion of the glass sample.

Publication

Sanders, G.A., and S. Ezekiel, "Measurement of Fresnel-Drag in Moving Media Using a Ring Resonator Technique," *J. Opt. Soc Am. B* (1988), to be published).
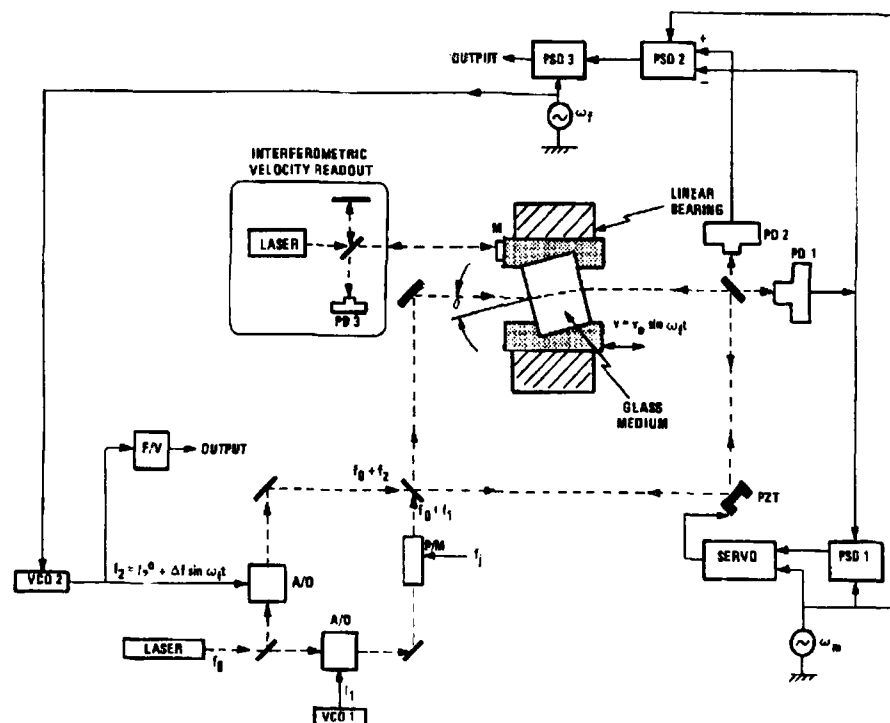
Figure 22.1 Experimental setup.

22.2 Observation of Ultra-Narrow Raman Ramsey Fringes in a Cesium Atomic Beam Using a Semiconductor Laser

We have observed an ultra narrow, 4 kHz wide Raman Ramsey fringe in a cesium atomic beam using a semiconductor laser with a free running linewidth of 45 MHz. To

our knowledge, this is the narrowest atomic resonance recorded using a semiconductor laser and has applications in the development of new time and frequency standards. A clock based on the resonance Raman effect in cesium could be smaller, simpler and less expensive than a conventional cesium clock.

The stimulated resonance Raman process is illustrated in figure 22.2 where we show a Raman transition between two long-lived states, 1 and 3, induced by two laser fields at frequencies ω_1 and ω_2. As is well-known, the Raman transition linewidth for weak copropagating laser fields is primarily determined by the decay rates of the long lived states 1 and 3. Thus, the linewidth is set by the transit time. To achieve an effectively long transit time, and thus a very narrow linewidth, Ramsey's technique of separated field excitation is used.
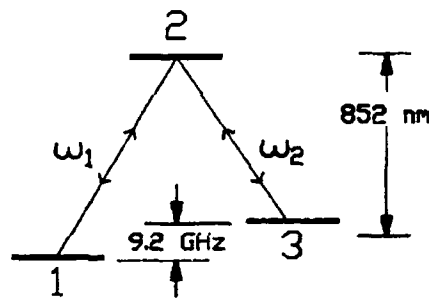
Figure 22.2 Schematic of Raman transition in cesium.

In our present experiment, the long-lived states 1 and 3 in figure 22.2 are respectively the $6^2S_{1/2}(F = 3)$ and $(F=4)$ ground state hyperfine levels in cesium separated by 9.2 GHz, and state 2 is the $6^2P_{3/2}(F = 4)$ level. The optical transitions are components of the cesium D_2 line at 852 nm.

The experimental setup is shown schematically in figure 22.3. The laser diode is a single frequency, double heterostructure, AlGaAs laser (Hitachi HLP-1400) operating at 852 nm and mounted on a thermoelectric device. The linewidth of the laser was 45 MHz as measured by a Fabry Perot interferometer.

Generation of the two optical fields, ω_1 and ω_2 is accomplished by modulating the laser current at 4.6 GHz with a microwave VCO, shown in figure 22.3, thus yielding two amplitude modulation sidebands separated by 9.2 GHz. By generating ω_1 and ω_2 in this manner, the effect of laser jitter can be eliminated. In our previous work using a sodium beam and a dye laser, the second optical field was generated by frequency shifting in an external Bragg cell.

Figure 22.4(a) shows the modulation sidebands of the modulated laser as measured by a short, plane-parallel, scanning Fabry-Perot cavity with a free spectral range of 25 GHz. As can be seen, the separation between sidebands is 4.6 GHz and that there is no evidence of any laser instabilities. In contrast, figure 22.4(b) shows the spectrum of the unmodulated single mode laser.
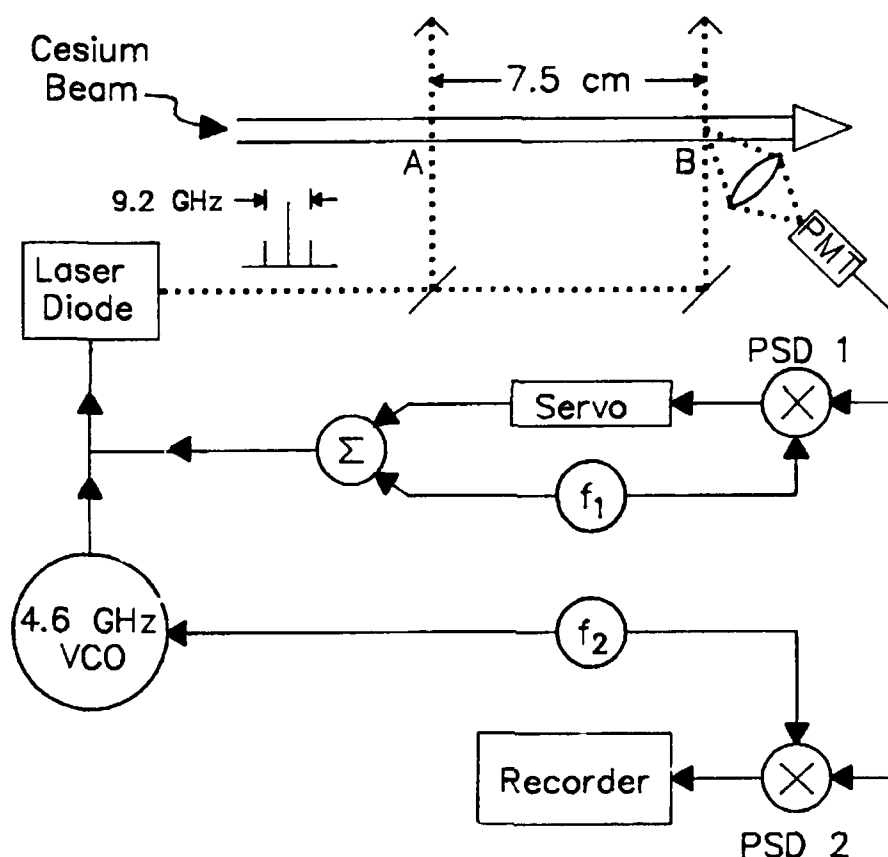
Figure 22.3. Experimental setup.

As indicated in figure 22.3, the output from the modulated laser interacts with the cesium atomic beam in zones "A" and "B," and the fluorescence from zone "B" is collected onto a photomultiplier tube. Figure 22.5 shows the demodulated fluorescence from zone "B" which exhibits the Ramsey fringes as the microwave oscillator is slowly swept through the center of one of the cesium Zeeman transitions. As shown in the figure, the central fringe has a width of 4 kHz, which is in good agreement with the predicted width for a 7.5 cm zone separation and a 200°C oven temperature. To observe the Raman transition, the laser and sidebands were held by means of a servo near the maximum of the fluorescence lineshape in zone "B." It should be noted that these Ramsey fringes are still preliminary and the details of the fringe shapes have yet to be carefully investigated.

As in the sodium Raman clock studies, the central Ramsey fringe associated with the magnetic field insensitive m = 0, δ m = 0 transition can be used as a reference for the stabilization of the microwave oscillator. The Raman clock would have an advantage over the conventional cesium clock, in that it does not require state selection magnets, nor a microwave cavity.
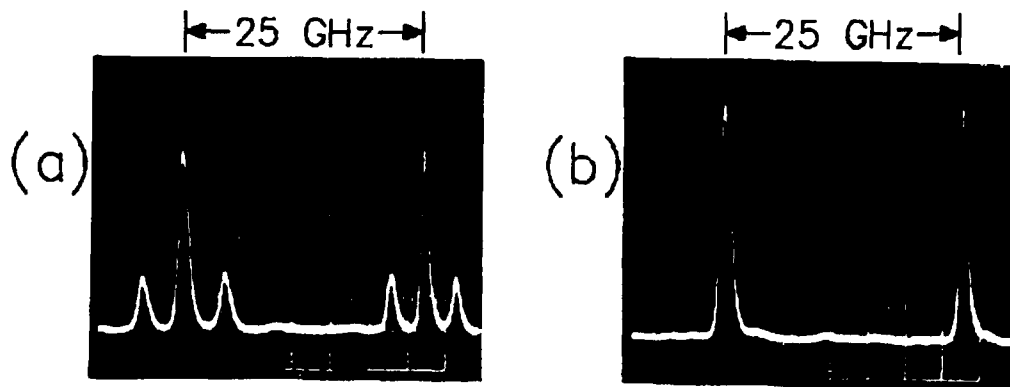
Figure 22.4 Spectrum of: (a) Modulated laser at 4.6 GHz (b) Unmodulated laser.
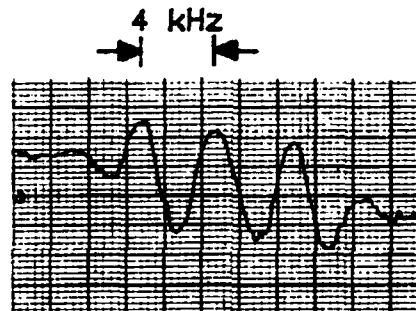
Figure 22.5 Ramsey fringes for a 7.5 cm zone separation.

Although optical pumping has recently been considered as a replacement for the state selection magnets in the conventional cesium clock, the microwave cavity, however, is still needed.

Future work will be focused on the study of error sources in semiconductor excited cesium Raman clocks. In addition, several improvements to our present setup are being considered. For example, we propose to use a laser with a spectral width equal to or less than the cesium natural width of 5 MHz instead of the present 45 MHz. Also, we wish to consider simple methods of laser cooling the cesium beam, to increase the transit time for a given zone separation and oven temperature.

Since semiconductor lasers are also available at 780 nm near the resonance excitation of rubidium, it would be worthwhile to consider a rubidium Raman clock in addition to cesium. Finally, the possibility of a millimeter wave Raman clock is also being explored.

Publication

22.3 Coupled Pendulum Model of the Stimulated Resonance Raman Effect

The stimulated resonance Raman effect has found numerous potential applications in such diverse areas as spectroscopy, collisional studies and Raman lasers. In addition, we are exploring the possibility of using the stimulated resonance Raman interaction for portable clock development (see section 22.2 above). To date, there has not been a simple physical model to describe this interaction. Theoretical treatments using either perturbation theory or dressed states have been devised. The dressed state approach has been more successful because it describes the existence of a "trapped state" which is transparent to resonant excitation fields. This accounts for the non-absorption resonances which have been observed experimentally by a number of researchers. However, these models do not offer a simple physical explanation of either the formation of the trapped state or the influence of experimental conditions on observables.

In our research we have shown that the analogy between the stimulated resonance Raman interaction and the well-known system of three classical coupled pendulums can provide considerable physical insight. A set of three classical coupled pendulums is used to model the stimulated resonance Raman interaction. This model provides a simple, intuitive, physical description of the resonance Raman process and can also be used to interpret experimental observations, including the dynamics of Raman induced transparency, the physical nature of Ramsey fringes in separated field excitation, and the effects of off-resonant laser excitation. The model has also been extended to suggest what might be observed for very strong laser fields.

Publication

22.4 Laser Raman Clock Using Sodium

We have continued our precision studies of dye laser induced stimulated resonance Raman interactions in a sodium atomic beam with emphasis on Ramsey's method of separated oscillatory fields. We observed Raman-Ramsey fringes for a field separation of up to 30 cm, and the data were consistent with theoretical predictions. We have also been investigating the performance of a clock based on this interaction in a sodium atomic beam to determine the feasibility of such a scheme and to demonstrate any possible advantages over conventional microwave excited clocks. Recent performance of our sodium Raman clock showed a stability of 1×10^{-11} for a 5000 second averaging time. This compares favorably with commercial cesium clocks when difference in atom transit time and transition frequency are taken into consideration.

Currently we are studying potential sources of long term frequency error in a Raman clock. Some of the error sources are similar to those in microwave clocks, such as the effects of path length shift, external magnetic fields, background slope, atomic beam misalignment and second order Doppler. The other error sources are unique to the Raman clock and include laser frequency detuning, laser intensity changes, laser beam misalignment, optical atomic recoil, the presence of nearby hyperfine levels, and other small effects.

Recently we have performed theoretical and experimental studies of an important error source related to Ramsey fringe phaseshift as a function of laser detuning in a two zone Raman excitation scheme. In our set up, laser detuning arises from many reasons such as laser drift away from the optical resonance (see section 22.2 above), misalignment of beams, and so on. Experimentally, we found that the Ramsey fringe phase shift depends strongly on initial state preparation, as well as, laser intensity in the interaction regions. We have used the Bloch vector approach to model the Raman interaction in the separated field excitation and have found that the observed phase shift is simply the phase of the 1-3 off-diagonal density matrix element at the end of the first interaction zone. This phase shift is therefore of fundamental interest and, in fact, is directly related to the phase difference between the atom-field dressed states.

The model we developed renders the Raman system almost as simple as the two level microwave system, and yet is complete enough to predict experimental observables with quantitative accuracy. Figures 22.6 (a) and 22.6 (b) show experimentally observed shift in the clock frequency as a function of laser detuning under two different sets of conditions. Figure 22.6 (c) and 22.6 (d) show theoretical predictions, according to our model, of the frequency shift we should expect corresponding to the same conditions. As can be seen, the results agree quite well both qualitatively and quantitatively. Moreover, we have verified this agreement over a wide range of parameters.

Specifically, we have investigated the effects of varying, independently, the initial population difference between levels 1 and 3 and the laser intensity in the interaction zones. Figures 22.6 (b) and 22.6 (d) correspond to a large initial population difference and low intensity. As can be seen, the clock frequency is extremely sensitive to laser detuning under this condition. Theory predicts, as shown in figure 22.6 (c), that this sensitivity becomes very small for small detuning if we use high intensity along with a small difference in population. Figure 22.6 (a) confirms this experimentally.

In summary, we are now able to choose operating conditions under which the clock is least sensitive to laser detuning. Theory also shows that under such conditions, the clock is also least sensitive to changes in laser intensity and population difference.

Our current atomic beam design is such that we were not able to run the clock under such an optimal condition. We recently finished construction of a new beam that will run under the desired conditions. Moreover, the new beam is designed to have increased signal-to-noise ratio, be more stable, and be less sensitive to external magnetic fields.
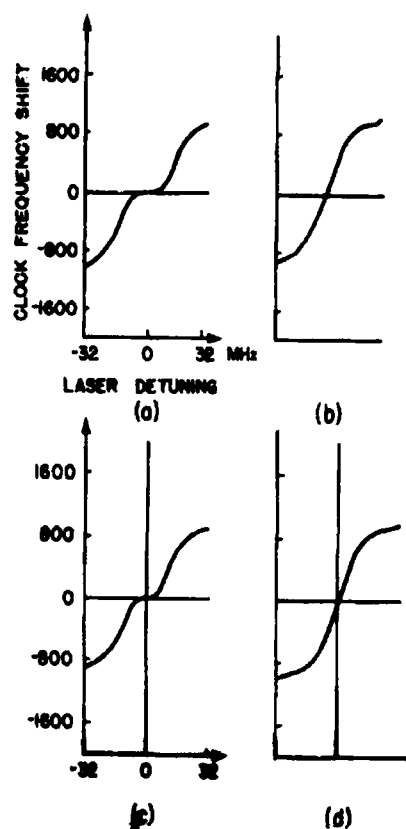
Figure 22.6   Comparison of experimental results with theoretical predictions of Raman clock frequency shift as a function of laser detuning.

22.5   Alignment Insensitive Technique for Wideband and Tuning of an Unmodified Semiconductor Laser

Many applications such as laser spectroscopy, optical pumping and isotope separation require a tunable narrow-linewidth source in the near infrared. Semiconductor lasers are an attractive alternative for these applications due to their relatively low cost, small size, and simplicity of operation. However, to date, semiconductor lasers have found limited spectroscopic applications because of their inability to be tuned to arbitrary frequencies of interest within the laser gain curve. To alleviate this problem, optical feedback schemes have been devised using diffraction gratings or etalons to provide frequency selective feedback. However, all these techniques require the use of antireflection-coated lasers and, in addition, are very sensitive to alignment of the external optics. These factors detract from the simplicity and low cost aspects inherent in semiconductor lasers.

We have developed a simple optical feedback technique that permits an ordinary semiconductor diode laser with no antireflection-coated facets to be tuned to arbitrary frequencies within the laser gain curve. In addition, this method is not highly sensitive to optical misalignments. Briefly, a one piece cat's eye retro-reflector serves as the

feedback mirror and a tilted intra-cavity solid etalon provides frequency selectivity. The use of a one piece retro-reflector contributes greatly to the simplicity of the technique because it eliminates the need for angular adjustment of the feedback mirror. The etalon, having approximately one-fifth the optical thickness of the semiconductor laser, forces the laser to lase in the longitudinal mode of interest.

Using our set up we were able to excite the D_2 line in atomic Cesium very repeatably using a nominally 852 nm laser. If the laser were used without feedback, it would not have been possible to excite the cesium transition reliably using either injection current or temperature tuning.

Publication

Bernacki, B.E., P.R. Hemmer, S.P. Smith and S. Ezekiel, "Alignment Insensitive Technique for Wideband Tuning of an Unmodified Semiconductor Laser," submitted to *Optics Lett.*

Professor Daniel Kleppner

23.0 Atomic Resonance and Scattering

Academic and Research Staff

Prof. D. Kleppner, Prof. D.E. Pritchard

Visiting Scientist

T.W. Ducas[1]

Postdoctoral Associates

G.P. Lafyatis, A.G. Martin

Graduate Students

V.S. Bagnato, K. Boyce, P.P. Chang, E.A. Cornell, T.J. Gentile, K. Helmerson, L. Hsu, B. Hughey, C-H. Iu, M.M. Kash, D.W. Keith, B.G. Oldaker, S. Paine, E.L. Raab, R.E. Stoner, R.M. Weiskoff, G.R. Welch

Undergraduate Students

D. Lew, J. Landry, A.H. Miklich, G. Zeglin

23.1 Basic Atomic Physics

23.1.1 Rydberg Atoms in a Magnetic Field

Michael M. Kash, George R. Welch, Chun-Ho Iu, Long Hsu, Daniel Kleppner

We have produced Rydberg atoms in a lithium atomic beam using cw dye lasers, developed the technology for cw detection of these atoms with static electric field ionization, and performed accurate measurement of the atomic energy levels in a strong magnetic field. A procedure for c rmining accurately the magnetic field strength has been implemented. These measuren..nts allow the characterization of important spectral features, including the size and location of level anticrossings.

Understanding the diamagnetic spectrum of an atom with a single valence electron presents a formidable challenge to theory and experiment.[1] The quantum mechanical equations of motion are easily constructed, but in spite of the simplicity of the problem the solutions are elusive and our understanding is far from complete. Numerical techniques have been developed that are accurate for relatively low energy and field. However, even in this regime, these calculations provide little insight into the physics

---

[1] Wellesley College

of the anticrossings. The widely held view is that *hydrogen* atomic energy levels very nearly cross, so lithium anticrossings are a manifestation of the valence electron - atomic core interaction.[2] Our measurements provide a one-hundred fold increase in accuracy over previous studies,[3] so any model of the core can be tested strenuously.

The excitation of lithium Rydberg atoms is performed with a two-step, three-photon process. The first step is a two-photon transition from the 2s to the 3s state. This step is detected by observing the cascade fluorescence (3s → 2p, 2p → 2s) through a fiber optic bundle with a sensitive photomultiplier tube. The transition is excited by 735 nm light from a ring dye laser. The 2p → 2s fluorescence is used to stabilize the laser against slow drift. The second step is a one-photon transition from the 3s state to the *n*p state, accomplished with radiation from a second ring dye laser. This resonance is observed by counting electrons which are produced in ionizing the excited atoms as they move from the interaction volume into a region of static electric field, 5-10kV/cm. The electrons are counted with a surface barrier diode. Standard devices such as electron multiplier tubes, channeltron multipliers, or micro-channel plates do not operate in a strong magnetic field (greater than 1 Tesla).

To minimize the electric field in the atom's rest frame, an atomic beam of lithium is used with velocity parallel to the axis of a superconducting solenoid. The interaction region consists of an aluminum cylinder whose axis is parallel to the atomic beam. The cylinder also contains prisms to deflect the lasers so that the laser and atomic beams intersect at right angles, to minimize Doppler broadening. The interaction region combines efficient collection of cascade fluorescence with good geometric rejection of *scattered laser light. Measurement of the magnetic field uses the linear Zeeman effect:* the energy difference between corresponding states with $m = +1$ and $m = -1$ is equal to the Bohr magneton times the field. With this technique, the field can be determined to about 20 gauss.

Figure 23.1 shows a theoretical prediction of energy levels in atomic lithium as a function of magnetic field with $m=0$, odd parity, near $n=25$. The three indicated anticrossings have been experimentally studied. The first anticrossing data are displayed in figure 23.2. The data are generated by fixing the magnetic field and scanning the second laser over the indicated energy range. The anticrossing is a manifestation of perturbations to the hydrogenic Hamiltonian by the non-hydrogenic potential within lithium core electrons. The decrease of transition probability in the upper state reveals that this state is an antisymmetric combination of hydrogen states, while the lower state is a symmetric combination. The resonance linewidth is about 30 MHz. In figure 23.3 the theory and experiment are compared. The anticrossing size is the minimum energy separation of the two levels; the anticrossing position is the field location of this minimum. These are determined by fitting a hyperbola to the data. The experimental uncertainty in the position of anticrossings 1 and 3 is reduced over that of 2 because we improved the field measurement technique: for 2 we had only a magneto-resistor probe. The agreement between theory and experiment of anticrossing location seems reasonable, but in the case of anticrossing 1, there appears to be a small but real discrepancy. This is probably caused by a stray electric field in the interaction region.

In the next phase of the research we plan to extend the study of anticrossings and to expand our spectroscopic survey to study global properties of the system including the evolution of the spectrum from regions of orderly to disorderly classical motion.

23.1.2 Microwave Quantum Optics

Theodore W. Ducas, Thomas J. Gentile, Barbara Hughey, Daniel Kleppner

The interaction of an atom with electromagnetic fields, including the vacuum field, is modified by conducting surfaces. A cavity tuned to an atomic transition will enhance the absorption and emission rates of that transition above their free space values. If the cavity damping time is long (high Q), there can be an oscillatory exchange of energy between the atom and the cavity. An experiment is in progress to study these effects using Rydberg states of calcium in the TM010 mode of a cylindrical superconducting cavity at 35 GHz.

An atomic beam of calcium is generated by a tube oven and a collimating aperture. Rydberg states of calcium are produced by a three-step pulsed laser excitation. A Quanta-Ray DCR-1A Nd:Yag laser is used to pump three dye lasers. The first dye laser drives the 4s4s → 4s4p transition at 423 nm. The second step is the 4s4p → 4s5s transition at 1035 nm. The 1035 nm light is produced by generating the difference frequency of a dye laser (525 nm) and the Nd:Yag fundamental (1064 nm) in a KD*P crystal. Finally the third laser drives the 4s5s → 4snp transition. By tuning the wavelength of the third laser, nearly any 4snp Rydberg state can be excited.

Calcium was chosen for this experiment because its dominant isotope (calcium 40, 97% abundance) has no hyperfine structure. Moreover, calcium has two valence electrons which can combine into either a singlet or a triplet state. By choosing the singlet state, we also avoid fine structure. This allows us to have a true two-level system for the cavity experiment.

The atomic transition we have chosen for this experiment is 46p → 46s. Rydberg states ionize in modest electric fields; a particular Rydberg state can be identified by the value of the electric field required for ionization. This technique is used to resolve the two Rydberg states involved in the transition. We use ramped electric field plates that ionize the two states at distinct positions along the atomic beam direction. The ramp is optimized for the 46p → 46s transition, but can be used for a variety of Rydberg state transitions. The electrons released by the ionization are detected by channel electron multipliers, which generate a distinct electrical pulse for each detected electron. Consequently, we can count the number of atoms in the two Rydberg states involved in the transition.

The oscillatory exchange of energy between the atom and the cavity can be destroyed by the presence of blackbody radiation at the transition frequency. For this reason, and also to achieve a sufficiently high Q using a superconducting cavity, this experiment is carried out at low temperatures. To achieve this goal, the interaction region of the apparatus is attached to the bottom of a liquid helium dewar. We expect to reach 1.5 degrees Kelvin by lowering the pressure above the helium bath. We have recently modified the dewar apparatus and achieved the following goals: improved microwave and electrical access to the apparatus; better cryogenic design; installation of the channel electron multipliers and magnetic shielding; and greater overall flexibility and convenience.

We have performed preliminary experiments in which Rydberg state transitions are driven by a high resolution microwave source. The source is an HP 8690B sweep oscillator locked to an HP 8662A synthesizer. These experiments have allowed us to test the resolution of the detector. In addition, we have accurately measured the frequency of the 46p → 46s transition, which is necessary for the design of the cavity. The study of these microwave transitions is also an excellent diagnostic for systematic problems in our apparatus. Because of the extreme sensitivity of Rydberg atoms, small electric fields can broaden the spectral linewidth of the transition and destroy the coherent exchange of energy between the atom and the cavity. The measurement of the spectral linewidth of the Rydberg state transitions and the observation of coherent effects have allowed us to diagnose and reduce stray electric fields. The reduction of stray electric fields is directly related to the cleanliness of the vacuum system and to the alignment and properties of the lasers. Figure 23.4 shows a frequency scan of the microwave source over the 46p → 46s transition. The observed linewidth of 300 kHz is dominated by the transit time across the waveguide in which the transition occurs. Since our system is so well suited to measuring the transition frequencies of these Rydberg state transitions, we plan to measure a variety of transition frequencies in calcium. We expect these measurements to have a resolution of approximately 10^6. Figures 23.5 and 23.6 are examples of coherent phenomena that we have studied. Figure 23.5 shows the evolution of the magnetic sublevels of the 46p state in the ambient magnetic field. (This field will be greatly reduced by shielding in the cavity experiment, but its presence is useful for these diagnostic experiments.) Figure 23.6 shows the dependence of the Rabi oscillation frequency on microwave power with and without the magnetic shielding. In the presence of microwaves tuned to the Rydberg state transition frequency, the atomic population will oscillate between the two Rydberg states involved in the transition. These oscillations are reminiscent of the coherent exchange of energy between the atom and the cavity.

The cavity mode that we have chosen is the TM010 mode of a right circular cylindrical cavity because the electric field in this mode is constant along the length of the cavity. The atoms travel parallel to the cavity axis, and the constant electric field simplifies the analysis of our experiment. Another advantage of this mode is that it allows us to conveniently probe the time dependence of the atom-cavity interaction. With the TM010 mode, the cavity can be split lengthwise into two halves without greatly perturbing the mode structure. We can then electrically isolate the two halves and apply a small voltage to one half at various times during the atom-cavity interaction. This small dc electric field shifts the atomic resonance away from the cavity resonance, thus stopping the atom-cavity interaction and "freezing" the atomic population. This enables us to trace out the oscillation of the atomic population between the 46p and 46s states in the cavity. The split cavity can be tuned by varying the size of the gap between the halves. To achieve $Q > 10^7$ in the split cavity we must minimize the leakage of microwaves out of the crack separating the halves. This is accomplished by machining a small "choke" groove around the cavity.

The cavity is analyzed by coupling it to a waveguide through a small aperture and detecting the reflected power from the cavity as a function of frequency. The locked, narrowband microwave system described above is necessary to observe these high Q cavities (for $Q = 10^7$, the source needs to be stable to better than 500 Hz). The properties of the decrease in the reflected power near resonance are used to determine the intrinsic Q of the cavity, Q_0.

A vacuum chamber with a small liquid helium dewar is used to test the cavities. The pressure above the helium is reduced in order to lower the temperature of the cavity to less than 1.8K. Figure 23.7 shows the measured Q as a function of temperature of a lead-plated copper split cavity with a choke groove. The Q increases exponentially as the temperature decreases, as is predicted by the BCS theory for superconductors. Work is in progress to tune this cavity while maintaining a high Q.
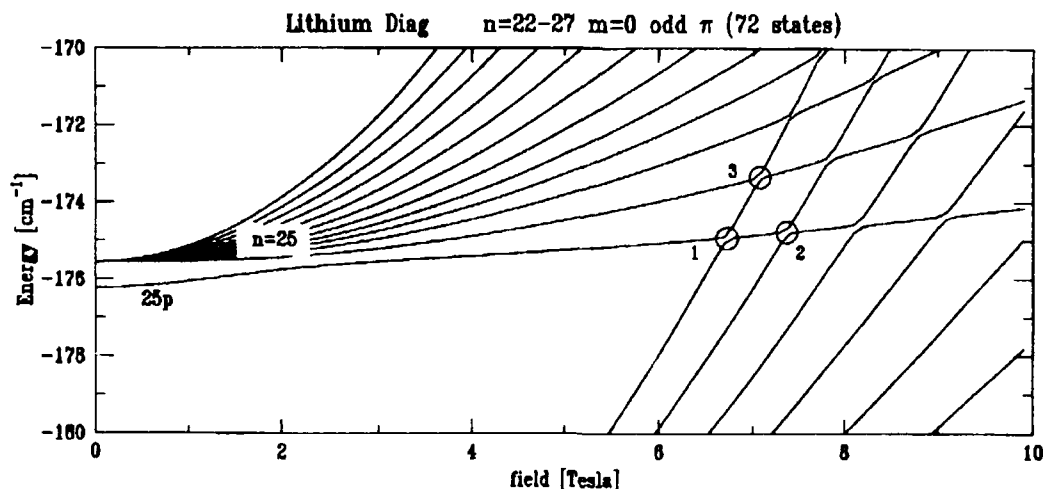
Lithium Diag   n=22-27 m=0 odd π (72 states)

Figure 23.1 Theoretical prediction of atomic lithium energy levels with $m-0$, odd parity near $n=25$.

n=24,25 m=0 oddπ "1st" anticrossing (Data)
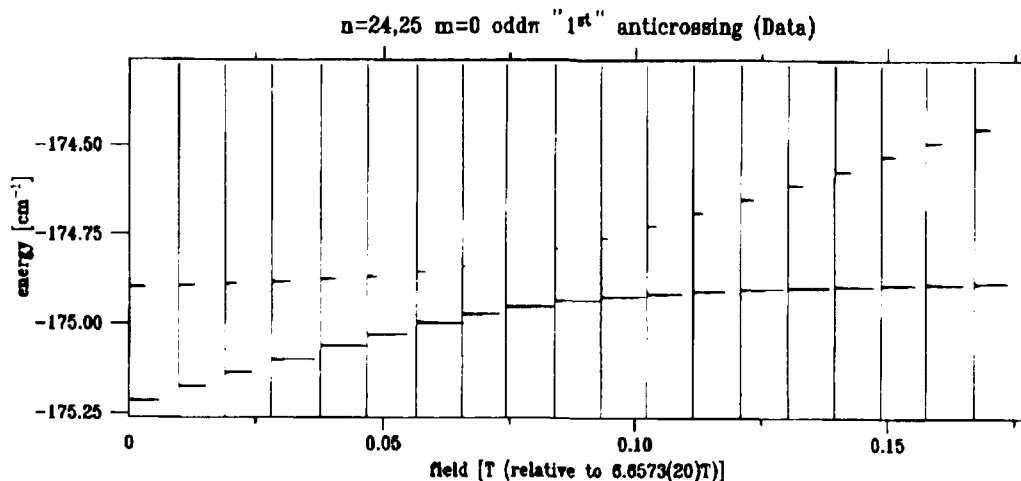
Figure 23.2 Experimental study of anticrossing 1. The baseline of each laser scan determines the magnetic field. The base of each resonance is the energy of the state at the corresponding field.

n=24,25 m=0 oddπ anticrossings: theory -vs- experiment
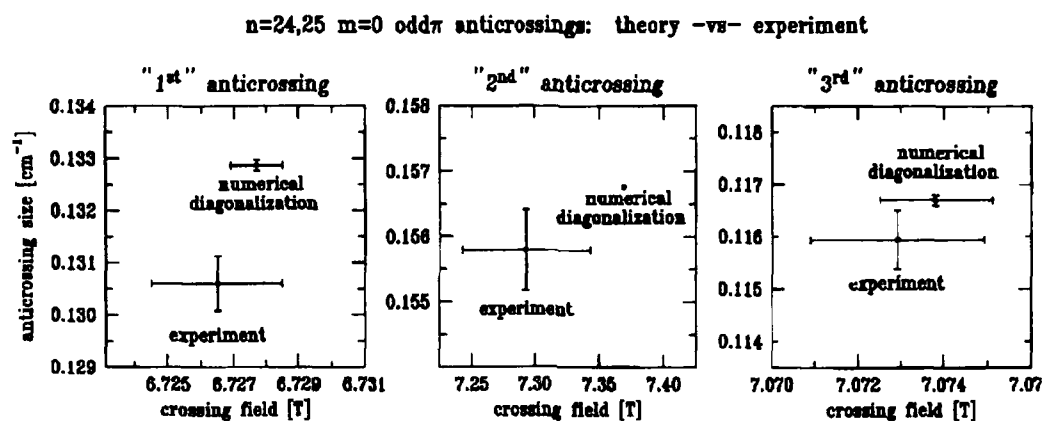
Figure 23.3 Comparison of theory and experiment. The bars on the theory indicate the extent of convergence in the calculation.
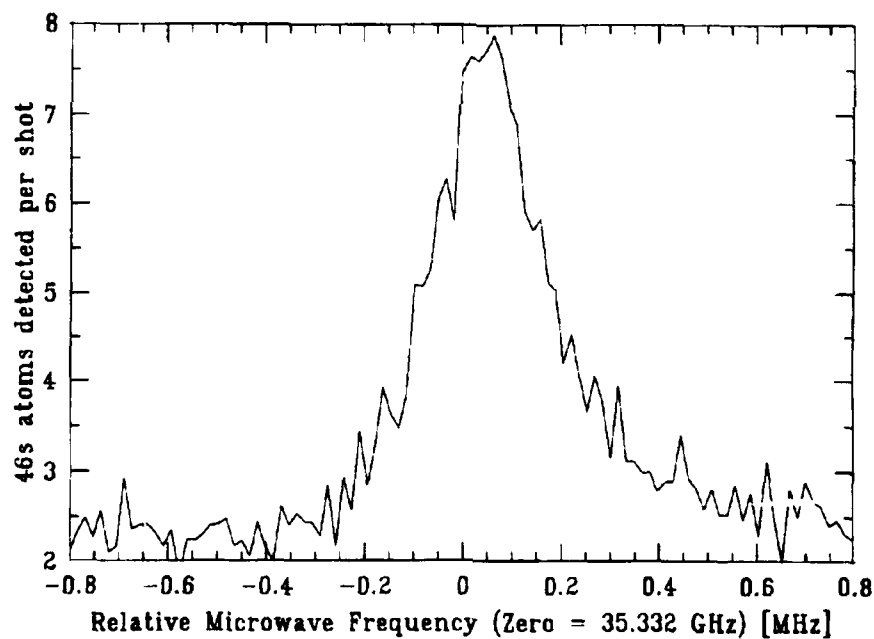
Figure 23.4. Low power frequency scan of the microwave source over the calcium 46p → 46s transition. Power is ~ 10^{-14} Watts.
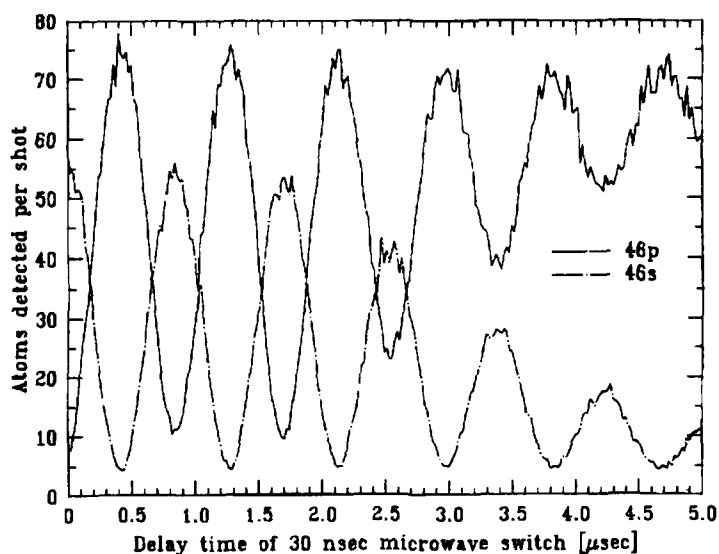
Figure 23.5 M-level evolution in the ambient magnetic field of 0.42 gauss. The 46p atoms reflect the population in the 46p m = ± −1 states and the 46s atoms reflect the population in the 46p m=0 state before the 30 nsec microwave switch is applied.
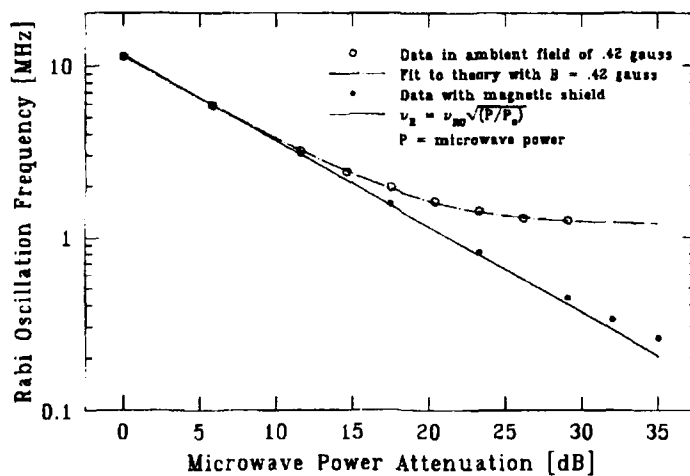
Figure 23.6 Rabi oscillation frequency of the calcium $46p \rightarrow 46s$ transition as a function of microwave power. The data were taken with and without the magnetic shield. The solid curve is $\nu_R \propto$ microwave electric field strength. The dashed line is a fit to the observed oscillation frequency in the presence of the magnetic field: $\nu_{osc} = \sqrt{\nu_R^2 + 4\nu_L^2}$ where ν_L is the Larmor frequency.
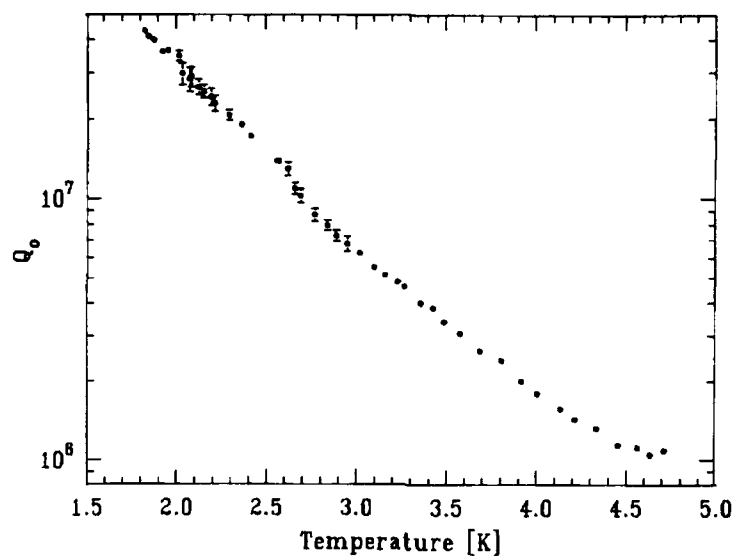
Figure 23.7 Unloaded Q of TM_{010} mode of a lead plated split cavity as a function of temperature.

23.1.3 Millimeter Wave Measurements of Rydberg Constant

Pin P. Chang, Scott Paine, Daniel Kleppner

We are undertaking a determination of the Rydberg constant of hydrogen by measuring the frequency of the transition $n = 29 \rightarrow n = 30$, at 256 GHz. Our approach differs from that of previous determinations in that the Rydberg is measured in frequency units. This avoids the problems of wavelength metrology that limit optical measurements. The design goal is an accuracy of 1 part in 10^{11}, approximately thirty times higher than optical measurements.

We have started construction of an atomic beam apparatus, and have carried out preliminary studies on the optical excitation of Rydberg atoms. Our first goal will be to prepare the atoms in "circular" states using a novel method recently proposed by Delande and Gay.[4]

References

[1] J.C. Gay, "High Magnetic Field Atomic Physics." In *Progress in Atomic Spectroscopy*, eds. H.J. Beyer and H. Kleinpoppen. New York: Plenum, 1984.

[2] M.L. Zimmerman, M.M. Kash, and G.R. Welch, *J. Phys.* 43:C2-113 (1982).

[3] P. Cacciani, E. Luc-Koenig, J. Pinard, C. Thomas, and S. Liberman, *J. Phys. B* 19:L519 (1986).

[4] D. Delande and J.C. Gay, *Europhys. Lett.* 5:303 (1988).

23.2 Magnetic Trap for Neutral Atoms

Vanderlei S. Bagnato, Gregory P. Lafyatis, Alexander G. Martin, Kristian Helmerson, David E. Pritchard, Joseph Landry

We are working on a program to trap large numbers of atoms and cool them to microkelvin temperatures. The objective - a dense sample of ultra cold atoms - promises to open up new and exciting areas of physics. The lack of interaction of the trapped atoms with any confining walls, their low velocities due to their reduced thermal motion, and the possibility of indefinitely long interaction times makes such samples of trapped atoms ideal for high resolution spectroscopy and for use as atomic frequency standards. High density samples of ultra-cold atoms also promise to open up new areas of research in the study of both interatomic collisions and collective effects, such as Bose condensation.

Following the completion and successful demonstration of our superconducting magnetic trap for neutral atoms in 1986,[1] we have worked to elevate neutral traps from laboratory curiosities to powerful tools for new research in physics.

Our chief accomplishments in 1987 include: trapping greater numbers of atoms; inducing R.F. transitions amongst the various magnetic substates; and doppler cooling of the atoms to milli-kelvin temperatures.

We have succeeded in trapping $\sim 2\times10^{10}$ Na atoms. This is a sufficient number of atoms to make the sample optically dense, so that up to 60% of a weak probe beam is absorbed during one pass through the sample. Figure 23.8 (a) shows a typical absorption spectrum of trapped atoms. The shape of the absorption spectrum reflects the longitudinal magnetic field profile.[1]

We have also doppler-cooled the trapped atoms. A laser beam is sent down the axis of the trap and retro-reflected back on itself. Tuned to the red of the atomic transition frequency the standing wave forms a one-dimensional version of "optical molasses".[2] In this manner, we have succeeded in cooling our sample to approximately 4 mK. Figure 23.8 (b) shows a typical absorption spectrum of doppler cooled atoms. The increase (decrease) in the absorption at the low (high) frequency side of the curve corresponds to an increase (decrease) in the density of atoms at the low (high) magnetic field values (they have been sufficiently cooled so that they no longer have enough energy to reach the high magnetic field region).

Our greatest success in 1987 was the first observation of R.F. induced transitions on trapped atoms. With the application of R.F. we have succeeded in transferring the populations among the various ground state hyperfine levels of sodium, which we de-

tect through fluorescence induced by a weak probe laser beam. Figure 23.9 (a) shows a typical fluorescence spectrum of trapped atoms taken just after loading the trap. The atoms are in the F=2, M=2 hyperfine level, the state selected by our slowing and stopping lasers. Figure 23.9 (b) is a fluorescence spectrum of trapped atoms after repeated application of R.F. pulses to induce transitions from the initial F=2, M=2 to F=2, M=1,0,-1 hyperfine levels. Each of the peaks corresponds to one of these four ground state hyperfine levels, shifted in frequency by the presence of the external magnetic field, the only states in which weak-field seeking atoms can be trapped.

In addition, we have obtained a R.F. resonance curve for the F=2, M=2 to F=2, M=1 transition by measuring the relative peak heights of the two states in the fluorescence spectrum as a function of the frequency of the applied R.F. pulse. Figure 23.10 is such a curve. A fit to the curve from a model indicates the temperature of the atoms to be $\sim$ 60mK These first observations of R.F. transitions on trapped atoms are of great interest, not only because they provide us with a measurement of the temperature of our atoms, but also because they are essential to a scheme which we have proposed to cool atoms to micro-kelvin temperatures using combined R.F. optical techniques.[3] Such supercooling is the key to both high resolution spectroscopy and collective effects.

References

[1] V.S. Bagnato, G.P. Lafyatis, A.G. Martin, E.L. Raab, R.N. Ahmad-Bitar, D.E. Pritchard, *Phys. Rev. Lett.* 58:2194 (1987).

[2] S. Chu, L. Hollberg, J.E. Bjorkholm, A. Cable, and A. Ashkin, *Phys. Rev. Lett.* 55:48 (1985).

[3] D.E. Pritchard, *Phys. Rev. Lett.* 54:1336 (1983).
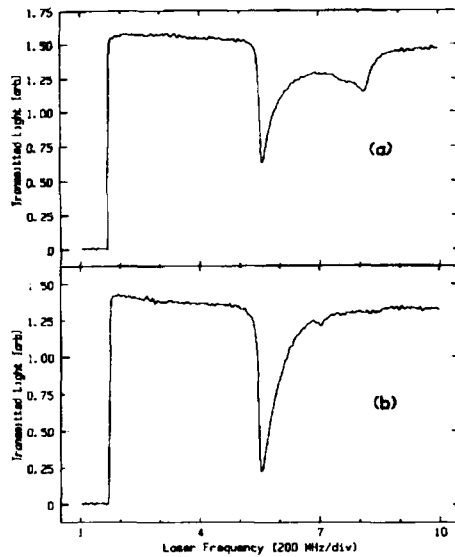
Figure 23.8 (a) Absorption spectrum of magnetically trapped sodium atoms taken just after loading of trap.

23.8 (b) Absorption spectrum taken after application of doppler cooling.
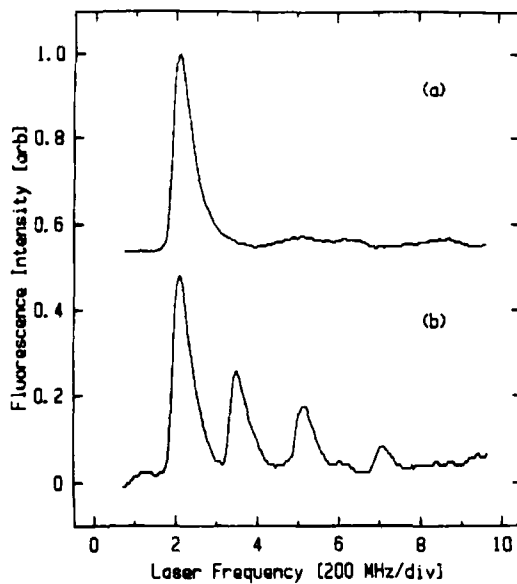
Figure 23.9 (a) is a fluorescence spectrum of atoms trapped in the F=2, M=2 state.

23.9 (b) is a spectrum showing population in all four trapped magnetic substates, F=2, M=2,1,0,-1.
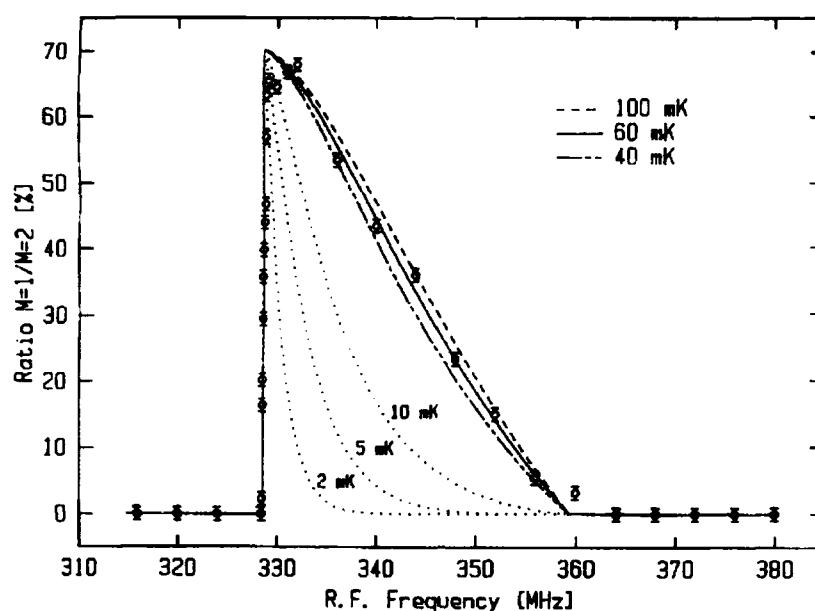
Figure 23.10 is a R.F. resonance lineshape (points) for the F=2, M=1 to F=2, M=2 transition. The calculated lineshapes (curves) allow us to estimate the temperature of the trapped atoms. The calculations for 2,5 and 10 mK show the greatly increased sensitivity to temperature for colder samples.

23.2.1 Light Trap

Alexander G. Martin, Eric L. Raab, Richard E. Stoner, Debra Lew, David E. Pritchard

We are constructing an apparatus to slow, confine, and cool neutral atoms with laser light. The apparatus will enable us to produce clouds of $>10^8$ sodium or lithium atoms with temperatures of less than 500 μk and densities of $>10^{11}$atoms/cm^3. With these cold, dense gases we will study long range molecules,[1] associative ionization,[2]

$$(Na^* + Na^* \rightarrow Na_2^+ + e^-)^2,\tag{1}$$
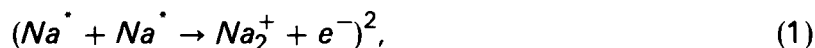
and low-energy collision processes.

Low-energy collisions provide challenges to both theorist and experimentalist because the duration of an ultra-cold excited-state collision is several natural lifetimes! Such a collision process, in which a spontaneous decay is probable, has yet to be observed or modeled.

In 1987 we demonstrated the first spontaneous force light trap in experiments at Bell Laboratories in collaboration with Mara Prentiss, Alex Cable, and Steve Chu.[3] This trap relies on the use of a magnetic field to induce the atoms to preferentially absorb light propagating towards trap center.[4] In this experiment we trapped over 10^7 neutral atoms for over 2 minutes in a trap with a confinement volume of several cm^3 and a depth >0.4K. The density of atoms was about 2×10^{11}atoms/cm^3; the temperature was ap-

proximately 600 μk. The observation of escape of atoms from the trap (inferred from the decay of the fluorescence from the trap, figure 23.11) revealed a loss mechanism manifest at high densities proportional to the square of the density of trapped atoms.

Figure 23.12 depicts the new MIT apparatus. Atoms coming up through the dewar bottom will be slowed by a laser beam propagating counter to the atomic beam. A tapered solenoid superconducting magnet (the "slower" of figure 23.12) creates a Zeeman shift of the atomic levels which compensates for the changing Doppler shift of the atoms as they decelerate. Three pairs of counterpropagating laser beams intersecting at the center of the "anti-Helmholtz" trap coils (i.e., two coils oriented coaxially with oppositely-directed dipole moments) comprise the trap (figure 23.13).

The continuous loading capability to be afforded by the tapered solenoid slower, as well as the high central field gradient attainable by the superconducting trap coils, will afford us a significant improvement in density over that of the Bell Laboratories trap. The improved vacuum resulting from the LHe dewar cryo-pumping should substantially increase the trap lifetime. The new apparatus will be operational by mid-1988.

References

[1] W. Stwalley, *Contemp. Phys.* 19:65 (1979).

[2] P. Gould et al., to be published.

[3] E. Raab et al., *Phys. Rev. Lett.* 59:109 (1987).

[4] D.E. Pritchard et al., *Phys. Rev. Lett.* 57:310 (1986); the particular trap demonstrated at Bell Laboratories grew out of discussions with J. Dalibard.
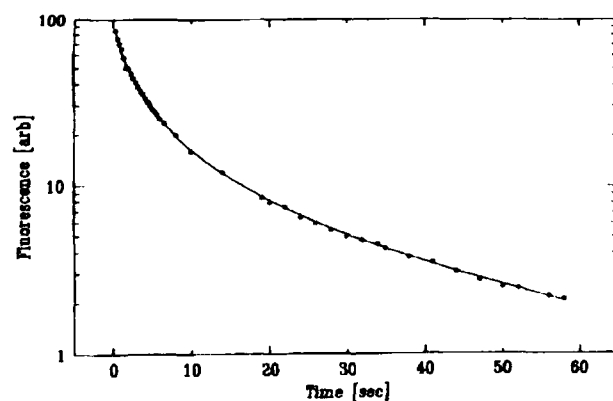
Figure 23.11 Decay of the fluorescence from the trapped atoms when the initial density was high. We see that at early times, the decay deviates from a simple exponential, indicating the presence of non-linear decay. The solid line represents a fit of Eq. (1) to the data.
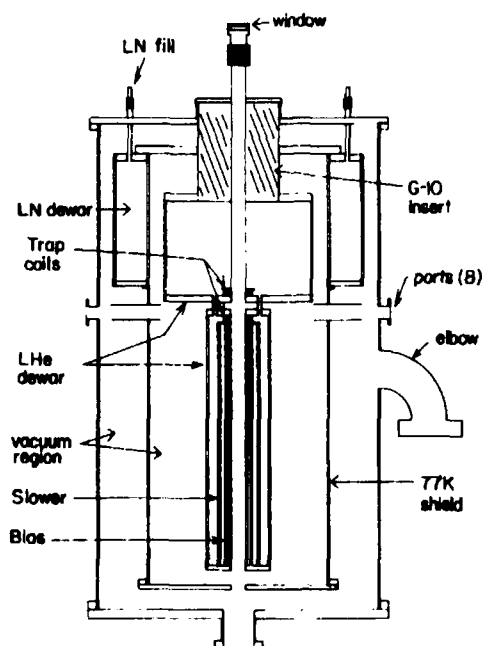
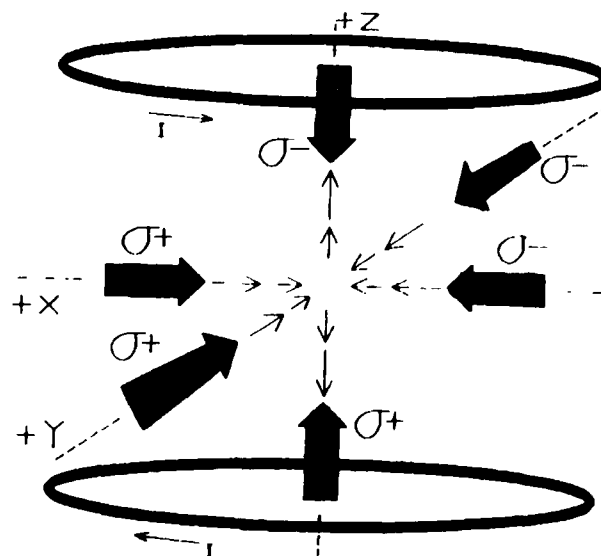Figure 23.12 Schematic of apparatus.

Figure 23.13. Trapping scheme in three dimensions. The "spherical quadrupole" field is generated by two coils of opposing current placed along the z axis approximately as shown. The field along the axes, indicated by the light arrows is parallel to its respective axis. Laser light, indicated by the heavy arrows, counter-propagates along x, y, z and is polarized as shown with respect to the axis of propagation.

23.2.2 Atom Wave Interferometer

David W. Keith, Bruce G. Oldaker, Garth Zeglin, David E. Pritchard

We are beginning a program to make an atom interferometer (one which interferes atomic deBroglie waves). In order to realize such a device on needs components analogous to those employed in conventional optics. We are currently investigating different technologies that could serve as elements of an "atomic optical" system. Two sorts of atomic optical elements are contemplated; those that exert forces on atoms through their interaction with near-resonant light, and grazing incidence diffraction gratings or micro fabricated transmission optics designed for x-rays of comparable wavelengths.

The key component for an interferometer is a coherent beam splitter. In 1986 our group was the first to demonstrate an atomic beam splitter.[1] We used the near resonant Kapitza-Dirac effect in which an atom is diffracted through a standing wave of laser light. However, this technique has several disadvantages, it requires a complex, stabilized laser and results in very small beam separations, on the order of 10^{-4} rads. In addition, such a technique is limited to atoms that have easily accessible laser transitions, which are not the atomic species most suitable for many conceivable applications of atom interferometers.

The observation of specular reflection of thermal alkali atoms from surfaces at grazing incidence[2] implies the possibility of observing diffraction of our atomic beam from a x-ray diffraction grating designed for comparable wavelengths. Gratings have been demonstrated for x-rays with wavelengths below 1 Å; they produce diffracted angles in the order of 10^{-2} rad. This technology would be ideal for use as an atomic beam splitter. Gratings are cheap and reliable (compared to lasers), and they could produce much larger angular beam separations resulting in more compact or sensitive interferometers. We have constructed an addition to our existing high resolution sodium beam machine to allow us to investigate grazing incidence reflections. During the last few months we have tested two simple gratings.

Interferometers measure the difference in the phase accumulated by particles traveling between two points by spatially separated paths. Thus an interferometer is sensitive to length changes caused by absolute rotation or relative mechanical displacements of its parts as well as to energy shifts caused by electromagnetic or gravitational interactions. To date interferometers have been made for photons and neutrons. For almost all purposes atoms would be better for matter wave interferometers than neutrons. Atoms are far more sensitive to electromagnetic interactions, they are available with ~ 10 times shorter wavelengths, and from cheap compact sources (neutrons come from reactors). The fluxes available in atomic beams are 10^8 times larger than those for neutrons; high fluxes would enable an atomic interferometer to make use of the fringe splitting techniques developed for optical interferometers. An atomic interferometer is intrinsically 10^5 times more sensitive to mechanical displacement than an optical interferometer. Since atoms travel many times slower than light, atomic interferometers are 10^{10} more sensitive to rotations than laser gyros. Atomic interferometers could be used to make precise measurements of atomic properties as well as to make funda-

mental tests in physics including Berry's phase, and the phase shift on rotation of bosons and fermions

References

[1] A. Anderson, S. Haroche, E.A. Hinds, W. Jhe, D. Meschede, and L. Moi, *Phys. Rev. A* 34:3513 (1986).

[2] P.L. Gould, G.A. Ruff, and D.E. Pritchard, *Phys. Rev. Lett.* 56:827 (1986).

23.2.3 Precision Mass Spectroscopy of Ions

Kevin R. Boyce, Eric A. Cornell, Gregory P. Lafyatis, David E. Pritchard, Robert M. Weisskoff

We are developing an experiment to determine the mass of individual atomic and molecular ions at precisions of 10^{-11}. This technique will allow us to do a variety of experiments which address issues of both fundamental and applied physics:

- The $^3H^+ - ^3He^+$ mass difference is an important parameter in ongoing experiments to measure the electron neutrino rest mass.

- Excitation and binding energies of typical atomic and molecular ions might be studied by "weighing" the small increase in energy: $\Delta m = E_{bind}/c^2$.

- Experiments that weigh γ-rays can be used in a new method to determine Avogadro's number, N_A, a key fundamental constant.

- Traditional applications of mass spectroscopy should benefit from the several orders of magnitude improvement in both accuracy and the sensitivity our approach offers over conventional techniques.

We will measure ratios of cyclotron frequencies, and therefore masses, of a small number of atomic or molecular ions in a Penning trap at 4.2K. To attain the precision we seek, it will be necessary to work with only one, or at most two ions in the trap. Space charge from other ions would lead to undesirable frequency shifts. Thus or mass spectrometer will have the ultimate sensitivity - a single molecule.

We will use ion trapping techniques based on methods developed at the University of Washington, where they have made precision measurements on protons, electrons and positrons at the 10^{-11} level. Trapped ions are detected by the small currents which they induce in the trap electrodes as they move. However, because atomic and molecular ions have larger masses, and thus lower resonant frequencies, they induce much smaller currents than the particles studied at Washington. Consequently, we developed a detector using a SQUID (Superconducting QUantum Interference Device) and superconducting electronics to measure these small induced currents, typically $< 10^{-14}$A.

This year, following several improvements on the apparatus and the detector,[1] we began systematic high-precision measurements on small clouds of ions (typically $\sim 5 - 10 N_2^+$ ions) stored in our trap. We learned how to minimize the non-harmonic electric fields, and, in addition, how to cool the trapped ions so that the remaining perturbations have smaller effects. We have used these cooled ions to make our first precision cyclotron measurements using a novel "avoided-crossing" technique.

Figure 23.14 shows a typical example of compensation decreasing the anharmonicity of the trap. The asymmetry in the left and right peaks come from a quartic term in the trapping potential. In the center peak, we have minimized this term using an additional set of electrodes in the trap. C_4 is a measure of the size of the quartic term.)

Figure 23.15 is an avoided-crossing cyclotron measurement. For this measurement, we have coupled the axial and cyclotron modes together with an inhomogeneous electric field, oscillating near their difference frequency, $v_c' - v_z$. When resonant, this electric field splits the axial mode. Figure 23.15 yields a 5×10^{-8} measurement of the cyclotron frequency and, in addition, provides information about the strength of the coupling field.

In the coming year, we expect to observe these effects with single ions and continue precision measurement work.

Reference

[1] R. Weisskoff et al., *J. Appl. Phys.* 63:4599 (1988).

Axial Line Shapes: Improved Harmonicity

Figure 23.14

Cyclotron Resonance by Avoided Crossing
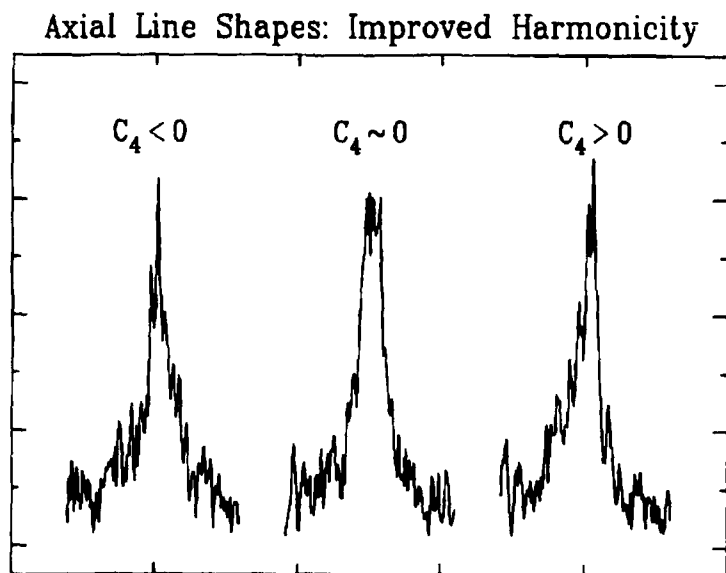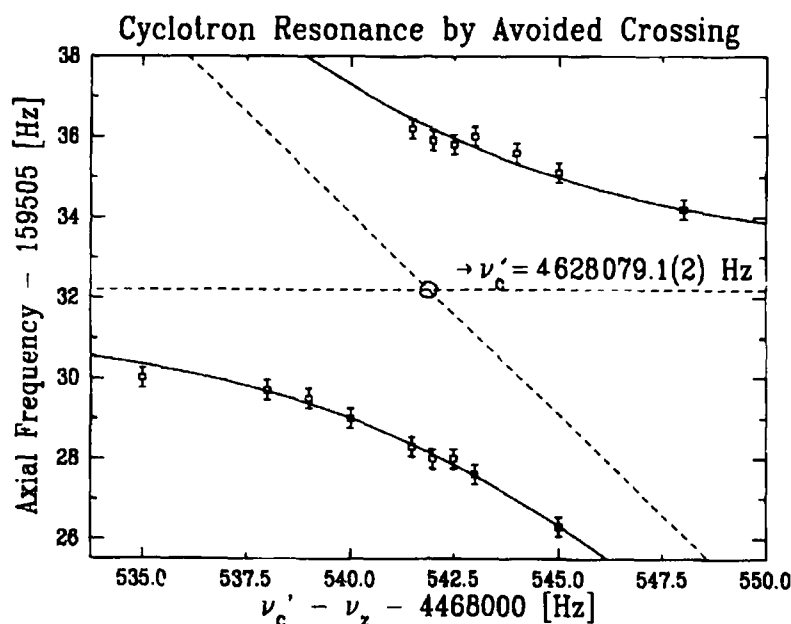
Figure 23.15

23.2.4 Experimental Study of Momentum Transfer to Atoms by Light

David W. Keith, Bruce G. Oldaker, Andrew H. Miklich, David E. Pritchard

We are investigating the radiative forces experienced by a two-level atom interacting with light. These forces provide a new way to study the fundamental interaction between atoms and radiation, and also have important applications in the slowing, cooling, and trapping of neutral atoms using light. By deflecting a highly collimated (0.7 $\hbar$ FWHM resolution), state-selected, and velocity selected (11% FWHM) atomic sodium beam with a well-characterized light wave, we are able to make quantitative measurements of many aspects of momentum transfer to atoms by light. The transverse momentum resolution gives us the only apparatus in the world capable of single photon resolution.

Emphasis this year has been on momentum transfer by a standing wave. Here the momentum transfer can be viewed in terms of a classical force (the dipole force) which arises from the interaction of the induced electric dipole moment with the gradient of the standing-wave electric field. If the laser is detuned far enough from resonance, spontaneous emission is negligible and the process can be described by a semi-classical Hamiltonian. The momentum transfer can also be described as absorption/stimulated emission of photon pairs from the two counterpropagating traveling waves which make up the standing wave (see figure 23.16), a view which predicts momentum transfer in discrete units of 2 $\hbar$k as we observed. If the standing wave is considered as a grating, 2 $\hbar$k is the reciprocal lattice vector in which momentum is transferred if the grating is not excited.

The major breakthrough this year has been the observation of Bragg scattering of atomic waves off a standing wave light "crystal." If the atomic beam is viewed as a plane wave and the antinodes of the standing wave define crystal planes, then large resonances for momentum transfer occur for incident angles, θ, satisfying the Bragg law,

$$2d \sin \theta = n\lambda_{D.B.}, \text{ where } d = \frac{\lambda_{light}}{2}, \lambda_{D.B.} = \frac{h}{mv}$$

is the DeBroglie wavelength of the atomic wave, and n is an integer (see figures 23.17 and 23.18).[1]

Evidence of this new phenomenon opens up new possibilities for the construction of an "atomic interferometer;" basically, a device that interferes atomic waves.

Reference

[1] P.J. Martin, B.G. Oldaker, A.H. Miklich, and D.E. Pritchard, *Phys. Rev. Lett.* 60:515 (1988).

Publication

Pritchard, D.E., and P.L. Gould, *J. Opt. Soc. Am. B* 2:1799 (1985).
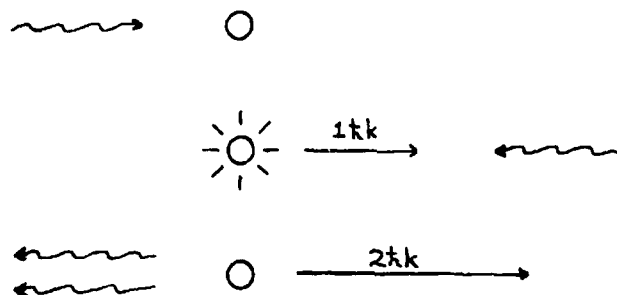
Figure 23.16 This shows schematically the absorption/stimulated emission process. a) Atom at rest absorbs a photon and 1 $\hbar k$ of momentum. b) A photon from the counterpropagating traveling wave causes stimulated emission by the excited atom. c) Atom in ground state moves with 2 $\hbar k$ of momentum and a photon has been traded from one traveling wave to the other.
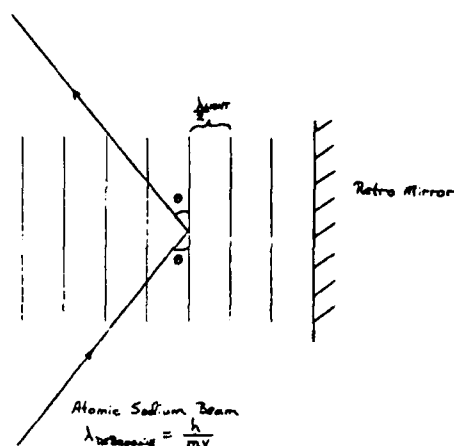
Figure 23.17 Schematic of Bragg scattering of an atomic sodium wave off a standing light wave.

a) First order Bragg scattering: P = 6 mW; D = 800 MHz, t = 6.4 ms (DW = 3.2 mm).

b) First order Bragg scattering: P = 10mW; D = 800 MHz; t = 6.4 ms.

c) Second order Bragg scattering: P = 4mW; D = 500 MHz; t = 3.2 ms (DW = 1.6 mm). The angle of the standing light wave nodes with respect to the atomic beam was 30 mrad times the order, m.
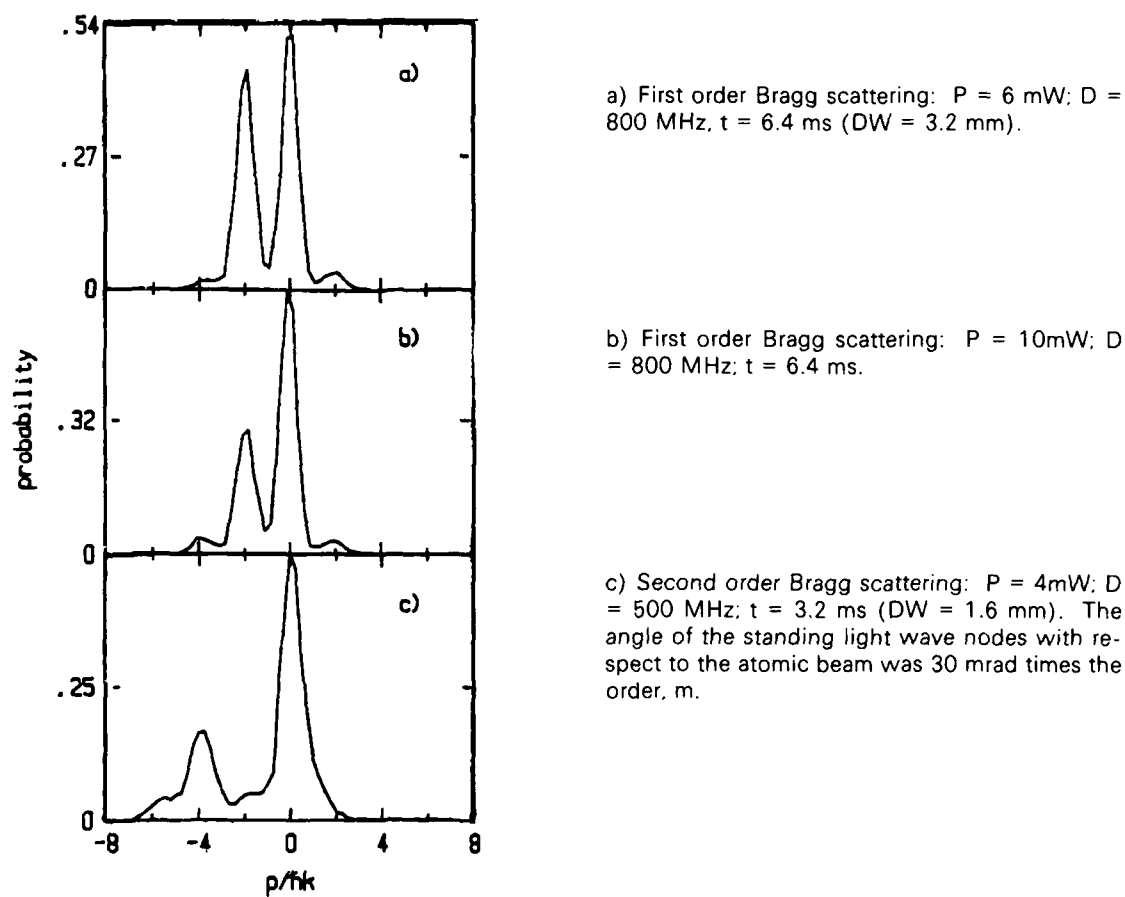
Figure 23.18 Experimental data of Bragg scattering.

24.0 Plasma Dynamics

Academic and Research Staff

Prof. G. Bekefi, Prof. A. Bers, Prof. B. Coppi, Prof. M. Porkolab, Prof. J.S. Wurtele, Dr. K-I. Chen, Dr. S-C. Chen, Dr. R.C. Englade, Dr. S.C. Luckhardt, Dr. S. Migliuolo, Dr. F. Porcelli, Dr. A. Ram, Dr. L. Sugiyama, I. Mastovsky

Visiting Scientists

V. Fuchs[1], R.A. Cairns, [2] P. Detragiache, Dr. C. Leibovitch, Dr. K. Xu, X.H. Lu

Graduate Students

G.A. Allen, R. Betti, C. Chow, S. Coda, J. Colborn, M. Conde, C. DeGraff, A.C. DiRienzo, R. Kirkwood, K. Kupfer, Y-K. Pu, J. Puchala, J.P. Squire, J.N.S. Villasenor

24.1 Relativistic Electron Beams

George Bekefi, Kongyi Xu, Chaim Leibovitch, Ivan Mastovsky

24.1.1 Coherent, Free-Electron Radiation Sources

The primary objective of the group is to develop a basic experimental and theoretical understanding of coherent generation by free electrons for wavelengths in the 1 μm to 10 cm range. Particular emphasis is placed on free electron lasers, Cerenkov sources, relativistic magnetrons, and other novel radiation sources.

The experiments are carried out on four high-voltage pulsed accelerators available in our laboratory. Their characteristics are summarized on the next page.

---

[1] I.R.E.Q., Quebec, Canada

[2] University of St. Andrews, North Haugh, St. Andrew, Scotland

PHYSICS INTERNATIONAL PULSERAD 110A ACCELERATOR

Voltage	1.5 MV
Current	20 kA
Pulse Length	30 nsec

NEREUS ACCELERATOR

Voltage	600 kV
Current	150 kA
Pulse Length	30 nsec

PHYSICS INTERNATIONAL 615MR PULSERAD

Voltage	500 kV
Current	4 kA
Pulse Length	1 μsec

HIGH VOLTAGE MODULATOR

Voltage	750 kV
Current	600 A
Pulse Length	1 μsec
Repetition Range	4 pps

In the area of free electron lasers (FEL's), experimental studies have been carried out on the amplification and phase coherence,[1] nonlinear saturation,[2] beam quality,[3] and optical guiding in a free electron laser.[4] These results contribute to the basic understanding of this important new type of coherent radiation source. An outstanding issue in free electron laser research is the problem of optical guiding. One of the remarkable properties of the free electron laser, apart from its wavelength tunability and high efficiency, is the large phase shift which the resonant interaction induces in the amplified electromagnetic wave. Under proper circumstances this phase shift can have a sign such that the electromagnetic wave is refracted towards the axis of the electron beam, in a manner somewhat akin to the guiding properties of an optical fiber. This theoretically predicted behavior has important implications. Optical guiding would mitigate the effects of diffraction, and thereby allow the length of FEL wigglers to exceed the Rayleigh range. Such long wigglers are needed if free electron lasers are to operate either in the vacuum ultraviolet (VUV) or at high efficiencies in the infrared wavelength regime. Using the MIT free electron laser facility, the phenomenon of optical guiding has been observed. This is the first such experimental demonstration.[4]

In addition to the above work, a new type of permanent magnet helical wiggler has been developed for free electron and gyrotron application. The system consists of an assembly of staggered samarium-cobalt magnets.[5,6] Other innovative magnetostatic wiggler configurations are being investigated, including a circular wiggler in which a rotating electron beam is surrounded by an assembly of samarium-cobalt magnets.[7]

The physics of the FEL interaction when the magnetostatic wiggler is replaced by an electromagnetic wave is being studied theoretically. A novel FEL device using a gyrotron powered electromagnetic wave wiggler has been designed.[8]

A long-pulse relativistic magnetron microwave source using a superconducting magnet has also been designed and is under construction.[9] A 35 GHz cyclotron autoresonance maser (CARM) amplifier with high efficiency has been designed, and experiments have begun.[10]

Recently, a novel technique of studying intense relativistic electron beams has been developed and tested.[11,12] It permits time resolved measurements of the beam with subnanosecond time resolution. In this method one observes the Cerenkov light through a fast electrooptic shutter and thereby obtains a two-dimensional picture of the beam on a piece of regular photographic film.

References

[1] J. Fajans and G. Bekefi, *Phys. Fluids* 29:3461 (1986).

[2] J. Fajans, J.S. Wurtele, G. Bekefi, D.S. Knowles, and K. Xu, *Phys. Rev. Lett.* 57:579 (1986).

[3] J. Fajans and G. Bekefi, MIT Plasma Fusion Center Report No. PFC/JA-86-57, 1986.

[4] F. Hartemann, K. Xu, G. Bekefi, J.S. Wurtele, and J. Fajans, *Phys. Rev. Lett.* 59:1177 (1987).

[5] G. Bekefi and J. Ashkenazy, *Appl. Phys. Lett.* 51:700 (1987).

[6] J. Ashkenazy and G. Bekefi, MIT Plasma Fusion Center Report No. PFC/JA-87-45.

[7] F. Hartemann and G. Bekefi, *Phys. Fluids* 30:3283 (1987).

[8] B.D. Danly, G. Bekefi, R.C. Davidson, R.J. Temkin, T.M. Train, and J.S. Wurkele, *IEEE J. Quantum Electron.* QE-23:103 (1987).

[9] S-C. Chen, G. Bekefi, and R.J. Temkin, In *Proceedings of the International Society for Optical Engineering*, January 1988, p. 873.

[10] A.C. DiRienzo, G. Bekefi, and C. Leibovitch, IEEE International Conference on Plasma Science, Seattle, Washington, 1987 (to be published).

[11] F. Hartemann and G. Bekefi, *Appl. Phys. Lett.* 49:1680 (1986).

[12] G. Bekefi, F. Hartemann, and D.A. Kirkpatrick, *J. Appl. Phys.* 62:1564 (1987).

24.2 Plasma Wave Interactions - RF Heating and Current Generation

Abraham Bers, Vladimir Fuchs, R. Alan Cairns, Abhay Ram, Kenneth Kupfer, Carson Chow

The work of this group is generally concerned with theoretical and computational studies on the *Electrodynamics of Plasmas.* Such studies encompass the linear and nonlinear excitation and propagation of stable and unstable waves in plasmas, and the nonlinear interactions involved in energy and momentum exchange among waves and between waves and plasma particles. Much of our work is directly related to *plasma heating and current generation* by electromagnetic fields coupled to a plasma from external power sources. This work is also relevant and coupled to ongoing experiments in toroidaly confined plasmas at MIT (Versator and Alcator) and elsewhere. Other basic studies are concerned with the *space-time evolution of instabilities*; these studies have extended to problems outside plasma dynamics and found applications in fluid dynamics and other continua. Our interest has also focused on nonlinear phenomena of *intrinsic stochasticity and chaos* in plasma electrodynamics. A more in-depth overview of our research can be obtained from the progress reports of the past few years (RLE Progress Report Nos. 124 through 129).

In the following four subsections we describe our work over the past year. In 24.2.1 we outline some initial work aimed at understanding the diffusion and transport induced by waves in a plasma. This builds upon our previous studies on intrinsic stochasticity and Fokker-Planck studies of the particle distribution function evolution in the presence waves. Subsection 24.2.2 describes our progress in achieving a much simplified (reduced) description of mode conversion at singular layers in inhomogeneous, hot plasmas. Away from such layers, ray tracing is an important tool in studying the wave energy flow and deposition in complex geometries of magnetically confined plasmas; this is described in subsection 24.2.3. Finally, in subsection 24.2.4 we describe the importance of an elecromagnetic (kinetic) mode at ion-cyclrotron harmonics and how it modifies our usual understanding of wave propagation and damping for waves at such frequencies.

24.2.1 Diffusion in Velocity and Configuration Space due to Waves

As part of our studies on intrinsic stochasticity, we are turning our attention to understanding the diffusion of plasma particles that results when stochasticity is induced by finite amplitude waves. The most familiar situation is that of a homogeneous plasma where wavepackets induce diffusion in velocity space, e.g., the well-known quasilinear diffusion. In inhomogeneous plasmas velocity-space and configuration-space diffusion are, in general, coupled. We have clearly seen this in our studies of FM induced stochasticity for charged particles in a potential well,[1] as reported in previous Progress Reports. To understand this and other similar situations of diffusion in wave-particle interactions in an inhomogeneous plasma, we have been studying a Fokker-

Planck formulation which couples wave driven flows in velocity space to transport flows in configuration space. To simplify the situation further, we have initiated such a specific study for electrons in the tail of a distribution function maintained by rf fields, a situation that is very familiar to us from our past studies of current genration by rf waves in plasmas.

24.2.1.1 Transport Due to RF Generation of Energetic Tail Particles

Anisotropic distribution functions can be easily created in plasmas by having electromagnetic/electrostatic waves interact with the tail particles of the distribution function. For instance, in lower-hybrid current drive, an energetic electron tail is created by the lower hybrid waves; in ion-cyclotron heating of a two ion-species plasma an energetic minority species tail is created by the incident fast Alfvén wave coupled to an ion-Bernstein wave. These wave-particle interactions result in velocity space diffusion and the creation of a broad energetic tail to the distribution function. Since such tails are maintained by the waves and may contain a large fraction of the total plasma energy, it is important to understand their transport properties.

In general there are several mechanisms which can lead to the transport of energy from a tail. A stable tail will exhibit transport resulting from its interactions with the bulk plasma turbulence, the ripple magnetic field, and the wave fields themselves. Collisional transport is comparatively unimportant for tail particles because of their low collision frequency. An unstable tail can exhibit all of the above as well as the direct liberation of energy in the form of collective oscillations.

In the case of a stable tail, the fluctuations causing transport (including the waves themselves) are all supported by the bulk plasma. We have been studying these effects using a Fokker-Planck equation which in its most general form couples the wave driven flows in velocity space to transport flows in configuration space.[2] We have been concerned primarily with formulating this Fokker-Planck equation correctly in toroidal geometry while retaining a physical understanding of the various processes which contribute to the diffusion tensor. We have also done some numerical studies investigating the effect of a finite confinement time for fast electrons. This work is also coupled to our previous studies on lower hyrid current drive[3] and stochasticity.[4] The correct formulation of the diffusion coefficients that appear in the Fokker-Planck equation requires detailed understanding of the wave-particle interaction and the subsequent phase-space diffusion. Our stochasticity studies provide the basis for the diffusion and its correct analytical modelling; it can then be incorporated into our transport analysis. When studying phase-space diffusion in stochastic processes, it was convenient, at times, to describe diffusion in action-angle coordinates.[1] We find that similar transformations of the Fokker-Planck equation are necesary to facilitate the transport analysis. A gyro-center kinetic theory for rf transport in tokamaks with the appropriate physics has been setup in action-angle coordinates. The diffusion coefficients include the relevant toroidal dynamics of the tail particles in the spatially localized rf fields. An analysis of this equation is in progress to eventually determine the effect of rf on the transport of the tail particles.

References

[1] A.K. Ram, K. Hizanidis, and A. Bers, *Phys. Rev. Lett.* 56:147 (1986).

[2] K. Kupfer, A. Bers, A.K. Ram, V. Fuchs, and M.M. Shoucri, "Energy Transport in Lower Hybrid Current Driven Plasmas," *Bull. Am. Phys. Soc.* 32:1793 (1987).

[3] V. Fuchs, R.A. Cairns, M.M. Shoucri, K. Hizanidis, and A. Bers, *Phys. Fluids* 28:319 (1985).

[4] V. Fuchs, V. Krapchev, A. Ram, and A. Bers, *Physica D* 14D:141 (1985).

24.2.2 Singular Layer Reduction Theory for Wave Propagation in ICRH

The treatment of singular layers in wave propagation in inhomogeneous plasmas, where geometric optics techniques break down, is a long-standing unsolved problem for plasmas whose dynamics are described by the Vlasov equation. In regions around such singular layers, the natural waves of the plasma are coupled so that a wave incident upon such a region may be partially converted to another wave, partially reflected, and partially transmitted. What is of primary interest is the magnitude of each of these processes, i.e., determining the so-called transmission, reflection and mode-conversion coefficients of such singular layers. In the absence of kinetic (Landau-type) dissipation and for cases where the coupling of waves is only pairwise, we have shown, some time ago,[1] that the singular layer region can be described by appropriate second-order differential equations, and, thus, several important characteristic problems in propagation across a magnetic field were solved.[2]

For propagation that involves a nonzero wavenumber parallel to the magnetic field, and in particular near cyclotron and cyclotron harmonic resonances, dissipation cannot be ignored and the coupling problem is intrinsically fourth-order or higher. Up to now, the solution to such specific problems was obtained only by difficult numerical integrations of the differential equations (of fourth and sixth order). Recently, we have been successful in showing that this type of coupling problem can be reduced to a set of simpler, first and second-order, problems, some of which can be solved analytically.[3] Thus we have shown that the transmission through the singular layer can be reduced to a first-order differential equation and solved for analytically.[4] This was based upon extending well-known perturbation techniques for homogeneous plasmas[5] to inhomogeneous plasmas, and was a direct outflow of the Ph.D. dissertation work[6] we reported in last year's Progress Report. In addition, we have shown that the transmission and reflection at the singular layer can be obtained from an appropriate second-order equation whose numerical solution is very easy.[7] Both of these results have been tested against results obtained by integrating the fourth and sixth-order equations[8,9] and shown to be in excellent agreement.

Currently we are in the process of formulating an appropriate second-order equation to describe transmission or reflection and mode-conversion. Success in this endeavor will complete this reduced description of kinetic wave propagation at singular layers, since with the knowledge of the transmission, reflection, and mode conversion, the dissipation can be deduced from conservation of energy flow.

References

[1] V. Fuchs, K. Ko, and A. Bers, *Phys. Fluids* 24:1251 (1981).

[2] V. Fuchs, A. Bers, and L. Harten, *Phys. Fluids* 28:177 (1985).

[3] A. Bers, G. Francis, V. Fuchs, C.N. Lashmore-Davies, and A.K. Ram, "Analytic Descriptions of Ion Cyclotron Absorption," In 14th European Conference on Controlled Fusion and Plasma Physics, Madrid, June 22-26, 1987, Vol. 11D, Part III, p. 995 A-C. Geneva: European Physical Society, 1987.

[5] A. Bers, In *Plasmas Physics - Les Houches 1972*, ed. C. DeWitt and J. Peyraud. New York: Gordon and Breach Science Publishers, 1975.

[6] G. Francis, Ph.D. diss., Dept. of Physics, MIT, 1987.

[7] C.N. Lashmore-Davies, V. Fuchs, G. Francis, A.K. Ram, A. Bers, L. Gauthier, AIP Conference Proceedings 159 (7th Topical Conference on Applications of R. F. Power to Plasmas, Kissimmee, Florida 1987) eds. S. Bernabei and R.W. Motley, 366-369, New York: American Institute of Physics, 1987. Also Plasma Fusion Center Report PFC/JA-87-35, MIT, 1987. Also submitted to *Phys. Fluids*.

[8] P.L. Colestock and R.J. Kashuba, *Nucl. Fusion* 23:763 (1983).

[9] H. Romero and J. Scharer, *Nucl. Fusion* 27:363 (1987).

24.3 Ray Tracing for the Mode Converted IBW in ICRH

The fast wave component of the externally launched ICRF wave undergoes mode-conversion to the ion-Bernstein wave (IBW) near the ion-ion hybrid resonance (in a two ion species plasma). In last year's progress report we described the detailed numerical analysis that was being carried out with the help of a ray trajectory code that we had developed. This code was for following rays in a hot, Maxwellian plasma in toroidal geometry with gradients in density, temperature, toroidal and poloidal magnetic fields, included in a WKB sense. One of the major conclusions of this work[1,2,3] was that the IBW can Landau damp onto the electrons by significant upshift of the $k_\parallel$ spectrum along the rays in a torus. The externally launched $k_\parallel$ spectrum was not capable of accomplishing this.

The ray tracing analysis which we have used so far relies on a basic assumption that the anti-hermitian part of the conductivity tensor describing the plasma be much greater than the hermitian part. The ray tracing equations that are derived with this assumption are then the standard geometric optics ray equations. In our analysis of the propagation of the ion-Bernstein wave in a toroidal plasma, we find that this particular assumption breaks down along the rays. A next order correction to the conventional ray trajectory equations is needed to follow the rays through such regions.[4] We are in the process of modifying our ray tracing code to include the next order correction. With that in place we will be able to complete these studies on the propagtion of ion-Bernstein waves and the electron heating by such waves as they propagate in toroidal geometry.

References

[1] A.K. Ram and A. Bers, "Ray Tracing Analysis of the Mode Converted Ion-Bernstein Wave in ICRF Heating," Sherwood Controlled Fusion Theory Conference, San Diego, California, April 1987.

[2] A.K. Ram and A. Bers, *AIP Conference Proceedings* 159 (7th Topical Conference on Applic. of R. F. Power to Plasma, Kissimmee, Florida, 1987), eds. S. Bernabei and R. W. Motley, 402-405. New York: American Institute of Physics, 1987.

[3] A.K. Ram and A. Bers, "Analytical Modelling of the Propagation of Ion-Bernstein Waves in ICRF Heated Toroidal Plasmas," *Bull. Am. Phys. Soc.* 32:1948 (1987).

[4] I.B. Bernstein and L. Friedland, Chapter 2.5, In *Handbook of Plasma Physics*, Vol. 1, eds. M.N. Rosenbluth and R.Z. Galeev. North Holland, 1983.

24.3.1 Kinetic EM Mode Near Ion-Cyclotron Harmonics

For low β plasma ($\beta = 2\mu nkT/B^2$, where n is the density, T is the temperature and B is the magnetic field), one usually considers that there are two well-known modes that propogate perpendicular to the magnetic field near the first harmonic, $2\omega_c$, of the ion-cyclotron frequency. One of them is the electromagnetic fast-Alfvén wave which is usually shown to cross the cyclotron harmonic, and the other one is the electrostatic ion-Bernstein wave. However, at any finite value of β, we find that there is also another kinetic mode near $2\omega_c$.[1,2] The characteristic of this mode is that it is an elliptically polarized electromagnetic wave, and it remains so for all values of $k_\perp$ (the wave vector perpendicular to $\vec{B}$). Furthermore, its frequency ω, is such that $\omega/\omega_c \lesssim 2 - \beta$ through the entire range of $k_\perp$. The fast-Alfvén wave couples to this mode and this eliminates the erroneous crossing of the harmonic which is usually shown for the dispersion diagram of the fast-Alfvén wave. We have carried out detailed numerical and analytical work on this new, kinetic electromagnetic mode (see figure 24.1). For very slightly oblique propagation this mode tends to become evanescent, and rapidly enters into the complex k -plane as the obliqueness is increased. A version of this new mode exists in a two ion-species plasma as well. Here the new mode is also near the first harmonic of the cyclotron frequency and couples to the Alfvén wave branch which comes from the ion-ion hybrid cutoff (see figure 24.2).

The effect of this new mode on the transmission, mode conversion and reflection properties of the incident fast wave are presently being examined. For most β's of interest to fusion plasmas, we find that the new kinetic mode is well-defined (i.e., $k_\perp$ is essentially real) for only a very small range of $k_\parallel$'s around zero, and that it remains highly localized in the vicinity of the cutoff at $2\omega_c$. To account for this mode in the vicinity of the fast-Alfvén wave, the dispersion relation must be expanded to order $(k_\perp\rho)^6 \sim \beta^3$. The damping of the fast wave is then found to be much larger than what one usually calculates from dispersion relations that are correct to order $(k_\perp\rho)^2$ only (see figure 24.3).

References

[1] This mode was first discussed in: A.B. Kitsenko and K.N. Stepanov, *Nucl. Fusion* 4:272 (1964).

[2] C. Chow, A.K. Ram, and A. Bers, "Mode-Conversion and Damping in ICRF at Finite Ion-Betas," *Bull. Am. Phys. Soc.* 32:1948 (1987).
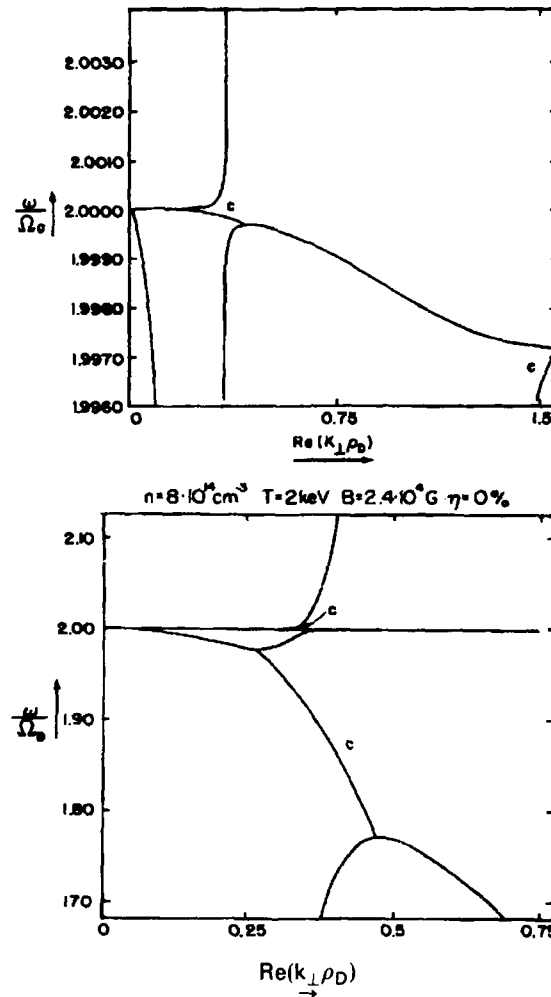
Figure 24.3.1 (a) Dispersion diagram near the first harmonic of the ion-cyclotron frequency for a single ion-species (deuterium) plasma. Branches denoted by C are real parts of complex $k_\perp$ -roots. (b) Detail near $\omega = 2\Omega_D$
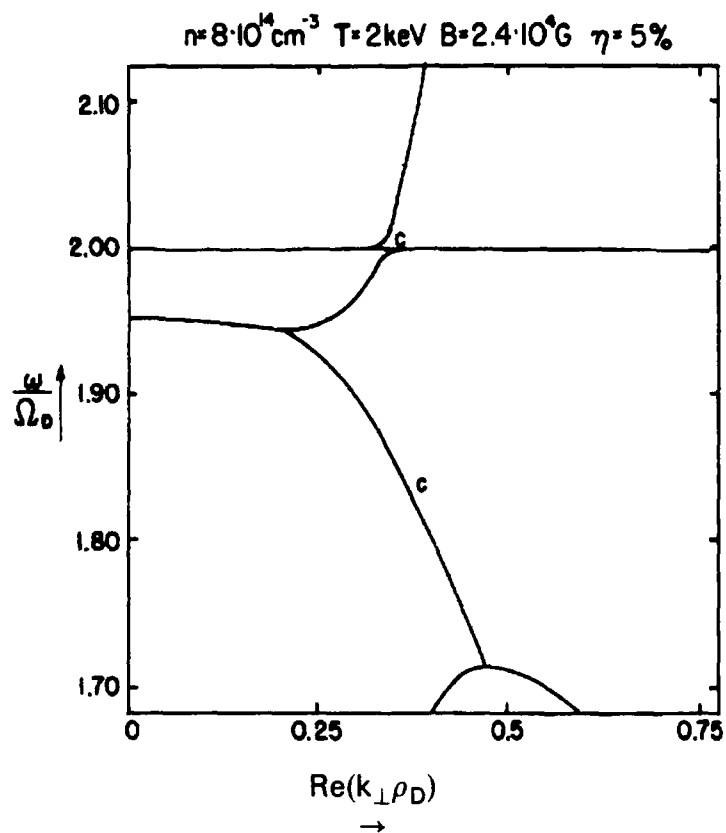
Figure 24.3.2 Dispersion diagram near the first harmonic of the deuterium cyclotron frequency for a two ion-species plasma $D(H)$. Branches denoted by C are real parts of complex $k_\perp$ -roots.

$$n = 8 \times 10^{14} \text{cm}^{-3} \quad T = 2\text{keV} \quad B = 2.9 \times 10^4 \text{G}$$
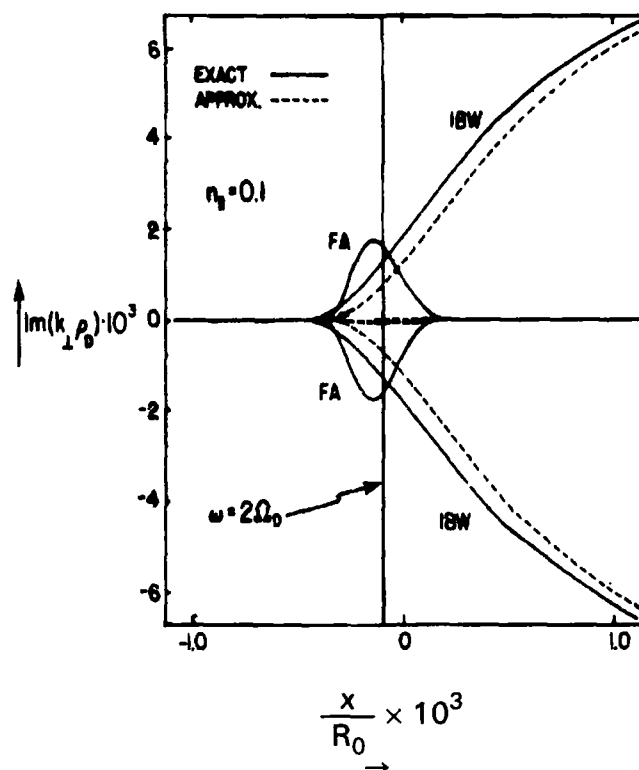
Figure 24.3.3 Damping and evanescence for finite $n_\parallel = ck_\parallel/\omega$ in the vicinity of the $2\Omega_D$ layer in a toroidal plasma. The approximate results are from dispersion relations correct to order $(k_\perp\rho)^2$.

24.4 Physics of Thermonuclear Plasmas

Bruno Coppi, A. Becker, Ricardo Betti, Stefano Coda, Paolo Detragiache, Ronald C. Englade, Stefano Migliuolo, Yi-Kang Pu, Linda Sugiyama

The main theme of this program is the theoretical study of magnetically confined plasmas in regimes of thermonuclear interest. A variety of physical regimes that fall in this category characterize both present-day experiments on toroidal plasmas (Alcator, TFTR, JET,...) as well as future ones that will contain ignited plasmas employing either first generation fuels, namely a deuterium-tritium mixture (Ignitor, CIT), or more advanced fuels such as deuterium-deuterium or deuterium-helium (Candor). A coordinated effort of collaboration between the design group of CIT, the U.S. compact ignition experiment, and the European Ignitor has been set up with our participation. At MIT, the Alcator C-Mod facility is under construction. This experiment combines the favorable features of elongated plasma cross-sections with those of high field compact geometries. These features have been embodied earlier in both the Ignitor and the CIT designs, as well as in a machine (proposed by us in the early 1970's) called Megator.

193

A recently proposed MIT program called Versator-Upgrade, has, as its main purpose, to achieve the "second stability" region for ideal MHD balooning modes. We were the first group to discover this stability region in the winter of 1977-1978, and to outline the experimental procedure by which to reach it. This consists of starting with a tight aspect ratio configuration, and raising the value of q (the inverse of the local rotational transform) on the magnetic axis above a certain level, such as 1.4, while increasing the value of the plasma pressure parameter, β_P, to those typical of the second stability region.

Our research program is now oriented along two major avenues. First, the basic physical processes of thermonuclear plasmas (equilibrium, stability, transport, ...) are being studied as they apply to existing or near-turn future systems. In this, we closely collaborate with our experimental colleagues. Second, we explore advanced regimes of thermonuclear burning, including those employing low neutron yield fuels (D-^{3}He and "catalyzed" D-D). We consider both the design of machines to contain these ultra-high temperature plasmas as well as the physics that governs their behavior.

Below, we present some salient results on topics pursued by our group this past year, as well as from current research.

24.4.1 Anomalous Ion Thermal Conductivity

Over the past few years we have undertaken a comprehensive analytic and numerical study of the anomalous ion thermal transport associated with a microinstability known variously as the ion temperature gradient mode, η_i, mode or ion mixing mode. Many of the relevant properties of this mode were outlined by our group[1] as part of the analysis of the mechanism responsible for inward particle transport in toroidal devices. Subsequently, the increased energy confinement times τ_E and record values of the confinement parameter achieved by pellet injection[2] in Alcator C have validated our previously suggested[3] "cure," for the observed inadequate energy confinement times in the plasmas produced by Alcator C, that significant anomalous ion thermal conductivity could be avoided by producing peaked density profiles.

Our recent investigations focused on the spatial profile and parameter dependence of the mixing mode in toroidal devices. Simulations[4] successfully reproduced present day regimes and have been employed in predictions regarding high field experiments in ignited regimes.

24.4.2 Profile Consistency: Global and Nonlinear Transport

It is well established experimentally that the steady-state electron temperature profile in tokamak discharges is relatively independent of the spatial deposition of auxiliary power and assumes a canonical shape that can be related to that of a macroscopically stable and relaxed current density profile outside the region of sawtooth activity. This behavior is often referred to as the "principle of profile consistency."[5] In addition, the readjustment of the profile distortion caused by pellet injection and the propagation of heat pulses associated with sawtooth crashes or transient bursts of spatially localized microwave power deposition are observed to proceed on time scales considerably faster than the steady-state electron thermal energy transport time.

These considerations have led us to conclude[6] that the relevant electron cross-field heat flux is the result of at least two different transport processes described as fast and slow. The slow process can be appropriately described by a standard diffusion term that is linear in the temperature gradient, but the fast process is strongly determined by the departure of the electron temperature from the canonical profile and has a nonlinear temperature gradient dependence in our formulation. In neither case is the magnitude of transport required to explicitly depend on the profile and strength of the source of electron thermal energy even though the solution of the energy balance equation adheres reasonably closely to the "principle of profile consistency."

24.4.3 Sawtooth and Fishbone Stabilization in Auxiliary Heated and Fusion Burning Plasmas

Recent experiments at JET[7] have shown that ion cyclotron resonance heating (ICRH) can stabilize "sawtooth" oscillations. Shortly after ICRM turn-off, a sawtooth crash occurs with a delay time that is a finite fraction of the slowing down time of energetic ions produced by the RF fields.[8] In collaboration with the JET theory group, we have undertaken a study of the interaction of global $n° = 1$, $m° \simeq 1$ internal modes (which are responsible for the sawtooth) with a high energy ion population. Standard MHD theory[9] yields an instability parameter for these internal modes, denoted λ_H. The energetic ions: 1) contribute to a reduction in this parameter $\lambda_H \rightarrow \lambda_H + \mathrm{Re}(\lambda_K) < \lambda_H$; and 2) provide a viscous-like dissipation term, $\mathrm{Im}(\lambda_K)$ that arises from a resonance between the mode and trapped energetic ions that precess around the torus due to the curvature of the equilibrium magnetic field.

In high temperature plasmas, where finite ion diamagnetic frequency has brought the ideal $m° \simeq 1$ kink to marginal stability, the residual growth is provided by electrical resistivity. This growth can be negated by hot ion effects (a)-(b). This provides a qualitative understanding[10] of the mechanism that stabilizes sawtooth crashes. Detailed calculations are underway, examining plasma regimes and energetic ion distribution functions for which stabilization actually occurs.

24.4.4 Density Limit and D-T ignition Conditions

Relatively high values of the plasma density are required to insure a confinement parameter $n\tau_E$ (central electron density times energy confinement time) sufficient to reach ignition even for deuterium-tritium fuel. Collisional ion thermal conductivity and bremsstrahlung radiation, both proportional to the square of the particle density, play a strong role in the global energy value up to temperatures somewhat above T_m, the "minimum ignition temperature." Near and above T_m, the presence of anomalous ion thermal conductivity can have significant effects. Investigation of the microinstability known as the ion temperature gradient mode (also the η_i or ion mixing mode) shows that it can give rise to an ion thermal conductivity that scales as $nT_i^{3/2}$. In collaboration with W. Tang of the Princeton Plasma Physics Laboratory, we have analyzed an approximate model equation for the steady state energy balance in the central region of a tokamak plasma which includes this type of transport.[11] Multivalued solutions for the density are obtained as a function of temperature, ion thermal anomaly strength and power.

If no ion anomaly is active, the density must remain below a certain maximum value for the plasma to attain the minimum ignition temperature T_m, but any density is allowed beyond T_m. In the presence of anomalous transport, a critical heating power deposition that increases with the magnitude of the anomaly is required to open a channel between regions of allowed density for temperatures above and below T_m. Since the rate of change of the fusion cross-section decreases with temperature, the density must be progressively increased above a minimal value, to heat the plasma to steady-state temperatures considerably higher than T_m.

24.4.5 Alpha Particle Induced Fishbone Oscillations in Fusion Burning Plasmas

The "fishbone" is a burst of oscillations that occurs in some experiments in which plasmas have two components, a main plasma and an energetic ion population. The fishbone has toroidal $n° \simeq 1$ and poloidal $m° \simeq 1$ spatial dependence and a frequency close to the diamagnetic frequency of the core (main plasma) ions.[12] Three requirements must be met to have instability: 1) high enough temperatures are produced so that finite diamagnetic frequency brings the ideal mode to marginal stability; 2) the core plasma beta must exceed a threshold value; and 3) a viscous-like resonant interaction of the wave with trapped energetic ions, that precess due to the curvature of the magnetic field, must exist. For parameters relevant to an Ignitor device[13] alpha particles with energies near 300 keV resonate with the fishbone oscillation.

Work in progress[14] is concentrating on the stabilization of this mode (as well as that of the internal kink, see the preceding section) as a consequence of the energetic particle contribution, $\lambda_K(\omega)$, to the effective instability parameter $\lambda_H + \lambda_K(\omega)$. Here λ_H is the parameter given by standard[9] ideal MHD theory. The real part of λ_K is negative for modes with $\omega \simeq \omega_{di}$ much lower than $\omega_{D\alpha M}$ which is a measure of the precession drift frequency of alphas at their birth energy. Thus, the effective instability parameter decreases and the fishbone restabilizes at high enough α-particle pressure.

We have also found that another $m° \simeq 1$ oscillation can exist, but only at very high α pressure ($\beta_{p\alpha} > 1$). This oscillation is at higher frequency ($\omega \gtrsim \omega_{D\alpha M}/3$) and can be entirely supported by trapped energetic ions which provide a destabilizing contribution: $\text{Re}[\lambda_K(\omega \gtrsim \omega_{D\alpha M}/3)] > 0$.

24.4.6 Transport Simulations of Thermonuclear Ignition in Compact Experiments

The attainment of ignition in a toroidal device depends critically on the net balance between bulk heating of the plasma and energy loss due mainly to anomalous electron and ion thermal conductivity, bremsstrahlung, synchrotron radiation, and macroscopic processes such as sawtooth oscillations. Using a modified version of the BALDUR one and one-half-dimensional transport code,[15] we have investigated the impact of these processes on the time evolution of D-T plasmas in a compact, high field device of the Ignitor type with strong ohmic heating.[4]

We have used the generalization of Coppi-Mazzucato-Gruber diffusion to model electron heat transport as well as alpha particle heating contributions. For an anoma-

lous ion heat diffusion coefficient peaked halfway out in the discharge and sawtooth repetition times down to 0.3 seconds, ohmic ignition could be achieved over a fairly wide density range. A central electron density near $8 \, 10^{14} \mathrm{cm}^{-3}$ was optimal in the sense of allowing relatively rapid approach to the state in which fusion heating dominates ohmic heating. A slightly higher density allows faster heating to fusion burning regimes. The overall magnitude of electron heat transport could be increased about a factor of two before ignition was prevented, while the magnitude of ion heat transport was not a sensitive parameter. In addition, we have studied the effects of variations in the form of electrical resistivity, plasma impurity level, and flux surface equilibrium configuration on the approach to ignition. Simulation of the CIT device illustrates the rather strong auxiliary heating requirements of that design.

24.4.7   Transport Simulations of Ohmic TFTR Discharges

We have demonstrated the validity of a one-dimensional transport model for Ohmic TFTR plasmas. Some 40 representative discharges were simulated, including current, density, and toroidal magnetic field scans from four operating periods extending from 1983 to 1986. Most of these cases were dominated by an anomalous energy transport carried by the electrons. Our work shows that a model based on the idea of "profile consistency"[5] successfully reproduces the total energy confinement times of these discharges even though the electron energy confinement model had a different form.

24.4.8   The Role of the Ubiquitous Mode in Anomalous Electron Energy Transport

Electron thermal energy transport in magnetically confined plasmas is one of the most important subjects in fusion research. Experiments indicate that such a transport process is anomalous, namely that the observed electron energy confinement time is an order of magnitude smaller than the one predicted by collisional neoclassical theory. We find that the ubiquitous mode[16] satisfies the required[6] properties for driving the anomalous transport:

1. It is driven by the electron temperature gradient;

2. It is active over a significant portion of the plasma column and is not sharply reduced in regions of considerable collisionality ($v_e / E\omega_{be} \lesssim 1$);

3. Its wavelength is long enough to produce substantial energy transport over a significant portion of the plasma;

4. The energy transport is up to an order of magnitude larger than the corresponding particle transport.

References

[1] T. Antonsen, B. Coppi, and R. Englade, *Nucl. Fusion* 19:641 (1979).

[2] S. Wolfe, et al., *Nucl. Fusion* 26:329 (1986).

[3] B. Coppi, invited paper in *Abstracts of the 1984 Annual Controlled Fusion Theory Conference,* Lawrence Livermore National Laboratory, Lake Tahoe, Nevada, 1984.

[4] R. Englade, RLE PTP-87/12 (1987).

[5] B. Coppi, *Comm. Plasma Phys. Cont. Fusion* 5:261 (1980).

[6] B. Coppi, *Phys. Lett. A* (1988), in press.

[7] D. J. Campbell, et al., *Bull. Am. Phys. Soc.* 32:1838 (1987).

[8] F. Porcelli and F. Pegoraro, Second European Fusion Theory Meeting, Varenna, Italy, 1987.

[9] M. N. Bussac, R. Pellat, D. Edery, and J. L. Soule, *Phys. Rev. Lett.* 35:1638 (1975).

[10] P. Detragiache, B. Coppi, R. J. Hastie, F. Pegoraro, and F. Porcelli, Sherwood Controlled Fusion Theory Meeting, Gatlinburg, Tennessee, 1988.

[11] B. Coppi and W.M. Tang, submitted to *Phys. Fluids.*

[12] B. Coppi and F. Porcelli, *Phys. Rev. Lett.* 57:2272 (1986). Also B. Coppi, S. Migliuolo and F. Porcelli, *Phys. Fluids* (1988), in press.

[13] B. Coppi, L. Lanzavecchia, and the Ignitor Design Group, *Comm. Plasma Phys. Cont. Nucl. Fusion* 11:47 (1987).

[14] B. Coppi and F. Porcelli, *Fusion Technology* 13:447 (1988). Also B. Coppi, S. Migliuolo and F. Porcelli, RLE PTP-88/4 (1988).

[15] G. Bateman, Spring College on Plasma Physics, Trieste, Italy, 1985.

[16] B. Coppi and F. Pegoraro, *Nuclear Fusion* 17:969 (1977).

24.5 Tokamak Research: RF Heating and Current Drive

Mikolos Porkolab, Stanley C. Luckhardt, Kuo-in Chen, Edward W. Fitzgerald, John C. Nickerson, Stephano Coda, Jeffrey A. Colborn, Robert Kirkwood, Jared P. Squire, Jesus N.S. Villasenor

The purpose of the Versator II tokamak research program is the following: 1) to carry out a series of RF heating experiments near the lower-hybrid frequency on the Versator II tokamak, and to study toroidal current generation by RF waves using a unidirectionally injected slow (lower hybrid) wave; 2) to study the efficiency of RF current generation with combined ECRH/LHRF power injection; 3) to study RF preionization and startup with lower-hybrid waves in combination with ECRH assist; 4) to study high β_P plasmas at low toroidal currents, and the stability of the associated plasma; and 5) to study fast wave launching and coupling with a dielectric loaded

waveguide phased array (grill) as well as with an extended radiating-hole structure. For the heating and current drive experiments a four-waveguide phased array (grill) is used to inject microwave power with pulse lengths up to 20msec at a frequency of 800 MHz or 40 msec at a frequency of 2.45 GHz. The 800 MHz klystron provides RF powers up to 150 kW, and the 2.45 GHz system consists of two 50 kW klystrons providing up to 100 kW of total power. For the ECRH system, a linearly polarized radiation pattern is injected from the high field side by means of a rotatable mirror.

24.5.1 Combined Electron Cyclotron Heating and Current Drive Experiments

The versator ECRH/LHCD experiment uses ECRH and LHCD to generate current and heating of the suprathermal tail component as a means to provide preionization, start-up, ramp-up and control of the steady state current driven distribution funciton. Start-up of the tokamak plasma constists of two stages: 1) the preionization stage in which the neutral fill gas is broken down and an initial low temperature plasma is formed; and 2) the current ramp-up stage in which the plasma current is increased from zero or near zero to the desired operation current and closed magnetic surfaces are produced.

In the ECRH preionization experiment, ECRH power is injected into a neutral gas filling with the cyclotron resonance layer at the center of the vacuum vessel, $B_o = 12.5$ kG. Dense plasmas to allow effecient coupling of the lower-hybrid waves were produced easily. Time evolution of the spatial profiles of the density and the H_α emission were measured. The most surprising result of these experiments was that the ionization and peak in the density profile was shifted outward from the cyclotron resonance layer toward the location of the upper hybrid layer. This can be seen in figures 24.5.1 and 24.5.2 which show the time evolution of the density and hyrdogen emission along with the location of the upper hybrid resonance, $\omega^2 = \omega_{pe}^2 + \omega_{ce}^2$. The fact that the density and H_α light peaks between the cyclotron layer and the upper hybrid layer, is evidence that the power absorption in the preionization plasma is not due to cyclotron resonance absorption. The mechanism for the absorption may be through mode conversion to the electron Bernstein wave or as a result of a non-linear process.
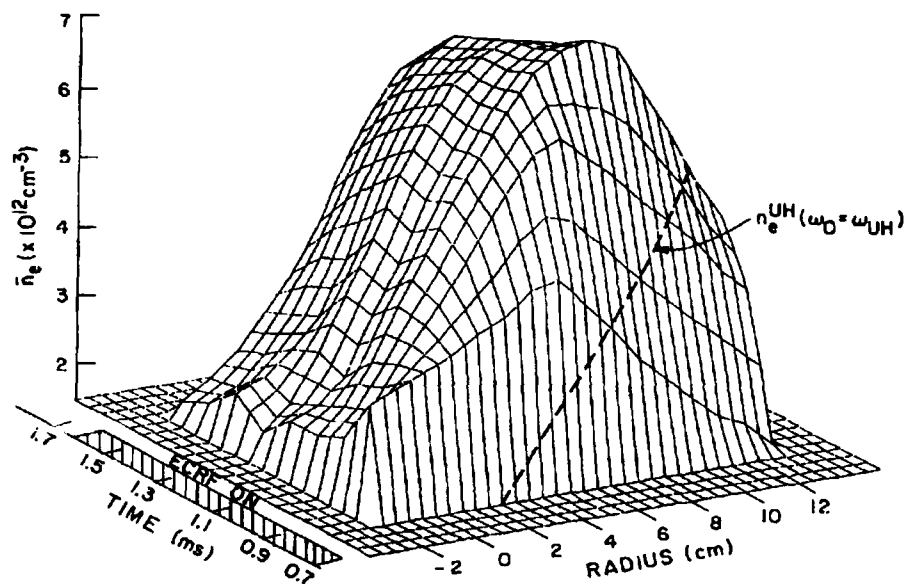
Figure 24.5.1 Temporal evolution of the density profile during 35 GHz ECRH preionization experiments (H_2 pressure = 2×10^{-4} torr, Prf = $\sim$(40-50) kW, $B_T(0)$ = 12.5 kG).

The start-up of the plasma current with ECRH and combined ECRH and LHCD was accomplished using ECRH to preionize an initial gas fill pressure of typically 5×10^{-5} torr hydrogen. During the ECRH phase the density rises to $4 \times 10^{12} cm^{-3}$ and then decays due to low recycling over a 2 msec time period. A small amount of current (< 2kA) is driven by the ECRH. When ECRH and LHCD are combined the current can be ramped up from 0 to 11 kA over a 4.5 msec period, see figure 24.5.3 Although, it was necessary to apply a small inductive voltage (less than 3 volts) to obtain this ramp up result, we believe that this voltage can be eliminated completely by improving the equilibrium control of the plasma vertical position. Note that this inductive voltage is still an order of magnitude lower than that needed for inductive start-up of the Versator plasma (typically, v_ℓ= 30-35 volts).

The principal unresolved physics question in the current start-up experiment is the large spectral gap existing between the phase velocity of the lower-hybrid waves and the initial low temperature plasma produced by ECRH. Non-linear effects have been invoked to provide waves with a range of phase velocities needed to bridge the gap to low electron energies. On Versator II initial experiments have been carried out with RF probes to detect the non-linearly produced waves. RF probes at the plasma edge during the ECRH/LHCD start-up experiment have detected evidence of low frequency wave generation in the plasma near the ion plasma frequency during both the ECRH phase and LH phase of the plasma start-up. Production of the energetic electron tail has been verified with electron energies in the range of 2-40 keV.
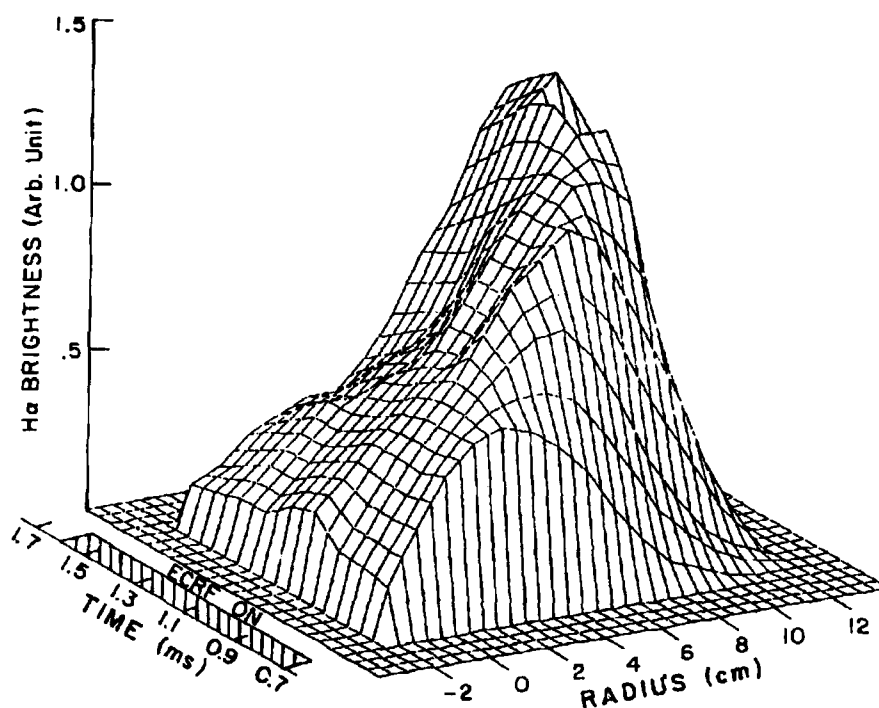
Figure 24.5.2 The temporal evolution of the H_α emission during 35 GHz ECRF preionization experiments (same conditions as in figure 24.5.1).

24.5.2   High β_P Plasma Equilibria by LHCD and ECRH Heating

The production of tokamak plasma equilibria with high values of $\epsilon \beta_P$ (>1) is important for determining the tokamak plasma β limits and for reaching the second stability regime of tokamk operation. On Versator II we have recently been successful in producing equilibria with values of β_P up to 3.8 and $\epsilon \beta_P$ up to 1.3 by means of RF current drive. In these experiments, plasma is fully sustained by RF drive with the inductive drive shut off, and the kinetic pressure from the RF driven energetic electron component provides the high plasma pressure needed to raise β_P. While the ultimate aim of high β tokamak operation is to increase the β_P of the bulk thermal plasma, the MHD equilibria, stability thresholds for ballooning modes, and other physics issues can be studied in these plasmas where the plasma pressure is produced by the energetic tail electrons.

The fact that the current is carried by energetic electrons in these plasmas allows us to obtain information about the current profile from our extensive set of x-ray diagnostics. This information is usually not available for inductively driven plasmas because of the the difficulty of current profile measurements in ohmic plasmas. The spatial distribution of the RF driven current was determined by measurement of the spatial width and profile of the hard x-ray bremmstrahlung spatial profile.   The x-ray profile was found to be shifted outward also a result of high β_P. The internal inductance of the rf driven current profile, ℓi, was obtained from the width of the x-ray profile, and this allowed us to use the equilibrium measurement of $\beta_P + \ell i/2$ to determine β_P itself.

201

VERSATOR II   ECRH / LHCD START - EXP.
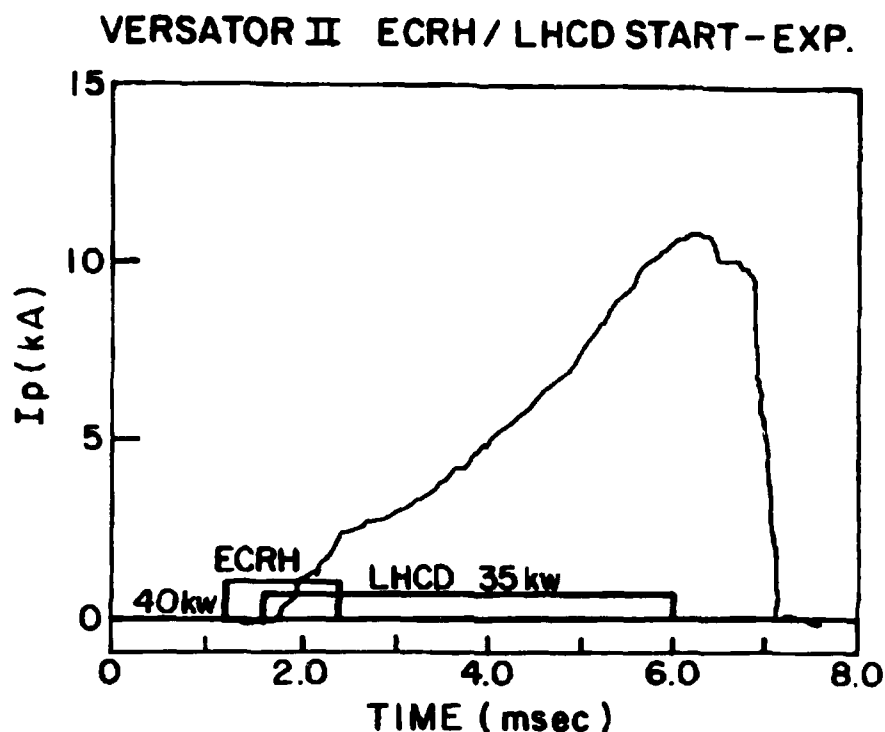
Figure 24.5.3 Plasma start-up by combined ECRH and LHCD.

The value of $\ell i/2$, the internal inductance of the RF current, was obtained by measuring the width of the current carrying energetic electron population with a hard x-ray PHA spectroscopy diagnostic. The width of the x-ray profile, figure 24.5.4, may be taken as the width, w, needed to calculate the internal inductance, $\ell i = .5 + 2 \times \ln(a/w)$ giving $\ell i/2 = 1.2$, where a is the minor radius of the discharge.

Another information about the shift of the magnetic axis as a result of reaching high β_p has been obtained from measurement of the density profile as a function of major radius. The outward shift of the density profile is an indication of the magnitude of the Shafranov shift of the magnetic axis. The spatial profile of the density was measured and was indeed found to shift outward at high β_p, see figure 24.5.5. The flux surface shift was inferred from the density profile shift. The time evolution of the density as a function of major radius shows an outward shift of the peark density as β_p increases. When the steady state RF driven flattop phase is reached the outward shift of the density profile is 6 cm (see figure 25.5.5 (d)), and the shift normalized to the minor radius is .46.

24.5.3   800 MHz Fast Wave Current Drive Experiments

The fast wave branch of the cold plasma dispersion in the lower hybrid range of frequencies promises to have a better current drive efficiency in reactor grade plasmas than the well established slow wave branch. The fast wave has a lower damping coefficient than the slow wave and has no resonance layer where it can be thermally absorbed. Therefore, the fast wave should penetrate into the plasma interior at high
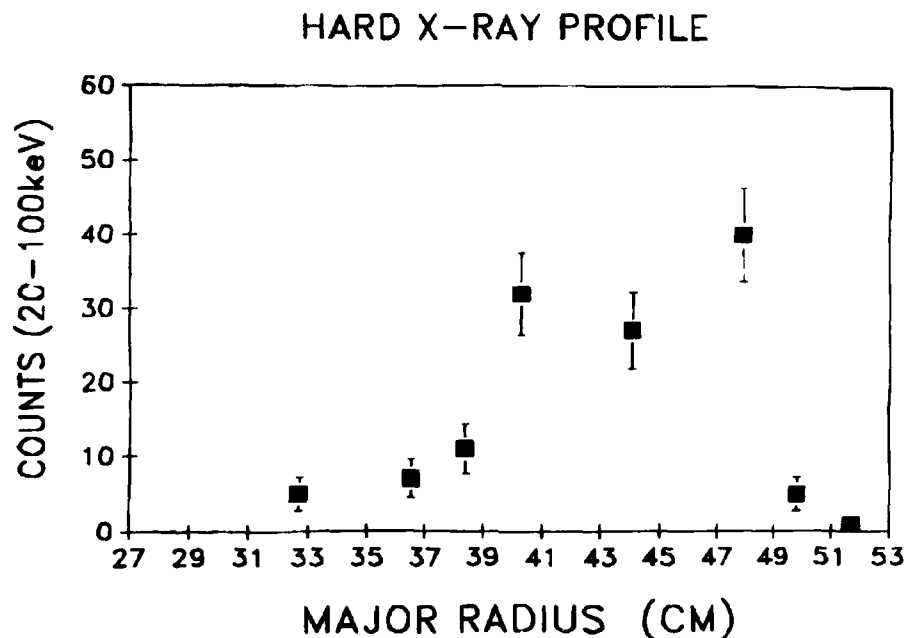
HARD X—RAY PROFILE

Figure 24.5.4 The hard x-ray profile of fully RF driven dicharge with high β_p. The major raidus of the vacuum chamber is 40 cm.

densities. This allows lower frequencies to be used, which also lowers the minimum $N_\parallel$ needed for the lower hybrid waves *accessibility to the center. Low $N_\parallel$ waves excite* higher velocity electrons, which are more efficient for current drive. Thus, assuming that non-linear effects do not dominate near the plasma surface, fast waves may be more efficient for current drive than slow waves.

The experiment is also strongly motivated by our earlier discovery of the current drive density limit which degrades slow wave current drive at high densities ($\bar{n}_e = 6 \times 10^{12} \text{cm}^{-3}$ for Versator II at 800 MHz). The physical processes which causes the density limit is not understood as yet although we believe that parametric decay processes are the prime candidate. Comparison of the results of fast wave current drive with the previous slow wave results done at 800 MHz in Versator should help gain insight into the problem.

The fast wave antenna system has been completed and is now being installed on the Versator II tokamak. The antenna is an array of four dielectric loaded waveguides (material: TiO, dielectric loaded constant $\epsilon = 80$, loss tangent < .0005) suitably fanned to correspond to the major radius of the tokamak. The dominant $N_\parallel$ is 3.5 for 90 degree phasing. The fast wave experiment will commence in mid-1988.
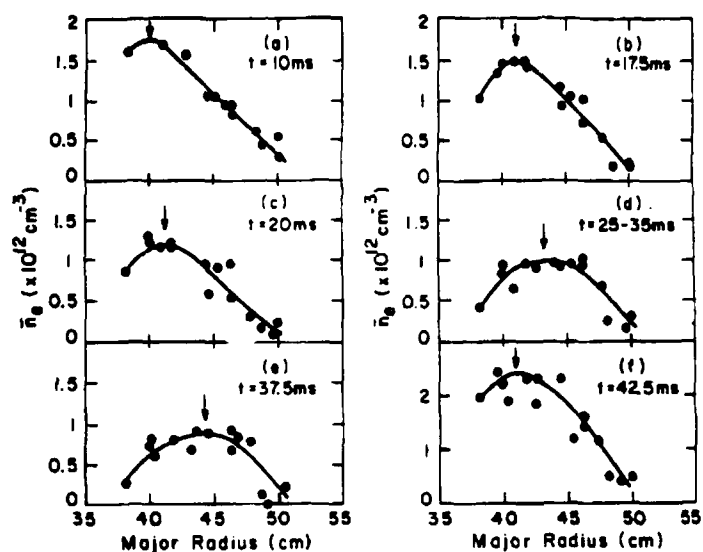
Figure 24.5.5 The outward shift of the density profile when β_P increases. Note that the RF was on from 20.5 ms to 41 ms.

25.0 Digital Signal Processing

Academic and Research Staff

Prof. A.V. Oppenheim, Prof. J.S. Lim, Prof. B.R. Musicus, Prof. A.B. Baggeroer, Dr. M. Feder, G. Aliberti

Graduate Students

M. Bace, J. Bondaryk, D. Cobra, M. Covell, D. Griffin, D. Harasty, J. Hardwick, S. Isabelle, J. Jachner, T. Joo, T. Pappas, G. Wornell, R. Wright, A. Zakhor

Support Staff

P. Eiro, D. Gage, C. LeBlanc

Part-Time Assistants/Special Projects

A. Donato, M. Dove, H. Gharavy

25.1 Introduction

The Digital Signal Processing Group is carrying out research in the general area of signal processing. In addition to specific projects handled on campus, there is close interaction with Lincoln Laboratory and the Woods Hole Oceanographic Institution. While a major part of our activities focuses on the development of new algorithms, there is a strong conviction that theoretical developments must be closely tied to applications. We are involved with the application areas of speech, image, video, and geophysical signal processing. We also believe that algorithm development should be closely tied to issues of implementation because the efficiency of an algorithm depends not only on how many operations it requires, but also on how suitable it is for the computer architecture it runs on. Also strongly affecting our research directions is the sense that while, historically, signal processing has principally emphasized numerical techniques, it will increasingly exploit a combination of numerical and symbolic processing, a direction that we refer to as knowledge-based signal processing.

In the area of knowledge-based signal processing, there are currently two research projects. One involves the concept of symbolic correlation, which is concerned with the problem of signal matching using multiple levels of description. This idea is being investigated in the context of vector coding of speech signals. Symbolic correlation will entail the use of both symbolic and numeric information to efficiently match a speech signal with stored code vectors. The second project in this area deals with the representation and manipulation of knowledge and expressions in the context of signal processing. This work examines issues such as the representation of knowledge, derivation of new knowledge from that which is given, and strategies for controlling the use of this knowledge.

In the area of speech processing, we have, over the past several years, worked on the development of systems for bandwidth compression of speech, parametric speech modeling, time-scale modification of speech, and enhancement of degraded speech. Recently, a new model-based speech analysis/synthesis system was developed. This system is capable of high-quality speech production, and it is being used in several low- and mid-rate speech coding systems. Our newest speech coding system has achieved a bit rate of 4.8 kbps while maintaining high speech quality. Research continues on adaptive noise cancellation techniques in a multiple microphone environment. An approach based on maximum likelihood estimation has shown substantial improvements over previous techniques.

In image processing, several restoration and enhancement projects were completed recently. One project involved the estimation of coronary artery boundaries in angiograms. This research produced a more robust model of the coronary angiograms which, consequently, improved the estimates of the arterial dimensions. A second image processing project studied the removal of ghosts from television signals. This form of degradation is caused by multi-path channels and can be removed by the use of an appropriate inverse filter. The stable filter which results is in general non-causal and, therefore, some form of time reversal must be used to implement the filter. Other research included motion compensation for moving pictures, and magnitude only reconstruction of images.

In the area of geophysical signal processing, our research is focused on the transformation of side scan sonar data. In practice, this data is corrupted by a number of factors related to the underwater environment. Our goal is to explore digital signal processing techniques for extracting the topographic information from the actual sonographs. Concepts under study include the removal of distortions caused by towfish instability and reconstruction based on multiple sonographs taken from different angles.

We are pursuing a number of projects which are directed toward the development of new algorithms with broad potential applications. For some time, we have had a considerable interest in the broad question of signal reconstruction from partial information, such as, Fourier transform phase or magnitude. We have shown theoretically how, under very mild conditions, signals can be reconstructed from Fourier transform phase information alone. This work has been extended to the reconstruction of multi-dimensional signals from one bit of phase and, exploiting duality, zero-crossing and threshold crossing information. Current research includes reconstruction from distorted zero-crossings. In addition, the reconstruction from multiple threshold crossings is being studied. This problem has been shown to be better conditioned than reconstruction using only a single crossing. Also, we are examining the problem of narrowband signal detection in wideband noise. This project intends to compare several different techniques under a number of computational constraints. Research continues on relationships between information theory and stochastic estimation. We are exploring applications to statistical problems, iterative signal reconstruction, short-time analysis/synthesis, and parameter estimation.

With the advent of VLSI technology, it is possible to build customized computer systems of astonishing complexity for very low cost. However, exploiting this capability requires the design of algorithms which use few operations but have a high degree of regularity and parallelism, or can be pipelined easily. We are exploring directions which include systematic methods for designing multi-processor arrays for signal processing,

isolating signal processing primitives for hardware implementation, and searching for algorithms for multidimensional processing that exhibit a high degree of parallelism. We are also investigating highly parallel computer architectures for signal understanding, in which a mixture of intensive computation and symbolic reasoning must be executed in an integrated environment.

25.2 Motion Compensation for Undersea Cameras

Jae S. Lim, Matthew M. Bace

Undersea cameras have been used for many years in undersea exploration, reconnaissance, and salvage operations to go where divers cannot. While these cameras have proven to be very useful, they are still somewhat limited by their motion stability.

Typically, an undersea camera is towed behind a boat at a depth of several feet above the ocean floor. The video from the camera is displayed on monitors in the boat. Because the camera is not rigidly attached to anything, motion instabilities arise due to several major sources. Waves on the ocean surface cause the boat and therefore the towed camera to move slowly up and down. Variations in the currents near the ocean floor lead to unpredictable changes in the pitch and roll of the camera. The combined motion produces very disturbing effects in the resulting video sequence, even to the point of inducing sea-sickness in the technicians viewing the display monitors. The variations in camera depth and angle are also a source of difficulty in producing large "mosaic" pictures from sequences of pictures taken from horizontally adjacent positions. The ideal camera would cruise at constant depth with a constant angle.

While it may be impossible to mechanically stabilize an undersea camera, recent work in the field of image processing indicates that it may be possible to process the video from the camera in such a way so that it appears as if the camera is stable. The goal of this research is to develop an algorithm for accomplishing this motion compensation. First, an estimate of the motion of the undersea camera will be obtained from the input video sequence. Then, the motion estimate will be used to compensate for the vertical and rotational components of the camera's motion so that only the horizontal component of the motion is present in the output video sequence.

25.3 Reconstruction Of Nonlinearly Distorted Images From Zero Crossings

Alan V. Oppenheim, Joseph E. Bondaryk

It has been shown theoretically that bandlimited, multidimensional signals can be specified to within a constant factor by the information contained in the locations of their zero crossings. It has been shown experimentally that two-dimensional,

bandlimited signals can be reconstructed to within a constant factor from zero crossing information alone. The two-dimensional signals used were derived from images and their zero crossings corresponded to the threshold crossings of the images.

In this research, the problem considered is that of two-dimensional, bandlimited signals which have been affected by memoryless, nonlinear distortions. It is shown that such distortions retain the information required by the above theory, if they contain a monotonic region. Therefore, reconstruction to within a scale factor of an original, bandlimited image from the threshold crossing information of a distorted image is made possible. The zero crossing coordinates of the two-dimensional signal derived from a distorted image are substituted into a Fourier Series representation of the original signal to form a set of homogeneous, linear equations with the Fourier coefficients of the original signal as unknowns. The least squares solution to this set of equations is used to find the Fourier coefficients of the original signal, which are inverse Fourier transformed to recover the original image. By comparison of the distorted and reconstructed images, the nature of the distortion can be described. Some of the numerical problems associated with the reconstruction algorithm are also considered.

The reconstruction process is particularly stable for images which have bandedge Fourier components of high magnitude. It is shown that reconstruction from the zero crossing information of these images is similar to reconstruction from halftones, binary-valued images used to represent images which contain a continuous range of tones. This theory is finally extended to include reconstruction of bandlimited images from the zero crossings of distorted halftones.

25.4   Digital Processing of Side Scan Sonographs

Alan V. Oppenheim, Daniel T. Cobra

Since its introduction in the early sixties, side scan sonar has proved to be a very important tool for underwater exploration and,in particular, for marine geology. Its applications include surveying the sea floor, the search and location of objects on the bottom of the sea, and the prospection of mineral deposits.

The information contained in reflected sound waves is used by side scan sonar to produce a graphic record, called a sonograph, which constitutes a composite representation of the topographic features and the relative reflectivity of the various materials on the sea bed. Due to several factors, however, sonographs do not provide a precise depiction of the topology. Geometric distortions can be caused by motion instability of the towfish on which the transducers are mounted. This can be due to a number of factors, including variable ship speed and sea currents. The record can also suffer from interferences such as those caused by dense particle suspension in the water, shoals of fish, or by ultrasonic waves generated by passing ships. As a result, the interpretation of sonographs often requires extensive practice and can be a tedious and time-consuming task.

Our general goal is to explore the application of digital signal processing techniques to side scan sonar data, with the purpose of producing enhanced sonographs. At present, we are studying the specific problem of estimating and correcting the distortions caused by towfish instability. This project is being conducted under MIT's joint program with the Woods Hole Oceanographic Institution, with the cooperation of the U.S. Geological Survey.

25.5 Representation and Manipulation of Signal Processing Knowledge and Expressions

Alan V. Oppenheim, Michele M. Covell

The phrase "signal processing" is used to refer to both "symbolic" and "numeric" manipulation of signals. "Symbolic" signal processing manipulates the signal description as opposed to the signal values with which "numeric" signal processing is primarily concerned. Efforts have been made to create computer environments for both types of signal processing.[1,2] Some issues that arise as a result of this work concern uniform representation of knowledge, derivation of new knowledge from that which is given, and strategies for controlling the use of this knowledge. This research will be *concerned with these areas and how they apply to digital signal processing.*

Representations that have been used in symbolic signal processing[1,2,3] have been largely distinct from those used in numeric signal processing.[1,4] The types of representations used are further separated by the control structures that the numeric and symbolic information commonly assume, the distinction essentially being the same as the distinction between Algol-like languages and logic programming languages. This dichotomy results from the differing amounts of available knowledge about appropriate approaches to the problems being addressed. By separating the control structure from application knowledge, this dichotomy can be avoided.

Strategies for controlling when knowledge about a signal is used should be provided and new strategies should be definable, since these control structures provide additional information about the problem space, namely, approaches that are expected to be profitable. Control strategies can also be used to outline new approaches to a problem, approaches that would not be considered by simple trigger-activated reasoning.

Finally, the ability to derive new knowledge from that which is given is desirable. This ability would allow the amount of information initially provided by the user to be minimized. The environment could increase its data base with new conclusions and their sufficient pre-conditions. Two immediate advantages of providing the environment with this ability are the reduction in the programming requirements and the possible "personalization" of the data-base. A reduction in programming requirements is available since information that is derivable from given information need not be explicitly encoded. Commonly, this type of information is provided to improve the performance of the derivation process. Secondly, since the environment would add information

to the data set according to conclusions prompted by the user's queries, the data set would expand in those areas which the user had actively explored.

References

[1] C. Myers, *Signal Representation for Symbolic and Numeric Processing*, Ph.D. diss., MIT, 1986.

[2] W. Dove, *Knowledge-based Pitch Detection*, Ph.D. diss., MIT, 1986.

[3] E. Milios, *Signal Processing and Interpretation using Multilevel Signal Abstractions*, Ph.D. diss., MIT, 1986.

[4] G. Kopec, *The Representation of Discrete-Time Signals and Systems in Programs*, Ph.D. d'~s., MIT, 1980.

25.6 Iterative Algorithms for Parameter Estimation from Incomplete Data and their Applications to Signal Processing

Alan V. Oppenheim, Meir Feder

Many signal processing problems may be posed as statistical parameter estimation problems. A desired solution for the statistical problem is obtained by maximizing the Likelihood (ML), the A-Posteriori probability (MAP) or some other criterion, depending on the a-priori knowledge. However, in many practical situations the original signal processing problem may generate a complicated optimization problem, e.g., when the observed signals are noisy and "incomplete."

An iterative framework for maximizing the likelihood, the EM algorithm, is widely used in statistics. In the EM algorithm, the observations are considered "incomplete" and the algorithm iterates between estimating the sufficient statistics of the "complete data" given the observations and a current estimate of the parameters (the E step), and maximizing the likelihood of the complete data, using the estimated sufficient statistics (the M step). When this algorithm is applied to signal processing problems, it yields, in many cases, an intuitively appealing processing scheme.

In the first part of this research, we investigate and extend the EM framework. By changing the "complete data" in each step of the algorithm, we can achieve algorithms with better convergence properties. In addition, we suggest EM type algorithms to optimize other (non ML) criteria. We also develop sequential and adaptive versions of the EM algorithm.

In the second part of this research we examine some applications of this extended framework of algorithms. In particular we consider:

1. Parameter estimation of composite signals, i.e., signals that can be represented as a decomposition of simpler signals. Examples include:

   ● Multiple source location (or bearing) estimation

   ● Multipath or multi-echo time delay estimation

2. Noise cancellation in a multiple microphone environment (speech enhancement)

3. Signal reconstruction from partial information (e.g., Fourier transform magnitude).

The EM-type algorithms suggested for solving the above "real" problems provide new and promising procedures, and they thus establish the EM framework as an important tool to be used by a signal processing algorithm designer.

25.7   Multi-Band Excitation Vocoder

Jae S. Lim, Daniel W. Griffin

The problem of analyzing and synthesizing speech has a large number of applications, and as a result has received considerable attention in the literature. One class of speech analysis/synthesis systems (vocoders) which have been extensively studied and used in practice are based on an underlying model of speech. For this class of vocoders, speech is analyzed by first segmenting speech using a window such as a Hamming window. Then, for each segment of speech, the excitation parameters and system parameters are determined. The excitation parameters consist of the voiced/unvoiced decision and the pitch period. The system parameters consist of the spectral envelope or the impulse response of the system. In order to synthesize speech, the excitation parameters are used to synthesize an excitation signal consisting of a periodic impulse train in voiced regions or random noise in unvoiced regions. This excitation signal is then filtered using the estimated system parameters.

Even though vocoders based on this underlying speech model have been quite successful in synthesizing intelligible speech, they have not been successful in synthesizing high-quality speech. For clean speech, the synthesized speech often exhibits a "buzzy" quality. For noisy speech, severe "buzziness" and other degradations often occur resulting in a large drop in intelligibility scores. The poor quality of the synthesized speech is, in part, due to the excitation models and the parameter estimation methods used in existing vocoders.

The Multi-Band Excitation Vocoder contains a speech model which allows the band around each harmonic of the fundamental frequency to be declared voiced or unvoiced. Accurate and robust estimation methods for the parameters of the new speech model

were developed, as well as methods for synthesizing speech from the model parameters and methods for coding the speech model parameters. An 8 kbps vocoder was developed as well.

This 8 kbps Multi-Band Excitation (MBE) Vocoder was compared with a more conventional Single Band Excitation (SBE) Vocoder (1 V/UV bit per frame) in terms of quality and intelligibility. Informal listening indicated that the "buzzy" quality of the SBE Vocoder was eliminated by the MBE Vocoder with the improvement being most dramatic in noisy speech. Intelligibility tests (Diagnostic Rhyme Tests) for speech corrupted by additive white noise (approximately 5 dB SNR) produced an average score of 58.0 points for the MBE Vocoder, 12 points better than the average score of 46.0 for the SBE Vocoder. In addition, the average score for the MBE Vocoder was only about 5 points below the average DRT score of 63.1 for the uncoded noisy speech. This represents a much smaller intelligibility decrease in noise experienced by most vocoders.

This project was completed in March 1987.

25.8 Television Signal Deghosting by Noncausal Recursive Filtering

Alan V. Oppenheim, Daniel J. Harasty

A ghosting channel is typically modeled by a finite impulse response filter. Such a filter has an all-zero system function. A deghosting system, the inverse of the ghosting channel, mitigates the effects of the ghosting. For a nonminimum phase channel, that is, for a filter which has a discrete-time system function with zeros outside the unit circle, the deghosting system has poles outside the unit circle. Such a deghosting system has a stable, noncausal infinite impulse response, which can be decomposed into components which are strictly causal and strictly anticausal. Our research considered the implementation of a deghosting system.

A recursive filter can be used to implement the time-flipped impulse response of the anticausal component of the deghosting system. However, the input and output signals must also be flipped in time. Rather than flipping the signals in their entirety, piecewise time reversal is used: This algorithm partitions the signal into overlapping blocks which are independently time reversed in flip buffers. The overlap accommodates the transient response of the recursive filter implementing the time-flipped anticausal impulse response. A consequence of piecewise time reversal is that the anticausal impulse response is no longer infinite, but the flip buffer and overlap lengths can be chosen to provide an arbitrarily close approximation.

A discrete-time ghosting channel model, deghosting system decomposition, and piecewise time reversal were studied. The advantages of the direct form recursive filter over other filter structures were studied, as well as the simulation program and experimental results.

25.9   A 4.8 Kbps Multi-Band Excitation Speech Coder

Jae S. Lim, John C. Hardwick

Recently completed research has led to the development of a new speech model. This model, referred to as the Multi-Band Excitation Speech Model, has been shown to be capable of producing speech without the artifacts common to model-based speech systems.[1] This ability makes the model particularly applicable to speech coding systems requiring high-quality reproduction at a low bit rate. In reference 2, a 9.6 kbps speech coder based on this model was first described. Later work resulted in an 8.0 kbps speech coding system. Both of these systems have been shown to be capable of high-quality speech reproduction in both low and high SNR conditions.

The purpose of this research is to explore methods of using the new speech model at lower bit rates. Results indicate that a substantial amount of redundancy exists between the model parameters. Recent research efforts have focused on methods of exploiting this redundancy in order to more efficiently quantize the model parameters. A 4.8 Kbps speech coder has been developed as part of this research. Preliminary tests have shown that this bit rate has been achieved with the same quality level as found in the previously developed coding system. Extensive evaluations of this new 4.8 kbps speech coding system are currently being conducted.

References

[1] D.W. Griffin and J.S. Lim, "A New Model-Based Speech Analysis/Synthesis System," IEEE International Conference on Acoustics, Speech, and Signal Processing, Tampa, Florida, March 26-29, 1985, 513-516.

[2] D.W. Griffin and J.S. Lim, "A High Quality 9.6 kbps Speech Coding System," IEEE International Conference on Acoustics, Speech, and Signal Processing, Tokyo, Japan, April 8-11, 1986.

25.10   Image Interpolation Using Edge Information

Jae S. Lim, Steven H. Isabelle

One application of interpolation in the area of digital image processing is in the increase of scale or resolution of still images. In this application, unknown sample values

of a continuous 2-D image function must be approximated based on the known sample values of a digital image. This interpolated image is an approximation to the ideal digital image created by sampling the original continuous image on a more dense sampling grid. This approximated image should be in some sense close to the ideal digital image. Because pictures are meant to be viewed by humans, the idea of closeness of the interpolated image to the ideal image is related to the response of the human visual system. For human viewers, edges convey much of the information in images; therefore, an interpolation system should place emphasis on recreating edge information accurately.

This research is aimed at developing an image interpolation system which incorporates edge information. This edge orientation information is computed using a simple edge model along with local characteristics of the image. Preliminary results indicate that artifacts introduced by conventional approaches such as pixel averaging can be substantially reduced using this method.

25.11 Multi-Level Signal Matching for Vector Quantization

Alan V. Oppenheim, Jacek Jachner

Our research investigates the use of multi-level signal representations, or hierarchies of signal representations with increasing levels of abstraction of detail, to perform efficient signal matching for Vector Quantization in a speech coder. The signal representations range from the numeric sequence that completely characterizes a signal, to high-level representations that abstract detail and group signals into broad classes.

The use of abstraction of detail in signal matching has been proposed in the context of a helicopter sound signature detection problem.[1] The current work focuses on low-bit-rate speech coding, for which recently proposed approaches, such as the Code Excited Linear Predictor (CELP) structure,[2] rely on a Vector Quantizer to code the residual signal after linear prediction stages. The residual is matched with one codeword signal out of a codebook of such signals, such that an error criterion between input and codeword signals is minimized. In the CELP coder, the error criterion is a time-varying linearly weighted mean-square error. The signal matching operations required for Vector Quantization (VQ) represent the major source of complexity in the CELP structure, and limit the practical size, hence performance, of VQ codebooks.

Our work seeks to reduce matching complexity by using multi-level signal representations simplified by abstraction of detail. The computational benefit of such signal representations is twofold. First, the matching operations on simplified or partial signal representations, termed partial errors, are substantially simpler to perform than applying

the error criterion to the complete signal representation. Next, the simplified signal representations partition the codebook into equivalence classes of code words that share a partial signal representation value. The partial error is the same for all code words in a class and needs to be computed only once. The partial errors are useful when they provide sufficient information to eliminate some code words from further consideration. By matching using multiple signal representations with progressively greater representation detail, a branch-and-bound procedure[3] is used to prune the set of eligible code words. The computational advantage of this approach stems from the substitution of simpler partial error evaluations for the more complex application of the error criterion to the complete representation.

The formulation and evaluation of suitable multi-level representations and partial error functions for VQ in the CELP coder are the main directions of our current work. Performance simulations are conducted using the SPLICE[4] signal processing environment on LISP machines.

References

[1] E. Milios, *Signal Processing and Interpretation using Multi-level Signal Abstraction*, Ph.D. diss., MIT, 1986.

[2] M. Schroeder and B. Atal, "Code-Excited Linear Prediction (CELP): High-Quality Speech at Very Low Bit Rates," IEEE International Conference on Acoustics, Speech, and Signal Processing, 1985.

[3] E. Lawler and D. Wood, "Branch-and-Bound Methods: a Survey," *Operations Research* 14(4):699-719, 1966.

[4] C. Myers, *Signal Representations for Symbolic and Numerical Processing*, Ph.D. diss., MIT, 1986.

25.12 Detection of Narrowband Signal in Wideband Noise

Alan V. Oppenheim, Tae H. Joo

The search for radio signals transmitted by extraterrestrials is a complex, multidimensional search problem because little is known about the transmitted signal. Current searches for extraterrestrial intelligence (SETI) collect data from a predetermined range of signals. These data are then processed to detect all synthetic components. (Synthetic components of signals are those which do not originate naturally. This assumes that the synthetic component is generated by extraterrestrials.) The assumption that the transmitted signal is a continuous wave (CW) at certain frequencies is commonly used in determining the range. Existing SETI systems use a frequency of 1450 MHz, atomic hydrogen line.

Due to uncertainties in the transmitter location, the relative velocities and the receiver antenna beamwidth, the frequency of the CW signal is unknown but is within 200 KHz of 1420 MHz. The propagation experiences multi-path which spreads the CW signal to a bandwidth of about 0.05 Hz. Therefore, SETI systems must search a wide frequency band (approximately 400 KHz) to detect a very narrowband (0.05 Hz) signal in poor signal-to-noise ratio (SNR) conditions.

Current SETI systems use FFT's to compute the spectrum. Each spectrum is then compared to a threshold to detect a peak. Because the SNR is low, the frequency bin size of the FFT is matched to the bandwidth of the narrowband signal. Therefore, a 2^{23}, or approximately 400 KHz/0.05 Hz, length FFT is required. In an existing system known as mega-channel extraterrestrial array (META)[1], this FFT is computed in two steps. First, the signal is filtered by 128 band-pass filters. Second, each band-pass filtered signal is transformed by a 64K length FFT. These computations are made using fixed point arithmetic. There are alternative implementations of this DFT-based method. The performance of different implementations, within constraints of the finite register length and other computational limitations, will be examined.

If the received signal is modeled as a sinusoid in white noise, modern spectrum estimators (e.g., the maximum entropy method) or frequency estimators (e.g., Pisarenko's method) can be employed. The performance and applicability of these algorithms, within constraints of computational limitations, will be examined.

Reference

[1] P. Horowitz, J. Forster, and I. Linscott, "The 8-Million Channel Narrowband Analyzer," In *The Search for Extraterrestrial Life: Recent Developments,* ed. M.D. Papagiannis, 361, 371. Hingham, Massachusetts: Kluwer Academic Publishers, 1985.

25.13 Estimation of Coronary Artery Dimensions from Angiograms

Jae S. Lim, Thrasyvoulos N. Pappas

A new approach was developed for the measurement of the severity of coronary obstructions from coronary angiograms. An angiogram is an x-ray picture of arteries in which a contrast agent has been injected. Existing techniques are heuristic and their performance is not satisfactory. Our approach exploited the characteristics of the signals involved. A model of the film density of the coronary angiograms was developed and used to estimate the diameter and cross-sectional area at each point along the vessel. Our model accounts for the structure of the vessel and background, as well as the distortions introduced by the imaging system. Both a one-dimensional and a two-dimensional model of the angiograms were studied. The algorithms were tested on synthetic data, on x-rays of contrast-medium-filled cylindrical phantoms, and on real coronary angiograms. Both algorithms were shown to have better performance than

current methods. Moreover, the two-dimensional algorithm was shown to be better than the one-dimensional algorithm.

This research was completed in April 1987.

25.14 Chaotic Dynamics in Digital Signal Processing

U.S. Navy - Office of Naval Research (Contract N00014-81-K-0742)

Alan V. Oppenheim, Gregory W. Wornell

This research is aimed at exploiting the rapidly emerging theory of chaotic dynamical systems in problems of interest to the digital signal processing community. Chaotic dynamical systems are deterministic systems capable of exhibiting highly stochastic behavior. Due to their exponentially sensitive dependence on initial conditions, the state evolution of these systems becomes increasingly unpredictable. It is well-known that chaotic phenomena are not restricted to high-order systems; very complex, chaotic behavior can be observed in simple non-linear dynamical systems of arbitrarily low-order.

Present work is aimed at identifying and characterizing chaotic dynamics at work in some digital signal processing scenarios. For example, the effect of quantization in digital filtering is clearly a deterministic, non-linear phenomena typically modeled as noise-like. It is conceivable that a chaotic model of quantization effects (rather than an additive-noise model) may lead to improved techniques for reducing these effects.

Other phenomena under investigation as chaotics systems include speech generation, non-linear signal distortion, and signal modulation.

25.15 Image Texture Modeling

U.S. Navy - Office of Naval Research (Contract N00014-81-K-0742)

Jae S. Lim, Rosalind H. Wright

Textured regions are the nemesis of many image processing algorithms such as those used for segmentation or compression. Such algorithms rely on assumptions of stationarity or on a high deg ee of correlation of the image gray-level data. In textured regions, where correlation n iy exist between spatial patterns instead of between gray-levels, these assumptions are inadequate. It is desirable to develop a model which captures the texture's inherent pattern in a concise way.

One desirable property of a texture model is an ability to synthesize syntactically regular "structural" textures (e.g., a tiled wall) as well as the more random "stochastic" textures (e.g., shrubbery). Current models usually assume only one of these cases. This research has so far focused on the appropriateness of causal and non-causal 2-D Markov random fields as a model for image texture. The Gibbs distribution of statistical mechanics, which is equivalent to the Markov model, offers a milieu which is better suited to studying the regular neighborhood interactions which

give textures their "texture" quality. The use of the (stochastic) Gibbs model in modeling and randomizing structural textures will be explored. The computation required to analyze and synthesize 2-D non-causal texture models is high, and encourages the examination of two more issues. The first issue involves modeling texture after reducing the number of gray-levels. The second issue involves determining the spatial resolution necessary to characterize the texture.

The goal of this research is to develop a model which is capable of synthesizing a continuum of structural and stochastic textures. Although analysis is a major part of the synthesis effort, the focus is on synthesis to see if one can characterize the texture "completely" as opposed to just extracting features which discriminate it from another texture. Such a model can later be used to justify features for texture classification and discrimination, as well as for controlled experimentation with human perception of visual pattern.

25.16 Reconstruction of Multidimensional Signals from Multiple Level Threshold Crossings

Alan V. Oppenheim, Avideh Zakhor

It has been shown theoretically that under mild conditions multidimensional signals can be recovered from one-level crossings (e.g., zero crossings). However, the accuracy with which locations of the one-level crossings need to be specified is large enough to limit the applicability of such a method in many practical situations. In this research, we have found two major sampling strategies for reconstruction of signals from multiple-level crossings.

In our first approach, we extend new theoretical results in multivariate polynomial interpolation theory, in order to define a variety of semi-implicit sampling strategies. These strategies, which provide sufficient conditions for recovery of multidimensional signals from non-uniform samples on lines of rational slope, are ultimately applied to the problem of reconstruction from multiple-level crossings. Although these semi-implicit results are general enough to be used for recovery from signal crossings with arbitrary functions, they do not provide conditions for reconstruction of signals from an arbitrarily small number of thresholds. In order to circumvent this difficulty, we are taking a second approach which is implicit, and uses algebraic geometric concepts to find conditions under which a signal is almost always reconstructible from its multilevel threshold crossings.

A problem distinct from that of uniquely specifying signals with level crossings is that of developing specific algorithms for recovering them from level crossing information, once it is known that the signals satisfy the appropriate constraints. We have developed a variety of reconstruction algorithms for each of our two approaches, and demonstrated results for several images. Preliminary investigation of their quantization characteristics seems to indicate that the dynamic range and bandwidth requirements for representation of signals via multiple level threshold crossings lie in between those of Nyquist

and zero crossing representation. Moreover, under certain circumstances, our semi-implicit and implicit sampling strategies become identical to Nyquist sampling. This bridges the gap between explicit, semi-implicit, and implicit sampling strategies, unifies seemingly unrelated sampling schemes, and provides a spectrum of sampling schemes for multidimensional signals.

This research was completed in October 1987.

Professor Alan V. Oppenheim

Professor Donald E. Troxel

26.0   Cognitive Information Processing

Academic and Research Staff

Prof. W.F. Schreiber, Prof. D.H. Staelin, Prof. D.E. Troxel, Prof. S. Benton, Prof. R-S. Gong, Dr. C.W. Lynn, Dr. L. Picard, J. Ward

Graduate Students

M. Heytens, R. Jayavant, S. Kommrusch, P. Monta, J. Ono, T. Tsakiris, R. Vinciguerra S. Hsu, T.T. Huang, E. Krause, D. Kuo, C. Lee, S. Marshall, D. Pian, J. Piot, J. Preisig, J.-P. Schott, J. Shapiro, E. Simoncelli, B. Szabo, A. Tom, J. Wang, G. Wornell

Undergraduate Students

A. Cherkassky, J. Kaliszewski

26.1   Advanced Television Research Program

26.1.1   Goals

The purpose of this program is to conduct research relevant to the improvement of broadcast television systems. Some of the work is carried out at RLE and some at other parts of MIT, including the Media Laboratory by Prof. Andrew Lippman, Prof. Edward Adelson, Prof. Stephen Benton, and Adjunct Prof. Arun Netravali. Audience research is carried out by Prof. W. R. Neuman in the Political Science Department. Reporting is by means of theses and published papers.

26.1.2   Background

The Japan Broadcasting Company (NHK) has demonstrated a high definition television system of 1125 lines, 30 frames, 60 fields, 25 MHz bandwidth, with image quality comparable to 35 mm motion pictures. A bandwidth-compressed version requiring an 8.1 MHz baseband has been developed. Both of these systems were originally intended for use in DBS (direct broadcasting from satellites) systems. A so-far unsuccessful attempt has also been made to have the wideband version adopted as an international standard for production and program interchange. Japanese interests have announced their intention to introduce some version of this system into the United States in 1990 via recorded media such as tape cassettes and video disks.

The latter possibility is widely seen as a serious threat to the financial stability of American television broadcasters, and the Federal Communicaitons Commission has

launched an inquiry into the situation. The MIT group is fully participating in the Inquiry.

26.1.3 Research Activities

In this contract year, we have put into operation a simulation facility that permits computed image sequences to be observed in real time. This is being used to study *problems in motion rendition. We have also started developing new systems that might be used for transmission of improved TV images, both enhanced (EDTV) and "true" high definition (HDTV), using only one standard TV channel.

We have carried out a number of studies at the Audience Research Facility in Danvers, Massachusetts for the principal purpose of determining viewer reaction to improved images and sound, and, in particular, to finding out whether audiences are willing to pay a premium for better pictures independent of program material.

We are continuing our studies of motion estimation and perception; motion-compensated interpolation, noise reduction, and demodulation; optimum filtering; and TV system modeling.

Publications

Herrmann, F.P., *A Four-Input Digital Video Combiner with High Definition Output,* S.B. thesis, Dept. Electr. Eng. and Comp. Sci., MIT, 1987.

Jesurum, D.A., *A Microprocessor-Controlled Dyanmic Raster Convergence System,* S.B. thesis, Dept. Eletr. Eng. and Comp. Sci., MIT, 1987.

Kuo, D.D., *Design of Dual Frame Rate Image Coding Systems,* S.M. thesis, Dept. of Electr. Eng. and Comp. Sci., MIT, 1987.

Krause, E.A., *Motion Estimation for Frame-Rate Conversion,* Ph.D. diss., Dept. of Electr. Eng. and Comp. Sci., MIT, 1987.

Kung, K., *Evaluation of a Single Channel High Definition Television System,* S.B. thesis, Dept. of Electr. Eng. and Comp. Sci., MIT, 1987.

Oh, M.H., *Improved NTSC,* S.B. thesis, Dept. of Electr. Eng. and Comp. Sci., MIT, 1987.

Schreiber, W.F., "Improved Television Systems: NTSC and Beyond," *SMPTE J.* 66(8) (1987).

Schreiber, W.F., "HDTV Technology: Advanced Television Systems and Public Policy Options," *Telecommun.* (1987).

Singer, L.A., *An Ultra-High-Resolution Display Monitor,* S.M. thesis, Dept. of Electr. Eng. and Comp. Sci., MIT, 1987.

Teng, P., *Design and Construction of a 1K x 1K Frame Buffer*, S.B. thesis, Dept. of Electr. Eng. and Comp. Sci., MIT, 1987.

26.2 Computer-Aided Fabrication System Structure

DARPA/U.S. Navy - Office of Naval Research (Contract N00014-85-K-0213)

Donald E. Troxel, Michael Heytens, Rajeev Jayavant, Steve Kommrusch, Peter Monta, Joseph Kaliszewski

26.2.1 Abstract

The Computer-Aided Fabrication (CAF) system structure carried out within RLE is part of a larger project within MTL. The overall goal of the CAF project is to integrate computers into the control, data collection, modeling, and scheduling of the integrated circuit fabrication process.

26.2.2 Computer-Aided Fabrication System Structure

The Computer-Aided Fabrication (CAF) system structure carried out within RLE is part of a larger project within MTL. The overall aim of the CAF project is to integrate computers into the control, data collection, modelling, and scheduling of the integrated circuit fabrication process. The goals of Computer-Aided Fabrication (CAF) of integrated circuits can be stated in different ways. One is to provide effective management of information associated with the fabrication of integrated circuits to improve flexibility, portability, and quality and to minimize turnaround time, development cost, confusion, error, and manufacturing cost. Another is to provide a way to operate a fabrication facility without using paper in the clean room. Another is to provide a framework for the creation of information that has usually not been available in a concise or precise way.

To realize these goals we must provide mechanisms and tools for data acquisition, analyses, reports, and instructions (guidance) for the actual operation of the fabrication equipment. Some data collection, analysis, and report generation is ongoing and automated. However, most of the data collected is either entered or entry is initiated by a person.

During the past year we have defined and installed both a hardware configuration and an initial CAF software system architecture. Central to the hardware architecture is the use of computer networking, both to provide integration of functions performed on different computers and to provide access to these computers from the integrated circuit processing facility and also from the users' offices.

The primary computer used for the actual operation of the CAF system within the integrated circuit processing facility consists solely of a Sun 3/280 processor with disk and network interface. Our processing facilities and offices are equipped with ASCII terminals which are interfaced to diskless terminal concentrators, which in turn provide network connections to any available computer. There are eight terminal concentrators, each of which has provision for up to 48 9600 baud RS 232 ports. These concentrators

also provide for communication paths and connection of some of the actual integrated circuit processing equipment.

Another Sun 3/280 is used as a development test bed for enhancements, tests, and debugging fixes. This insulates the users of the primary CAF system from the introduction of untested software, and it also helps to provide faster response time for the present users in that they do not have to share their cpu resources with the developers of new software. The second Sun 3/280 allows the developers of new software in particular to experiment with data base application programs without corrupting the actual data base used for ongoing processing of integrated circuits.

A third computer system consisting of a DEC 785 serves as a common meeting ground for the somewhat wider community of people concerned with integrated circuit design and manufacture. This computer provides the bulk of the text processing, printing, mail, simulation, and other facilities which are related to, but not directly concerned with, the actual operations in the integrated circuit processing facility. The 785 also provides a connection to an MIT Physical Plant computer and maintains an active alarm log for the building containing the integrated circuits fabrication facility.

Our initial CAFE (Computer-Aided Fabrication Environment) software system was based on the Berkeley Roving Shell with a file based data storage system. Our present CAFE system is based on the Berkeley system with an enhanced user interface menu and uses a commercial version of RTI INGRES data base system. Users log into this facility in the gowning room and then attach to the CAFE system at a terminal close by the equipment to be operated.

We have provided an ever growing number of functions to be accessed via the CAFE system. We have implemented a personal laboratory notebook facility. We have developed a standard forms based user interface mechanism which is used for most of our applications functions. Our implementation of an equipment reservation mechanism has been enthusiastically accepted by our laboratory users. We have implemented a number of transaction type applications such as defining of facilities and machines, starting lots, and reports which show machine status and the status of lots being fabricated. Just recently we have implemented an initial version of a process flow language and have provided two interpreters and a browser for this language.

We have interfaced to some processing and measuring equipment. The Dektak profilometer has been interfaced with the CAF computer, and software has been developed for transmitting screen plots and for printing these plots on either a laser printer or a terminal. The Nanospec has been interfaced and data collection software installed. We have also provided a connection to the BTU furnace controller both for creating and downloading furnace recipes.

We have continued our development of a generalized forms based user interface program, fabform. This single program, when called with a parameter file, produces a terminal display and allows a user to move from field to field and enter data. The type and content of the screen display are specified by an ASCII file which is referenced by data included in the parameter file. The form may have arbitrary length and the user can scroll up or down. At present, user interface commands are much like EMACS commands. When the user exits, or saves the data, an updated parameter file is written.

Using fabform, we have implemented a new version of the equipment reservations program which enables users to sign up for multiple machines at once. Users specify a list of machines that they will use in their next processing operation and access the data base for the current status of reservations. A locking mechanism has been devised so that multiple users cannot make conflicting entries. However different users may make reservations for different machines or different days. This program is in daily use and stores the sign up data in our data base.

We have also used fabform to implement a new multilevel menu system for the CAFE shell. We required a multilevel menu as we are accumulating quite a number of functions and were running out of space on the two level menu system that we ported from Berkeley. By using fabform we were able to implement this change fairly smoothly and also provide users with a more uniform interface.

We have continued to make substantial progress in the development of a data model and schema. Our system architecture is based on the Multibase system developed at CCA. This provides a uniform query interface to data residing in multiple autonomous, heterogeneous data bases.

Our data model is the functional model with support of extended data types, including various temporal types as well as inexact, interval, and null values. The schema captures several important aspects of plant and process management: fabrication facilities and equipment, users, equipment reservations, lots, lot tracking, wafers, process flow descriptions, work in progress (wip) tracking, and lab activity information.

Primarily because of the interface layer between the application programs and the data base accesses we were able to change the data base out from under the application programs without requiring changes in those applications when we ported the data base to the Suns and RTI INGRES.

We have continued to progress on the development of a process flow language (PFL). The creation of a PFL and associated interpreters is the key to our approach for generating actual fabrication instructions and for collecting the data resulting from actual fabrication steps. The interpreters provide the actual meaning of the process flows expressed in the flow language. Our PFL development is based on a two stage process step model which relates the goal of a change in wafer state first to the physical treatment parameters and finally to the actual machine settings used to process the wafers.

We have completed initial versions of walk through and fabrication interpreters and a browser all of which utilize our generalized forms based user interface program, fabform. The walk-through interpreter enables a process developer or potential user to see what will happen when the process is executed. The fabrication interpreter is similar, but in addition, allows for convenient entry of data as the wafers are actually processed. We have also completed an initial version of a past history browser which allows a user to review what actually happened in the fabrication of a lot of wafers.

26.3   Programmable Frame Buffer Systems

International Business Machines, Inc.

Donald E. Troxel, Charles W. Lynn, Len Picard, Joanne Ono, Todd Tsakiris, Ralph Vinciguerra, Alexander Cherkassky

26.3.1   Abstract

Our research during the past five years has focused on the architecture of interactive graphics work stations, the user interface, the manipulation of subimages, and algorithms for shading, texture mapping, and antialiasing. This year we have implemented a window system for the IBM YODA, experimented with progressive rendering of graphics images, completed a graphics system processor based on the TMS34010, and continued our investigation of the antialiasing of color graphics images.

26.3.2   Frame Buffer Systems

Our research during the past five years has focused on the architecture of interactive graphics work stations, the user interface, the manipulation of subimages, algorithms for shading, texture mapping, and antialiasing, and the raster display itself.

The use of color in computer graphics is now prevalent in many areas and at many levels of sophistication. *Color provides additional realism to images and greatly enhances visual presentation quality.* Spatial aliasing on finite resolution color displays remains a problem, however, although the problem has many applicable solutions for monochromatic images. In most cases the same monochromatic techniques are generally applied to color images, treating each color channel as a separate image to be antialiased and later merged for the full color result. This produces various problems with the color transition involving dark fringes and incorrect lightness rates along edges which are antialiased. Solutions to general color antialiasing have been developed which allow multicolored objects to be rendered on backgrounds of nonuniform color with minimum aliasing artifacts. These solutions involve optimized trajectories through a perceptually appropriate hybrid color space, parameterized by the position across each antialiased edge. Several related issues concerning local adaptation and proper system modeling and calibration are described. Data from tests of the algorithm on a set of human viewers is also presented in support of these new solutions. These solutions can also provide perceptually pleasing transparency effects, boundary blending for image composition, color correct scaling and zooming, and multivalued function displays. The tools developed for the determination of the solution also provide a convenient framework for the manipulation of color on graphic display systems.

A recently completed master's thesis by Joanne Ono developed software for a demand paged window manager. The objective of this thesis was to develop and implement in C language a method to efficiently redisplay the window information that is exposed as a result of a screen modification. The implementation uses offscreen display memory and PC main memory to store bit maps of the obscured portions of the windows currently in use. The method utilizes the offscreen memory that is available in the display memory for a demand paged type of storage between main memory and the

display. The program is implemented for a desk top window system currently being developed for the IBM YODA and its updated version, BETTY, that will run on an IBM XT, RT, or AT.

A recently completed bachelor's thesis by Alexander P. Cherkassky concerned a general purpose graphics system based on a TMS34010. The architecture of this graphics system provides a cost effective means for achieving high performance in color (as well as in monochrome) bit mapped graphics displays for personal computers and work stations. Much of the power of this system is due to the use of TMS34010 Graphics System Processor. This system can be adapted to a variety of resolutions and scanning frequencies and can be used in color as well as monochrome modes. It is capable of handling 1024 by 1024 resolution displays with four bits per pixel, and can contain up to 16 frame buffers in memory. Alternatively, this system can handle up to 16 bits per pixel with corresponding decrease in frame buffer storage. For demonstration purposes, the system was programmed to deliver resolution of 320 pixels per line, there being 250 lines per screen, four bits in a pixel.

A simple progressive rendering system for computer graphic images was developed to explore the trade off of computation time versus image quality. Five distinct levels of improving image quality were implemented, and a sequence of algorithms was developed that would generate the images sequentially. Algorithms were chosen that mesh well together, share as much information as possible, and minimize redundant calculations. The main use of such techniques is in interactive environments where the amount of time needed to produce a very realistic version of the image may be substantial. The idea of progressive rendering is well known in the area of image transmission, but relatively new to the computer graphics field. The challenge is to display as realistic an image as possible given a fixed computation time, and then to subsequently improve image realism in the most time efficient manner, making pass after pass, until some action by the viewer requires that the rendering process be started all over again on a new image (perhaps a zoomed or rotated view of the previous image). The desired set of algorithms should have the property that each builds upon the one before it, using results obtained by the latter so that the final image is approached in an incremental fashion.

Professor Jin Au Kong

27.0 Electromagnetic Wave Theory and Applications

Academic and Research Staff

Prof. J.A. Kong, Dr. S. Ali, Dr. A. Priou, Dr. R.T. Shin, Dr. T.M. Habashy, Dr. I.V. Lindell, Dr. M.C. Lee, Dr. S.Y. Poh, Q. Gu, A. Sihvola, Z. Li, N. Lu, T. Savarino, W.K. Wang, M. Zhai

Graduate Students

C. Adams, D. Arnold, R. Atkins, M. Borgeaud, I. Chang, D. Gaylor, K. Groves, H.C. Han, J.F. Kiang, C.W. Lam, C.F. Lee, K. Li, F.C. Lin, S.V. Nghiem, S. Rogers, L. Sichan, A. Swartz, M.J. Tsuk, A. Tulintseff, N. Yamashita, Y.E. Yang, H.A. Yueh, G. Zancewicz,

27.1 Electromagnetic Waves in Multilayer Media

Jin A. Kong, Samuel Ali, Tarek M. Habashy, Ying-Ching E. Yang, Michael J. Tsuk, Soon Y. Poh, Qizheng Gu, Jean-Fu Kiang, Ann Tulintseff

A general method of analyzing the time-domain bi-directional coupling of a pair of nonuniformly coupled dispersionless transmission lines has been devised. The transmission line equations are decoupled using the method of characteristics and the equations are solved iteratively. In the cases with linear loads, the unit-step response can be obtained in closed-form to the first order approximation, and arbitrary excitations can be handled by convolution. General approximate solutions to the transient response on two identical, nonuniformly coupled transmission lines terminated with linear or nonlinear loads have been obtained through an iterative scheme. The iterative method is very useful when the coupling coefficients are slowly varying with position since the zeroth order or first order approximation would be sufficiently accurate yet much easier to calculate. Furthermore, with the help of newly devised special transformations, we have shown that both the codirectional coupling and contradirectional coupling of the problem with unit-step excitation and linear loads have closed form expressions up to the first order approximation. Arbitrary excitation can then be taken into account by convolution. This method is hence most efficient. As for nonlinear terminations, numerical integrations are performed along the characteristics. Examples have been given for both cases to illustrate the use of this method. Extension to problems in which the phase velocities of coupled lines are not equal, or where more than two coupled lines are involved, is also under consideration.

We have also applied the technique of wave transmission matrices in periodic structures to examine transmission and reflection properties in striplines under the influence of meshed ground planes. Responses at different frequencies are calculated, followed by numerical Fourier inversion to obtain the time-domain response. The resistances of ground planes and strips have been taken into account. The results support the conclusion of the aforementioned research.

Many integrated circuits contain strip lines at different heights that run parallel or perpendicular to each other. We have investigated reliable models for these structures. First the capacitances associated with two offset parallel strips at different heights between ground planes are computed using the conformal mapping approach. As an extension, a simplified circuit of parallel-plate lines with transverse ridges is introduced to model two parallel strips with perpendicularly crossing strips on top. We treated it as a distributed circuit consisting of transmission lines segments with periodical capacitive loading. In order to calculate the coupling between two lines, we reduced this structure to two equivalent single line circuits, i.e., the even mode and the odd mode circuits. The Laplace transform approach can be easily applied to find out the transient response. The numerical computation carried out for various environments shows that the crossing strips will cause serious trouble for signals with a rise time of less than 50ps to propagate along a distances of 2cm or longer.

In applying the method of moments to solving the EM scattering problems, it is necessary to solve a large matrix when the dimension of the scatterer is larger than several wavelengths. Tremendous amount of computer CPU time will be spent on solving the matrix equation. When only the far field properties such as scattering cross section is of interest, we can use the sparse matrix technique to reduce the amount of computation. Some algorithms are compared to solve the sparse matrix. The Gaussian elimination algorithm, Cholesky decompositon algorithm and several versions of conjugate gradient methods are used. The number of multiplications and divisions (flops) are counted for comparing the efficiency of these algorithms. The effect of the nonzero element positions to the efficiency is also studied by defining the clustering index.

Another way of incorporating the effect of complicated geometry is to use a continuous line model while considering the coupling between parallel lines in multilayered integrated circuits to be nonuniform. In addition to the scheme that combines the method of characteristics and perturbational series to simplify the computation of the transient response from the coupled transmission line equations, new transformation for decoupling enables us to generalize this formulation to calculate the near-end and far-end crosstalks to very high accuracy, given arbitrary positional dependence for both capacitive and inductive coupling coefficients.

Basically, vias in a multilayered integrated circuits are treated like transmission lines with loadings where they encounter holes in ground planes separating different layers. We have modeled a ground plane with a hole and a circular conductor at the center of the hole as a radial waveguide, which in turn is connected to the via, another section of transmission line. Thus by computing the characteristic impedance of the former, we have derived the equivalent load impedance of the via hole. The load impedance is one important parameter in calculating the transient propagation along vias.

In order to investigate the validity of the quasi-TEM approximation for the time-domain wave propagation, we have developed an iterative approach to perform

quasi-TEM analysis in the time-domain. By assuming first that the longitudinal field components are small, it is shown that the transversal components can be obtainted from statics equations analogous to those applied for sinusoidal steady states. They also lead to solutions to the propagation velocities and voltage distributions of diferent quasi-TEM modes. The convergence criterion is shown to depend upon the time derivative of signals and inhomogeneity of the media.

Theory for quasi-TEM modes propagating in a transversely inhomogeneous (multidielectric) longitudinally uniform transmission line, previously derived for time-harmonic waves, is derived for transient signals. It is seen that, while the starting point for the theory is completely different, the result is similar to the time-harmonic theory, and previously derived properties for propagating modes also apply in the transient case. The range of applicability is discussed with a simple example.

Three methods are given with which bounded electromagnetic sources can be decomposed into two parts radiating, respectively, TE and TM fields with respect to a given constant direction in space. Source equivalence and nonradiating sources are discussed and taken into account in the theory, which leads to a recursive method or two different differential equations for the TE and TM components of the original source. It is seen that for a point source, a decomposition can be made with the aid of a line source, a plane source, or a set of point sources. A combination of these is also possible. The result is discussed and the planar decomposition is seen to match to an earlier result given by Clemmow in 1963. Also, it is demonstrated that the general exact image expression for the Sommerfeld half-space problem can be obtained through the present decomposition method.

The double-deformation technique is a modal technique based on identifying and extracting singularities from the Fourier integrals in the complex frequency and wave number domains. With this method, we have been able to obtain both early and late time response for vertical electric dipole and line source excitations in a two-layer medium very efficiently. We have also discovered a general scheme of breaking up the integrands so that sources with arbitrary time and space dependences can be easily handled without sacrificing convergence.

The analysis of resonance, input impedance and radiation of the elliptic disk, microstrip structure is rigorously formulated in this paper, using the Scalar and Vector Mathieu Transforms. With the help of these transforms, the resonance frequencies of the structure can be derived exactly using Galerkin's method and approximately using a perturbational approach. Expressions for the input impedance and the radiation pattern are also obtained.

Simple approximation for diffraction surface currents on a conducting half plane, due to an incoming plane wave, is given in terms of a line current (monofile) in complex space. When compared to the approximation by a current located at the edge, the diffraction pattern is seen to improve by an order of magnitude for a minimal increase in computation effort. Thus, the inconvenient Fresnel integral functions can be avoided in quick calculations of diffracted fields and the accuracy is seen to be good in other directions than along the half plane. The method can be generally applied to problems involving planar metal edges.

Exact image method, recently introduced for the solution of electromagnetic field *problems involving sources above a planar interface between two homogeneous media,* is shown to be valid also for sources located in complex space, which makes its application possible for Gaussian beam analysis. It is demonstrated that the Goos-Hanchen shift and the angular shift of a *TE* polarized beam are correctly given as asymptotic results by the exact reflection image theory. Also, the apparent image location giving the correct Gaussian beam transmitted through the interface is obtained a₃ another asymptotic check. The present theory makes it possible to calculate the exact coupling from the Gaussian beam to the reflected and refracted beams as well as to the surface wave.

The transient electromagnetic radiation by a vertical electric dipole on a two-layer medium is analysed using the double deformation technique, which is a modal technique based on identification of singularities in the complex frequency and wavenumber planes. Previous application of the double deformation technique to the solution of this problem is incomplete in the the early time response. In this paper we show that the existence of a pole locus on the negative imaginary frequency axis, which dominates the early time response, proves crucial in obtaining the solution for all times. A variety of combinations of paremeters are used to illustrate the double deformation technique, and results will be compared with those obtained via explicit inversion, and a single deformation method.

The transient response of fundamental sources, such as dipole and line current, was carefully analyzed. With the double-deformation technique, which is a modal technique based on identification of singularities in the complex frequency and wave number planes, we are able to obtain both early and late time response very efficiently. Some results for vertical electric dipole excitation on a two-layer medium have been published. Recently, we have discovered a general scheme of breaking up the integrands so that sources with arbitrary time and space dependence can be incorporated into our formulation without sacrificing convergence.

Publications

Gaylor, D., T.M. Habashy, and J.A. Kong, "Fields Due to a Dipole Antenna Mounted on Top of a Conducting Pad of Finite Extent in a Layered Stratified Medium," National Radio Science Meeting, Philadelphia, Pennsylvania, June 9-13, 1986.

Gu, Q., J.A. Kong, and Y.E. Yang, "Time Domain Analysis of Nonuniformly Coupled Lines," *J. Electromag. Waves Appl.* 1 (2):111 (1987).

Gu, Q., and J.A. Kong, "Transient Analysis of Single and Coupled Lines with Capacitively-Loaded Junctions," *IEEE Trans. Microwave Theory Tech.* MTT-34 (9):952 (1986).

Habashy, T.M., J.A. Kong, and W.C. Chew, "Resonance and Radiation of the Elliptic Disk Microstrip Structure, Part I: Formulation," *IEEE Trans. Antennas Propag.* AP-35:877 (1987).

Kiang, J.F., J.A. Kong, and D.A. Shnidman, "Comparison of Algorithms to Solve Sparse Matrix in EM Scattering Problem," National Radio Science Meeting, Philadelphia, Pennsylvania, June 9-13, 1986.

Poh, S.Y., and J. A. Kong, "Transient Response of a Vertical Electric Dipole on a Two-Layer Medium," *J. Electromag. Waves Appl.* 1 (2):135 (1987).

Poh, S.Y., J.A. Kong, M. Tsuk, "Transient Response of Dipole Antennas on Two-Layer Media," National Radio Science Meeting, Philadelphia, Pennsylvania, June 9-13, 1986.

Yang, Y.E., J.A. Kong, and Q. Gu, "Time Domain Perturbational Analysis of Nonuniformly Coupled Transmission Lines," *IEEE Trans. Microwave Theory Tech.* MTT-33 (11):1120 (1985).

27.2   Remote Sensing of Earth Terrain

Jin A. Kong, Robert T. Shin, Freeman C. Lin, Maurice Borgeaud

A systematic approach for the identification of terrain media such as vegetation canopy, forest, and snow-covered fields is developed using the optimum polarimetric classifier. The covariance matrices for the various terrain cover are computed from theoretical models of random medium by evaluating the full polarimetric scattering matrix elements. The optimal classification scheme makes use of a quadratic distance measure and is applied to classify a vegetation canopy consisting of both trees and grass. Experimentally measured data are used to validate the classification scheme. Theoretical probability of classification error using the full polarimetric matrix are compared with classification based on single features including the phase difference between the VV and HH polarization returns. It is shown that the full polarimetric results are optimal and provide better classification performance than single feature measurements.

We modeled earth terrain covers as random media characterized by different dielectric constants and correlation functions. In order to model sea ice with brine inclusions and vegetation with row structures, the random medium is assumed to be anisotropic. A three-layer model will be used to simulate a vegetation field or a snow-covered ice field with the top layer being snow or leaves, the middle layer being ice or trunks, and the bottom layer being sea water or ground.

The strong fluctuation theory with the distorted Born approximation is applied to the solution of the radar backscattering coefficients. In order to take into account the polarimetric information, we relate the backscattered Stokes vector to the incident Stokes vector by the Mueller matrix, which completely describes the scattering (in amplitude, phase, frequency, and polarization) from the three-layer anisotropic random medium. The Mueller matrix properties, as well as the covariance matrix issues, relevant to the radar backscattering will be examined. It is shown that for an isotropic medium, eight of the 16 elements of the Mueller matrix are identically zero. However, the tilted anisotropic permittivity of the middle layer (sea ice or trunks) generates a full nonzero Mueller matrix.

The Mueller matrix and polarization covariance matrix are studied for polarimetric radar systems. The clutter is modeled by a layer of random permittivity, described by a three-dimensional correlation function, with variance, and horizontal and vertical correlation lengths. This model is applied, using the wave theory with Born approximations carried to the second order, to find the backscattering elements of the polarimetric matrices. It is found that eight out of 16 elements of the Mueller matrix are identically zero, corresponding to a covariance matrix with four zero elements. Theoretical predictions are matched with experimental data for vegetation fields.

We have used the strong fluctuation theory to derive the backscattering cross sections. The study of the strong fluctuation theory for a bounded layer of random discrete scatterers is further extended to include higher order co-polarized and cross-polarized second moments. The backscattering cross sections per unit area are calculated by including the mutual coherence of the fields due to the coincidental ray paths and that due to the opposite ray paths which are corresponding to the ladder and cross terms in the Feynman diagrammatic representation. It is proved that the contributions from ladder and cross terms for co-polarized backscattering cross sections are the same, while the contributions for the cross-polarized ones are of the same order. The bistatic scattering coefficients in the second-order approximation for both the ladder and cross terms are also obtained. The enhancement in the backscattering direction can be attributed to the contributions from the cross terms.

A two-layer anisotropic random medium model is developed for the active and passive microwave remote sensing of ice fields. The dyadic Green's function for this two-layer anisotropic medium is derived. With a specified correlation function for the randomness of the dielectric constant, the backscattering cross sections are calculated with the Born approximation. It is shown that the depolarization effects exist in the single-scattering process. Treating sea ice as a tilted uniaxial medium, the observed strong cross-polarized return in the bistatic scattering coefficients is successfully predicted from the theoretical model. It is also shown that the backscattering cross section of horizontal polarization can be greater than that of vertical polarization even in the half-space case. The principle of reciprocity and the principle of energy conservation are invoked to calculate the brightness temperatures. The bistatic scattering coefficients are first calculated and then integrated over the upper hemisphere to be subtracted from unity, in order to obtain the emissivity for the random medium layer. It is shown that both the absorptive and randomly fluctuating properties of the anisotropic medium affect the behavior of the resulting brightness temperatures both in theory and in actual controlled field measurements. The active and passive results match favorably well with the experimental data obtained from the first-year and the multiyear sea ice as well as from the corn stalks with detailed ground-truth information.

The Feynman diagrammatic technique is used to derive the Dyson equation for the mean field and the Bethe-Salpeter equation for the correlation or the covariance of the field for electromagnetic wave propagation and scattering in an anisotropic random medium. With the random permittivity expressed in a general form, the bilocal and the nonlinear approximations are employed to solve the Dyson equation and the ladder approximation to the Bethe-Salpeter equation. The mean dyadic Green's function for a two-layer anisotropic random medium with arbitrary three-dimensional correlation functions has been investigated with the zeroth-order solutions to the Dyson equation under the nonlinear approximation. The effective propagation constants are calculated for the four characteristic waves associated with the coherent vector fields propagating

in an anisotropic random medium layer, which are the ordinary and extraordinary waves with upward and downward propagating vectors.

A three-layer random medium model is adopted to study the volume scattering effects for the active and passive microwave remote sensing of snow-covered ice fields. We simulate the snow layer by an isotropic random medium and the ice layer by an anisotropic random medium. In snow, the fluctuation of the permittivity and the physical sizes of the granular ice particles are characterized by the variance and two correlation lengths. In ice, the anisotropic effect is attributed to the elongated structures and the specific orientations of the air bubbles, the brine inclusions, and other inhomogeneities. Two variances are required to characterize the fluctuations of the permittivities along or perpendicular to the tilted optic axis. The physical sizes of those scattering elements are also described by two correlation lengths.

The vegetation canopy and snow-covered ice field have been studied with a three-layer model, an isotropic random medium layer overlying an anisotropic random medium. We have calculated the dyadic Green's functions of the three-layer medium and the scattered electromagnetic intensities with Born approximation. The backscattering cross sections are evaluated for active microwave remote sensing. The theoretical approach can be extended to derive the bistatic scattering coefficients. After integrating the bistatic scattering coefficients over the upper hemisphere and substracting from unity, we can also compute the radiometric brightness temperatures for passive microwave remote sensing by invoking the principle of reciprocity.

Publications

Borgeaud, M., R.T. Shin, and J.A. Kong, "Theoretical Models for Polarimetric Radar Clutter," *J. Electromag. Waves Appl.* 1 (1):73 (1987).

Borgeaud, M., J.A. Kong, and F.C. Lin, *Microwave Remote Sensing of Snow-Covered Sea Ice*, 1986 International Geoscience and Remote Sensing Symposium, Zurich, Switzerland, September 8-11, 1986.

Borgeaud, M., J.A. Kong, and R.T. Shin, "Polarimetric Radar Clutter Modeling with a Two-Layered Anisotropic Random Medium," International Union of Radio Science Commission F Open Symposium, University of New Hampshire, Durham, New Hampshire, July 28-August 1, 1986.

Borgeaud, M., R.T. Shin, and J.A. Kong, "Theoretical Modeling of Polarimetric Radar Clutter," National Radio Science Meeting, Philadelphia, Pennsylvania, June 9-13, 1986.

Kong, J.A., *Electromagnetic Wave Theory.* New York: Wiley-Interscience, 1986.

Lee, J.K., and J.A. Kong, "Modified Radiative Transfer Theory for a Two-Layer Anisotropic Random Medium," National Radio Science Meeting, Philadelphia, Pennsylvania, June 9-13, 1986.

Lee, C., and R.T. Shin, "Radar Cross Section Prediction Using a Hybrid Method," National Radio Science Meeting, Philadelphia, Pennsylvania, June 9-13, 1986.

Lin, F.C., and J.A. Kong, "Remote Sensing of Snow-Covered Sea Ice," International Union of Radio Science Commission F Open Symposium, University of New Hampshire, Durham, New Hampshire, July 28-August 1, 1986.

Lin, F.C., J.A. Kong, R.T. Shin, and Y.E. Yang, "Backscattering and Propagation of Radar Pulses in Earth Terrain Media," IEEE IMTC/86 Meeting, Boulder, Colorado, March 24-27, 1986.

Nghiem, S., M.C. Lee, and J.A. Kong, "Nonlinear EM Wave Interactions with the Neutral Atmosphere," International Union of Radio Science Commission F Open Symposium, University of New Hampshire, Durham, New Hampshire, July 28-August 1, 1986.

Rogers, S.W., and R.T. Shin, "Radar Cross Section Prediction for Coated Perfect Conductors with Arbitrary Geometries," National Radio Science Meeting, Philadelphia, Pennsylvania, June 9-13, 1986.

Sihvola, A., and J.A. Kong, "Effective Permittivity of Dielectric Mixtures," International Union of Radio Science Commission F Open Symposium, University of New Hampshire, Durham, New Hampshire, July 28-August 1, 1986.

27.3   Remote Sensing of Upper Atmosphere

Jin A. Kong, Robert T. Shin, Min C. Lee, Freeman C. Lin, Son V. Nghiem, Keith M. Groves, H.C. Han

Radio measurements of Total Electron Content (TEC) and optical detection of airglow variations show that large scale plasma patches appearing in the high latitude ionosphere have irregular structures, evidenced by the satellite phase and amplitude scintillations. Whistler waves, intense quasi-DC electric fields, atmospheric gravity waves, and electrojets are potential sources of various plasma instabilities. The role of thermal effects in generating ionospheric irregularities by these sources have been investigated. A model has been developed to explain the discrete spectrum of the resonant ULF waves that have been commonly observed in the magnetosphere. The resonant electron diffusion is suggested to be an effective saturation process of the auroral kilometric radiation. The calculated intensity of the saturated radiation has a significantly lower value in comparison with that caused by the quasi-linear diffusion process as an alternative saturation process.

Faraday Polarization Fluctuations (FPF) of transionospheric radio waves in the presence of random density irregularities have been studied. The irregularities are anisotropic and modeled by a correlation function containing different correlation lengths in the directions parallel and perpendicular to the Earth's magnetic field. Expression for the FPF variance is obtained under the underdense ionospheric plasma condition. The results show that the FPF variance depends on the ratio of the perpen-

dicular to the parallel correlation lengths and the anisotropic irregularity effect becomes more appreciable for the longitudinally propagating modes.

The ionospheric modification caused by an HF or MF heater wave can be enhanced with the subsequent illumination of the ionosphere by a powerful VLF wave. Let the HF or MF heater be operated in a pulse-wave mode to assure the excitation of short- rather than large-scale ionospheric density irregularities. These excited ionospheric density striations can effectively scatter the VLF wave into a lower hybrid wave via the nonlinear mode conversion provided that the scale lengths of ionospheric irregularities are much less than the wavelength of the VLF wave. For example, the wavelength of a VLF wave at the frequency of 10 kHz is of the order of 500 meters in the ionospheric F region. The preferential excitation of meter-scale ionospheric irregularities by the HF or MF heater wave can provide the subsequently injected VLF wave with a favorable condition for the nonlinear mode conversion. These density striations, in fact, can also be intensified by the powerful VLF wave via a plasma instability that can concomitantly generate lower hybrid waves. The ionosphere modified by the two heater waves is ex- pected to have intense lower hybrid waves and short-scale ionospheric density striations. These VLF wave-produced electrostatic waves can effectively heat the ionospheric plasma. Enhanced modification effects in, for instance, airglow and height distribution of plasma lines are expected. The proposed experiment can provide the controlled study of the spectral broadening effect of propagating VLF waves.

Nearly monochromatic signals at 13.6 kHz $\pm$ Hz injected from a ground-based VLF transmitter can experience a broadband expansion as high as 10% ($\sim$ 100 Hz) of the incident wave frequency as they traverse the ionosphere and reach satellite altitudes in the range of 600-3800 kilometers. We investigate two different source mechanisms that can potentially result in the observed spectral broadening of injected monochromatic VLF waves. One is the nonlinear scattering of VLF signals by induced ionospheric density fluctuations that renders the nonlinear mode conversion of VLF waves into lower hybrid waves. These quasi-electrostatic modes result when the injected VLF waves are scattered by ionospheric density fluctuations with scale lengths less than $0.7(c/f_p)(f_e/f_o)^{1/2}$ where c, f_p, f_e, and f_o are the speed of light in vacuum, the plasma fre- quency, the electron cyclotron frequency, and the VLF wave frequency, respectively. A second mechanism involves the excitation of electrostatic waves (lower hybrid waves, low frequency quasi-modes) by the injected VLF waves. This process tends to produce a spectrally broadened transmitted pulse with peaks at a discrete set of frequencies on both sides of the nominal carrier frequency.

Publications

Borgeaud, M., J.A. Kong, and R.T. Shin, "Polarimetric Microwave Remote Sensing of Anisotropic Earth Terrain with Strong Fluctuation Theory," IGARSS 87 and URSI Meeting, University of Michigan, Ann Arbor, Michigan, May 18-21, 1987.

Groves, K.M., M.C. Lee, and S.P. Kuo, "Mechanisms Leading to the Spectral Broaden- ing of Transmitted VLF Signals," *Proceedings of Ionospheric Effect Symposium*, May 1987.

Kuo, S.P., and M.C. Lee, "Parametric Excitation of Whistler Waves by HF Heater," *Proceedings of the International Symposium on Modification of the Ionosphere by Powerful Radio Waves*, 109, Suzdal/Moscow, U.S.S.R., September 9-12, 1986.

Kuo, S.P., and M.C. Lee, "Stimulated Backscattering of Lower Hybrid Waves," *Phys. Fluids* 29 (4):1024 (1986).

Lee, M.C., J.A. Kong, and S.P. Kuo, "On the Resonant Ionospheric Heating at the Electron Gyrofrequency," *Proceedings of the International Symposium on Modification of the Ionosphere by Powerful Radio Waves,* 111, Suzdal/Moscow, U.S.S.R., September 9-12, 1986.

Lee, M.C., K.M. Groves, H.C. Han, J.A. Kong, S.P. Kuo, and H.C. Carlson, Jr., "Ionospheric Modifications by Two Heater Waves," *Proceeding of Ionospheric Effect Symposium,* May 1987.

Lee, M.C., J.A. Kong, and S. P. Kuo, "Enhanced Ionospheric Modifications by the Combined Operation of HF and VLF Heaters," *Proceedings of the International Symposium on Modification of the Ionosphere by Powerful Radio Waves,* 146, Suzdal/Moscow, U.S.S.R., September 9-12, 1986.

Lin, F.C., J.A. Kong, and R.T. Shin, "Theoretical Models for Active and Passive Microwave Remote Sensing of Snow-Covered Sea Ice," IGARSS 87 and URSI Meeting, University of Michigan, Ann Arbor, Michigan, May 18-21, 1987.

Nghiem, S.V., J. Murad, and M.C. Lee, "On the Faraday Rotation Fluctuations of Radio Waves," *Proceedings of Ionospheric Effect Symposium,* May 1987.

27.4 Remote Sensing of Sea Ice

Jin A. Kong, Robert T. Shin, Freeman C. Lin, Maurice Borgeaud

We have studied the volume scattering effects of snow-covered sea ice with a three-layer random medium model for microwave remote sensing. The strong fluctuation theory and the bilocal approximation are applied to calculate the effective permittivities for snow and sea ice. The wave scattering theory in conjunction with the distorted Born approximation is then used to compute bistatic coefficients and backscattering cross sections. Theoretical results are illustrated by matching experimental data for dry snow-covered thick first-year sea ice at Point Barrow. The radar backscattering cross sections are seen to increase with snow cover for snow-covered sea ice, due to the increased scattering effects in the snow layer. The results derived can also be applied to the passive remote sensing by calculating the emissivity from the bistatic scattering coefficients.

We have also derived a general mixing formula for discrete scatterers immersed in a host medium. The inclusion particles are assumed to be ellipsoidal. The electric field inside the scatterers is determined by quasistatic analysis, assuming the diameter of the inclusion particles to be much smaller than the wavelength. The results are applicable to general multiphase mixtures, and the scattering ellipsoids of the different phases can have different sizes and arbitrary ellipticity distribution and axis orientation, i.e., the mixture may be isotropic or anisotropic. The resulting mixing formula is nonlinear and

implicit for the effective complex dielectric constant, because the approach in calculating the internal field of scatterers is self-consistent. Still, the form is especially suitable for iterative solution. The formula contains a quantity called the apparent permittivity, and with different choices of this quantity, the result leads to the generalized Lorentz-Lorenz formula, the generalized Polder-van Santen formula, and the generalized coherent potential - quasicrystalline approximation formula. Finally, the results are applied to calculating the complex effective permittivity of snow and sea ice.

We have derived the dyadic Green's function for a two-layer anisotropic medium. The Born approximation is used to calculate the scattered fields. With a specified correlation function for the randomness of the dielectric constant, the backscattering cross sections are evaluated. The analytic expressions for backscattering coefficients are shown to include depolarization effects in the single-scattering approximation. It is also shown that the backscattering cross section (per unit area) of horizontal polarization can be greater than that of vertical polarization even in the case of half-space. The bistatic scattering coefficients are first calculated and then integrated over the upper hemisphere to be subtracted from unity, in order to obtain the emissivity. The principle of reciprocity is then invoked to calculate the brightness temperatures. It is shown that both the absorptive and randomly fluctuating properties of the anisotropic medium affect the behavior of the resulting brightness temperatures both in theory and in actual controlled field measurements. The active and passive results are favorably matched with the experimental data obtained from the first-year and the multiyear sea ice.

Electromagnetic wave propagation and scattering in an anisotropic random medium has been examined with Dyson equation for the mean field which is solved by bilocal and nonlinear approximations and with Bethe-Salpeter equation for the correlation of field was derived and solved by ladder approximation. The effective propagation constants are calculated for the four characteristic waves associated with the coherent vector fields propagating in an anisotropic random medium layer, which are the ordinary and extraordinary waves with upward and downward propagating vectors. The z-component of the effective propagation constant of the upward propagating wave is different from the negative of that of the downward propagating wave, not only for the extraordinary wave but also for the ordinary wave. This is due to the tilting of the optic axis which destroyes the azimuthal symmetry.

Since both snow and ice exhibit volume scattering effects, we model the snow-covered ice fields by a three-layer random medium model with an isotropic layer to simulate snow, an anisotropic layer to simulate ice, and the bottom one being ground or water. The snow and ice are characterized by different dielectric constants and correlation functions. The theoretical results are illustrated for thick first-year sea ice covered by dry snow at Point Barrow and for artificial thin first-year sea ice covered by wet snow at CRREL. The radar backscattering cross sections are seen to increase with snow cover for snow-covered sea ice, because snow gives more scattering than ice. The results are also used to interpret experimental data obtained from field measurements.

Publications

Borgeaud, M., J.A. Kong, and R.T. Shin, "Polarimetric Microwave Remote Sensing of Anisotropic Earth Terrain with Strong Fluctuation Theory," IGARSS 87 and URSI Meeting, University of Michigan, Ann Arbor, Michigan, May 18-21, 1987.

Borgeaud, M., R.T. Shin, and J.A. Kong, "Theoretical Models for Polarimetric Radar Clutter," *J. Electromag. Waves Appl.* 1 (1):73 (1987).

Borgeaud, M., J.A. Kong, and F.C. Lin, "Microwave Remote Sensing of Snow-Covered Sea Ice," 1986 International Geoscience and Remote Sensing Symposium, Zurich, Switzerland, 8-11, September 1986.

Borgeaud, M., J.A. Kong, and R.T. Shin, "Polarimetric Radar Clutter Modeling with a Two-Layered Anisotropic Random Medium," International Union of Radio Science Commission F Open Symposium, University of New Hampshire, Durham, New Hampshire, July 28-August 1, 1986.

Kong, J.A., A.A. Swartz, H.A. Yueh, L.M. Novak, and R.T. Shin, "Identification of Terrain Cover Using the Optimum Polarimetric Classifier," *J. Electromag. Waves Appl.* 1 (4): (1987).

Kong, J.A., *Electromagnetic Wave Theory.* New York: Wiley-Interscience, 1986.

Lee, J.K., and J.A. Kong, "Modified Radiative Transfer Theory for a Two-Layer Anisotropic Random Medium," National Radio Science Meeting, Philadelphia, Pennsylvania, June 9-13, 1986.

Lin, F.C., J.A. Kong, and R.T. Shin, "Theoretical Models for Active and Passive Microwave Remote Sensing of Snow-Covered Sea Ice," IGARSS 87 and URSI Meeting, University of Michigan, Ann Arbor, Michigan, May 18-21, 1987.

Lin, F.C., and J.A. Kong, "Remote Sensing of Snow-Covered Sea Ice," International Union of Radio Science Commission F Open Symposium, University of New Hampshire, Durham, New Hampshire, July 28-August 1, 1986.

Sihvola, A., and J.A. Kong, "Effective Permittivity of Dielectric Mixtures," International Union of Radio Science Commission F Open Symposium, University of New Hampshire, Durham, New Hampshire, July 28-August 1, 1986.

27.5 SAR Image Interpretaion and Simulation

Jin A. Kong, Freeman C. Lin, Robert T. Shin, Al Schwartz, Herng A. Yueh

Using the random medium model, synthetic aperture radar (SAR) simulations can now be generated based on ground truth data from a given terrain site. We first match the various elements within the data to the physical parameters previously discussed, which are compiled in a database generated from correlation function studies. Based on these physical terrain parameters, we next use the random medium model to predict the radar backscatter from the various terrain elements in order to generate a range cross-range terrain profile. We have taken into account the change of incident angle

along the ground swath as well as the terrain local incident angle, when the terrain backscatter is computed. Finally the effects of fading (i.e., speckle) are incorporated into the simulated imagery. Utilizing this procedure, we are able to simulate the radar measurements which would have been actually recorded had this terrain been imaged by an airborne SAR. There simulations are fully polarimetric. The advantage to terrain simulation using the random medium model is that, in general, most airborne radars operate at either a single frequency, of over some relatively small bandwidth. However, the random medium model allows us to generate simulations of the same terrain for a variety of operating frequencies. In light of this fact, we see that terrain simulation based on the random medium model is an extremely useful tool.

Development of high resolution and autocorrelation range profile algorithms, which are a special case of the above mentioned terrain simulation, has continued. Modification to the algorithms, discussed in previous reports, were detailed at SIMTECH. The primary modification altered the way in which the terrain was sectioned into high resolution range bins. Formerly these bins were evenly spaced on a flat terrain, however, spacing was not uniform when terrain elevation information was added. The new methodology takes this effect into account. Now the terrain scattering elements, located in each range bin are evenly separated both in the case of a flat terrain and for regions in which ground elevation occurs. Since most terrain regions are not uniformly flat, this new algorithm for partitioning the terrain represents an improvement over the previous model.

We have developed a data processing algorithm which produces maximum contrast between two scattering classes, each represented by its respective covariance matrix. We will derive an optimal linear decision vector or decision functional which maximizes the contrast or expected power return ratio between the two scattering classes. The suboptimal case of a fixed transmit polarization will also be considered. The maximization procedure involves solving an eigenvalue problem in which the eigenvector yielding this maxima will correspond to the decision functional we seek. To demonstrate the physical significance of the linear weighting decision vector, we transform it into its associated transmit and receive polarization state, in terms of horizontal and vertical vector components. This technique is then applied to radar imagery to enhancement contrast between different classes within a given database.

The scattering of electromagnetic waves from a randomly perturbed periodic surface is solved using the Extended Boundary Condition (EBC) method. The scattering from periodic surface is solved exactly using the EBC method and this solution is used in the small perturbation method to solve for the scattered field from a randomly perturbed periodic surface. The random perturbation is modeled as a Gaussian random process and the surface currents and the scattered fields are expanded and solved up to the second order. The theoretical results are illustrated by calculating the bistatic and backscattering coefficients. It is shown that as the correlation length of the random roughness increases, the bistatic scattering pattern of the scattered fields show several beams associated with each Bragg diffraction direction of the periodic surface. When the correlation length becomes smaller, then the shape of the beams become broader. The results obtained using the EBC method is also compared with the results obtained using the Kirchhoff approximation. It is shown that the Kirchhoff approximation results show quite a good agreement with EBC method results for the VV and HH polarized backscattering coefficients for small angles of incidences. However, the Kirchhoff approximation does not give depolarized returns in the backscattering direction whereas

the results obtained using the EBC method give significant depolarized returns when the incident direction is not perpendicular to the row direction of the periodic surface.

Polarimetric radar backscatter data have been used extensively to classify terrain cover. Since it is difficult to calibrate out the effects of amplitude and phase errors induced by atmospheric effects, path loss, etc., absolute amplitude and phase of radar returns are not reliable features for terrain classification purposes. The use of normalized polarimetric data is proposed so that only the relative magnitudes and phases will be utilized to discriminate different terrain elements. It is shown that the Bayes classification error does not depend on the form of the normalization function if the unknown radar system calibration factor is modeled as a multiplicative term in the received signal. This holds true for arbitrary probabilistic distributed polarizations. Assuming a multivariate Gaussian distribution for the un-normalized polarimetric data, the probability density function (PDF) of the normalized data and the corresponding Bayes classifier distance measure for the normalized data are derived. Furthermore, by assuming a specific form of the covariance matrix for the polarimetric data, exact PDFs are given for HH, HV, VV and span type normalization schemes. Corresponding classification errors are evaluated to verify their independence from all normalization functions.

We have studied the Mueller matrix and polarization covariance matrix for polarimetric radar systems. The clutter is modeled by a layer of random permittivity, described by a three-dimensional correlation function, with variance, and horizontal and vertical correlation lengths. This model is applied, using the wave theory with Born approximations carried to the second order, to find the backscattering elements of the polarimetric matrices. It is found that eight out of 16 elements of the Mueller matrix are identically zero, corresponding to a covariance matrix with four zero elements. Theoretical predictions are matched with experimental data for vegetation fields.

Publications

Borgeaud, M., J.A. Kong, and R.T. Shin, "Polarimetric Radar Clutter Modeling with a Two-Layered Anisotropic Random Medium," International Union of Radio Science Commission F Open Symposium, University of New Hampshire, Durham, New Hampshire, July 28-August 1, 1986.

Borgeaud, M., J.A. Kong, and R.T. Shin, "Polarimetric Microwave Remote Sensing of Anisotropic Earth Terrain with Strong Fluctuation Theory," IGARSS 87 and URSI Meeting, University of Michigan, Ann Arbor, Michigan, May 18-21, 1987.

Borgeaud, M., R.T. Shin, and J.A. Kong, "Theoretical Models for Polarimetric Radar Clutter," *J. Electromag. Waves Appl.* 1 (1):73 (1987).

Borgeaud, M., J.A. Kong, and F.C. Lin, "Microwave Remote Sensing of Snow-Covered Sea Ice," 1986 International Geoscience and Remote Sensing Symposium, Zurich, Switzerland, 8-11, September 1986.

Borgeaud, M., R.T. Shin, and J.A. Kong, "Theoretical Modeling of Polarimetric Radar Clutter," National Radio Science Meeting, Philadelphia, Pennsylvania, June 9-13, 1986.

Chen, C.F., and G. Freeman, "A New Formula for Partial Fraction Expansion of a Transfer Matrix," *Comp. Maths. with Appls.* 12A (9):963 (1986).

Kong, J.A., *Electromagnetic Wave Theory.* New York: Wiley-Interscience, 1986.

Kuo, S.P., and M.C. Lee, "Parametric Excitation of Whistler Waves by HF Heater," *Proceedings of the International Symposium on Modification of the Ionosphere by Powerful Radio Waves,* 109, Suzdal/Moscow, U.S.S.R., September 9-12, 1986.

Kuo, S.P., and M.C. Lee, "Stimulated Backscattering of Lower Hybrid Waves," *Phys. Fluids* 29 (4):1024 (1986).

Lee, C., and R.T. Shin, "Radar Cross Section Prediction Using a Hybrid Method," National Radio Science Meeting, Philadelphia, Pennsylvania, June 9-13, 1986.

Lee, C., and R.T. Shin, "Radar Cross Section Prediction Using a Hybrid Method," National Radio Science Meeting, Philadelphia, Pennsylvania, June 9-13, 1986.

Lee, J.K. and J.A. Kong, "Modified Radiative Transfer Theory for a Two-Layer Anisotropic Random Medium," National Radio Science Meeting, Philadelphia, Pennsylvania, June 9-13, 1986.

Lee, M.C., J.A. Kong, and S.P. Kuo, "On the Resonant Ionospheric Heating at the Electron Gyrofrequency," *Proceedings of the International Symposium on Modification of the Ionosphere by Powerful Radio Waves,* 111, Suzdal/Moscow, U.S.S.R., September 9-12, 1986.

Lee, M.C., J.A. Kong, and S.P. Kuo, "Enhanced Ionospheric Modifications by the Combined Operation of HF and VLF Heaters," *Proceedings of the International Symposium on Modification of the Ionosphere by Powerful Radio Waves,* 146, Suzdal/Moscow, U.S.S.R., September 9-12, 1986.

Lee, M.C., and S.P. Kuo, "Resonant Electron Diffusion as a Saturation Process of the Synchrotron Maser Instability," *J. Plasma Phys.* 35 part 1:177 (1986).

Lin, F.C., J.A. Kong, and R.T. Shin, "Theoretical Models for Active and Passive Microwave Remote Sensing of Snow-Covered Sea Ice," IGARSS 87 and URSI Meeting, University of Michigan, Ann Arbor, Michigan, May 18-21, 1987.

Lin, F.C., and J.A. Kong, "Remote Sensing of Snow-Covered Sea Ice," International Union of Radio Science Commission F Open Symposium, University of New Hampshire, Durham, New Hampshire, July 28-August 1, 1986.

Lin, F.C., J.A. Kong, R.T. Shin, and Y.E. Yang, "Backscattering and Propagation of Radar Pulses in Earth Terrain Media," IEEE IMTC/86 Meeting, Boulder, Colorado, March 24-27, 1986.

Rogers, S.W., and R.T. Shin, "Radar Cross Section Prediction for Coated Perfect Conductors with Arbitrary Geometries," National Radio Science Meeting, Philadelphia, Pennsylvania, June 9-13, 1986.

Rogers, S.W., and R.T. Shin, "Radar Cross Section Prediction for Coated Perfect Conductors with Arbitrary Geometries," National Radio Science Meeting, Philadelphia, Pennsylvania, June 9-13, 1986.

Tsang, L., J.A. Kong, and R.T. Shin, *Theory of Microwave Remote Sensing.* New York: Wiley-Interscience, 1985.

Left to right: Research Assistant Maurice Borgeaud, Visiting Scientist Qizheng Gu, Secretary Young-Mi Kim, Research Assistant Check-Fu Lee, and Visiting Scientist Zhuzhen Li

28.0   Microwave and Quantum Magnetics

Academic and Research Staff

Prof. F.R. Morgenthaler

Graduate Student

C.M. Rappaport

28.1   Microwave Hyperthermia

Frederic R. Morgenthaler, Carey M. Rappaport

Our understanding of both physics and physiology is challenged in trying to optimize techniques for heat production and for the thermometry associated with Hyperthermia modalities used in connection with cancer therapy. Fundamental considerations are based on designing proper microwave applicators which must be able to handle the microwave power required to raise the temperature of the tumor. They must also minimize the amounts of microwave power being delivered to the healthy tissue or being radiated into free space.

The Ph.D. dissertation research of Carey Rappaport has been completed. The abstract, table of contents and conclusions are reproduced below:

28.2   Synthesis of Optimum Microwave Antenna Applicators for Use in Treating Deep Localized Tumors

Carey M. Rappaport

Submitted to the Department of Electrical Engineering and Computer Science on May 26, 1987 in partial fulfillment of the requirements for the Degree of Doctor of Philosophy.

28.2.1   Abstract

The optimal electromagnetic source distributions for depositing power at depth in biological tissue are derived and analyzed. The fundamental microwave penetration limits, against which all other applicator performance can be measured, is determined.

Focussed power patterns are computed for planar, circular cylindrical and spherical source geometries, which have as much or greater power at a centrally located tumor as in the surrounding normal tissue. Focussing is shown to increase the planar pene-

tration depth by a factor of three over a uniform source. Analysis of performance as a function of frequency shows that for smaller body parts, 915 MHz maximizes penetration without sacrificing power pattern peak resolution.

A leaky-wave antenna, the troughguide, is introduced as a flexible applicator with built-in power monitoring lines, amplitude control, and a continuous aperture with supports a distribution that is unaffected by tissue loading variations. An artificial dielectric composed of conducting spheres imbedded in boron nitride is used to match to tissue while providing surface cooling. Experiments were performed on a troughguide in conjunction with the artificial dielectric at 915 MHz radiating into simulated biological tissue. Power and temperature contours which show a localized power maximum are presented.

28.2.2 Table of Contents

Appendix H: Program Description and Listing, "CMRGL"

Appendix I: Derivation of Snell's Law for Lossy Media

Appendix J: Derivation of Impedance Matching Layer Equations

Appendix K: Program Description and Listing, "CONGEN/CONTR"

References

28.3 Microwave Ferrites

Frederic R. Morgenthaler

The February 1988 issue of the IEEE Proceedings will be devoted, in part, to the subject of microwave ferrites. A review paper by F.R. Morgenthaler titled "An Overview of Electromagnetic and Spin Angular Movement Mechanical Waves in Ferrite Media" will be included. The abstract, table of contents, introduction and summary are reproduced below:

28.3.1 Abstract

We review the principal characteristics of gyromagnetic materials that are useful for microwave applications and give both the large-and small-signal models that govern wave propagation at microwave frequencies. Uniform and nonuniform plane waves in a unbounded ferrite medium are considered form the complementary view points of electromagnetics and mechanics.

Both electromagnetic ($\overline{E}X\overline{H}$) and quantum-mechanical exchange channels of power exist in such materials which can be ascribed to either waves or quasiparticles.

Regimes of wave propagation that are magnetostatic in character are shown to exist, as well as the relationships between the Walker modes of a small spheroid and the magnetostatic waves propagation in thin films.

When the power densities within these waves or modes exceeds certain thresholds, the linear model breaks down and parametric instabilities can create a form of "magnetic turbulence." We review the thresholds of such for both first - and second-order processes that involve the uniform precession mode and "parallel-pumping" process that do not.

28.3.2 Table of Contents

1. Introduction

2. Large-Signal Model of a Magnetized Ferrite

3. Small-Signal (Linearized) Model

28.3.3   Introduction

The desired characteristics of a magnetic material for use at microwave frequencies are:

1.   <u>Magnetic Order.</u> A relatively high density of magnetic ions is necessary in order that the magnetic interactions be large. Strong nearest neighbor coupling leads to spontaneous magnetization below some critical temperature, T_c , which should be high enough for practical applications.

2. <u>Very high resistiveity.</u> A large skin depth is required to allow penetration of electromagnetic energy inside the sample, where the $\bar{h}$ field can interact with the magnetic moments.

3. <u>Low magnetic loss.</u> To reduce magnetic resonance damping, the magnetic ions should be weakly coupled to the lattice, therefore spin-orbit coupling effects should be small. For a given material, losses also depend upon the configuration of the magnetization and can be minimized by applying a large enough external dc magnetic field to remove all domain walls (and hence all wall resonances). It is desirable that the material saturate in a reasonable field.

4. <u>Low elastic loss.</u> This is important for microwave acoustic applications, but can be ignored otherwise.

Fortunately, a number of actual materials combine these properties and belong to the class termed ferrimagnetic.[1] These materials commonly called ferrites are oxides of the ferromagnetic metals which may also contain ions of one or more nonmagnetic atoms.[1] Examples are Fe_3O_4 (magnetite), $BaFe_2O_4$, $MnFe_2O_4$, $CoFe_2O_4$, and $Y_3Fe_5O_{12}$ (yttrium iron garnet). The first of these (also known as lodestone) was the first magnetic material discovered by man but is of limited importance for microwave applications because it suffers from a fairly low resistivity. The last (commonly abbreviated YIG) is of great practical importance because of its unusually low magnetic and elastic losses.

Ferrites are available in polycrystalline ceramic and single crystal forms. The former are much used in the fabrication of nonreciprocal microwave devices that operate with material wavelengths very much larger than the crystallite grain size, the latter are required for short wavelength magnetostatic wave devices and/or microwave acoustic applications because wave scattering at grain boundaries is undesirable, because it creates high attenuation.

In this review paper, we develop both large-signal and small-signal models of a rigid ferrimagnetic material that is magnetized to saturation by an external dc magnetic field. Magnetic anisotropy, quantum-mechanical exchange, and dissipation effects are included. For the linear model, and for steady-state wave propagation at frequency ω , two complementary view points are developed. In the first, and most common, the ferrite material is "black-boxed" to yield the Polder magnetic susceptibility tensor; that constitutive law is then combined with Maxwell's Equations. The primary emphasis in on the small-signal electric and magnetic fields, $\bar{e}$ and $\bar{h}$ and the waves are considered electromagnetic in character. In the second, it is Maxwell's Equations that are "black-boxed" to yield $\bar{e}$ and $\bar{h}$ in terms of the small-signal magnetization $\bar{m}$. The primary emphasis is on the small-signal angular momentum vector associated with $\bar{m}$ and the waves are considered as mechanical in character. Naturally, both view points lead to the same final result of waves that, in general, have both electromagnetic and mechanical characteristics; when a particular character predominates the corresponding view point is especially helpful.

---

[1] Some authors prefer to reserve the term "ferrite" for a particular subclass of magnetic oxides, nameley $MeOFe_2O_3$ (where Me is any divalent metal ion). We make no such distinction here.

Coupling between mechanical and electromagnetic components of the wave exists because, at an atomic level, electrons that carry angular momentum also carry a magnetic moment. When the magnetic moments in a solid are parallel to one another, organized angular momentum also exists and is the basis of magnetic resonance effects in ferrites.

Because a precessing mechanical top (and thus angular momentum waves) are inherently nonreciprocal, so too are associated electromagnetic waves when the mechanical component is sufficiently strong. This fact is the underlying reason why nonreciprocal ferrite devices[2] such as isolators, circulators and gyrators have proved to be possible.

After developing the linearized models, we review plane wave propagation in an unbounded ferrite medium and derive the dispersion relations between angualr frequency ω and the propagation wave vector. The fields of those portions of the spectrum where mechanical properties prediominate, are shown to satisfy the condition $\nabla \times \bar{h} \cong 0$; these so-called magnetostatic waves are discussed in detail. In contrast, when $\nabla \times \bar{h} \neq 0$, the waves are primarily electromagnetic in character.

In comparatively long wave length wave regions, where quantum-mechanical exchange effects are of negligible importance, wave power is associated with the $\bar{E} \times \bar{E}$ power flux and is governed by the normal Maxwellian boundary conditions on $\bar{E}$ and $\bar{H}$ when the wavelengths are sufficiently short, power is also carried by exchange mechanisms and additional boundary conditions are required.

Based upon the linearized-model, we formulate small-signal energy, power and stress, momentum conservation laws. An alternative interpretation to the wave description is given in terms of quasiparticles. At the macroscipic continuum level, the connection between photons, magnons and waves is provided by energy-momentum considerations. After the boundary conditions on both static and rf fields are considered, the magnetostatic modes of small spheroids are discussed with particular attention being given the family of modes that contain the uniform precession, or Kittel resonance. magnetostatic surface waves of a rectangular thin film are shown to be directly related to that family of modes; they provide and explanation of field-displacement modes; they provide an explanation of field-displacement nonreciprocity. Forward and backward volume waves propagating in such films are also reviewed.

Coupling between the linear modes of a saturated ferrite occurs because the total magnetization vector is conserved; this leads to nonlinear frequency mixing and parametric instabilities that cause a type of magnetic turbulence that can limit the amplitude of the linear response. Such indirect first-and second-order instabilities involve the linear susceptibilityu between an applied rf field and some mode (commonly the uniform precession) which nonlinearly pumps unstable spin waves. These processes are reviewed along with first-order "parallel-pumping" processes that directly couple an applied rf magnetic field to unstable spin waves or other magnetostatic modes. A particle interpretation of parametric instabilities, concludes this review of basic microwave resonance and propagation effects in ferrite media.

28.3.4 Summary

We have reviewed the underlying large-signal model of a rigid magnetically-saturated (single-domain) ferrite medium and used it to develop the linearized equations that govern the small-signal model. Uniform and non-uniform wave propagation in an infinite medium was derived from both electromagnetic and mechanical view points; the mechanical view points; the latter is especially useful for dealing with magnetostatic wave regimes.

Power-energy and momentum theorems revealed the connection between wave and quasi-particle representations.

Magnetostatic Walker modes in small ferrite ellipsoids were discussed with special attention given to the Kittel uniform precession mode.

Both volume and surface magnetostatic wave propagation in thin films were also considered.

Finally, high power effects cause by parametrically unstable spin wave were reviewed and a unified treatment of first and second-order thresholds and parallel pumping thresholds was presented.

Professor Frederic R. Morgenthaler and Dr. Carey M. Rappoport

29.0   Radio Astronomy

Academic and Research Staff

Prof. A.H. Barrett, Prof. B.F. Burke, Prof. J.W. Dreher, Prof D.H. Staelin, Dr. H.S. Malvar, Dr. P.W. Rosenkranz, Dr. M. Shao, J.W. Barrett

Visiting Scientists

Prof. S. Brofferio, Prof. D.H. Roberts, Prof. E. Turner

Graduate Students

P.C. Bonanni, C.L. Carilli, S.R. Conner, V. Dhawan, S.F. Filippone, A.J. Gasiewski, M.B. Heflin, B.E. Hines, E.J. Kim, C.C. Kuo, G.I. Langston, J. Lehar, J.C. Preisig, J.M. Shapiro, B.I. Szabo, G.W. Wornell, G.J. Zanciewicz

Undergraduate Students

W.R. Bayer, J.R. Bochinski, C-H. Lee, S. Cheung, S.S. Eikenberry, M.M. Hou, R.R. Krishnaiah, G. Long, R. Mason, M. Medard, E. Ordentlich, L. Renna, C. Torres Vila, K.A. Tuson

29.1   Galactic and Extragalatic Research

John H. Dreher, Bernard F. Burke, Christopher Carilli, Jacqueline Hewitt, Glen Langston, Michael Heflin, Samuel Connor, Vivek Dhawan

A striking new gravitational lens candidate, MG1131+0456, was discovered in the course of the gravitational lens search project being carried out jointly with Princeton and California Technical State University. The radio source has the appearance of a nearly perfect, slightly elliptical ring, with two compact sources superimposed, one slightly outside the ring, the other slightly inside the ring but diametrically opposed. There is an additional, much fainter, source farther out on one side. The structure is consistent with the lens being a massive elliptical galaxy, the object being a multiple radio source. One of the components is almost perfectly aligned with the galaxy and is imaged into an "Einstein Ring," an idealized structure predicted by Einstein long ago. An ideal point mass, acting as a lens, imaging a compact distant object, deflects the light around all sides, the result being a ring-like image. If the lens has a gravitational quadrupole moment, as an elliptical galaxy would have, the ring would take the observed elliptical form. The compact sources, just inside and just outside the ring, are also consistent with the lensing hypothesis. If the object, in addition to having a component lined up with the lens to give the ring, also has a slightly off-axis component, its principal image would lie on the inside of the ring and its secondary image would fall diametrically opposite, but inside the ring and this is what is observed. The faint outer image would be from a third component, and it might well lie in the single-

image domain, but its secondary image in any event would be faint and could easily go undetected. A report with J.N. Hewitt as first author has been submitted to *Nature*.

An extension of the MG survey has been completed with the 300-ft transit telescope of the NRAO at Green Bank, West Virginia, and served as the thesis for G. Langston. This covers the declination range 4.25 - 20.25 hours, covering 1.464 steradians and containing 5354 sources brighter than 41 mJy. Completeness and reliability were investigated closely, and above 80 mJy it was established that a single scan gives 95 ± 3% completeness, a performance that has seldom been achieved in other surveys. Related work by Langston revealed several individual sources with unusual structure, and these are being investigated further. A deep survey of the region 1146+111 was carried out with the VLA. There are two quasars in this region that have apparently equal redshifts, whose wide separation (2.6 arc-min) raised the possibility that a gravitational lens of extraordinary character - perhaps a cosmic string - was involved. The deep radio map, however, lends no support to that hypothesis.

29.2   Millimeter-Wave VLBI

Bernard F. Burke, Vivek Dhawan

The 7 mm VLBI project, to establish that VLBI at that wavelength was reducible to standard engineering practice, reached completion with the Ph.D. dissertation of V. Dhawan. In that work, carried out jointly with colleagues around the world, he showed that mapping of radio sources was feasible, but that a sufficiently large network of large radio telescopes, all having reasonable efficiency, must be employed. The atmospheric phase shifts do not present a fundamental barrier, but high standards of accurate calibration must be achieved at all stations. Precision of frequency standards and phase-stability of the local oscillator chain are prerequisites. In addition to mapping the active galaxy 3C84 with 90 microarc-sec resolution, a selection of 16 compact sources were observed, with 15 successful detections on transatlantic baselines. The extension of these observations should provide a network of calibrators for the VLB array now being constructed by the NRAO.

29.3   Orbiting VLBI

Bernard F. Burke, Samuel Connor, Michael Heflin, John W. Barrett

The QUASAT project is a study of the feasibility of extending the baselines of VLB interferometers into space. The work is in the Phase A study process within the European Space Agency, and is receiving support by NASA for the data acquisition, missions operations, orbital prediction and analysis, scientific studies, and data reduction phases. Professor Burke is chairman of the United States Science Working Group, coordinating with Doctor J.F. Jordan of the Jet Propulsion Laboratory, who is the study manager.

The experimental aspect of the study has used the TDRSS Satellite, a data relay satellite in geosynchronous orbit over the Atlantic Ocean, in conjunction with ground stations in Japan and Australia, to perform a successful experiment at 2.3 GHz, with baselines over two earth diameters in length. The work has been carried out jointly with the Jet Propulsion Laboratory and Haystack Radio Observatory. The next step will be to extend operations to 15 GHz. The short wavelength (2 cm) will give angular resolution of the order of 60 micoarc-seconds. The ground receivers, which are cooled HEMT amplifiers, are being built by RLE, following NRAO design, and are expected to have execeptionally good low-noise performance.

29.4 Studies of Planetary Systems of Other Stars

Bernard F. Burke

A preliminary study of the feasibilty of directly imaging planets in other solar systems has been carried out by Professor Burke, and a preliminary report was given at the 1987 International Astronautics Federation Congress at Brighton, England. The conclusion is positive: with sufficient care, the direct detection of an earth-like planet is feasible if it is orbiting a star within ten parsecs from the sun. The critical elements are: 1) the construction of an orbiting optical interferometer of the order of 20-30 meters maximum baseline; 2) the provision of phase-stable optics and correlators; 3) the development of low-sidelobe optics; and 4) the adaptation of radio VLBI methods to the optical domain.

In the above list, item (3), low-sidelobe optics, is the most challenging. Tapering the aperture illumination is essential, but the "noise sidelobes" generated by optical imperfection must be rigorously controlled. The conclusion was reached that the rms deviation of the wavefront imposed by optical imperfections should not exceed $\lambda/80$ over spatial frequencies extending from 1 cm to the full aperture of the optics. The main elements would be off-axis paraboloidal mirrors in the 1.5 - 2 cm range, and would thus have to be different from ordinary optical practice. There seem to be no fundamental technological barriers, however. The radio experience is directly applicable to the optical case, except for the limitation that amplification on heterodyne missions is infeasible because of quantum noise. Optical techniques exist, however, to provide the necessary cross-correlation capability.

29.5 Long-Baseline Astrometric Int rferometer

David H. Staelin, Michael Shao, John W. Barrett, Braden E. Hines, Edward J. Kim

During 1987 development of the Mark III optical astrometric interferometer continued at the Mount Wilson Observatory, and initial scientific results were obtained. Several manuscripts were prepared for publication.

Work began on the electronics for the laser siderostat subsystem. This system measures the positions of the siderostat mirrors relative to their associated concrete

pedestals. Four laser interferometers measure the distances between a large hemispherical mirror bonded to the siderostat mirror and four reference points tied to an invar assembly, which is attached to one of the steel reinforced concrete pedestals located at the ends of the various baselines. The hemispherical mirror, 6.8 inches in diameter, is mounted on the back of each main movable siderostat mirror such that the center of curvature of the mirrors is located withon several microns of the surface of the main mirror and close to the intersection of its azimuth an elevation axes. The four measurements are redundant so that the existence of fringe counting errors can be detected. Initial observations reveal that errors occur under rapid slewing at intervals of several minutes. Because that is too frequent to be useful, additional changes in operational procedures and system design are contemplated.

Operation of the interferometer in a photon-starved non-tracking mode appears to be feasible, and the necessary polychromatic fringe measurement system is being developed. It uses a dispersive prism which projects the spectrum across the face of the same photon camera used for star-tracking. Measurements of the relative flicker rates of different optical spectral bands permits the fringe visibility and fringe centers to be estimated. Special high-speed electronics which operate on photon addresses and arrival times are being developed for this purpose.

Papers were prepared describing the initial scientific results regarding stellar diameter measurements,[1] measured star positions,[2] the two-color method for astrometry,[3] a description of the Mark III interferometer,[4] atmospheric phase measurements,[5] and the earlier Mark II results.[6]

References

[1] M. Shao, M.M. Colavita, B.E. Hines, D.H. Staelin, D.J. Hutter, K.J. Johnston, D. Mozurkewich, R.S. Simon, J.L. Hershey, J.A. Hughes, and G.H. Kaplan, "Initial Stellar Diameter Measurements with the Mark III Interferometer," to appear in *Astrophys. J.*, April 15, 1988.

[2] D. Mozurkewich, D.J. Hutter, K.J. Johnston, R.S. Simon, M. Shao, M.M. Colavita, D.H. Staelin, B. Hines, J.L. Hershey, J.A. Hughes, and G.H. Kaplan, "Preliminary Measurements of Star Positions with the Mark III Stellar Interferometer," submitted to *Astrophys. J.*

[3] M.M. Colavita, M. Shao, and D.H. Staelin, "Two-Color Method of Optical Astrometry: Theory and Preliminary Measurements with the Mark III Stellar Interferometer," *Appl. Optics* 26:4113 (1987).

[4] M. Shao, M.M. Colavita, B.E. Hines, D.H. Staelin, D.J. Hutter, K.J. Johnston, D. Mozurkewich, R.S. Simon, J.L. Hershey, J.A. Hughes, and G.H. Kaplan, "The Mark III Stellar Interferometer," submitted to *Astron. Astrophys.* (1987).

[5] M.M. Colavita, M. Shao, and D.H. Staelin, "Atmospheric Phase Measurements with the Mark III Stellar Interferometer," *Appl. Optics* 26:4106 (1987).

[6] M. Shao, M.M. Colavita, D.H. Staelin, K.J. Johnston, R.S. Simon, J.A. Hughes, and J.L. Hershey, "Application of Interferometry to Optical Astrometry," *Astron. J.* 93:1280 (1987).

29.6 Tiros-N Satellite Microwave Sounder

SM Systems and Research, Inc.

Phillip W. Rosenkranz, David H. Staelin, Charlene C. Kuo

Four-channel passive microwave spectrometers (MSU) have been used operationally on the National Oceanic and Atmospheric Administration (NOAA) polar orbiting weather satellites since 1977. They will be superseded in the early 1990's by the Advanced Microwave Sounding Unit (AMSU) which has 15 channels that image the earth with 50-km resolution every 12 hours at frequencies distributed from 23 to 90 GHz, and an additional five channels that simultaneously image the earth with 15-km resolution at frequencies distributed from 90 to 183 GHz. This effort involves scientific support of the AMSU program, with emphasis on physics and retrieval methods.

A new approach to estimating the interference coneufficients between the separate 5-mm wavelength oxygen lines has been developed and used to improve expressions for the absorption coefficient of oxygen in air.[1] Additional studies of the transmittance of atmospheric oxygen in the stratosphere and mesosphere have also led to definition of an extension to AMSU that could usefully sound temperature profiles up to 70 km altitude.[2]

Earlier work on methods for sounding water vapor using the 183-GHz resonance foundered when temperature inversions or quasi-isothermal regions existed in the troposphere. A new approach to this problem has been developed. It involves an iterative combination of nonlinear physics with *a priori* statistics. This new method is much more robust in the presence of the intrinsic singularities associated with these retrievals. Improved theoretical expressions for pressure broadening of the rotational bands of water vapor from 300 to 1100 cm^{-1} were also developed.[3]

A conference was organized and held June 1-3, 1987, at Williamsburg, Virginia, to discuss AMSU and the extension of this technology to operational systems in geosynchronous orbit. Study of such geosychronous systems was begun and was documented for the proceedings of this NOAA-sponsored conference, to be published in 1988.

References

[1] P.W. Rosenkranz, "Interference Coefficients for Overlapping Oxygen Lines in Air," submitted to *J. Quant. Spectrosc. Radiat. Trans.*, (1987).

[2] P.W. Rosenkranz, and D.H. Staelin, "Polarized Thermal Microwave Emission from Oxygen in the Mesosphere," submitted to *Radio Astron.*, (1988).

[3] P.W. Rosenkranz, "Pressure Broadening of Rotational Bands. II. Water Vapor from 300 to 1100 cm^{-1}," *J. Chem. Phys.* 87:163 (1987).

29.7 High Resolution Passive Microwave Imaging of Atmospheric Structure

David H. Staelin, Philip W. Rosenkranz, John W. Barrett, Pierino G. Bonanni, Albin J. Gasiewski, Gregory J. Zanciewicz

Considerable progress was made in reducing and analyzing the data obtained during 1986 using the new imaging millimeter-wavelength temperature sounder (MTS). The eight-channel MTS operates near the 118-GHz resonance of oxygen. The cross-track scan sampled the atmosphere at 14 spots convering the region $\pm$ 45° from nadir with a 7.5° spot beamwidth. The MTS was flown on the NASA ER-2 aircraft near 65,000 ft for 14 missions during the experiments GALE (February 1986) and for 21 missions for the experiments COHMEX (June-July 1986). Research efforts have involved development of microwave scattering models for use in interpreting this data, a study of the apparent degrees of freedom in the radiance spectrum of clouds, the relative sensitivity of 53.6- and 118-GHz soundings to clouds and precipitation, and the accuracy of temperature profile retrievals obtained using the eight-channel MTS data.

29.8 Video Image Processing

David H. Staelin, Henrique S. Malvar, Sergio Brofferio, James C. Preisig, Jerome S. Shapiro, Bernard I. Szabo, Gregory W. Wornell, Shiufun Cheung, William I. Irving, Gordon M. Lum, Muriel Medard

This effort has involved the publication of prior research results, and continued work with motion estimation and coding techniques. A new method for fast computation of the discrete cosine transform and the discrete Hartley transfom[1] was published, as was scme of the work on the optimal FIR pre- and postfilters for decimation and interpolation of random signals,[2] which is particularly relevant to filter design for high-definition television systems.

The work on motion estimation has involved a comparative analysis of present methods for estimating local motion, and a more general method for optimally combining such local motion estimates to yield more accurate estimates of regional motion. Video coding work has involved a study of transform image coding with composite block source models, a method of coding where each type of block has its own optimal transform. Research continued on the use of pseudorandom noise in the quantization of random variables with nonuniform probability distributions. Small efforts were begun in character recognition of arbitrary fonts,[3,4] and the efficient recognition of the occurrence of widely separated scene repetitions in noisy television sequences.

References

[1] H.S. Malvar, "Fast Computation of the Discrete Cosine Transform and the Discrete Hartley Transform," *IEEE Trans. Acous., Speech, Signal Process.* ASSP-35:1484 (1987).

[2] H.S. Malvar and D.H. Staelin, "Optimal FIR Pre- and Postfilters for Decimation and Interpolation of Random Signals," *IEEE Trans. Commun.* 36:67 (1986).

[3] G.M. Lum, *An Open-Font Character Recognition System Using the Karhunen-Loeve Transform*, S.B. thesis, Dept. of Electr. Eng. and Comp. Sci., MIT, 1987.

[4] W.W. Irving, *Foundation of Open Font Character Recognition System*, S.B. thesis, Dept. of Electr. Eng. and Comp. Sci., MIT, (1987).

29.9   Nonthermal Radio Emission from the Jovian Planets

David H. Staelin, Tomas A. Arias, Roeland V. Hammerschlag, Stephen S. Eikenberry

The Planetary Radio Astronomy (PRA) experiment on the Voyager 1 and 2 spacecraft observed radio emission from Earth, Jupiter, Saturn, and Uranus in 198 channels distributed over the band from 1.2 KHz to 40.5 MHz. Study of the striated spectral activity (SSA) in Jovian and Saturnian radio emission has continued and has been submitted for publication.[1]

Theoretical studies of the Io-generated Alfven waves were continued. Obtaining a complete self-consistent wave/particle beam solution compatible with the launch geometry has proved elusive.

Reference

[1] J.R. Thieman, J.K. Alexander, D.H. Staelin, and T.A. Arias, "Modulated Spectral Activity (MSA) in Jovian and Saturnian Radio Emission," submitted to *J. Geophys. Res.*, 1987.

Professor Sylvia T. Ceyer

30.0 RLE Publications and Papers Presented

The first section of this bibliography includes papers presented at conferences and meetings by RLE faculty, staff and students during 1987, and is in chronological order by the month the conference was held. Reprints of papers may be obtained by contacting the authors directly.

Sections 30.2 and 30.3 are alphabetical listings by author of journal articles and letters to the editor that were published or accepted for publication. Chapters by RLE authors within books are given in Section 30.4. The last two sections of the bibliography list RLE technical reports and special publications.

30.1 Meeting Papers Presented

January 1987

Physics of Quantum Electronics Conference, Snowbird, Utah, January 3-7, 1987

Ippen, E.P., "Femtosecond Studies of Material and Devices."

169th Meeting of the American Astronomical Society, Pasadena, California, January 4-8, 1987

Abstracts in *Bull. Am. Astron. Soc.* 18(4) (1986):

Carilli, C.L., and J.H. van Gorkom, "Coincident 21 cm and Ca II Absorption Towards PKS2020-370," p. 969.

Dhawan, V., B. Burke, N. Bartel, I. Shapiro, A. Rogers, K. Johnston, J. Spencer, C. Lawrence, A. Readhead, D. Graham, I. Pauling-Toth, R. Booth, B. Rönnäng, and H. Hirabayashi, "VLBI at Seven-Millimeter Wavelength with 70 Marsec Resolution," p. 970.

Dreher, J.W., J. Lehar, D.H. Roberts, and A.G. deBruyn, "Rapid Time Variability of OJ 287 at Centimeter Wavelengths," p. 1046.

Jackson, J.M., W.J. Welch, and J.W. Dreher, "Identification of the Most Luminous Outflow Source in W49," p. 1029.

Langston, G.I., B.F. Burke, E.L. Turner, and C.R. Lawrence, "Faint Radio Sources in the Field of 1146+111 B, C: Tests Gravitational Lens Models," p. 9 50.

Roberts, D.H., J. Lehar, and J.W. Dreher, "Time Series Spectral Analysis with CLEAN," p. 945.

Shao, M., M.M. Colavita, B. Hines, D. Staelin, J. Hershey, J. Hughes, K. Johnston, D. Hutter, D. Mozurkevich, and R. Simon, "Preliminary Results from the Mark III Stellar Interferometer," p. 967.

Opto-Electronic Laser '87 and Electro-Optic Imaging Symposium, Los Angeles, California, January 11-16, 1987

Papers in *SPIE 751:*

Burke, B.F., "Aperture-Synthesis Interferometry at Optical Wavelengths," pp. 50-61.

National Radio Science Meeting, University of Colorado, Boulder, Colorado, January 12-15, 1987

Abstract in *Proceedings:*

Kuo, S.P., M.C. Lee, and F.T. Djuth, "New Interpretation of Plasma-Line Overshoot Phenomenon," p. 298.

Second Topical Meeting on Picosecond Electronics and Optoelectronics, Incline Village, Nevada, January 14-16, 1987

Brorson, S.D., J.G. Fujimoto, and E.P. Ippen, "Femtosecond Nonequilibrium Heat Transport in Thin Gold Films."

Colloquium on Energy, Polytechnic of Milan and University of Pavia, Voghera, Italy, January 17, 1987

Coppi, B., "Energy in the Universe."

February 1987

Midwinter Meeting of the Association for Research in Otolaryngology, Clearwater, Florida, February 1-6, 1987

Rosowski, J.J., C.R. Robinson, and W.T. Peake, "Accessory Acoustic Pathways to the Middle Ear of the Alligator Lizard: the Consequences of the Lack of a Bony Middle-Ear Capsule."

Second Airborne Science Workshop, University of Miami, Miami, Florida, February 3-6, 1987

Staelin, D.H., "Application of Airborne Passive Microwave Observations." (invited paper)

International Rosenbluth Symposium on Dynamics of Particles and Plasmas, University of Texas, Austin, Texas, February 5-6, 1987

Coppi, B., "Plasma Collective Modes and Transport."

Optical Society of America Symposium on the Microphysics of Surfaces, Beams, and Adsorbates, Santa Fe, New Mexico, February 14-17, 1987

Shedd, G.M., A.D. Dubner, H. Lezec, and J. Melngailis, "Focused Ion Beam Induced Deposition of Gold."

Speech-Research V Symposium, Washington, D.C., February 18-19, 1987

Feder, M., and A.V. Oppenheim, "Methods for Noise Cancellation Based on the E-M Logarithm."

International Solid State Circuits Conference, New York, February 25, 1987

Allen, J., Moderator for panel, "ASIC Architectures for the '90's."

National Energy Conference, Industry Commission, Italian Parliament, Rome, Italy, February 27, 1987

Coppi, B., "State and Problems on Nuclear Fusion Research."

March 1987

Advanced Course in Physics, University of Pavia, Pavia, Italy, March 4, 1987

Coppi, B., "Outstanding Plasma Problems in Astrophysics."

IEEE 1987 Particle Accelerator Conference, Washington, D.C., March 16-19, 1987

Abstract in *Proceedings*:

Hartemann, F., G. Bekefi, D.A. Kirkpatrick, R.E. Klinkowstein, and R.E. Shafer, "Evolution of Beam Emittance and Cathode Plasma Uniformity from a Field Emission Diode."

March Meeting of the American Physical Society, New York, March 16-20, 1987

Abstracts in *Proceedings*:

Bar-Yam, Y., S.T. Pantelides, and J.D. Joannopouios, " *Ab-Initio* Theory of Silicon Dioxide," p. 537.

Birgeneau, R.J., "Scattering Studies of Novel Low Dimensional Phases and Phase Transitions," p. 503.

Chung, J.W., E.D. Specht, K.W. Evans-Lutterodt, R.J. Birgeneau, A.R. Kortan, and P.J. Estrup, "Synchrotron X-Ray Study of Superlattice Diffraction Peaks from an Epitaxial Oxide Layer on a W(100) Surface," p. 452.

Ippen, E.P., "Femtosecond Phenomena and Their Applications," p. 743.

Kaxiras, E., "Variable Stoichiometry Surface Reconstruction: New Models and Phase Transitions on GaAs(111)2x2," p. 709. (invited paper)

Kaxiras, E., J.D. Joannopoulos, and K.C. Pandey, "New Models for the (2x4), c(2x8) and c(4x4) Surface Reconstructions of GaAs(100)," p. 710.

McIntyre, C.R., and P.A. Wolff, "A Variational Approach to Bound Magnetic Polarons in Dilute Magnetic Semiconductors," p. 527.

McKay, S.R., and A.N. Berker, "Hybrid Order Phase Transition of the d=3 Random-Field Ising Model from a Global Renormalization-Group Calculation," p. 823.

Needels, M.C., M.C. Payne, and J.D. Joannopoulos, " *Ab-Initio* Molecular Dynamics on the Ge(100) Surface," p. 572.

Payne, M.C., P.D. Bristowe, and J.D. Joannopoulos, "Calculation of the Structure of a $\Sigma = 5$ Twist Boundary in Germanium by Simulated Annealing," p. 721.

Smith, H.I., "X-Ray Nanolithography for Sub 100-nm Devices," p. 628. (invited paper)

Tarnow, E., M.C. Payne, and J.D. Joannopoulos, "Intrinsic Defects in c-As_2Se_3," p. 789.

Wong, S., P. Becla, and P.A. Wolff, "Magnetic Field Dependent Nonlinear Current-Voltage Characteristics in HgMnTe," p. 491.

New England Combined Chapter of the American Vacuum Society, Bedford, Massachusetts, March 18, 1987

Melngailis, J., "Focused Ion Beam Microfabrication." (invited paper)

Symposium on Interfaces and Thin Films, National Academy of Sciences, Washington, D.C., March 23-24, 1987

Birgeneau, R.J., "Liquids, Crystals and Liquid Crystals."

Stanford VLSI Conference, Palo Alto, California, March 23-27, 1987

Selvige, C., and L. Glasser, "*Power and Communications* Techniques for Physically Isolated Integrated Circuits. "

Speech Recognition Workshop, Defense Advanced Research Projects Agency, San Diego, California, March 24-26, 1987

Papers in *Proceedings:*

Glass, J.R., and V.W. Zue, "Acoustic Segmentation and Classification," pp. 38-43.

Seneff, S., "A New Model for the Transduction Stage of the Auditory Periphery," pp. 26-32.

Seneff, S., "Vowel Recognition Based on Line-Formants Derived from an Auditory-Based Spectral Representation," pp. 33-37.

April 1987

Sherwood Theory Conference, San Diego, California, April 6-8, 1987

Abstracts in *Proceedings:*

Bonoli, P., and M. Porkolab, "Analysis of Lower Hybrid RF Stabilization of Sawteeth in the Alcator C Tokomak," paper 1C23.

Coppi, B., "Profile Consistency: Global and Nonlinear Transport," paper 2D1.

Detregiache, P., B. Coppi, and F. Pegoraro, "Theory of $m^\circ = 1$ Modes in Regimes of Long Mean Free Path Relevant to Ignition Plasmas," paper 3B4.

Englade, R., "Profile Consistency and Transport Modelling," paper 3B15.

Francis, G., A.K. Ram, A. Bers, C.N. Lashmore-Davies, V. Fuchs, and L. Gauthier, "Analytic Models of Ion Cyclotron Absorption," paper 1D1.

Hsu, C.T., and D.J. Sigmar, "Cross-Species Collisional Viscosity," paper 2C6.

Pegoraro, F., F. Porcelli, and T.J. Schep, "Internal Kink Modes in the Large Larmor Regime," paper 1D5.

Porcelli, F., B. Coppi, and S. Migliuolo, "Fishbone Oscillation Bursts Initiated by Fusion Alpha Particles," paper 1C30.

Ram, A.K., and A. Bers, "Ray Tracing Analysis of the Mode Converted Ion-Bernstein Wave in ICRF Heating," paper 2D27.

Ramos, J.J., "Internal Kink Modes in Elongated Tokamaks with Flat Rotational Transform," paper 2D2.

Sugiyama, L.E., "Resolution of Anomalous Thermal Transport Models," paper 3A23.

Presentation to Texas Instruments, Dallas, Texas, April 6, 1987

Allen, J., "Future Directions in DSP Chips." (invited paper)

IEEE International Conference on Acoustics, Speech and Signal Processing, Dallas, Texas, April 6-9, 1987

Papers in *ICASSP '87:*

Allen, J., Chairman of panel, "VLSI Signal Processing Architectural Choices."

Feder, M., A.V. Oppenheim, and E. Weinstein, "Methods for Noise Cancellation Based on the EM Algorithm," pp. 201-204.

Jeong, H., and B.R. Musicus, "Masks Extraction from Optical Images of VLSI Circuits," pp. 602-605.

Musicus, B.R., and G.N.S. Prasanna, "A Small 16x16 Cellular Array for Image Processing," paper 33.7.

Myers, C., "Symbolic Representation and Manipulation of Signals," pp. 2400-2403.

Peterson, P.M., "Using Linearly-Constrained Adaptive Beamforming to Reduce Interference in Hearing Aids from Competing Talkers in Reverberant Rooms," pp. 2364-2367.

Peterson, P.M., and J.A. Frisbie, "An Interactive Environment for Signal Processing on a VAX Computer," pp. 1891-1894.

Rodriguez, J.J., J.S. Lim, and E. Singer, "Adaptive Noise Reduction in Aircraft Communication Systems," pp. 169-172.

Oak Ridge National Laboratory, Energy Division, Oak Ridge, Tennessee, April 16, 1987

Coppi, B., "Physics and Engineering Issues for Fusion Ignition Experiments."

Conference on Lasers and Electro-Optics, Baltimore, Maryland, April 26 - May 1, 1987

Papers in *CLEO '87:*

Shirasaki, M., H.A. Haus, and D.L. Wong, "A Nonlinear Fiber Interferometer and Logic Gates," pp. 284-286.

15th International Conference on Quantum Electronics, Baltimore, Maryland, April 27 -May 1, 1987

Papers in *IQEC '87:*

John, R.K., J.H. Shapiro, and P. Kumar, "Classical and Quantum Noise Transformations Produced by Self-Phase Modulation."

Lin, W.Z., R.W. Schoenlein, S.D. Brorson, J.G. Fujimoto, and E.P. Ippen, "Femtosecond Carrier Thermalization in GaAs and AlGaAs."

Shapiro, J.H., "Generation, Propagation, and Detection of Squeezed State Light." (invited paper)

IEEE Circuit Analysis and Design Workshop, Destin, Florida, April 28, 1987

Allen, J., Organizer and chairman of the session, "Performance Directed Synthesis."

GEC Hirst Research Center, Wembley, England, April 29, 1987

Melngailis, J., "Focused Ion Beam Fabrication." (invited seminar)

CNET, Grenoble, France, April 30, 1987

Melngailis, J., "Microfabrication par Faisceaux D'ion Focalises." (invited seminar)

May 1987

Seventh APS Topical Conference on Applications of Radio-Frequency Power to Plasmas, Kissimmee, Florida, May 4-6, 1987

Chen, K.I., S.C. Luckhardt, M. Mayberry, and M. Porkolab, "Particle Transport Simulation of Lower-Hybrid Current Drive Experiments on the Versator Tokamak."

Francis, G., A. Bers, and A.K. Ram, "Non-Resonant Mode-Coupling Model of ICRF Heating."

Fuchs, V., C.N. Lashmore-Davies, G. Francis, A.K. Ram, and A. Bers, "Fast-Wave Transmission and Reflection in Ion-Cyclotron Heating."

Luckhardt, S.C., K-I. Chen, R. Kirkwood, M. Porkolab, J. Squire, and Z. Lu, "Initial Operation of Combines ECRH and Lower-Hybrid Current Drive Experiments on the Versator II Tokamak."

Ram, A.K., and A. Bers, "Electron Heating by Mode-Converted Ion-Bernstein Waves in ICRF Heating of Tokamak Plasmas."

NATO Workshop on Emerging Technologies for In Situ Processing, Institute of Scientific Studies at Cargese, Corsica, France, May 4-8, 1987

Melngailis, J., Organizer and co-chairman of the workshop.

Melngailis, J., "Focused Ion Beam Induced Deposition."(invited paper)

Annual Spring Meeting of the Association for Research in Vision and Ophtalmology, Sarasota, Florida, May 4-8, 1987

Abstracts in *ARVO 1987:*

Fujimoto, J.G., C.A. Puliafito, J.M. Krauss, and W.Z. Lin, "Interferometric Laser Exposure Technique for Investigation of Retinal Thermal Damage," p. 114.

Hewlett Packard Internal Design Review Meeting, Berkeley, California, May 5, 1987

Allen, J., Keynote Speaker on Silicon Compilation

113th Meeting of the Acoustical Society of America, Indianapolis, Indiana, May 11-15, 1987

Abstracts in *J. Acoust. Soc. Am.* 81, Suppl. 1 (1987):

Eddington, D.K., "Cochlear Implants: What Are They and What Do They Accomplish?" p. S58.

Fisher, W.M., V.W. Zue, J. Bernstein, and D.S. Pallett, "On Acoustic-Phonetic Data Base," p. S92.

Kline, G.C., and H.S. Colburn, "Predictions for Binaural Masked Detection with Frozen-Noise Maskers," p. S27.

Koehnke, J., and H. S. Colburn, "The Dependence of Binaural Detection and Interaural Time and Intensity in Normal and Impaired Listeners," p. S27.

Reed, C.M., M.H. Power, K.K. Foss, N.I. Durlach, and L.D. Braida, "Development and Testing of Artificial Low-Frequency Speech Codes," p. S54.

CNET/CNRS, Bagneux, France, May 12, 1987

Melngailis, J., "Microfabrication par faisceaux d'ions focalises." (invited seminar)

Thompson CSF, Orsay, France, May 13, 1987

Melngailis, J., "Microfabrication par faisceaux d'ions focalises." (invited seminar)

Bull Research Center, Paris, France, May 14, 1987

Melngailis, J., "Microfabrication par faisceaux d'ions focalises." (invited seminar)

Technical Symposium Southeast on Optics, Electro-Optics and Sensors, SPIE '87, Orlando, Florida, May 17-22, 1987

Papers in *SPIE Proceedings* 783:

Mark, M.B., and J. H. Shapiro, "Multipixel, Multidimensional Laser Radar System Performance," pp.109-122.

International Geoscience and Remote Sensing Symposium and URSI Meeting, University of Michigan, Ann Arbor, Michigan, May 18-21, 1987

Borgeaud, M., J.A. Kong, and R.T. Shin, "Polarimetric Microwave Remote Sensing of Anisotropic Earth Terrain with Strong Fluctuation Theory," URSI Proceedings p. 127.

Lin, F.C., J. A. Kong, and R.T. Shin, "Theoretical Models for Microwave Remote Sensing of Snow-Covered Sea Ice," IGARSS '87, pp. 1121-1125.

Spring Meeting of the American Geophysical Union, Baltimore, Maryland, May 18-22, 1987

Thieman, J.R., J.K. Alexander, and D.H. Staelin, "Modulated Spectral Activity (MSA) in Jovian Radio Emission."

United States / Israel Workshop on VLSI Architecture and Design, Tiberias, Israel, May 23-31, 1987

Allen, J., "Performance-Directed Synthesis."

International Workshop on High-Speed Optical Processes and Optoelectronics Devices Based on Compound Semiconductors, University of Michigan, Ann Arbor, Michigan, May 27-29, 1987

Ippen, E.P., "Femtosecond Dynamics in AlGaAs Materials and Devices."

June 1987

Conference on Passive Microwave Observing from Environmental Satellites, Williamsburg, Virginia, June 1-4, 1987

Gasiewski, A.J., J.W. Barrett, P.G. Bonanni, and D.H. Staelin, "Temperature Sounding and Precipitation Cell Detection Using 118-GHz Passive Radiometric Observations."

Rosenkranz, P., "Recent Developments in Transmittance."

Staelin, D.H., "Surface Emissivity."

Staelin, D.H., "Precipitation and Water Vapor."

Fourth International Symposium on Gyrotron and Free Electron Laser, Chengdu, China, June 1-5, 1987

Bekefi, G., J. Fajans, D.S. Knowles, B. Lax, J.S. Wurtele, K. Xu, and Y.Z. Yin, "Measurements of Linear and Nonlinear Characteristics of a Collective Free Electron Laser."

Bekefi, G., F. Hartemann, D.A. Kirkpatrick, and R.E. Shefer, "Measurements of Beam Brightness from Field Emission Guns for Free Electron Laser Applications."

Picture Coding Symposium, Stockholm, Sweden, June 7-12, 1987

Martinez, D.M., and J.S. Lim, "Restoration and Interpolation of Motion Pictures by Motion Compensation."

IEEE Microwave and Millimeter-Wave Monolithic Circuits Symposium, Las Vegas, Nevada, June 8-9, 1987

Dagli, N., and C.G. Fonstad, "A New Method of Analyzing and Modeling Integrated Optoelectronic Components," pp. 39-41.

Second Haystack Observatory Meeting on Interstellar Matter, Barrett Symposium, Cambridge, Massachusetts, June 8-12, 1987

Burke, B.F., "Alan Barrett and Future Directions in Astronomy."

Burke, B.F., "Introduction of Charles H. Townes."

General Electric Company and Record Company of America Research Briefing, Massachusetts Institute of Technology, Cambridge, Massachusetts, June 10, 1987

Allan, J., "Microwave and Quantum Electronics, and Microelectronics: Outlook on RLE/Lincoln Supported Research."

170th Meeting of the American Astronomical Society, Vancouver, Canada, June 14-18, 1987

Dreher, J.W., C.L. Carilli, and R.A. Perley, "Discovery of the Counter Jet in Cygnus A."

Heflin, M.B., B.F. Burke, E.E. Falco, M.V. Gorenstein, I.I. Shapiro, J.N. Hewitt, A.E.E. Rogers, and C. Lawrence, "VLBI Observations of the Gravitational Lens System 2016+112."

Langston, G.I., and B.F. Burke, "MG 1355+083: Quartet of Double-lobed Radio Sources."

International Astronomical Union Colloquium on Bioastronomy - The Next Step, Balatonfured, Hungary, June 14-20, 1987

Burke, B.F., "Optical Interferometry and the Detection of Evidence of Life."

International Astronomical Union Symposium on Evolution of Large Scale Structures in the Universe, Balatonfured, Hungary, June 14-20, 1987

Burke, B.F., "Gravitational Lenses."

Department of Defence Alpha Particle Workshop, Germantown, Maryland, June 15-16, 1987

Coppi, B., "Plasma Oscillation Bursts and Scattering of Slowed-down MeV Particles."

10th Annual Conference, Rehabilitation Engineering Society of North America San Jose, California, June 21-23, 1987

Durlach, N.I., C. R. Corbett, M.V.C. McConnell, W.M. Rabinowitz, P.M. Peterson, and P.M. Zurek, "Multimicrophone Monoaural Hearing Aids."

Lin Symposium, Massachusetts Institute of Technology, Cambridge, Massachusetts, June 22-24, 1987

Coppi, B., "Physics of Space and Laboratory Plasmas."

Eighth International Conference on Laser Spectroscopy, Are, Sweden, June 22-26, 1987

Papers in *Proceedings:*

Pritchard, D.E., K. Helmerson, V.S. Bagnato, G.P. Lafyatis, and A.G. Martin, "Optical Pumping in Translation Space," pp. 68-72

Gordon Conference on Plasma Physics MHD and Transport, Plymouth, New Hampshire, June 22-26, 1987

Coppi, B., "Profile Consistency in Tokamaks."

14th European Conference on Controlled Fusion and Plasma Heating, Madrid, Spain, June 22-26, 1987

Coppi, B., P. Detregiache, and F. Pegoraro, "Internal Kink Modes in the Large Larmor Radius, Long Mean Free Path Regime."

Pegoraro, F., F. Porcelli, and T.J. Schep, "Kink Modes in the Large Gyroradius Regime."

Conference on Electron Properties of Microstructures, Santa Barbara, California, June 29 - July 2, 1987

Lee, P., "Conductance Fluctuations in Submicron Structures."

Gordon Research Conference on Implantable Auditory Protheses, New London, New Hampshire, June 29-July 3, 1987

Rabinowitz, W.M., "Tactile Aids for the Deaf." (invited presentation)

July 1987

Fifth International Conference on Hot Carriers in Semiconductors, Boston, Massachusetts, July 20-24, 1987

Papers in *Proceedings:*

Schoenlein, R.W., W.Z. Lin, S.D. Brorson, E.P. Ippen, and J.G. Fujimoto, "Femtosecond Hot Carrier Energy Redistribution in GaAs and AlGaAs,"

Shahidi, G.G., D.A. Antoniadis, and H.I. Smith, "Reduction of Hot-Electron Effects in Sub-100 nm Channel Length Si MOSFETs."

United States-Japan Seminar on Quantum Mechanical Aspects of Quantum Electronics, Monterey, California, July 21-24, 1987

Papers in *Proceedings:*

Ippen, E.P., and J.G. Fujimoto, "Femtosecond Studies of Hot Carrier Relaxation in GaAs and AlGaAs," p. 415.

Kumar, P., J.H. Shapiro, M.W. Maeda, S-T. Ho, and M. Madabushi, "Squeezing Via Travelling-Wave Forward Mixing in Atomic Vapors: Comparison with Nondegenerate Theory," p. 451.

Shapiro, J.H., "Open Questions in Closed-Loop Photodetection," p. 628.

Wolff, P.A., "Free Carrier Nonlinear Optics," p. 327.

Japan-United States Transcultural Seminar, Sendai, Japan, July 26-August 1, 1987

Kleppner, D., Plenary Address.

Gordon Research Conference on Nonlinear Optics and Lasers, Brewster Academy, Wolfeboro, New Hampshire, July 27 - August 1, 1987

Ippen, E.P., "Femtosecond Studies of Opto-electronic Materials and Devices."

NASA Global Scale Atmospheric Processes Research Program Review, Columbia, Maryland, July 29, 1987

Gasiewski, A.J., J.W. Barrett, P.G. Bonanni, C.C.L. Kuo, and D.H. Staelin, "High-Spatial-Resolution Passive Microwave Remote-Sended Spectra Observations Near Fronts: Experimental Results."

Rosenkranz, P.W., A.C. Briancon, and D.H.Staelin, "Impact of High-Spatial-Resolution Passive Remote Sensing Data Upon Numerical Weather Analyses and Predictions: Theoretical Studies."

August 1987

Eleventh International Congress of Phonetic Sciences, Tallinn, Estonia, August 1-7, 1987

Papers in *Proceedings:*

DiBenedetto, M-G., "On Vowel Height: Acoustic and Perceptual Representation by the Fundamental and the First Formant Frequency," Vol. 5, pp. 198-201.

Espy-Wilson, C.Y., "A Semivowel Recognition System," Vol. 5, pp. 403-406.

Hawkins, S., and K.N. Stevens, "Perceptual and Acoustical Analyses of Velar Stop Consonants," Vol. 5, pp. 342-345.

Lim, J.S., "Speech Enhancement," Vol. 1, pp. 285-291.

Randolph, M.A., and V.W. Zue, "The Role of Syllable Structure in the Acoustic Realizations of Stops," Vol. 2, pp. 360-363.

Seneff, S., "Vowel Recognition Based on "Line-Formants" Derived from an Auditory-Based Spectral Representation," Vol. 5, pp. 392-395.

Shattuck-Hufnagel, S., "Phonological Planning for Speech Production Speech Error Evidence for Word-Based vs. Syllable-Based Structure," Vol. 3, pp. 169-172.

Stevens, K.N., "Interaction Between Acoustic Sources and Vocal-Tract Configurations for Consonants," Vol. 3, pp. 385-389.

Stevens, K.N., "Relational Properties as Perceptual Correlates of Phonetic Features," Vol. 4, pp. 352-356.

19th General Assembly of the International Union of Geodesy and Geophysics, Vancouver, British Columbia, Canada, August 9-22, 1987

Gasiewski, A.J., J.W. Barrett, P.G. Bonanni, and D.H. Staelin, "Passive Microwave Imaging of Brain Cells Using the 118-GHZ Oxygen."

Energy Independence Conference on Fusion Energy and Plasma Physics, Rio de Janeiro, Brazil, August 17-21, 1987

Coppi, B., "First Ignition Experiments: Problems and Perspectives."

International Symposium on Signal Processing and Its Applications, Brisbane, Australia, August 24-28, 1987

Papers in *ISSPA '87:*

Griffin, W.D., and J.S. Lim, "A High Quality 8 Kbps Multi-Band Excitation," pp. 531-536.

September 1987

International Symposium on Feasibility of Aneutronic Power, Institute for Advanced Study, Princeton, New Jersey, September 10-11, 1987

Coppi, B., "Ignition Studies of D-He^3 Thermal Plasmas and the Second Stability Region."

Ninth International Free Electron Laser Conference, Williamsburg, Virginia, September 14-18, 1987

Ashkenazy, J., and G. Bekefi, "A Novel Permanent Magnet Helical Wiggler."

Bekefi, G., J. Fajans, F. Hartemann, J.S. Wurtele, and K. Xu, "Observation of Wave Profile Modification (Optical Guiding) Induced by the Free Electron Laser Interaction. "

Hartemann, F., and K. Xu, "Pulse Compression in a Free Electron Laser Amplifier."

Second CIT-Ignition Design Meeting, Massachusetts Institute of Technology, Cambridge, Massachusetts, September 21, 1987

Coppi, B., "Compact Ignition Experiments: Physics and Design Issues"

Microcircuit Engineering 87, International Conference on Microlithography, Jouy-en-Josas, France, September 22-25, 1987

Papers in *Proceedings:*

Anderson, E.H., D. Kern, and H.I. Smith, "Fabrication by Tri-Level Electron-Beam Lithography of X-Ray Masks with 50nm Linewidths, and Replication by X-Ray Nanolithography," pp. 541-546.

Schattenburg, M.L., I. Tanaka, and H.I. Smith, "Microgap X-Ray Nanolithography," pp. 273-279.

Workshop on Defects and Interfaces in Solids, Columbus, Ohio, September 29 - October 1, 1987

Joannopoulos, J.D., "Grain Boundary in Solids."

October 1987

Princeton Workshop on Algorithms, Architecture and Technology Issues in Models of Concurrent Computation, Princeton, New Jersey, October 1-2, 1987

Allen, J., "Representation Issues for System Synthesis."

IEEE Conference on Computer Design - VLSI in Computers, Rye, New York, October 7-9, 1987

Song, W.S., and B. Musicus, "A Fault-Tolerant Architecture for a Parallel Digital Signal Processing Machine."

38th International Astronautical Federation Congress, Brighton, England, October 10-17, 1987

Burke, B.F., "Detection of Life in Other Planetary Systems."

Optical Society of America Annual Meeting, Rochester, New York, October 18-23, 1987

Fujimoto, J.G., "Applications of Ultrashort Pulse and Measurement Techniques to Laser Medicine."

Workshop on Active Experiments in Space, Kyoto, Japan, October 19-20, 1987

Lee, M.C., K.M. Groves, H.C. Hang, and C.P. Liao, "Combined Operation of Two Ground Transmitters for Enhanced Ionospheric Heating."

Carnegie-Mellon University Seminar, Pittsburgh, Pennsylvania, October 22, 1987

Allen, J., "Performance-Directed Synthesis of Digital VLSI Circuits."

Workshop on Future Trends in EEC Curricula: United States, Brasil, Spain and Portugal, Lisbon, Portugal, October 26-27, 1987

Allen, J., Invited Presentation.

Topical Conference on Compound Semiconductor Growth, Processing, and Devices for the 1990's: Japan/United States Perspectives, Gainsville, Florida, October 26-28, 1987

Melngailis, J., "Focused Ion Beam Processing of Compound Semiconductor." (invited paper)

Workshop on Chemical Concepts for Ultrasmall Electronic Devices, Army Research Office, Cambridge, Massachusetts, October 28-29, 1987

Smith, H.I., "Fabrication and Performance of Sub-100 nm Electronic Devices."

November 1987

Fall Meeting of the Division of Plasma Physics, American Physical Society, San Diego, California, November 2-7, 1987

Abstracts in *Bull. Am. Phys. Soc.* 39:9 (1987):

Ashkenazy, J., and G. Bekefi, "A Novel Permanent Magnet Helical Wiggler."

Bekefi, G., "Measurements of Wave Profile Modification (Optical Guiding) Induced by the Free Electron Laser Interaction."

Chen, K-I., S.C.Luckhardt, Z.H. Lu, M. Porkolab, and S.C. Sherwood, "Emissivity Profiles of H_x During EC Start-up Experiments and Particle Transport Study During Combined EC/LH Current Drive Experiments on the Versator II Tokamak."

Chow, C., A.K. Ram, and A. Bers, "Mode-Conversion and Damping in ICRH at Finite Ion-Betas."

Coppi, B., Maxwell Prize Address, "New and Old Trends in Plasma Physics."

Coppi, B., "Global and Nonlinear Energy Transport."

Coppi, B., and the Ignitor Design Group, "Update on the Ignitor Experiments."

Detregiache, P., B. Coppi, and F. Pegoraro, "Resistive Kink Modes in Kinetic Plasma Regimes."

Englade, R., "Ohmic Ignition in a Compact Toroidal Device of Ignitor Type."

Francis, G., A. Bers, and A.K. Ram, "Mode-Boundary Expansion of Coupled Mode Instabilities in Inhomogeneous Plasmas."

Fuchs, V., R.A. Cairns, A.K. Ram, A. Bers, and C.N. Lashmore-Davies, "Mode-Conversion and Dissipation of the Fast Alfven Wave in Ion-Cyclotron Heating."

Hartemann, F., and G. Bekefi, "Microwave Radiation from a Tunable Circular Free Electron Laser."

Hartemann, F.V., S.C. Chen, and G. Bekefi, "Microwave Radiation from a Rippled-Bore Magnetron (Electrically Pumped Cross-Field Free Electron Laser)."

Kirkpatrick, D.A., G. Bekefi, and A.C. DiRienzo, "Experimental Studies of a Submillimeter Wavelength Free Electron Laser."

Kirkwood, R.K., K-I. Chen, I.H. Hutchinson, and S.C. Luckhardt, "Measurement of Electron Distribution in Versator II Using Electron-Cyclotron Absorption."

Kupfer, K., A. Bers, A.K. Ram, V. Fuchs, and M.M. Shoucri, "Energy Transport in Lower Hybrid Current Driven Plasmas."

Lu, Z-H., S.C. Luckhardt, K-I. Chen, D.A. Singleton, and M. Porkolab, "The EC Transmission System for the Versator II Tokamak and Measurements of Power Radiation."

Luckhardt, S.C., K-I. Chen, R. Kirkwood, Z. Lu, M. Porkolab, J. Squire, and J. Villasenor, "Electron Cyclotron Heating and Lower-Hybrid Current Drive Experiments on Versator II."

Migliuolo, S., L.E. Sugiyama, and S. Coda, "Ballooning Modes in Collisionless Plasmas with Anisotropic Electrons."

Porcelli, F., B. Coppi, and S. Migliuolo, "Plasma Oscillations Bursts and Scattering of Intermediate Energy α Particles."

Pu, Y.K., S. Migliuolo, and B. Coppi, "Collisional Ubiquitous Mode."

Ram, A.K., and A. Bers, "Analytical Modelling of the Propagation of Ion-Bernstein Waves in ICRF Heated Toroidal Plasmas."

Squire, J.P., K-I. Chen, R.K. Kirkwood, S.C. Luckhardt, and M. Porkolab, "Hard and Soft X-Ray Measurements During ECRH and LHCD Experiments on the Versator II Tokamak."

Sugiyama, L.E., "Ignition of Advanced Fuels in Compact Tokamaks."

Villasenor, J., M. Porkolab, S.C. Luckhardt, and K-I. Chen, "Lower-Hybrid Fast Wave Current Drive Experiments in the Versator II Tokamak."

Xu, K., and F. Hartemann, "Generation of Short Pulses of Coherent Electromagnetic Radiation in a Free Electron Laser Amplifier."

Speech Processing Symposium, Middletown, New Jersey, November 4-6, 1987

Lim, J.S., "4800 BPS High Quality Speech Coding System."

NEC, Kawasaki, Japan, November 10, 1987

Melngailis, J., "Focused Ion Beam Research at MIT." (invited seminar)

International Conference on Computer-Aided Design, Santa Clara, California, November 12, 1987

Allen, J., Chairman of session on control path synthesis.

NTT/Astugi Laboratories, Astugi, Japan, November 12, 1987

Melngailis, J., "Focused Ion Beam Research at MIT." (invited seminar)

Hitachi Research Center, Kokubunji, Japan, November 13, 1987

Melngailis, J., "Focused Ion Beam Research at MIT." (invited seminar)

Annual Convention of the American Speech-Language-Hearing Association, New Orleans, Louisiana, November 13-16, 1987

Braida, L., D. Bustamante, A. Montgomery, S. Revoile, and R. Uchanski, "Hearing-Aid Processed Speech." (Miniseminar)

Koehnke, J., and H. S. Colburn, "Binaural Detection and Discrimination in Normal-Hearing and Hearing-Impaired Listeners."

Levitt, H., W.M. Rabinowitz, and M. Weiss, "Noise Reduction Techniques." (Miniseminar)

Joint Japan/United States Seminar on Focused Ion Beam Technology and Applications, Osaka, Japan, November 15-20, 1987

Melngailis, J., U.S. chairman of the seminar.

Melngailis, J., T.O. Herndon, M. Shepard, and H. Lezec, "Planar Vias Through $Si_3 N_4$ Fabricated by Focused Ion Beam Implantation."

Ro, J.S., A.D. Dubner, C.V. Thompson, and J. Melngailis, "Ion Induced Deposition of Gold Films."

114th Meeting of the Acoustical Society of America, Miami, Florida, November 16-20, 1987

Glass, J.R., and S. Seneff, "Pulse Synchronous Analysis of Speech Using an Auditory Representation," p. S83.

Grant, K.W., "Evaluating the Articulation Index for the Auditory-Visual Input."

Isabelle, S.K., and H.S. Colburn, "Effects of Target Phase in Narrowband Frozen Noise Detection Data."

Klatt, D.H., "Acoustic Correlates of Breathiness: First Harmonic Amplitude, Turbulence Noise, and Tracheal Coupling."

Koehnke J., and S. Colburn, "Effects of Rowing Level on Binaural Detection and Discrimination On and Off Midline."

Lamel, L.F., "Identification of Stop Consonants from Continuous Speech in Limited Context," p. S80.

Rabinowitz, W.M., and P.M. Peterson, "Directional Processing for Interference Reduction in Hearing Aids."

Reed, C.M., L.A. Delhorne, and N.I. Durlach, "Tactile Reception of Fingerspelling and Sign Language."

Reed, C.M., W.M. Rabinowitz, and N.I.Durlach, "Tactile Speech Reception Using Augmented Tadoma."

Seneff, S., "A Model for Transduction Stage of Auditory Speech Processing," p. S80.

Wilson, T.A., "AGC Behavior of a Recovery Model for Auditory Neuron Firings," p. S118.

Fujitsu Laboratories, Atsugi, Japan, November 30, 1987

Melngailis, J., "Focused Ion Beam Research at MIT." (invited seminar)

Toshiba Laboratories, Kawasaki, Japan, November 30, 1987

Melngailis, J., "Focused Ion Beam Research at MIT." (invited seminar)

Materials Research Society Meeting, Boston, Massachusetts, November 30-December 5, 1987

Papers in *Proceedings:*

Lin, W.Z., R.W. Schoenlein, S.D. Brorson, E.P. Ippen, and J.G. Fujimoto, "Femtosecond Carrier Dynamics in Semiconductors and Metals."

Ro, J.S., A.D. Dubner, C.V. Thompson, and J. Melngailis, "Microstructure of Gold Films Grown by Ion Induced Deposition."

December 1987

Workshop on Femtosecond Physics in Semiconductors, Arizona State University, Tempe, Arizona, December 9-11, 1987

Fujimoto, J.G. "Femtosecond Transient Absorption Saturation Studies of Carrier Relaxation in GaAs."

National Science Foundation Workshop on Physics of Devices, Madras, India, December 10-12, 1987

Allen, J., "Performance Directed Synthesis of VLSI Systems."

Symposium on Speech Communication and Processing, Massachusetts Institute of Technology, Cambridge, Massachusetts, December 14, 1987

Allen, J., Welcome and introduction.

Braida, L.D., "Speech Processing Aids for the Handicapped."

Klatt, D.H., "Speech Synthesis: State of the Art, Current Research at MIT, Future Prospects."

Lim, J.S., "Coding, Enhancement, and Time Scale Modification of Speech."

Stevens, K.N., "Speech Production, Speech Perception, and Linguistic Units."

Zue, V., "Speech Recognition: State of the Art, Current Research at MIT, Future Prospects."

Symposium on Fundamental Limits on Coherent Lidar, Broadway, England, December 15-18, 1987

Shapiro, J.H., "Heterodyne Mixing Efficiency for Coherent Laser Radar." (invited paper)

58th Statistical Mechanics Meeting, Rutgers University, New Brunswick, New Jersey, December 17-18, 1987

Hui, K., "Reentrant Behavior of an Anti-Metamagnet in a Magnetic Field."

Marko, J.F., "Optimized Direct Correlations and Ordering in the Hard Ellipsoid Fluid."

30.2 Journal Articles

30.2.1 Published Journal Articles

Bekefi, G., F. Hartemann, and D.A. Kirkpatrick, "Temporal Evolution of Beam Emittance from a Field Emission Electron Gun," *J. Appl. Phys.* 62 (5):1564 (1987).

Birgeneau, R.J., "Liquids, Crystals, and Liquid Crystals," *Proc. Nat. Acad. Sci.* 84:4689 (1987).

Brown, M.C., "Morphology of Labeled Afferent Fibers in the Guinea Pig Cochlea," *J. Comp. Neurol.* 260:591 (1987).

Brown, M.C., "Morphology of Labeled Efferent Fibers in the Guinea Pig Cochlea," *J. Comp. Neurol.* 260:605 (1987).

Bustamante, D.K., and L.D. Braida, "Principal-Component Amplitude Compression for the Hearing Impaired," *J. Acoust. Soc. Am.* 82 (4):1227 (1987).

Carilli, C.L., and J.H. van Gorkom, "Discovery of Low Redshift, Neutral Hydrogen Absorption in the Radio Spectrum of PKS 2020-370," *Astrophys. J.* 319:683 (1987).

Colavita, M.M., M. Shao, and D.H. Staelin, "Atmospheric Phase Measurements with the Mark III Stellar Interferometer," *Appl. Optics* 26 (19):4106 (1987).

Colavita, M.M., M. Shao, and D.H. Staelin, "Two-Color Method for Optical Astrometry: Theory and Preliminary Measurements with the Mark III Stellar Interferometer," *Appl. Optics* 26 (19): 4113 (1987).

Coppi, B., L. Lanzavecchia, and the Ignitor Design Group, "Compact Ignition Experiments: Physics and Design Issues," *Comments on Plasma Phys. Contr. Fusion* 11 (1):47 (1987).

Dreher, J.W., C.L. Carilli, and R.A. Perley, "The Faraday Rotation of Cygnus A: Magnetic Fields in Cluster Gas," *Astrophys. J.* 316:611 (1987).

Dubner, A.D., G.M. Shedd, H. Lezec, and J. Melngailis, "Ion Beam Induced Deposition of Gold by Focused and Broad Beam Sources," *J. Vac. Sci. Technol. B* 5:1434 (1987).

Fajans, J., and G. Bekefi, "Effect of Electron Beam Temperature on the Gain of a Collective Free-Electron Laser," *IEEE J. Quantum Electron.* QE-23 (9):1617 (1987).

Garcia-Barreto, J.A., B.F. Burke, M.J. Reid, J.M. Moran, A.D. Haschick, and R.T. Schilizzi, "Magnetic Field Structure of the Star Forming Region W3(OH): VLBI Spectral Line Results," *Astrophys. J.* 326:954 (1988)

Fullerton, B.C., R.A. Levine, H.L. Hosford-Dunn, and N.Y.S. Kiang, "Comparison of Cat and Human Brain-Stem Auditory Evoked Potentials," *Electroencephalog. Clin. Neurophysiol.* 66:547 (1987).

Gifford, M.L., and J.J. Guinan, Jr., "Effects of Electrical Stimulation of Medial Olivocochlear Neurons on Ipsilateral and Contralateral Cochlear Responses," *Hear. Res.* 29:179 (1987).

Gomez-Santos, G., and J.D. Joannopoulos, "On the Application of the Spin Wave Theory to the Ground State of *XY* Quantum Hamiltonians," *Phys. Rev. B* 36 (16):8707 (1987).

Gould, P.L., G.A. Ruff, P.J. Martin, and D.E. Pritchard, "Preparation of a Single-State Atomic Beam by Optical Pumping and Radiative Deflection," *Phys. Rev. A* 36 (3):1478 (1987).

Grant, K.W., "Frequency Modulation Detection by Normally Hearing and Profoundly Hearing-Impaired Listeners," *J. Speech Hear. Res.* 30:558 (1987).

Gu, Q., J.A. Kong, and Y.E. Yang, "Time Domain Analysis of Nonuniformly Coupled Line Systems," *J. Electromag. Waves Appl.* 1 (1):109 (1987).

Habashi, T.M., J.A. Kong, and W.C. Chew, "Resonance and Radiation of the Elliptic Disk Microstrip Structure. Part I: Formulation," *IEEE Trans.* AP-35 (8):877 (1987).

Hartemann, F., and G. Bekefi, "Microwave Radiation from a Tunable Circular Free-Electron Laser," *Phys. Fluids* 30 (10):3283 (1987).

Haus, H.A., and G.A. Reider, "Enhancement of Surface Second Harmonic Generation with Waveguides," *Appl. Optics* 26 (21):4576 (1987).

Hewitt, J.N., E.L. Turner, C.R. Lawrence, D.P. Schneider, J.E. Gunn, C.L. Bennett, B.F. Burke, J.H. Mahoney, G.I. Langston, M. Schmidt, J.B. Oke, and J.G. Hoessel, "The Triple Radio Source 0023+171: A Candidate for a Dark Gravitational Lens," *Astrophys. J.* 321 (1987).

Izraelevitz, D., and J.S. Lim, "A New Direct Algorithm for Image Reconstruction from Fourier Transform Magnitude," *IEEE Trans.* ASSP-35 (4):511 (1987).

Kaxiras, E., Y. Bar-Yam, J.D. Joannopoulos, and K.C. Pandey, "*Ab Initio* Theory of Polar Semiconductor Surfaces: II (2x2) Reconstruction and Related Phase Transitions of GaAs(111)," *Phys. Rev. B* 35 (18):9636 (1987).

Klatt, D.H., "Review of Text-to-Speech Conversion for English," *J. Acoust. Soc. Am.* 82 (3):737 (1987).

Kuo, C-C. J., B.C. Levy, and B.R. Musicus, "A Local Relaxation Method for Solving Elliptic PDEs on Mesh-Connected Arrays," *SIAM J.* 8 (4):550 (1987).

Kuo, S.P., and M.C. Lee, "Thermal Filamentation Instability Driven by the Auroral Electrojet Current," *J. Geophys. Res.* 93 A1:265 (1988).

Kupfer, K., A. Bers, and A.K. Ram, "The Cusp Map in the Complex- Frequency Plane for Absolute Instabilities," *Phys. Fluids* 30 (10):3075 (1987).

Lee, M.C., and S.P. Kuo, "Resonant Electron Diffusion as a Saturation Process of the Synchrotron Maser Instability," *J. Plas. Phys.* 35 (part 1):177 (1986).

Luckhardt, S.C., "The Efficiency of RF Current Drive in the Presence of Fast Particle Losses," *Nucl. Fusion* 27 (11):1914 (1987).

Luckhardt, S.C., A. Bers, V. Fuchs, and M. Shoucri, "The Anomalous Doppler Instability During Lower-Hybrid Current Drive," *Phys. Fluids* 30 (7):2110 (1987).

Maeda, M.W., P. Kumar, and J.H. Shapiro, "Squeezing Experiments in Sodium Vapor," *J. Opt. Soc. Am.* 4 (10):1501 (1987).

Palmer, J.E., C.V. Thompson, and H.I. Smith, "Grain Growth and Grain Size Distributions in Thin Germanium Films," *J. Appl. Phys.* 62 (6):2492 (1987).

Poh, S.Y., and J.A. Kong, "Transient Response of a Vertical Electric Dipole (VED) on a Two-Layer Medium," *J. Electromag. Wave Appl.* 1 (2):133 (1987).

Porcelli, F., "Viscous Resistive Magnetic Reconnection," *Phys. Fluids* 30 (6):1734 (1987).

Rabe, K.M., and J.D. Joannopoulos, "Structural Properties of GeTe at $T = 0$," *Phys. Rev. B* 36 (6):3319 (1987).

Rabe, K.M., and J.D. Joannopoulos, "Theory of the Structural Phase Transition of GeTe," *Phys. Rev. B* 36 (12):6631 (1987).

Rabinowitz, W.M., A.J.M. Houtsma, N.I. Durlach, and L.A. Delhorne, "Multidimensional Tactile Displays: Identification of Vibratory Frequency, and Contactor Area," *J. Acoust. Soc. Am.* 82 (4):1243 (1987).

Rappaport, C.M., F.R. Morgenthaler, and P.P. Lele, "Experimental Study of the Controllable Microwave Troughguide Applicator," *J. Microwave Power (Hyperthermia Applicators)*, p. 71 (1987).

Rosenkranz, P.W., "Pressure Broadening of Rotational Bands. II. Water Vapor from 300 to 1100 cm^{-1}," *J. Chem. Phys.* 87 (1):163 (1987).

Saunders, J.C., E.M. Relkin, J.J. Rosowski, and C. Bahl, "Changes in Middle-Ear Input Admittance During Postnatal Auditory Development in Chicks," *Hear. Res.* 24:227 (1986).

Shapiro, J.H., G. Saplakoglu, S-T. Ho, P. Kumar, B.E.A. Saleh, and M.C. Teich, "Theory of Light Detection in the Presence of Feedback," *J. Opt. Soc. Am. B* 4 (10):1604 (1987).

Simonson, R.J., J.R. Wang, and S.T. Ceyer, "Spectroscopy Study of the Absorption of C_2H_4 and C_2H_2 on a Rare Earth Single Crystal. I. Metallic Gd(0001)," *J. Phys. Chem.* 91 (22):5681 (1987).

Vlannes, N.P., "Experimental Study of Microwave Magnetostatic Waves in Thin Film Yttrium-Iron-Garnett with a New Magnetic-Induction Probe," *J. Appl. Phys.* 61 (1):416 (1987).

Vlannes, N.P., "Optical Probing of Magnetostatic Forward Volume Waves in Thin Film Yttrium-Iron-Garnett," *J. Appl. Phys.* 62 (3):972 (1987).

Wintner, E., D.P. Chen, J. Melngailis, and E.P. Ippen, "Optical Generation and Phase-Sensitive Detection of Surface Acoustic Waves in InP," *IEEE Trans.* UFFS-34 (1):114 (1987).

Yam, Y., J.H. Lang, D.H. Staelin, and T.L. Johnson, "The Experimental Computer Control of a Two-Dimensional Hyperbolic System," *IEEE Trans.* AC-33 (1):79 (1988).

Yin, Y-Z., R-J. Ying, and G. Bekefi, "Generation of Electromagnetic Radiation from a Drifting and Rotating Electron Ring in a Rippled Magnetic Field," *IEEE J. Quantum Electron.* QE-23 (9):1610 (1987).

Yuen, S.Y., P.A. Wolff, P. Becla, and D. Nelson, "Free-Carrier Spin-Induced Faraday Rotation in HgCdTe and HgMnTe," *J. Vac. Sci. Technol. A* 5 (5):3040 (1987).

Zakhor, A., and A.V. Oppenheim, "Quantization Errors in the Computation of the Discrete HartleyTransform," *IEEE Trans.* ASSP-35 (11):1592 (1987).

Zurek, P.M., and L.A. Delhorne, "Consonant Reception in Noise by Listeners with Mild and Moderate Sensorineural Hearing Impairment," *J. Acoust. Soc. Am.* 82 (5):1548 (1987).

30.2.2 Articles Accepted for Publication in Journals

Ashkenazy, J., and G. Bekefi, "Analysis and Measurements of Permanent Magnet Bifilar Helical Wigglers," *IEEE J. Quantum Electron.*

Brorson, S.D., "What Is the Confocal Parameter?" *IEEE J. Quantum Electron.*

Brorson, S.D., and H.A. Haus, "Geometrical Limitations in Grating Pair Pulse Compression," *Appl. Optics.*

Brorson, S.D., and H.A. Haus, "Diffraction Gratings and Geometrical Optics," *J. Opt. Soc. Am.*

Coppi, B., "Near-Term Experiments on Fusion Burn Conditions by Neutronless Reactions," *Nucl. Instrum. Methods.*

Coppi, B., S. Migliuolo, and F. Porcelli, "Macroscopic Plasma Oscillation Bursts (Fishbones) Resulting from High Energy Populations," *Phys. Fluids.*

Coppi, B., and F. Porcelli, "Plasma Oscillation Bursts and Scattering of Intermediate Energy α Particles," *Fusion Technol.*

Feder. M., and E. Weinstein, "Parameter Estimation of Superimposed Signals Using the EM Algorithm," *IEEE Trans. ASSP.*

Glasser, L.A., and C.A. Zukowski, "Continuous Models for Communication Density Constraints on Multiprocessor Performance," *IEEE Trans. (C)*.

Ho, S-T., P. Kumar, and J.H. Shapiro, "Quantum Theory of Nondegenerate Multiwave Mixing: I. General Formulation," *Phys Rev. A*.

Kaxiras, E., and J.D. Joannopoulos, "Hydrogenation of Semiconductor Surfaces: Si and Ge (111)," *Phys. Rev. B*.

Malvar, H.S., and D.H. Staelin, "Optimal Pre-and Post-Filters for Multichannel Signal Processing," *IEEE Trans. ASSP*.

Payne, M.C., M. Needels, and J.D. Joannopoulos, "Symmetry Breaking in the Molecular Dynamics Method for *Ab-Initio* Total Energy Calculations," *Phys. Rev. B*.

Ro, J.S., A.D. Dubner, C.V. Thompson, and J. Melngailis, "Summary Abstract: Ion Induced Deposition of Gold Films," *J. Vac. Sci. Technol.*

Rose, C., and T.F. Weiss, "Frequency Dependence of Synchonization of Cochlear Nerve Fibers in the Alligator Lizard: Evidence for a Cochlear Origin of Timing and Non-Timing Neural Pathways," *Hear. Res.*

Sanders, G.A., and S. Ezekiel, "Measurement of Fresnel-Drag in Moving Media Using a Ring Resonator Technique," *J. Opt. Soc. Am.*

Simonson, R.J., J.R. Wang, and S.T. Ceyer, "Spectroscopy Study of the Adsorption of C_2H_4 and C_2H_2 on a Rare Earth Single Crystal. II. Oxidized Gd(0001)," *J. Phys. Chem.*

Weiss. T.F., and C. Rose, "Stages of Degradation of Timing Information in the Cochlea: A Comparison of Hair-Cell and Nerve-Fiber Responses in the Alligator Lizard," *Hear. Res.*

Weiss, T.F., and C. Rose, "A Comparison of Synchronization Filters in Different Auditory Receptor Organs," *Hear. Res.*

Wyatt, J.L., Jr., "Nonlinear Dynamic Maximum Power Theorem," *IEEE Trans. CAS*.

30.3 Letters to the Editor

30.3.1 Published Letters

Atwater, H.A., C.V. Thompson, and H.I. Smith, "Interface-Limited Grain-Boundary Motion During Ion Bombardment," *Phys. Rev. Lett.* 60 (2):112 (1988).

Bagnato, V.S., G.P. Lafyatis, A.G. Martin, E.L. Raab, and D.E. Pritchard, "Continuous Stopping and Trapping of Neutral Atoms," *Phys. Rev. Lett.* 58 (21):2194 (1987).

Bekefi, G., and J. Ashkenazy, "Permanent Magnet Helical Wiggler for Free Electron Laser and Cyclotron Maser Applications," *Appl. Phys. Lett.* 51 (9):700 (1987).

Brorson, S.D., J.G. Fujimoto, and E.P. Ippen, "Femtosecond Electronic Heat-Transport Dynamics in Thin Gold Films," *Phys, Rev. Lett.* 59 (17):1962 (1987).

Chung, J.W., K. Evans-Lutterodt, E.D. Specht, R.J. Birgeneau, P.J. Estrup, and A.K. Kortan, "Grazing-Incidence X-Ray Study of the Structures and Phase Transitions of Hydrogen on Tungsten(100)," *Phys. Rev. Lett.* 59 (19):2192 (1987).

Hartemann, F., K. Xu, G. Bekefi, J.S. Wurtele, and J. Fajans, "Wave Profile Modification (Optical Guiding) During Free Electron Laser Interaction," *Phys. Rev. Lett.* 59 (11):1177 (1987).

Kesler, M.P., and E.P. Ippen, "Subpicosecond Gain Dynamics in GaAlAs Laser Diodes," *Appl. Phys. Lett.* 51 (22):1765 (1987).

Lin, W.Z., J.G. Fujimoto, E.P. Ippen, and R.A. Logan, "Femtosecond Dynamics of Highly Excited Carriers in Al_xGa_{1-x} As," *Appl. Phys. Lett.* 51 (3):161 (1987).

Luckhardt, S.C., "The Efficiency of RF Current Drive in the Presence of Fast Particle Losses," *Nucl. Fusion* 27 (11):1914 (1987).

Martin, P.J., P.L. Gould, B.G. Oldaker, A.H. Miklich, and D.E. Pritchard, "Diffraction of Atoms Moving Through a Standing Light Wave," *Phys. Rev. A (Rapid Commun.)* 36 (5):2495 (1987).

Needels, M., M.C. Payne, and J.D. Joannopoulos, "*Ab-Initio* Molecular Dynamics on the Ge(100) Surface," *Phys. Rev. Lett.* 58 (17):1768 (1987).

Raab, E.L., M. Prentiss, A. Gable, and D.E. Pritchard, "Trapping of Neutral Sodium Atoms with Radiation Pressure," *Phys. Rev. Lett.* 59 (23):2631 (1987).

Rabe, K.M., and J.D. Joannopoulos, "*Ab Initio* Determination of a Structural Phase Transition Temperature," *Phys. Rev. Lett.* 59 (5):570 (1987).

Schoenlein, R.W., W.Z. Lin, E.P. Ippen, and J.G. Fujimoto, "Femtosecond Hot-Carrier Energy Relaxation in GaAs," *Appl. Phys. Lett.* 51 (18):1442 (1987).

Triantafyllou, G.S., K. Kupfer, and A. Bers, "Absolute Instabilities and Self-Sustained Oscillations in the Wake of Circular Cylinders," *Phys. Rev. Lett.* 59 (17):1914 (1987).

30.3.2 Letters to the Editor Accepted for Publication

Coppi, B., "Profile Consistency: Global and Nonlinear Transport," *Physics Lett.*

Martin, P.J., B.G. Oldaker, H.A. Miklich, and D.E. Pritchard, "Bragg Scattering of Atoms from a Standing Light Wave," *Phys. Rev. Lett.*

Shaidi, G.G., D.A. Antoniadis, and H.I. Smith, "Electron Velocity Overshoot at Room and Liquid Nitrogen Temperatures in Silicon Inversion Layers," *IEEE (EDL)*.

Stewart, B., P.D. Magill, T.P. Scott, J. Derouard, and D.E. Pritchard, "Quasi Resonant V $\longleftrightarrow$ R Transfer in Atom-Diatom Collisions," *Phys. Rev. Lett.*

30.4 Chapters in Books

Allen, J., "Introduction to VLSI Design," In *VLSI CAD Tools and Applications,* eds. W. Fichtner and M. Morf, 19-55. Norwell, Massachusetts: Kluwer Academic Publishers, 1987.

Bickley, C.A., and K.N. Stevens, "Effects of a Vocal Tract Constriction on the Glottal Source: Data from Voiced Consonants," In *Laryngeal Function in Phonation and Respiration,* eds. T. Baer, C. Sasaki, and K. Harris, 239-253. Boston, Massachusetts: Little, Brown and Company, 1987.

Burke, B.F., "Gravitational Lenses: Observations," In *Quasars,* eds. G. Swarup and V.K. Kapahi, 517-527. Dordrecht, Holland: Reidel Publishers, 1986.

Kleppner, D., "An Introduction to Rydberg Atoms," In *Atoms in Unusual Situations,* ed. J.P. Briand, 57-75. New York: Plenum Publishing Corporation, 1986.

30.5   Reports Published

These reports may be obtained from the Communications Office, 36-412, Research Laboratory of Electronics, Massachusetts Institute of Technology, Cambridge, Massachusetts 02139, at the cost listed. Please include a check made out to RLE and allow six to eight weeks for surface mail. Foreign airmail postage is an additional $4.00 for each report ordered.

Allen, J., and D. Kleppner, eds., *RLE Progress Report No. 129.* MIT, 1987. No charge.

Angelini, A., *Cooling of the Toroidal Magnet.* RLE PTP-87-10. MIT, 1987. $4.00.

Atwater, H.A., Jr., *Ion Beam Enhanced Grain Growth in Thin Films.* RLE TR-527. MIT, 1987. $15.00.

Brocco, L.M., *Macromodeling CMOS Circuits for Timing Simulation.* RLE TR-529. MIT, 1987. $8.00.

Coppi, B., *Direct Approach to Achieving Ignition Conditions.* RLE PTP-87-4. MIT, 1987. $5.00.

Coppi, B., *Near-Term Experiments on Fusion Burn Conditions by Neutronless Reactions.* RLE PTP-87-16. MIT, 1987. $3.00.

Coppi, B., *Transizione Dalla Fissione alla Fusione nell'Uso dell' Energia Nucleare.* RLE PTP-87-6. MIT, 1987. $3.00.

Coppi, B., *Comments on the Agreement between the U.S. and the U.S.S.R. on the Scientific and Technical Cooperation in the Field of the Peaceful Uses of Atomic Energy.* RLE PTP-87-13. $3.00.

Coppi, B., and R. Englade, *Proposal of a Minitex Experiment.* RLE PTP-87-9. MIT, 1987. $3.50.

Coppi, B., and A. Pellei, *La Fusione Termonucleare Controllata.* RLE PTP-87-8. MIT, 1987. $6.00.

Coppi, B., P. Detragiache, and F. Pegoraro, *Internal Kink Modes in the Large Larmor Radius, Long Mean Free Path Regime.* RLE PTP-87-14. MIT, 1987. $3.00.

Coppi, B., S. Migliuolo, and F. Porcelli, *Macroscopic Plasma Oscillation Bursts (Fishbones) Resulting from High Energy Populations.* RLE PTP-87-2. MIT, 1987. $6.00.

Coppi, B., and F. Pegoraro, *Salient Characteristics of the Ignitor Experiment.* RLE PTP-87-3. MIT, 1987. $3.50.

Coppi, B., and F. Porcelli, *Plasma Oscillation Bursts and Scattering of Intermediate Energy α Particles* RLE PTP-87-7. MIT, 1987. $3.00.

Coppi, B., and W.M. Tang, *Ignition Density Bounds and Collective Modes of Fusing Nuclei.* RLE PTP-87-17.

Dagli, N., *III-V Waveguides and Couplers for Integrated Optics.* RLE TR-533. MIT, 1987. $12.00.

Detragiache, P., and F. Pegoraro, *Internal Kink Modes in Weakly Collisional Plasma Regimes.* RLE PTP-87-15. MIT, 1987. $4.00.

Englade, R., *Ignition and Anomalous Transport Processes.* RLE PTP-87-12. MIT, 1987. $5.00.

Espy-Wilson, C.Y., *An Acoustic-Phonetic Approach to Speech Recognition: Application to the Semivowels.* RLE TR-531. MIT, 1987. $12.00.

Feder, M., *Statistical Signal Processing Using a Class of Iterative Estimation Algorithms.* RLE TR-532. MIT, 1987. $10.00.

Freeman, D.M., *Hydrodynamic Study of Stereociliary Tuft Motion in Hair Cell Organs.* RLE TR-523. MIT, 1987. $12.00.

Griffin, D.W., *Multi-Band Excitation Vocoder.* RLE TR- 524. MIT, 1987. $10.00.

Martinez, D.M., *Model-Based Motion Estimation and Its Application to Restoration and Interpolation of Motion Pictures.* RLE TR-530. MIT, 1987. $10.00.

Pappas, T.N., *Estimation of Coronary Artery Dimensions from Angiograms.* RLE TR-528. MIT, 1987. $10.00.

RLE Speech Communication Group. *Working Papers: Volume 5.* RLE SCG-5. MIT, 1987. $7.00.

Sugiyama, L.E., J. Martinell, and P.C. Efthimion, *1D Transport Code - User's Manual.* RLE PTP-87-5. MIT, 1987.

Sugiyama, L.E., *Predictive Transport Simulation of TFTR Ohmic Discharges.* RLE PTP-87-1. MIT, 1987. $5.50.

Towe, E., *Phase-Locked Semiconductor Quantum Well Laser Arrays.* RLE TR-526. MIT, 1987. $13.00.

Wyatt, J.L., Jr., *Nonlinear Dynamic Maximum Power Theorem.* RLE TR-525. MIT, 1987. $4.00.

Zimbardo, G., *Theoretical Model of Uranus's Bowshock.* RLE PTP-87-11. MIT, 1987. $5.00.

30.6 Special Publications

The publications listed below are available from RLE at no cost.

RLE Brochure. RLE SP-1. MIT, 1986.

Collegium Prospectus. RLE SP-2. MIT, 1987.

RLE Currents. RLE SP-3. Biannual newsletter.

Technical Reports Abstracts, 1983-1987. RLE SP-4. MIT, 1988.

RLE Publications Update, January 1987 - June 1988. RLE SP-5. MIT, 1988.

Seated: Senior Staff Assistant
Donna L. Gale.
Standing: Administrative
Assistant Cynthia Y. Kopf.
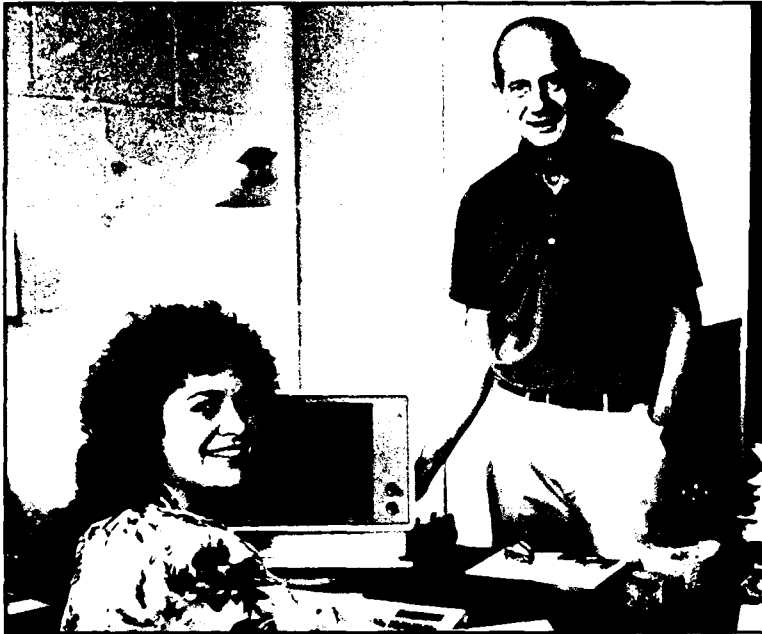
Administrative Assistant
Andrea L. Gelinas and
Technical Staff
John D. Kierstead.

Left to right:
Technical Staff John W. Barrett
and Research Associate
Dr. Phillip W. Rosenkranz.

Foreground: General Services
Supervisor Joseph Sincuk, Jr.,
background, left to right:
Senior Stock Clerk Joseph E.
Mitchell, Maintenance Mechanic
Edward R. Lavalle, Senior
Stock Clerk David M. Taylor,
Senior Tube Technician George
H. Leach, Instrument Maker
Robert W. Aalerud, Maintenance
Mechanic Donald A. Clements,
and Project Machinist
Manuel Cabral, Jr.

31.0 Current RLE Personnel

Director: Jonathan Allen
Associate Director: Daniel Kleppner

Professors

Jonathan Allen	Lawrence S. Frishkopf	William T. Peake
Dimitri A. Antoniadis	Hermann A. Haus	Miklos Porkolab
Arthur B. Baggeroer	Erich P. Ippen	David E. Pritchard
George Bekefi	John D. Joannopoulos	William F. Schreiber
A. Nihat Berker	Marc A. Kastner	Campbell L. Searle
Abraham Bers	Nelson Y-S. Kiang	Jeffrey H. Shapiro
Robert J. Birgeneau	John G. King	William M. Siebert
Amar G. Bose	Daniel Kleppner	Henry I. Smith
Louis D. Braida	Jin Au Kong	Louis D. Smullin*
Bernard E. Burke	Francis F. Lee	David H. Staelin
Sow-Hsin Chen	Patrick A. Lee	Kenneth N. Stevens
Bruno Coppi	Jerome Y. Lettvin	Donald E. Troxel
Thomas H. Dupree	J. David Litster	Thomas F. Weiss
Shaoul Ezekiel	Frederic R. Morgenthaler	Peter A. Wolff
Clifton G. Fonstad, Jr.	Alan V. Oppenheim	Henry J. Zimmermann*

Associate Professors

Sylvia T. Ceyer	Jeffrey H. Lang	Keith A. Nelson
John W. Dreher	Jae S. Lim	Carl V. Thompson II
James G. Fujimoto	Bruce R. Musicus	John L. Wyatt, Jr.
Peter L. Hagelstein		

Assistant Professors

Jesus A. del Alamo	Leslie A. Kolodziejski	Simon G.J. Mochrie
John M. Graybeal		Jacob K. White

Senior Research Scientists

Nathaniel I. Durlach	Dennis H. Klatt
Louis A. Kamentsky	Robert H. Rediker

Note
Faculty information current as of July 1, 1988. Asterisk (*) denotes emeritus professor.

Principal Research Scientists and Associates

H. Steven Colburn	Stanley C. Luckhardt	Joseph S. Perkell
John J. Guinan, Jr.	John Melngailis	Victor W. Zue

Postdoctoral Associates

Patricia G. Blauner	Francesco Porcelli	Elias Towe
Alexander Martin		Beat Zysset

Postdoctoral Fellows

Joseph Ashkenazy	Carol Espy-Wilson	Sharon Manuel
Robin L. Davis	Kenneth W. Grant	Karen Payton

Research Staff

Giovanni Aliberti	David H. Kaufman	John J. Rosowski
John W. Barrett	Min-Chang Lee	Stephanie Seneff
James M. Carter	Ivan Mastovsky	Stefanie Shattuck-Hufnagel
Marc Cohen	Stefano Migliuolo	Linda E. Sugiyama
Bertrand Delgutte	Harry Norris	Sue S. Syu
Lorraine A. Delhorne	Michael Phillips	Ngai Chuen Wong
Donald K. Eddington	William M. Rabinowitz	John Wroclawski
Ronald C. Englade	Charlotte M. Reed	Sunny Y.C. Yuen
Edward W. Fitzgerald	Philip W. Rosenkranz	Patrick M. Zurek
Dennis M. Freeman		

Visiting Scientists

Giuseppe Bertin	Jack Kotik	Thomas Savarino
Fielding Brown	Chris Lashmore-Davies	Bruce Schneider
Stefano Coda	Chaim Leibovitch	Thomas R. Sciascia
Paolo Detragiache	Zhuzhen Li	Randa Seif
Theodore W. Ducas	Neil A. Macmillan	Elias Snitzer
Alvin Essig	John Makhoul	King N. Tu
Gad Geiger	Paul Mataloni	Wen-ke Wang
Rong-shu Gong	Shigeru Oho	Kongyi Xu
Keikichi Hirose	Alain Priou	Xiuzhen Yu
Janet D. Koehnke	Stanley J. Rosenthal	

Research Affiliates

John S. Barlow	Mark L. Curby	Eva B. Holmberg
Bruce Bernacki	Richard S. Goldhor	Joseph A. Jarrell
Ian S. Boardman	Philip Hemmer	Haruko Kawasaki
Robert M. Brown	Robert E. Hillman	John D. Kierstead

Harlan Lane
Leah S. Larkey
John L. Locke
Leonard Picard
Irving Plotnik
Soon Yun Poh

L. Ramdas Ram-Mohan
Michael Shao
Robert T. Shin
Frank J. Stefanov-Wagner
David A. Steffens

Noriko Suzuki
Robert A. Ulichney
Akhileswar G. Vaidyanathan
Kenneth Wacks
Jane Webster

Research Assistants

Christopher J. Adam
Nasser A. Ahmad
Gary A. Allen
Andrew Alston
Erik H. Anderson
Kristin K. Anderson
Robert C. Armstrong
David V. Arnold
Vanderlei S. Bagnato
Donald G. Baltus
Cyrus S. Bamji
Pierino Bonnani
Maurice Borgeaud
Donald E. Bossi
Kevin Boyce
Stuart D. Brorson
Chrisopher Carilli
So Kuen Chan
Pin-P. Chang
Jaeshin Cho
Lawrence Clevenger
Samuel Conner
Christopher Corcoran
Michelle M. Covell
Vivek Dhawan
Andrew D. Dubner
Susan Dubois
Paul Duchnowski
Scott B.C. Dynes
Jerrold A. Floro
Gregory Francis
Albin J. Gasiewski
Thomas J. Gentile
David J. Gladstone
James R. Glass
Arthur C. Grant
Daniel W. Griffin
Keith Groves
Katherine Hall
Hsiu Chi Han
Stephen M. Hannon

Daniel Harasty
John C. Hardwick
Michael Heflin
Kristian Helmerson
Douglas Henderson
Braden E. Hines
Seng-Tiong Ho
Andrew W. Howitt
Long Hsu
Thomas T. Huang
Weiping Huang
William Huang
Barbara J. Hughey
Janice M. Huxley
Khalid Ishmail
Chun-Ho Iu
Rajeev Jayavant
Hong Jeong
Roy K. John
Hal Kahn
Michael M. Kash
Robert Kassel
Morris P. Kesler
Kelsey M. Key
Jean-Fu Kiang
Edward Kim
Richard Kim
Douglas A. Kirkpatrick
Yao-Ching Ku
Charlene Kuo
Kenneth Kupfer
Michael J. LaGasse
Lori F. Lamel
Suzanne Lau
Check Fu Lee
Kin-Wai Leong
Hong Chung Leung
Chungpin Liao
Chen-Shi Lin
Freeman Lin
Fu-Chin Liu

Ling-Yi Liu
Hai Longworth
Andrew Lumsdaine
Michael Machado
Peter D. Magill
Adam Malamy
Peter Martin
Lynne M. McCormick
Steven P. McCormick
Michael McCue
Marianne McGonigal
Udi Meirav
Lynne A. Molter-Orr
Peter A. Monta
Keith S. Nabors
Son Van Nghiem
Peter O'Brien
Scott Paine
Joyce E. Palmer
Lily Y. Pang
Dongwook Park
Samuel L. Park
Patrick M. Peterson
Mary Phillips
Julien Piot
John Pitrelli
Matthew Power
G.N. Srinivasa Prasanna
Gill Pratt
Yikang Pu
Jason Puchalla
Hui Meng Quek
Eric L. Raab
Mark M. Reichelt
Jaesang Ro
Jon C. Sandberg
Robert W. Schoenlein
John Scott-Thomas
Hugh Secker-Walker
Ghavam Shahidi
Mohammed Shahriar

289

Jerome M. Shapiro
Richard Singer
Stephen P. Smith
William S. Song
David Standley
Deborah Stephan
Brian Stewart
Richard Stoner
Ke-Xun Sun
Bernard I. Szabo

Eugene Tarnow
Barry L. Thompson
Ann Tulintseff
Rosalie Uchanski
Jesus N. Villasenor
James C. Vlcek
David B. Walrod
Robert Webster
Su-Min Wei
Robert Weisskoff

George R. Welch
Dilys K. Wong
Rosalind Wright
Ying-Ching Eric Yang
Anthony T. Yen
Peter T. Yu
Herng-Aung Yueh
Avideh Zakhor
Farhad Zarinetchi
Hong Zhang

Teaching Assistants

James S. Im
Harold H. Lim

Adam Tom

Dan Wang
Michael L. Zerkle

Graduate Students

Sergio Ajuria
Phillip F. Bagwell
Robert Barat
John D. Beckerle
Ricardo Betti
Bradley T. Binder
Kirk H. Chao
Cynthia R. Christensen
William Chu
Jeffrey A. Colburn
Nancy A. Daly
Manuel E. Conde
Anthony DiRienzo
Robert H. Enders
Robert B. Feinberg
Sheldon Gilbert

Julie E. Greenberg
Caroline Huang
Scott Isabelle
Lars U. Jaenchen
Marsha Jeung
Andrew D. Johnson
Michael J. Komichak
Laura MacGinitie
Jeffrey N. Marcus
John F. Marko
A.G. Martin
Scott E. Meredith
John Moores
Bruce G. Oldaker
Elizabeth Olson

Maurice J. Ostrov
Susan L. Phillips
Karim Roshd
Gurhan Saplakoglu
Michelle Schulberg
Scott R. Shephard
Barbara Shinn
Albert Swartz
Michael J. Tsuk
Carlos Vila
Weige Xue
Xinglong Yan
Qingyun Yang
Jenny Yu
Naomi E. Zirkind

Undergraduate Students

Anne Marie Atemio
Robert G. Atkins
Talal Bahrani
Leon Balents
Susmitha K. Bellam
Amy Bertin
J. Bevilaqua
David B. Blundin
Jason Bochinski
Joseph E. Bondaryk
Felipe Calderon

Roger Carpenter
Ike Chang
Thomas F. Chang
Vincent Chau
Judy Chen
Suephy Chen
Tak K. Cheng
Shiufun Cheung
Nicola Chin
Sunkyung Choi
Cynthia F. Chuang

Patricia Cuneo
David Duseau
Stephen Eikenberry
Thomas Farkas
Stuart Fiske
Marcelo F. Fogaca
Jaime Garza
William Greenberg
David Hamilton
Roeland V. Hammerschlag
Cynthia Harris

Mark A. Hausman
Timothy Hawkeye
Stacy S. Hawkind
Scott Hector
Brian T. Hou
Sue-Hane Hsu
Tsen-Yu Hung
Charles Jankowski
Hemantha Jayawardena
Illy King
Weng-Yew Ko
J. Kuchar
Debbie Kulik
Yinchieh Lai
Joseph C. Landry
Debra Lew
Ruby Li
Brian Luschwitz
Joyce Ma
Mark H. Mabry
Sanjay Manandhar
Edward L. Markowitz

Roderick K. Mason
Michael Matter
Muriel Medard
Leslie M. Melcer
H. Meng
Andrew W. Miklich
Bruce Mikura
Hirak Mitra
Christopher M. Neils
Garet Nenninger
Eugene Opsasnick
Erik Ordentlich
Christine Pao
Parag Patil
Ning P. Peng
Rebecca Perry
Mark Randolph
Leonardo Renna
Christopher Roller
Michael P. Ruf
Peter H. Schmidt
Andrew Shaw

Haris J. Sih
Richard W. Singerman
Prashant Singh
Genevieve C. Sparagna
Howard Stuart
Lisa Su
Javier G. Tam
Tali J. Tamir
A. Dushyanthi Thurairatnam
Rajeev Tewari
Sean Tierney
Mary F. Tong
Keith A. Tuson
Timothy Wilson
Amy Wong
Victor Wong
Chan A. Yoon
Gregory Zancewicz
Garth Zeglin
Lori L. Ziernan
H. Zolla

Administrative Staff

Donald F. Duffy
David W. Foss
Virginia R. Lauricella

Barbara J. Passero
John S. Peck
Joseph Sincuck, Jr.

Anita T. Sloan
Vicky-Lynn Taylor
Donna Maria Ticchi

Support and Technical Personnel

Robert W. Aelerud
Janice L. Balzer
Margery Brothers
Mary Ellen Butts
Manuel Cabral, Jr.
Kathleen E. Cairns
Donald A. Clements
John F. Cook
Alfredo D. Donato
Francis Doughty
Phyllis M. Eiro
Dorothy A. Fleischer
Ann Forestell
Deborah Gage
Donna L. Gale
Thalia Garalis

Andrea L. Gelinas
Kyra M. Hall
Maureen C. Howard
Venetia Kaloyanides
Barbara King
Cynthia Y. Kopf
Edward R. Lavalle
George H. Leach
Cynthia LeBlanc
Anh Lieu
Catherine Lorusso
Eleanora M. Luongo
John Mandile
Timothy McClure
Rita C. McKinnon
Christine T. Mendelsohn

Joseph E. Mitchell
Katherine S. Nash
Susan E. Nelson
John C. Nickerson
Donald K. North
Brian Ray
Veronica Romansky
Maxine P. Samuels
Clare F. Smith
Henry Stram
David M. Taylor
Mary Tighe
Eric P. Watson
John Weigel
Arlene Wint

Left to right: Technical Staff Edward W. Fitzgerald; Technicians John C. Nickerson,
Gerald Lorden, and John C. Weigel; and Research Specialist Ivan Mastovsky
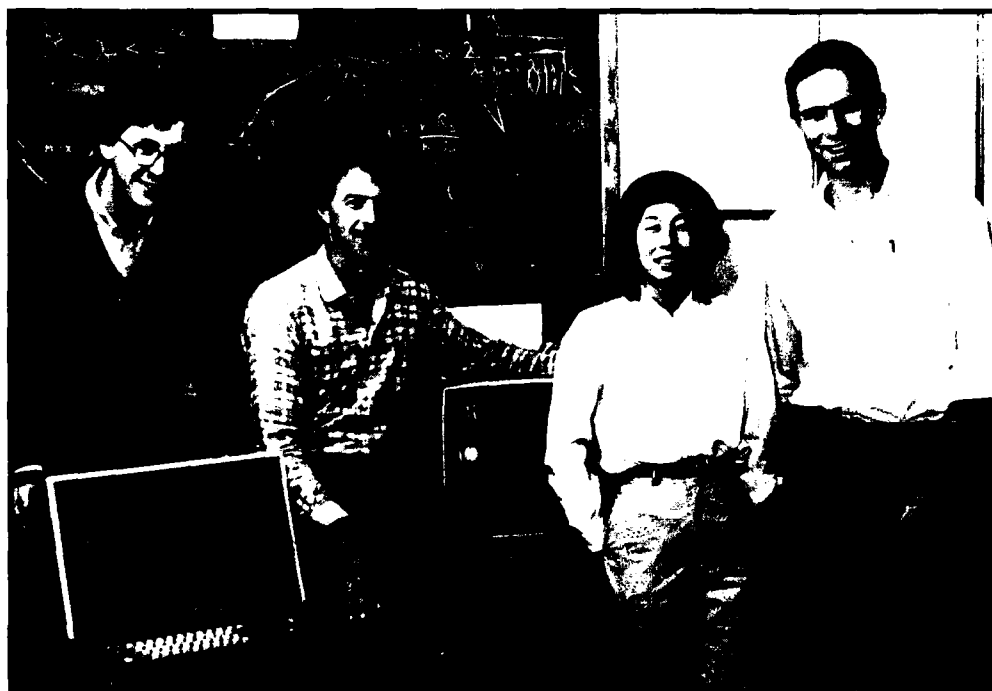
Left to right: Postdoctoral Associate Dr. Francesco Porcelli; Research Scientists
Dr. Ronald C. Englade, Dr. Linda E. Sugiyama, and Dr. Stefano Migliuolo

32.0   Research Support Index

Professor Keith A. Nelson

33.0 Research Project Staff Index

W

Wang, D.   92
Wang, X.Y.   93
Webster, R.   149
Wei, X.B.   93
Weiskoff, R.M.   178
Weiss, T.F.   132
Welch, G.R.   163
White, J.   104, 105, 106
Wolff, P.A.   67, 68
Wong, D.L.   33
Wong, N.C.   59
Wong, S.   68
Wornell, G.W.   217, 258
Wright, R.H.   217
Wu, C.F.   91
Wyatt, J.L., Jr.   102

X

Xu, K.Y.   183
Xue, W.   87

Y

Yang, Q.Y.   27, 30
Yang, Y.E.   229
Yen, A.T.   1, 5, 9
Yu, P.T.   57
Yueh, H.   240
Yuen, S.Y.C.   67

Z

Zakhor, A.   218
Zanciewicz, G.J.   258
Zeglin, G.   177
Zhao, N.M.   91
Zirkind, N.E.   62
Zurek, P.M.   141, 142
Zysset, B.   42, 46